Evaluation of FDOT Corrosion Prevention and Control Programs

DOT-RFP-19-9059-GH

Tallahassee, Florida

FINAL REPORT

May 20, 2022

WJE No. 2019.0352.0

PREPARED FOR:

Mr. Shannon Deese
Florida Department of Transportation
605 Suwannee Street, Mail Station 20
Tallahassee, Florida 32399-0450

PREPARED BY:

Wiss, Janney, Elstner Associates, Inc.
110 East Broward Boulevard, Suite 1860
Fort Lauderdale, Florida 33301

Evaluation of FDOT Corrosion Prevention and Control Programs

DOT-RFP-19-9059-GH

Tallahassee, Florida

FINAL REPORT

May 20, 2022

WJE No. 2019.0352.0

PREPARED FOR:

Mr. Shannon Deese
Florida Department of Transportation
605 Suwannee Street, Mail Station 20
Tallahassee, Florida 32399-0450

PREPARED BY:

DISCLAIMER

The opinions, findings, and conclusions expressed in this publication are those of the authors and not necessarily those of the Florida Department of Transportation.

1. Report No.	2. Government Accession No.	3. Recipient's Catalog No.
DOT-RFP-19-9059-GH		

4. Title and Subtitle	5. Report Date
Evaluation of FDOT Corrosion and Control Programs	May 2022
	6. Performing Organization Code

7. Author(s)	8. Performing Organization Report No.
Matthew Fadden, PhD, Casey Jones, John Lawler, PhD, Crisol Ortiz, Marwa Abdelrahman, PhD, Wiss, Janney, Elstner Associates, Inc. Kingsley Lau, PhD, Samanbar Permeh, Florida International University	

9. Performing Organization Name and Address	10. Work Unit No. (TRAIS)
Wiss, Janney, Elstner Associates, Inc. 110 East Broward Boulevard, Suite 1860 Fort Lauderdale, Florida 33301	11. Contract or Grant No. BE725

12. Sponsoring Agency Name and Address	13. Type of Report and Period Covered
Florida Department of Transportation 605 Suwannee Street, Mail Station 20 Tallahassee, Florida 32399	Final Report, 03/25/2019 through 05/31/2022
	14. Sponsoring Agency Code

15. Supplementary Notes

16. Abstract

Corrosion of Florida's bridge infrastructure has shown to be costly for FDOT, both due to the number of bridges and harsh environmental conditions across the State. While the mechanisms that describe corrosion within reinforced concrete bridge elements are well understood, the ability to limit corrosion in practice has led to many methods that aim to mitigate the effects of corrosion. These systems include durability-based design requirements for new bridges and rehabilitation efforts for existing bridges, summarized in this report. FDOT has implemented many of these systems on its bridges with varying degrees of success. This report also summarizes current FDOT design requirements and specifications regarding corrosion control for reinforced concrete bridge structures with a focus on substructure elements.

A comprehensive study that compares multiple practices and systems across various Florida bridges has been undertaken. As a result, comparative data related to their performances have been compiled and analyzed. Without this information, it is challenging for the State to understand the benefits of its corrosion control measures and the life-cycle cost analysis of the systems. Therefore, this study aims to evaluate and compare multiple practices and systems used across the State in terms of durability, cost, and long-term performance. Although every corrosion prevention and control program described in this report will not be incorporated into this research, this study includes the most used measures, including concrete cover, supplementary cementitious materials, epoxy coating, and cathodic protection (metalized, impressed current, and galvanic).

17. Key Word	18. Distribution Statement
Corrosion, bridge, cathodic protection, durability, cost	

19. Security Classif. (of this report)	20. Security Classif. (of this page)	21. No. of Pages	22. Price
Unclassified	Unclassified	196	

EXECUTIVE SUMMARY

The Florida Department of Transportation manages a network of over 6,500 bridges within its highway infrastructure system, many of which are constructed in severe corrosive environments. To extend the service life of bridges across the State, FDOT implements various corrosion prevention and control systems, including durability based design requirements of new bridges and rehabilitation efforts for existing bridges. This evaluation included a review of both performance and estimated costs of commonly used materials/systems to identify the most robust, effective, and cost-efficient methods for extending service lives of bridges. In addition field investigations were performed at four locations across the state and included eight individual bridges. These bridges were chosen in order to evaluate the most commonly utilized corrosion prevention and control systems installed in Florida's coastal environments.

The two corrosion control systems evaluated in this investigation are both cathodic protection installations and include galvanic pile jackets and impressed current jackets typically installed on the footing and/or pile cap elements. Results indicated that galvanic pile jackets are an effective method of mitigating corrosion on pile elements and can extend service life of pile elements by 20 years or more depending on the quality of installation, environment, and maintenance efforts. Similarly, conventional impressed current jackets powered by rectifiers are also effective at mitigating corrosion in larger substructure elements, however, these systems require periodic maintenance and adjustments. In 2020, FDOT replaced the traditional rectifiers with solar panels on select footing elements on three bridges on a trial basis. A review of data regarding one of these systems showed that while the solar powered systems provided some amount of cathodic protection, several limitations prevented the systems from performing comparably to the traditional rectifier-powered systems. Specifically, the solar-powered system did not provide adequate cathodic protection to the structure and daily shifts in provided current based on sunlight availability present challenges to be overcome in developing these systems.

Regarding corrosion prevention mechanisms, primarily those regarding construction materials included in the design of new bridges, this study evaluated performance of epoxy-coated reinforcing and inclusion of fly ash within concrete mix designs. The State has experienced mixed performances of bridges constructed with epoxy-coated reinforcing. This investigation compared a bridge substructure constructed with epoxy-coated reinforcement to a similar sister bridge constructed with traditional uncoated reinforcing steel. This investigation found that installation of epoxy-coated reinforcement has provided a minimum of three years of additional service life, and likely more, prior to repairs or corrosion control mechanisms would need to be considered. Inclusion of fly ash within concrete mix designs provided benefit regarding corrosion control by reducing pore size and increasing resistivity of the concrete, both of which reduce diffusivity of chlorides. However, quantitative conclusions were difficult to ascertain from data obtained during this investigation, as surface coatings unbeknownst to the research team had been applied to the bridge substructures, which likely affected surface concentrations and associated chloride profiles.

All of these results ultimately may lead to new criteria regarding installation, maintenance, and monitoring methods for cathodic protection systems, as well as consideration for construction materials for new bridge designs to increase durability and anticipated service life.

TABLE OF CONTENTS

LIST OF FIGURES

LIST OF TABLES

1. INTRODUCTION

Corrosion of steel in reinforced concrete bridges is a significant concern for the structural integrity, long-term durability, and maintenance of the Florida highway infrastructure. For example, statistics from a national study in 2002 indicated that approximately 15% of the national bridge inventory is structurally deficient because of corrosion, and the national annual direct cost exceeded $8 billion (Koch et al. 2002). As a result, research and recommendations have been made by technical organizations such as American Concrete Institute (ACI), Federal Highway Administration (FHWA), NACE International, and National Cooperative Highway Research Program (NCHRP) to promote corrosion durability of highway bridge infrastructures.

Transportation infrastructure costs typically exceed 10% of Florida's state budget. Florida's 2020-2021 fiscal year budget includes $9.9 billion to be allocated to the Florida Department of Transportation (FDOT), including $436.2 million for scheduled repairs of 57 bridges and replacement of 18 bridges and $2.8 billion for highway construction (Druga 2019). The typical design life expectation for the >6,500 bridges in the state highway infrastructure exceeds 50 years; however, approximately half of the bridges are in aggressive marine service. There is a need to continue to improve designs to control corrosion and develop tools to assess future performance and maintenance needs.

In Florida, corrosion is pervasive in many of the environments where transportation infrastructure exists, including buried steel and concrete pipes in soil, steel bridge superstructure and bearings, mechanically stabilized earth walls, steel cables and wires, steel piling, concrete tunnel segments, reinforced concrete decks, and pour-backs as well as reinforced concrete substructures. The corrosion mechanisms vary significantly due to the multitude of engineered highway systems with varying exposure environments, chemistry, and construction materials. However, of the many engineering systems in the state highway infrastructure, bridge substructures are most critically affected by corrosion of reinforcing steel. This critical nature is partly due to its high visibility to the general public, especially for highway bridges that serve public and private enterprises in large populations along the coast. Such highway bridges are vulnerable to aggressive coastal environments. Of the national annual direct costs for highway bridges, $2 billion was related to steel corrosion in bridge concrete substructures (Tinnea et al. 2006). The Florida bridge work plan identified bridge substructure repair as the second-highest maintenance need (Figure 1) (Lau et al. 2018).

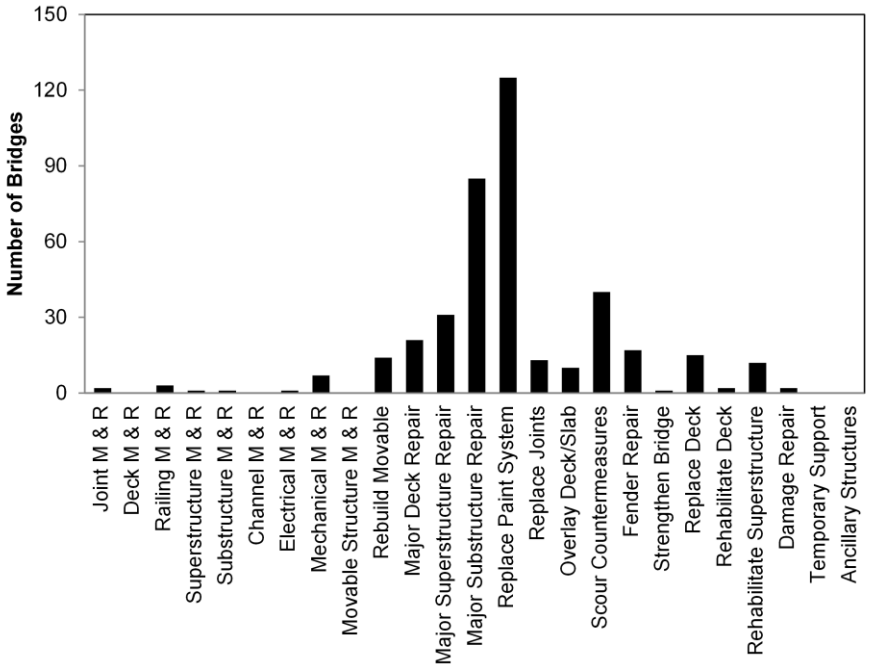

Figure 1. Florida Department of Transportation Bridge Work Plan for 2015. (Lau et al. 2018).

Continuing research by FDOT has advanced the engineering practice for corrosion control, especially for reinforced concrete substructures, and improved material specifications and design practices have been implemented over the last 30 years. These positive changes have provided safer and more durable structures. The maintenance of newer systems is not as intensive as for older bridges. Complexities of modern structural systems, the highly aggressive Florida exposure environments, changes in building and material technologies, and sometimes variability in construction quality provide bridge preservation challenges. Therefore, it is highly advantageous to evaluate the performances of implemented corrosion control measures in Florida bridges so that the most robust and effective methods for extending the service life of bridges can be identified.

Research Outline and Objectives

The overarching project objective is to determine the effectiveness of the current corrosion prevention and control programs used by the State. For this study, the research team has inspected eight bridges and considered the effects of improved construction practices and cathodic protection on bridges across the State. The following tasks which have been conducted outline the project objectives:

- **Task 1 - Literature Review:** The project team used its experience and familiarity with Florida infrastructure to conduct a review of literature that considers FDOT corrosion mitigation procedures.
- **Task 2 - Site Visits:** Working with FDOT, the project team identified bridges and systems for site inspection. Care was taken to limit the number of variables associated with each assessment in an effort to optimize the validity of the comparisons being made between the various bridges/CP systems.

- **Task 3 - Cost of Installed CP:** The project team analyzed design documents, BIRs, and other documents to determine an approximate order of magnitude lifetime cost estimate for each applicable CP system studied. The research team worked with FDOT to identify what CP systems/combinations are included and what life should be associated with the cost.
- **Tasks 4 and 5 - Analysis of Structures with and without Cathodic Protection:** Data mining of FDOT and other state resources has been carried out to estimate the service life of structures with and without CP. The research team has worked with FDOT to define threshold criteria for a service life that is applicable to FDOT's needs.
- **Task 6 - Comprehensive Assessment of Corrosion Prevention and Control Program:** The project team used its expertise and the knowledge gained through the previous tasks to quantify the effectiveness of the current FDOT corrosion prevention and control programs and summarize our findings.
- **Task 7 and 8 - Draft Final, Closeout Teleconference, and Final Report:** This final report will be submitted to FDOT for review, and a conference call will be held regarding the findings.

2. LITERATURE REVIEW

This literature review begins with a summary of the fundamental scientific principles that describe corrosion and corrosion control methodologies that have been developed. Following this, a review of the corrosion control methods used in Florida bridges and the implemented cathodic protection system are detailed. This review is intended to be comprehensive regarding the background and types of corrosion prevention systems used throughout Florida.

Science of Corrosion

To understand the corrosion degradation of reinforced concrete and application of mitigation technologies, the basics of the electrochemistry of these systems should be considered. At the most basic level, corrosion of the rebar in concrete is due to the development of an electrochemical cell that is made of the steel rebar and the concrete pore water. The cell supports two basic half-cell reactions:

$Fe \rightarrow Fe^{2+} + 2e^-$ Equation 1

$2H_2O + O_2 + 2e^- \rightarrow 4OH^-$ Equation 2

Equation 1 represents the anodic reaction that accounts for the material loss of the rebar, and Equation 2 represents the supporting cathodic oxygen reduction reaction. The components of the electrochemical cell are described next.

Steel Rebar Anode

The iron oxidation reaction occurs at portions of the steel rebar that serve as an anode. Very slow anodic reactions typically occur on steel rebar embedded in concrete when the steel is in a passive state due to the formation of a thin protective layer of iron hydroxides and oxides. However, chemical changes in the concrete pore water surrounding the steel rebar can disrupt the passive layer. In marine environments, this depassivation occurs when a critical level of chloride ions penetrate through the concrete cover to the surface of the steel rebar. A wide range of critical chloride threshold (CT) values have been reported (Angst et al. 2009), but values near 0.08% to 0.20% by weight cement content have been used by various

design and guideline documents. The effective CT may vary depending on several parameters, including polarization levels, pore water pH, and the binding capacity of the cement paste to entrap chloride ions from the solution. Engineering approaches require practical considerations so that CT may be used based on total chloride levels relative to cement content or by concrete volume. Still, it is important to recognize some uncertainty inherent in this approach.

The number of chloride ions penetrating the concrete cover is influenced by the concrete material, the reinforced concrete element geometry, and the severity of exposure to chloride ion sources. Reinforced concrete bridge substructure elements in marine environments have different exposure zones to water chloride ions and other potential contaminants. These zones include the submerged region, tidal region, splash region, and atmospheric region. Chloride ion diffusion and permeation can account for chloride ingress in concrete in the submerged region due to the chloride ion concentration gradient in the concrete pore water and the hydraulic pressure of the water. Chloride transport in concrete in the atmospheric regions where direct contact with water does not occur is much lower. In the tidal and splash regions, the cyclic wetting and drying allow for the salt concentration on the near-surface of the concrete to be significantly larger, which can be as high as 1.6 lb/ft^3 (Sagüés et al. 2001). This increase in the surface concentration of chloride ions promotes more rapid chloride ingress relative to the submerged and atmospheric regions.

Therefore, a localized region of depassivated steel often develops in the tidal and splash regions and produces locally high corrosion rates. This accounts for typical field observations where the concrete delamination and spalling typically occur in the tidal and splash zones.

Steel Rebar Cathode and Electrical Conductor

The anodic iron oxidation reaction is supported by the oxygen reduction reactions that occur on the surface of the reinforcing steel, typically relatively near the anode. Dissolved oxygen in the concrete pore water reacts, as shown in Equation 2, and the amount of available oxygen can control the rate of this reaction. Generally, the amount of available oxygen is greater in the splash/tidal and atmospheric regions than in the submerged regions. The greater access to oxygen helps accelerate corrosion in the tidal/splash zone, where the steel surface has been depassivated by the presence of chlorides.

The rebar itself acts as an electrical conductor that connects the anode portion of the rebar to its cathode surfaces. Large extended cathodes are available due to the long length of longitudinal rebar as well as the electrical coupling of other rebars by stirrups and tie wire. The large cathode surface area throughout the structure allows for larger rates of reduction reactions that, in turn, encourage polarization to occur and increase the iron oxidation rate at the anode site. This macro-cell coupling of the anode and the extended array of cathodes supports rapid corrosion.

Electrolyte and Ionic Bridge

The electrolyte, as part of the electrochemical cell, is made up of the concrete pore water that remains in the macro-, capillary-, and gel-pores of the hardened concrete. The concrete pore water is typically alkaline, greater than pH 13 during casting, and greater than pH 12 for mature concretes. As mentioned before, steel can develop a passive protective layer at these pH levels, but this can be compromised by chemical changes, including the accumulation of chloride ions.

The concrete pore water creates the ionic path that allows the completion of the electrical circuit (i.e., electrons flow from the anode to the cathode via the rebar itself, and ionic flow develops in the pore water). Concretes with low permeability create a less conductive ionic path. The polarization that occurs due to the coupling of the anode and cathode is reduced due to the voltage drop that occurs in concretes with high electrical resistivity. This loss in polarization reduces the rate of iron oxidation.

Corrosion Control Methodologies

Corrosion of steel in reinforced concrete substructures in marine exposure is largely associated with chloride-induced corrosion. However, carbonation-induced corrosion can occur in substructure components away from splash, where less moisture intrusion occurs. Cracking can also affect the overall corrosion durability of an element.

Corrosion control measures often address means to extend the time to corrosion initiation as the associated corrosion engineering principles are widely understood. The most common approaches include increasing the time it takes for chloride transport to the reinforcing steel surface. This can be accomplished by increasing the concrete cover, utilizing less permeable materials such as concrete incorporating supplementary cementitious materials (SCMs), or applying coatings or overlays on the concrete. Also, it is possible to increase the critical chloride threshold levels for corrosion initiation by using corrosion-resistant steel alloys and the application of coatings on the rebar. Other approaches include the application of admixed inhibitors to develop surface films or modify electrochemical characteristics of the corrosion system. Active approaches to delay or prevent corrosion initiation include the application of electrochemical techniques, such as cathodic protection (CP), chloride extraction, and realkalization.

CP and the use of inhibitors may also be considered as methods to reduce corrosion rates and extend the time to corrosion propagation. Crack repairs on concrete substructures may also delay the development of corrosion-related damage. Crack repair techniques can include epoxy injection and penetrating sealers.

The following sections describe, in detail, design specification and corrosion control methodologies that have been developed and implemented in Florida.

Concrete Structure Design and Construction

The design and detailing of reinforced and prestressed concrete elements play a critical role in determining the service life of the structures. In addition to corrosion-inhibiting admixtures and sealers discussed previously, factors affecting the corrosion resistance of reinforced and prestressed concrete elements include, but are not limited to, concrete mix designs, reinforcing steel cover depth, and method of curing for precast concrete elements.

Concrete Mix Designs

The typical constituents to produce concrete include aggregate, cement, water, SCMs, and admixtures. Each constituent's physical and chemical properties can vary depending on the source; quantities of each can be adjusted and modified, which can make the development of concrete mix designs challenging to meet the strength, durability, and corrosion resistance requirements of a given element.

To produce reinforced concrete structures resistant to corrosion, there are several critical components. The first of which is the water-to-cementitious material ratio (w/c), which is the ratio of the weight of water versus that of cement plus any SCMs. Typical values of w/c in conventional concrete are approximately 0.25 to 0.55. As part of the 1987 FHWA study, corrosion resistance of sample specimens with varying w/c was investigated. Samples were cast with w/c = 0.51, 0.40, and 0.28, and test results found that long-term chloride permeability to the 1-inch depth was reduced by approximately 80 and 95 percent when w/c was lowered from 0.51 to 0.40 and to 0.28, respectively (Pfeifer et al. 1987). The study concluded that after corrosion activity was started under a given set of conditions, the subsequent severity of the corrosion process was reduced significantly for lower w/c concrete samples. This included both conventional concrete and samples containing calcium nitrate and recommended to use w/c in the 0.44 to 0.32 range for substructure concrete members and new precast, prestressed concrete members for bridges.

A second important variable of concrete mix design is the use of SCMs, which can improve the workability of plastic concrete, increase strength, and lower permeability, leading to improved resistance to chloride ion ingress. The three most common SCMs today are slag cement, fly ash, and silica fume, which are byproducts of steel production, coal combustion, and the production of silicon metal or similar alloys. Each of these SCMs participates in different chemical reactions within the paste of the concrete; however, each generally serves to fill capillaries and reduce pore size, thus reducing the permeability of the concrete. Another conclusion from the 1987 FHWA study was that reinforcing steel in slabs that contained silica fume did not develop corrosion. Chloride contents at the 1-inch or greater depth were reduced by about 98 percent after the year-long cyclic saltwater exposure test when compared to the same conventional mix design without silica fume (Pfeifer et al. 1987). Similarly, a 1986 study on concrete containing fly ash indicated that corrosion resistance of concrete is improved when fly ash is used at rates up to 50 percent of the total cementitious material (Halstead 1986).

Concrete Cover Requirements

Another important variable in the corrosion resistance of reinforced and prestressed concrete elements is the thickness of concrete between the outer face of an element and the reinforcing steel, referred to as the concrete cover. As corrosion initiates when chlorides accumulate to a critical threshold concentration at the steel depth, increasing the distance the chlorides must migrate to reach steel will increase the amount of time until the initiation of corrosion. Although corrosion resistance of reinforced concrete elements can be increased using a greater cover, implementation of too much cover can result in wide cracks where cracking occurs perpendicular to the primary longitudinal steel. ACI 222R-19 provides a discussion on the correlation between cracks and their effect on the corrosion resistance of the element with varying findings between several studies; however, it concludes that larger cracks can negatively influence the corrosion performance of reinforced concrete structures and actions should be taken to prevent, or seal, large cracks. ACI 318-19 (as well as historical versions) and ACI 222.3R-11 both provide guidance on reinforced concrete when exposed to external sources of chlorides in service, which requires a minimum concrete cover of 2 inches for walls and slabs and 2-1/2 inches for other members, while this can be reduced to 1-1/2 and 2 inches for precast concrete walls and slabs, respectively (ACI 222.3R-11). AASHTO LRFD Bridge Design Specifications (9th Ed.) also provides additional guidance on the design of concrete covers based on element type, exposures, reinforcing material, and design w/c (AASHTO 2020). Applicable minimum covers per AASHTO are summarized in Table 1. Additionally, the design guide

provides modification factors for the provided values based on w/c ratios of the base concrete, which are also provided below:

- w/c ≤ 0.40 ..... 0.8
- 0.40 < w/c < 0.50 ..... 1.0
- w/c ≥ 0.50 .....1.2

Precast Concrete Curing

Concrete hydration is an exothermic chemical reaction between cement and water that occurs in the early ages of concrete after placement. This hydration process consumes water in the concrete but causes the concrete to harden and develop strength. However, excess heat or an excessive amount of moisture loss due to surface evaporation can result in cracking or a weakened surface. Several methods of providing moisture to concrete surfaces, after placement, referred to as curing, are typically employed. Research has shown the effectiveness of curing will influence the physical properties and corrosion resistance of a given element.

Today, several methods of curing exist for reinforced and prestressed concrete construction. For cast-in-place concrete elements, methods of curing are restricted due to access and equipment restrictions. Methods are generally limited to requiring forms be left in place for a certain period and covering them with a moisture barrier, such as a tarp, to restrict the escape of moisture, application of membrane curing compounds, and wet curing, which may include the periodic application of external water to the bare surface or temporary water-absorbing material, such as burlap. Additional methods are available in precast plant facilities for precast concrete elements, including heat curing and steam curing. Research has shown that steel in heat-cured precast, prestressed concrete members was better protected from chloride-induced corrosion than the same element cured using moisture-curing at ambient temperatures (Pfeifer et al. 1987).

Table 1. Summary of Applicable AASHTO Minimum Covers for Main Reinforcing Steel

Situation	Reinforcing Material Category		
	A	B	C
Severe to Moderate Exposure			
Direct exposure to saltwater	4.0	2.5	2.5
Cast against earth	3.0	2.0	2.0
Coastal	3.0	2.0	2.0
Limited Exposure			
Up to No. 11 Bar (not in the soffit of cast-in-place slabs or form panels)	1.5	1.0	1.0
No. 14 and No. 18 bars (not in the soffit of cast-in-place slabs or form panels)	2.0	2.0	2.0
Piling			
Precast reinforced piles - noncorrosive environments	2.0	1.5	1.0
Precast reinforced piles - corrosive environments	3.0	2.5	2.0
Precast prestressed piles	2.0	1.0	1.0
Cast-in-place piles - noncorrosive environments	2.0	1.5	1.5
Cast-in-place piles - corrosive environments	3.0	2.5	2.0
Cast-in-place piles - shells	2.0	1.5	1.0
Cast-in-place piles - auger-cast, tremie concrete, or slurry construction	3.0	2.5	2.0

Source: AASHTO 2020, Table 5.10.1-1 (Category A - Uncoated reinforcing steel meeting AASHTO M 31M, Category B - Epoxy coated or galvanized meeting ASTM A775, Category C - Materials meeting AASHTO M 334M)

Florida Concrete Specifications

Current standards for both new construction and maintenance of roads and bridge within Florida are governed by "Standards Specifications for Road and Bridge Construction" issued by FDOT in July 2020. These standard specifications provide design and construction requirements for a variety of construction operations, materials, and elements. Additional specific requirements may be developed for a given structure or project, and such are typically included for larger projects. Standard specifications applicable to reinforced and/or prestressed concrete bridge structures include, but are not limited to:

- Section 346 - Structural Portland Cement Concrete
- Section 400 - Concrete Structures
- Section 415 - Reinforcing for Concrete
- Section 455 - Structures Foundations
- Section 901 - Coarse Aggregate
- Section 902 - Fine Aggregate
- Section 921 - Portland Cement and Blended Cement
- Section 923 - Water for Concrete
- Section 924 - Admixtures for Concrete

- Section 925 - Curing Materials for Concrete
- Section 929 - Supplementary Cementitious Materials

Section 346 provides guidance for both cast-in-place and precast concrete mixtures, including material requirements, cement use by environmental classification, recommended SCM proportions, admixtures, and both plastic and hardened properties. A total of twelve standard classes of concrete are listed with 28-day specified minimum compressive strengths ranging from 3,000 to 10,000 psi. For each class, minimum total cementitious material contents and maximum w/c are also provided. Section 346 also references multiple Section 900 series specifications that provide chemical and physical requirements, required material testing, and any other requirements for concrete constituents and materials.

Standard specifications also provide guidance on reinforcing materials, construction practices, and allowable methods of curing. FDOT currently only permits the following concrete reinforcement materials in bridge structures: carbon steel bar, carbon steel welded wire mesh, fiber reinforcing polymer (FRP), stainless steel, and low carbon chromium steel. Current specifications exclude epoxy-coated reinforcing (ECR) or galvanized steel reinforcement from use in this application. FDOT currently requires a minimum duration of 72 hours for the concrete curing period and except when specific curing methods are specified, allows for curing to be performed by continuous moisture, membrane curing compound, curing blankets, or several methods of accelerated cure. If the concrete contains silica fume, the only allowable curing method is continuous moisture application for 72 hours.

Corrosion Resistant Reinforcement

Carbon steel has low resistance to the effects of chloride ions to depassivate its protective oxide layer. Different alloys have been developed to provide corrosion resistance. Corrosion-resistant reinforcing steels include hot-dipped galvanized (HDG), low carbon chromium steel, and stainless steel, among others. The corrosion-resistant reinforcing steels typically have greater critical chloride thresholds. For low carbon chromium steel and stainless steel, the addition of chromium allows for a greater critical passivation current density, which minimizes conditions where pitting corrosion can develop. Due to the higher CT, the steel can remain in passive condition for a wider range of chloride exposure environments. HDG allows for some level of beneficial cathodic polarization due to the sacrificial corrosion of the zinc-rich layers. However, much of the protection provided to the reinforcing is afforded by the barrier characteristics of the alloyed galvanizing layers (Broomfield 1997).

Reinforcing Steel Coatings

To improve corrosion protection of carbon reinforcing steel embedded in portland cement concrete, multiple types of coatings and surface treatments have been developed over the past several decades. Fusion-bonded, epoxy-coated reinforcement was the first widely adopted coating technology for reinforcing steel and has been used in the United States since approximately 1975. Since then, several other coating technologies have entered the market, including breeds of organic, inorganic, ceramic, and metallic coatings. Today, the most common corrosion mitigation technologies are ECR (ASTM A775), galvanized reinforcing (ASTM A1094), or dual-coated reinforcing steel incorporating a zinc-alloy first coat with an epoxy topcoat (ASTM A1055). Such surface applications are intended to provide additional corrosion resistance for the reinforcing steel bars by impeding oxygen, water, and chlorides from reaching

the surface of the bars. Florida commenced bridge construction using ECR in the late 1970s and as of 1994, over 300 FDOT bridges had been constructed incorporating ECR (Sagüés et al. 1994).

A previous study conducted by the Federal Highway Association (FHWA) to determine the long-term performance of ECR in salt-contaminated concrete found that corrosion resistance of ECRs in uncracked concrete can approach the corrosion-resistant level of stainless-steel reinforcement (Lee and Krauss, 2004). Coating defects and cracking of the concrete substrate, however, can result in corrosion of the embedded reinforcing steel. While some number of concrete cracking is expected across a structure, coating defects, such as holidays, can result in points of corrosion initiation, resulting in localized corrosion and coating disbondment of the adjacent coating. Coating defects can be formed during the coating process or transport, handling, or installation, as is more commonly the case with modern coating technologies. Current standards not only provide specific information on necessary surface preparations, chemical and performance requirements of the coatings, permissible defects in the coatings but also provide guidelines for construction practices (ASTM A775 Appendix X1).

Concrete Coatings/Sealers

Concrete coatings and/or sealers are used to provide corrosion protection to reinforced concrete elements by protecting against the intrusion of moisture and chlorides into the concrete substrate, thus increasing the amount of time until the initiation of corrosion. Multiple types of concrete coatings and/or sealers have been developed to be applied to new and/or existing bridges, such as boiled linseed oil, epoxies, polyurethanes, silicones, and others. Project 12-19A, conducted by the National Cooperative Highway Research Program in 1981, was implemented to develop a basis for comparison of multiple types of concrete coatings/sealers for objective performance evaluation, and the findings of this study are presented in NCHRP Report 244 (Pfeifer and Scali 1981). As part of this testing, several new test methods were developed, and testing was performed on fifty-two concrete coatings/sealers available at that time. Based on test methods designed to evaluate reduction of water absorption into concrete, reduction in chloride content in concrete, and visual performance, the three best performing products were alkyl-alkoxy silane, one epoxy composition, and methyl methacrylate. In a laboratory test designed to model chloride ingress based on conditions in the southern climate coastal regions, referred to as Southern Climate Exposure, these materials reduced chloride content by 97, 93, and 99 percent, respectively (Pfeifer and Scali 1981).

Today, Section 413 of FDOT Standard Specifications for Road and Bridge Construction outlines current requirements for installing surface sealers of concrete elements, which specifies alkyl-alkoxy silane as the penetrant sealer. Maximum limits of chloride ion penetration and water absorption are listed in the physical properties, as proven by multiple referenced tests. Additionally, surface preparation requirements are listed, which vary if the penetrant sealer is applied to new construction or existing concrete. High-molecular weight methacrylate is also specified for application to seal cracks on horizontal and slightly sloped concrete surfaces.

Admixed Inhibitors

Admixed corrosion inhibitor is a chemical substance that is incorporated into the concrete at the time of mixing to delay the onset of corrosion. There are also surface-applied migrating corrosion inhibitors that can be incorporated into repair systems to reduce the corrosion rate in existing structures. There are active

inhibitors that inhibit corrosion through a chemical reaction between steel and inhibitors that result in the formation of a protective film, by adsorption on the steel surface resulting in a protective layer, or through depletion of oxygen. Passive corrosion inhibitors work by reducing the rate of chloride ion ingress. There are multiple commercially available corrosion-inhibiting admixture products that feature active or passive systems or a combination of the two.

A range of organic and inorganic materials have been investigated as corrosion inhibitors, but some have shown adverse side effects on the mechanical properties of concrete. Calcium nitrate is widely used as a 30 percent solution and added at dosages of between 2 to 6 gallons per cubic yard, depending on the expected chloride levels in the vicinity of the reinforcing steel through the structure's design life. The effectiveness of calcium nitrate inhibitors in reducing the risk of corrosion has been demonstrated by extensive laboratory and field studies, where the onset of corrosion was considerably delayed, and after corrosion initiation, the corrosion rates were reduced. These studies included field assessment of existing structures that have been exposed for up to 20 years (Bamforth 2004). Previous studies have indicated the little impact of calcium nitrate-based inhibitors, used at recommended levels, on concrete properties except for accelerated setting time and early-age strength development at the dosages needed for corrosion mitigation. Some commercially available calcium nitrate admixtures are formulated with retarders to counter the accelerating effect. Generally, it is recommended that corrosion inhibitors not be used alone but in combination with high-quality concrete with enough concrete cover over the reinforcing steel to reduce the risk for corrosion in chloride contaminated concrete.

Cathodic Protection

The electrochemical reaction resulting in corrosion of reinforcing steel within concrete is contingent on the depassivation of the steel, which occurs when a critical level of chloride ions penetrates through the concrete cover to the surface of the steel rebar. After depassivation, localized corrosion cells are formed on the surface of the steel at a microscopic level between localized anodic and cathodic sites. The concept of cathodic protection (CP) involves providing an external current designed to reduce the potential difference between these anodic and cathodic sites to zero to eliminate the flow of corrosion current. By impressing a current on the reinforcing steel from an external electrode, the cathodic sites can be polarized in an electronegative direction. When the applied currents shift the potential of each cathodic site to the open circuit potential of the most anodic locations, the corrosion cells are eliminated, and the reinforcing steel becomes the cathode for the external electrode.

Florida has employed CP systems for corrosion mitigation of numerous bridges. CP for reinforced concrete comes in many varieties and has been used for multiple purposes. The two main varieties of CP systems include impressed current CP (ICCP) systems, where the current is supplied from an external power source, and galvanic systems, where active metals are used to provide the external current using galvanic action. Impressed current systems have used various anode materials often designed and incorporated with pile and/or pile cap jackets. The most commonly used galvanic CP systems are integral jackets installed on pile or shaft elements, which may include submergedbulk anodes, embedded discrete anodes, and/or anode meshes. Concrete-embedded and/or surface-applied galvanic anodes such as arc-spray anodes can also be designed in conjunction with integral repair jackets. Many FDOT bridges from the Florida Keys to Jacksonville have a useful application of CP systems.

Based on the information provided to date, details of commonly installed systems are described in the following sections. In addition to special technical provisions developed for specific projects, the FDOT standard specification Section 457 - Integral Pile and Column Jackets govern jacket systems. It should be noted that a variety of other cathodic protection systems have been installed on bridges across the United States and Canada, as outlined in a 2001 publication by FHWA describing a variety of CP systems and their long-term performance on highway structures. The systems described include conductive coating-based ICCP systems, conductive polymer-based ICCP systems, and coke breeze-based ICCP systems; however, CP systems that are not believed to be installed in Florida are omitted from the following subsections.

Impressed Current CP Systems

ICCP systems are generally installed on larger reinforced concrete substructure elements in the splash and/or tidal zones. Although galvanic CP systems, described in the following section, are more commonly used on large elements such as pile footings, ICCP systems are also being used across the State to provide CP for piles. For elements with a large surface area of reinforcing steel requiring cathodic protection, developing the necessary current density to polarize the reinforcing steel may not be feasible using a galvanic system. As such, an ICCP system is generally selected as current levels can be adjusted as necessary to polarize the reinforcing steel. The vast majority of ICCP systems use transformer-rectifier units (rectifiers), which convert externally provided alternating current (AC) to direct current (DC) for the CP system as power sources. Rectifiers can be installed with remote-monitoring units (RMUs) to monitor the performance of the system remotely, and in some cases, rectifiers can be controlled to adjust voltage and/or current output. Power sources that may be installed without external power include photovoltaic solar panels and batteries. However, these systems are less common due to the limited life spans and required maintenance.

A review of FDOT rehabilitation drawings shows these systems generally being installed as a form of a jacket. Negative and positive leads from the power supplies connect to the existing reinforcing steel and the system electrode(s), respectively, to drive current from the electrode to the reinforcing steel and shift the potential of the reinforcing steel in an electronegative direction. The system electrode(s) are encapsulated in a low-resistivity material such as portland cement concrete or gunite that serves as the electrolyte permitting current flow. To extend the service life of the electrodes noble metals are used, most commonly titanium mesh. For proper performance of these ICCP systems, electrical isolation of the reinforcing steel and the system electrode is critical, as a system short can restrict cathodic protection currents to the reinforcing steel.

Galvanic CP Systems

The most common galvanic CP system installed across the State is a galvanic CP jacket, typically installed on reinforced or prestressed concrete pile elements in the splash and tidal exposure zones. Several variations of CP jackets currently exist across the State; however, jackets generally consist of one or two stay-in-place form(s), installed around the piles and connect at one or more vertical seam(s) to encapsulate the pile. Jacket forms are commonly fiberglass, fiber-reinforced polymer (FRP), or PVC; however, other materials have been used. Each jacket contains a sacrificial anode for the CP system within the annular space of the jacket, which is most commonly a diamond pattern zinc mesh; however, strip zinc has been installed in some systems. After installing the external jacket and sacrificial anode, the annular space was filled with the CP system electrolyte. Low resistant, flowable materials with some level of

inherent strength after curing are typically used as the electrolyte; options include portland cement grout fillers for non-structural jackets and concrete fillers for structural jackets. After curingthe electrolyte, epoxy is installed on top of the grout and jacket as a seal from external moisture and contaminants. Typically, wiring from the negative connections to the reinforcing and/or prestressing steel and the wiring from the positive connections to the anode are wired through a protective conduit into a junction box, where electrical connections are made. Providing the electrical connection of the corrosion cell within the junction box allows the circuit to be disconnected during routine inspections of system performance. Additionally, the owner can install an RMU to remotely monitor performance, albeit this is uncommon for pile jackets. In addition to the CP jackets mitigating corrosion, the stay-in-place jacket is a barrier against additional chloride penetration.

Two primary variations of galvanic CP jackets exist today. The first variation of galvanic CP jackets includes the installation of submerged bulk anodes, which are installed beneath the water line in conjunction with the previously described jackets to provide a supplemental source of current to the submerged portion of the pile. Like the embedded sacrificial anode, the most commonly used material for this anode is zinc. The second variation is a structural galvanic CP jacket, specified to be installed on piles for which capacity may have been reduced due to section loss of prestressing or reinforcing steel. For these jackets, supplementary reinforcing steel is installed within the annular space between the jacket form and the existing pile to provide supplemental strength. In these jackets, the CP anodes must be designed to recognize that the additional reinforcing steel will draw additional current.

In addition to the previously mentioned CP jacket variations, detailing for these systems can vary based on design intent, installation procedures, geometric properties of a bridge, and several other factors. This detailing may vary across different bridges or on different piles within a given bridge. The encapsulated mass of zinc within the jacket can be adjusted depending on the surface area of reinforcing and/or prestressing steel to be protected. The installed height and elevation of CP jackets will determine the length of pile protection and may be designed based on the geometry of the piles and the extent of observed distress. Additional details that may vary include the quantity and type of established connections, protection mechanisms for these connections, and wiring types.

Metalizing

Thermal spray metalizing (metalizing) is the process of depositing metals or alloys in a liquid state onto a substrate. The process of metalizing involves running alloy wires through metalizing spray equipment, the most common of which are electric arc-type systems. The equipment drives the wire through the nozzle and is melted by the arc into particles blown onto the surface using the compressed air, typically applied to thicknesses ranging from 15 to 20 mils. Historically, the most common alloy used for metalizing was pure zinc in accordance with ASTM B6 and B833; however, zinc-aluminum alloy mixtures are also used across the State.

Metalizing provides three primary benefits related to corrosion protection of existing reinforced concrete elements. First, multiple external connections are installed to electrically connect the coating anode to the reinforcing steel cathode, creating conditions for galvanic cathodic protection to be provided to the existing reinforcing steel. These connections are generally installed by shorting the metalizing anode directly to the reinforcing steel by drilling and tapping galvanized or stainless steel rods into a steel bar connected to steel plates and the metalizing anodes on the surface of the concrete. This means no

external wiring that may be damaged or deteriorate over time is required. (Note: Occasionally, electric connections are wired through a junction box to allow monitoring of the systems.) Second, metalizing provides a generally cost-effective method to cover large areas of structure without requiring excavating cavities within the concrete or build-out of the structure. Finally, metalizing provides some level of barrier protection against the ingress of oxygen, water, and soluble salts to help slow the rate of ongoing corrosion. Topcoats such as water-based inorganic zinc silicate primers can be applied over the metalizing anode to deter self-corrosion. As the metalizing anode is consumed over time due toproviding cathodic protection to the embedded reinforcing steel, the effectiveness of the barrier coating is also reduced and/or eliminated.

Across Florida, metalizing is commonly used as part of the rehabilitation of concrete structures and oftentimes is used in conjunction with ICCP systems and/or galvanic CP systems; two examples of which are metalizing the strut beams spanning between pile footings with ICCP systems or the tops of prestressed concrete piles above the top of CP jackets. Metalizing is commonly applied to elements within the splash and lower atmospheric exposure zones and is generally not installed near the tidal zone due to water level and wave action.

Other Electrochemical Mitigation Techniques

Corrosion mitigation techniques include Electrochemical Chloride Extraction (ECE) and concrete realkalization. These non-destructive techniques are implemented temporarily to stop or prevent future corrosion in chloride contaminated or carbonated concrete, respectively, and extend the service life of the existing structure.

Electrochemical Chloride Extraction (ECE)

ECE is the process of removing chloride ions from existing, contaminated concrete while increasing the alkalinity near the reinforcing steel returning it into the passive state. Chlorides are removed from a reinforced concrete element via ionic migration. Ionic migration is the movement of ions, such as chloride and hydroxyl ions, due to an applied electric field. The electric field is created by passing a strong electrical current between an externally applied temporary anode (typically a metallic mesh) and the internal embedded reinforcing steel. This concept is illustrated in Figure 2. To maintain a neutral charge, free chloride ions in the concrete migrate away from the reinforcing steel and toward the temporary anode on the surface. A porous covering containing an alkaline electrolyte solution, also applied to the concrete surface, collects the chlorides that migrate out of the concrete, while the alkaline solution penetrates the concrete surface to help repassivate the reinforcing steel. Repassivation also occurs due to the generation of new hydroxyl ions at the reinforcing bar due to the applied voltage. When the treatment is completed, after approximately 4 to 8 weeks, the temporary mesh anode and the porous electrolyte are removed, taking the chlorides extracted from the concrete.

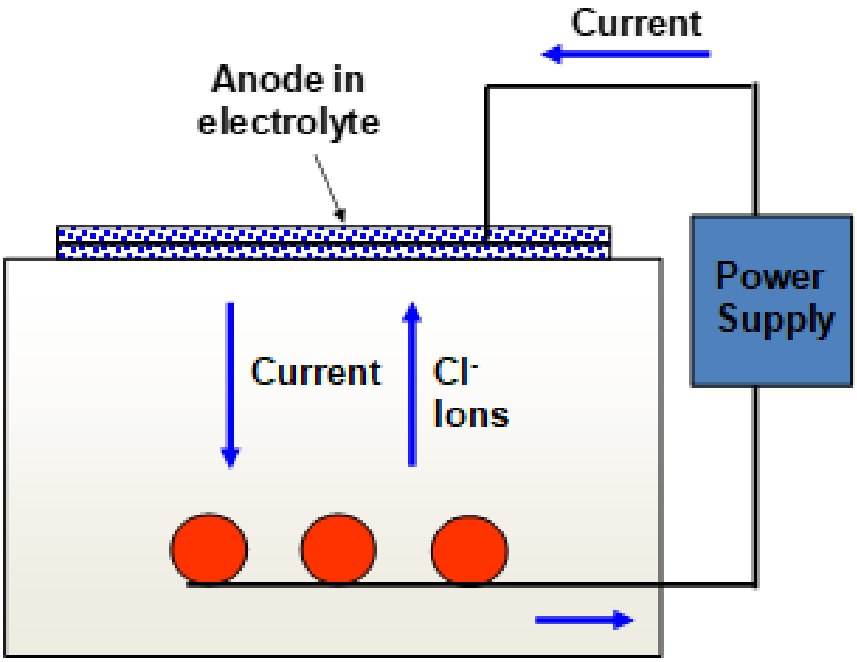

Figure 2. Schematic of electrochemical chloride extraction.

The ECE method was first developed in the 1970s to remove chloride ions from the concrete through an applied electric field (Lankard, Slater, Hedden, & Niesz, 1975; Morrison, Virmani, Stratton, & Gilliland, 1976). Early versions of the ECE process applied high current densities (over 20 A/m^2) to the concrete in an attempt to drive the chlorides out within a 24-hour period; however, this had the unintended consequences of disrupting the bond between the concrete and the reinforcing steel and increasing the permeability of the concrete (Clemena & Jackson, 2000). After additional study through multiple Strategic Highway Research Program (SHRP) projects (Bennett & Schue, 1993), the current densities applied to the concrete during treatment were reduced to below 4 A/m^2. The treatment time was extended to weeks so that sufficient chloride ions could be removed from the concrete without detrimental impact on the concrete or the concrete-to-steel bond (Broomfield, 2007).

Since the SHRP and demonstration projects of the early 1990s, ECE treatments have been applied to more than 30 reinforced concrete structures in the United States and Canada, including bridge piles at the B.B. McCormick Bridge, SR 212 in Jacksonville, Florida, with 500 total square feet of concrete surface area treated in 1992.

Based on chloride contents measured in structures before and after receiving ECE treatment, it has been reported that ECE treatment can remove up to 90 percent of chlorides from contaminated concrete, with most ECE treatments removing between 60 to 80 percent of chlorides in the outer 1 inch of the concrete surface. The most effective chloride reduction is reported to occur near the concrete surface and immediately adjacent to the reinforcing steel (Broomfield, 2007). Overall, the effectiveness of ECE treatment is a function of the amount of reinforcing steel in the element, the rebar spacing, the initial chloride content of the concrete, the voltage applied and treatment duration, and the presence of carbonation on the surface of the concrete (Sharp, Clemena, Virmani, Stone, & Kelly, 2002; Broomfield, 2007).

Treatments using ECE have proven to be effective at removing chlorides from reinforced concrete structures, but the effectiveness in reducing future corrosion is not well understood, and there are some additional potential consequences of ECE treatment that should be considered. If treatment is not well controlled, there may be a risk of potential loss of reinforcing bond and concrete damage due to excessively high current applications. Another concern is the movement of alkali metal ions, such as potassium and sodium. Alkali metal ions have an opposite charge from the chloride ions removed by the treatment and are more likely to migrate in the opposite direction of the chloride ions under the applied electric field toward the reinforcing steel. Therefore, caution should be used on concrete structures containing aggregates susceptible to an alkali-silica reaction as ECE treatment may accumulate locally high amounts of alkali ions that may stimulate alkali-silica reaction with potentially reactive aggregates in the concrete. The treatment is not likely to remove chlorides from beneath the outer mat of reinforcement, and removal effectiveness may diminish between individual reinforcing bars.

Realkalization of Reinforced Concrete

The electrochemical realkalization (ER) is the process of restoring the alkalinity of the pore solution for carbonated concrete to stop or prevent the corrosion of the reinforcing steel. A current of about 1 to 2 A/m^2 is passed to the reinforcing steel by means of an external anode embedded in an alkaline electrolyte that is temporarily attached to the concrete surface, as illustrated in Figure 3 (Broomfield 2004). Steel and Titanium-activated meshes are usually used as anodes. Anodes are immersed in electrolytes that conduct electricity and provide alkalis to be drawn into the carbonated concrete. A 1 M sodium carbonate solution (Na_2CO_3) has been used and referred to as the preferred electrolyte for realkalization treatments in several studies (Broomfield 2004, C. Andrade et al. 1999). However, Sodium ions may accelerate alkali-silica reaction (ASR) in concrete with reactive aggregates. Potassium carbonate (K_2CO_3) solution is a commonly used electrolyte, especially for ASR susceptible concrete. The time and applied electric field of ER depend on several factors, including cement type and mineral admixture, and the concrete cover thickness (Guo et al. 2020).

Several studies have proved the effectiveness of the concrete realkalization technique in restoring the alkalinity of carbonated concrete without removing sound concrete (J. Mietz 1998, COST 509 1996). However, whether that pH increase is enough to repassivate the steel reinforcement is still in question. Long term effectiveness of the treatment is also not well established in the literature.

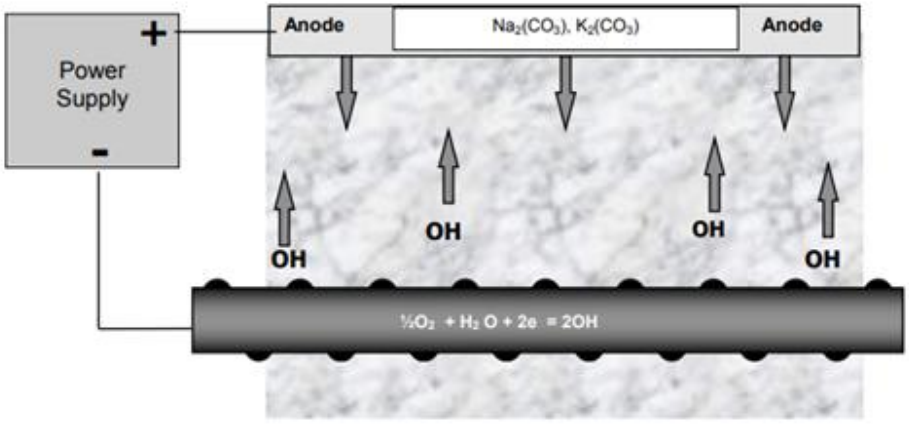

Figure 3. Schematic of electrochemical realkalization (reprinted from Broomfield 1997)

Corrosion Control in Florida Bridges

FDOT has widely adopted the strategy of extending the time to corrosion initiation by increasing concrete cover and using high performance concretes. SCMs have been shown to decrease the concrete chloride ion diffusivity. Notable bridges with high performance concrete include the piles and columns of the Sunshine Skyway Bridge, built in 1988. Some piles and approach columns in Sunshine Skyway exhibited deep, narrow cracks to reinforcement depths. At cracks, preferential chloride transport occurred, but steel corrosion was limited due to the high overall resistance of the concrete. Ternary blend concretes (i.e., mixes with cement and two additional SCMs) have shown good behavior as well. Piles manufactured with other construction methods, such as spun-cast cylinder piles, have been shown to produce concretes with low permeability. Notable Florida bridges with spun-cast piles include the St. George Island Bridge, built in 2003, and the Pensacola Bay Bridge, built in 1960. Current Florida specifications allow reduced concrete cover depths if low permeability can be shown.

Although no longer specified by the State, due to severe corrosion developing in as little as 5 years in some bridges built in the 1980s in the Florida Keys, fusion-bonded epoxy-coated rebar (ECR) has been in continued use (particularly for bridge decks) in northern States. Various researchers have identified coating defects as the initiation sites for corrosion-related damage. Some have claimed that this and associated coating disbondment largely compromises the protection provided by the coating. However, a few bridges exist in the State bridge inventory, including twin bridges in Melbourne built in the early 1980s where both ECR and conventional rebar were used. There, corrosion damage of reinforced concrete had begun to manifest when plain rebar was used but not with ECR. Further development of epoxy-coated rebar includes dual-coated rebar (DCR), where epoxy was applied over arc-sprayed zinc.

Florida has employed CP systems for corrosion mitigation of many bridges. CP for reinforced concrete comes in many varieties and purposes. The two main varieties of CP systems include impressed current systems, where current is supplied from an external power source, and galvanic systems, where active metals are used to provide beneficial galvanic polarization. Impressed current systems have used various anode materials often designed to be incorporated with pile jackets. Galvanic CP systems include bulk anodes, embedded discrete anodes, meshes, and arc-sprayed anodes. The galvanic CP systems can mitigate incipient anodes that develop in concrete repairs or are placed as an array in concrete before concrete spalling. Concrete-embedded and surface-anodes can also be designed for use with repair jackets. Many FDOT bridges from the Florida Keys to Jacksonville have an application of CP systems. Recent research with FDOT indicated that marine fouling organisms could affect polarization and current distribution on submerged steel piles (Permah et al., 2017). Fouling organisms also attach to concrete structures, and similar deficiencies in CP may occur. Durability issues related to the bond of wraps, jackets, coatings, anodes, and chemical changes to anode backfill and encapsulation materials, are not well understood or documented and may ultimately govern the life of the CP system.

3. FIELD INVESTIGATIONS OF CORROSION PREVENTION AND CONTROL PROGRAMS

The field investigation portion of this research includes the on-site and laboratory testing of the bridge structures to evaluate and verify the performance of the implemented corrosion prevention techniques and/or improved construction practices. The scope of work for this project task includes the study of twelve different bridge corrosion protection systems and/or construction materials/practices. When selecting bridges, FDOT and consultants considered the following three primary factors as related to corrosion prevention and control programs:

- Environment (chloride content of water, air, water temperature, etc.)
- Construction Materials/Practices (ECR, concrete mix designs, coatings, etc.)
- Corrosion Control Systems (Galvanic CP, Impressed Current CP, Metalizing, etc.)

The research team performed site visits at eight individual bridges, selected based on the criteria described above. Additionally, bridges were grouped based on geography to minimize the environment variation as a significant performance factor of the corrosion prevention means. The eight bridges evaluated were performed in four separate field investigations. Table 2 shows the location and bridges for each field investigation, while Table 3 shows which corrosion control systems were evaluated at each bridge. Detailed information is provided for each field investigation within the following subsections.

Table 2. Bridge Selection by Field Investigation

Field Investigation	Location	Bridge Name	FDOT Bridge Identification Number
1	Tampa, Florida	Gandy	100300
		Howard Frankland	150107
2	Melbourne, Florida	WB Melbourne (US-192)	700174
		EB Melbourne (US-192)	700181
3	Fort Lauderdale, Florida	EB Sunrise Boulevard	860467
		WB Sunrise Boulevard	860466
		St. Andrews Ave.	860319
4	St. Petersburg, Florida	Sunshine Skyway	150189 (Unit Key 0)

Table 3. Corrosion Control Systems Matrix

Bridge	Construction Practice	Galvanic CP	Impressed Current CP	Metalizing
Gandy		X	X	X[4]
Howard Frankland		X	X	X[4]
WB Melbourne (US-192)			X	
EB Melbourne (US-192)	X[1]			
EB Sunrise Boulevard	X[2]			
WB Sunrise Boulevard	X[1]			
St. Andrews Ave.	X[3]			
Sunshine Skyway			X	

[1] ECR, [2] ECR and inclusion of fly ash in mix design, [3] ECR and protective coating

[4] Only a cursory review of metalizing was performed, the primary purpose of this mobilization was to investigate the cathodic protection systems.

Descriptions of Electrical Measurements at Bridges with CP

Multiple electrical measurements and test methods were used to evaluate the corrosion prevention and control programs. Specifically, electrical measurements were used to evaluate the performance of CP systems against industry standards, while select test methods were used to evaluate materials and/or other properties regarding corrosion activity.

The following section provides specifics of the electrical measurements evaluated as part of the investigations regarding CP systems. It also contains guidance based on industry standards regarding the adequacy of the installed CP systems.

Current Output - Using a shunt with a known resistance, the measured voltage drop of the circuit can be converted to current using Ohm's law. All other things being equal, current flow is expected to correspond with increased polarization of the cathode, meaning that larger voltage drop measurements (and corresponding higher current flow) indicate more CP being offered by the anodes. Current alone is not an indicator of sufficient CP, as the current output will naturally decrease as the cathode is polarized. Additional factors such as tide, concrete cover, and temperature also play a role in output current.

Potential Measurements – Structure potential measurements can indicate the effectiveness of the CP systems and are obtained by making a positive electrical connection to the structure (e.g., reinforcing steel) and creating a circuit by placing a reference electrode on the surface of the concrete or within the water below and measuring the voltage drop across the circuit. For all reviewed pile jacket data, measurements were obtained in units of mV versus a Copper-Copper Sulfate (CSE) reference electrode both in the monitoring ports and within the water adjacent to the pile. A review of provided CP monitoring data showed that four individual potential measurements were obtained at these two locations for each pile at different periods related to the initial installation and disconnection of the CP system for monitoring purposes. Similar measurements are obtained by FDOT as routine measurements for the ICCP systems using Silver Silver-Chloride (Ag/Ag-Cl) reference electrodes. Specific measurements evaluated in this research are described below:

Static or Native or Base Potential –Potential of the structure prior to the electrical connection of the CP system, meaning the CP system does not affect this measurement. This measurement was obtained by testing during the initial installation of the CP pile jackets, known as commissioning.

On Potential – Potential measurement obtained at any time while the CP system is operating.

Instant-Off Potential - To account for the voltage offset resulting from the flow of current across a resistance, known as IR drop, "instant off" potentials are measured immediately after disconnecting the CP system to obtain the effective polarized potential. These measurements were obtained after initial commissioning and during typical monitoring efforts.

Decay Potential – Decay potential measurements are taken after disconnection of the CP system to allow the structure to shift towards its native potential. A review of data for this project indicated that the minimum time allotment for this shift, known as decay time, was 24 hours. However, up to 70 days were allowed on some piles depending on access. Decay potentials for reinforced concrete elements in marine environments will continue to shift the longer the CP system is disconnected until the final depolarized potential is reached; typically, a minimum of 24 hours is allotted for decay before recording a measurement.

Polarization Development / Depolarization - Polarization measurements, i.e. the change in measured potential of the structure, can be utilized to determine the CP's performance in comparison with industry standards.

Polarization development is calculated during the initial commissioning of the CP pile jackets and indicates the change in the structure's potential between the static potential and the instant-off potential. A properly installed CP system will shift the potential toward the negative when comparing the instant-off potential to the static potential.

Depolarization, on the other hand, is calculated after creating an open circuit (disconnecting the anodes from the structure within the junction boxes) and comparing the instant-off potential to the decay potential. Polarization decay is determined by subtracting the subsequent decay readings from the instant-off readings resulting in a positive shift in potential. The magnitude of these shifts can be compared to determine the adequacy of the installed CP, provided sufficient time has been allowed for polarization to develop or decay. Some industry documents refer to depolarization as polarization decay, but, depolarization is used throughout this document to match terminology from provided monitoring documentation.

Guidance from Industry Standards - NACE SP0216-2016 and NACE SP0408-2019 give guidance for CP systems on reinforced concrete structures. Based on the guidelines in the referenced documents, the following criteria were used in this assessment:

1. If the decay potential of the steel in wet, saturated concrete is more negative than -720 mV vs. CSE, then the reinforcing steel is considered not to be corroding.
2. If a minimum of 100 mV shift is achieved at the most anodic location, then the reinforcing steel is considered protected. During initial commissioning, this shift refers to polarization and is generally utilized to determine adequate protection. However, during routine monitoring, this shift refers to depolarization.

3. If the decay potential is less negative than -200 mV CSE, then the reinforcing steel is considered passive and no minimum polarization is required.

Some level of protection is provided for polarization/depolarization less than 100 mV, particularly for structures where the decay potential is less negative than -350 mV CSE. NACE TR21463-2020 provides additional commentary related to partial protection of reinforcing steel within concrete elements when one of the previous criteria is not met. These criteria are summarized visually in Figure 4.

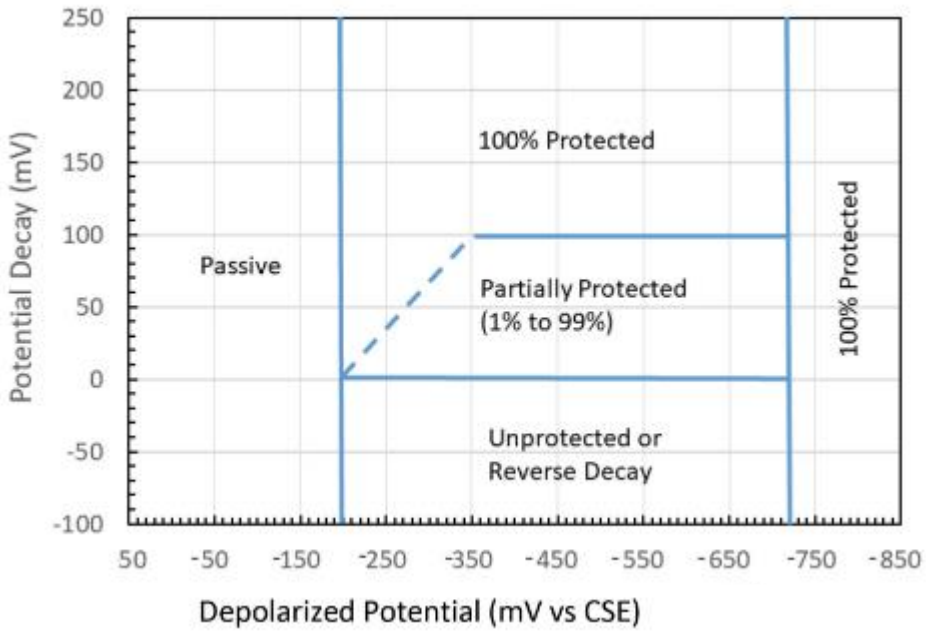

Figure 4. Corrosion protection status chart (adapted from NACE TR21463-2020).

Descriptions of Test Methods at Bridges without CP

Physical tests methods were also utilized to evaluate materials and/or corrosion conditions of select elements. Such test methods are described below and were utilized on bridges evaluated in these field investigations that did not include CP.

Petrographic Examination - Petrographic examination of concrete is performed in general accordance with ASTM C856, *Standard Guide for Petrographic Examination of Hardened Concrete*, to evaluate the properties of concrete, including assisting in determining the cause(s) of any concrete distress and determining the overall quality of the concrete.

Half-Cell Potential Testing - Half-cell potential (HCP) testing is used to determine the likelihood of ongoing corrosion activity of the reinforcing steel and can provide information as to whether corrosion could be a cause of the observed distress. HCP testing is performed inaccordance with ASTM C876, *Standard Test Method for Corrosion Potentials of Uncoated Reinforcing Steel in Concrete,* which offers guidance on interpreting the measured voltages for concrete structures with uncoated steel reinforcement. While these values are not directly applicable to epoxy-coated reinforcement, similar behavior (i.e., variations in half-cell potential) may be observed if corrosion of the reinforcement is occurring. Overall magnitudes of measured potentials may provide unreliable correlations with ongoing

corrosion; however, localized regions of more negative potentials may indicate locations of coating defects and/or corrosion activity.

HCP readings are influenced by a number of parameters, including, but not limited to, temperature and concrete resistivity. Concrete resistivity is affected by moisture, chloride content, and surface carbonation. Saturated concrete results in highly negative potentials because the oxygen availability is limited and thus affects the electro-chemical behavior of the bar, while carbonated concrete has a higher resistivity than uncarbonated concrete, which can lead to a positive shift in measured potentials. Typical ranges for HCPs for various conditions are provided in Table 4, while the guidelines for interpreting HCP data given in ASTM C876 are provided in Table 5.

Note that the values provided in all cases are for uncoated, black-bar reinforcing steel. In addition to the data interpretation references related to the magnitude of the readings listed below, gradients in HCP values greater than 100 mV over a 3-foot spacing typically correlate with corrosion activity of the reinforcing steel.

Table 4. Typical Half-Cell Potential Data Ranges

Concrete Condition	**Typical Range of HCPs, mV vs. CSE, with [risk of corrosion activity]**		
	Chloride Contaminated	Carbonated	Chloride Free
Humid, non-saturated	-600 to -400 [high]	-400 to +100 [moderate]	-200 to +100 [low]
Saturated, oxygen-starved	-1000 to -900 [low]	No data	-1000 to -900 [low]
Dry	No data	0 to +200 [low]	0 to +200 [low]

Source: Rilem TC 154-EMC

Table 5. Half-Cell Potential Corrosion Risk

HCP, mV vs. CSE	**Probability of Corrosion**
> -200	Low, <10%
-200 to -350	Moderate, 10 - 90%
< -350	High, >90%

Source: ASTM C876-15

Surface Resistivity - An important physical property of the concrete as it relates to corrosion resistance is the concrete resistivity. As the concrete serves as the electrolyte in a typical corrosion cell for reinforcing steel embedded in concrete, increased resistance reduces the ability of the corrosion current to flow. In these investigations, surface resistivity measurements were obtained, which generally indicates the electrical distance from the surface of the concrete to a depth of approximately 2 inches. Surface resistivity measurements were obtained using a 4-point Wenner probe for these investigations. As resistivity increases, the probability and rate of corrosion decrease. The categories described in Table 6 were used to correlate resistivity measurements to the risk of corrosion.

Table 6. Interpretation of Resistivity Measurements

Resistivity (kΩ-cm)	Corrosion Risk and Rate
> 100	Negligible. Cannot distinguish between active and passive steel.
50 to 100	Low risk. Corrosion rates are likely to be low.
10 to 50	Moderate risk. Moderate to high corrosion rates are possible in active areas.
< 10	High risk. Resistivity is not the controlling factor in corrosion rates.

Sources: Proceq Resipod Family Operating Manual.

Field Investigation 1 – Gandy and Howard Frankland Bridges

Multiple types of CP systems have been installed on the Gandy (Bridge No. 100300) and Howard Frankland (Bridge No. 150107) Bridges over multiple decades, including CP jackets and impressed current CP systems installed on piles and pier footings, respectively. As a result of multiple generations of CP systems, this investigation allowed for a direct comparison of long-term performance of the CP systems, as well as the primary factor(s) governing the end of life for these systems.

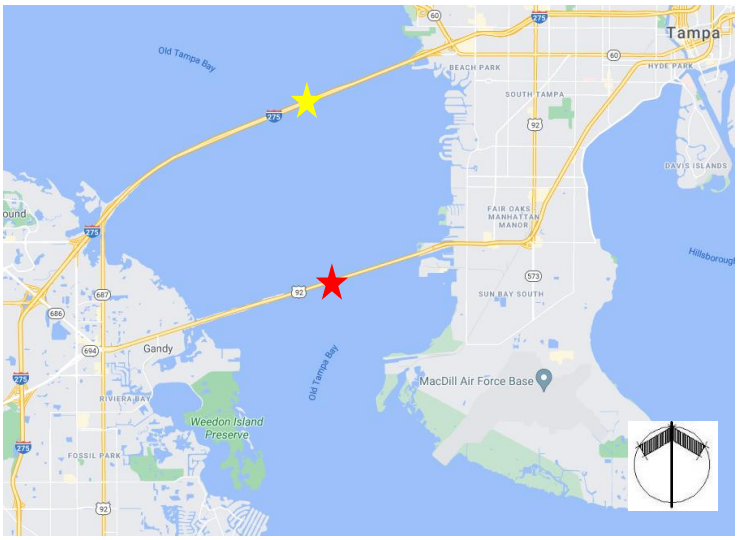

Figure 5. Location of the Gandy and Howard Frankland Bridges across Tampa Bay, identified by the red and yellow star, respectively (image from Google Maps©).

Assessment Objectives and Methodology

The installation of multiple generations of CP systems provides a unique opportunity to evaluate the systems as a function of age. As such, Field Investigation 1 is split into independent assessments of the galvanic CP pile jackets and the impressed current CP systems on the pile caps. The primary objectives of this field investigation are outlined below, followed by the tasks performed to evaluate the given objectives.

CP Pile Jackets

- Assess the long-term performance of galvanic CP jacket systems for pile repair/rehabilitation in marine exposures.
  - Consider functionality of each jacket at reducing distress based on visual condition of protected pile
  - Compare electrochemical performance of jackets of various ages based on current output and depolarization from provided monitoring data
  - Consider extent of zinc consumption
  - Consider variability in system resistance between generations of jackets and over time
- Determine the primary factor(s) governing the end of life of galvanic CP jacket systems for pile repair/rehabilitation.
  - Compare the following for functioning and non-functioning jackets:
    - Zinc consumption and quality
    - Circuit resistance (corrosion product build-up, moisture content of grout, etc.)
    - Fiber glass condition - impact on grout, local zinc consumption
    - Bond between grout and concrete

In an attempt to assess the previous objectives, the following field investigation tasks were performed to assess the CP pile jackets of the Gandy and Howard Frankland bridges.

- Review available structure information, including available data for trends from the most recent FDOT Bridge Inspection Report and routine monitoring data.

  Trends to identify include the following:
  - Elemental ratings for jacketed piles
  - Elemental ratings of CP jackets
  - Elemental ratings for non-jacketed piles
  - Performance data regarding electrical monitoring data of CP jackets. At least three generations and both structural and non-structural systems were installed.
- Perform a cursory visual inspection of piles identified for in-depth study, which will be used to confirm the findings of the January 2019 FDOT Bridge Inspection Report. Piles with jackets, as well as the jackets, will be rated in accordance with the NHI elemental rating system.
- Perform an in-depth study at select pile jackets by obtaining material samples in order to evaluate the performance of the jackets by evaluating the material constituents. Select pile jackets were selected for sampling based on electrical monitoring performance data in an attempt to compare material properties with electrical performance.

  The following material testing was performed on extracted samples:
  - Surface resistivity of grout
  - Bulk resistivity testing of samples in as-received and saturated conditions
  - Microscopic examination of zinc mesh samples using stereoscopic microscope to make observations related to oxidation or consumption
  - Measure thickness and/or weigh samples to determine consumption

Impressed Current CP Systems

- Assess the long-term performance of ICCP systems for footing repair/rehabilitation in marine exposures.
  - Consider functionality of each system in reducing distress based on visual condition of protected footings
  - Compare electrochemical performance of ICCP systems of various ages based on remote monitoring unit (RMU) data
  - Per specifications in the drawings, RMUs monitor voltage, current, and reference electrode potentials
  - Consider extent of titanium anode mesh consumption
  - Examine condition of rectifier, rectifier enclosure, and wiring system
- Determine the primary factor(s) governing the end of life of ICCP systems for footing repair/rehabilitation.
  - Compare performance of ICCP systems of various ages based on current output and depolarization

    Consider the following:
    - Titanium condition and quality
    - Circuit resistance (corrosion product build-up, moisture content of concrete jacket, distance from negative connections…)
    - Bond between concrete jacket and base concrete (dowels)

To assess the previous objectives, the following field investigation tasks were performed to assess the impressed current CP systems of the Gandy and Howard Frankland bridges.

- Evaluate available structure information, including available data for trends from the most recent FDOT Bridge Inspection Report and routine monitoring data in order to select study piers to perform in-depth studies.

  Trends to identify include the following:
  - Elemental ratings for pier footings
  - Elemental ratings of ICCP pier jackets
  - Performance data regarding electrical monitoring data of ICCP systems from RMUs
- Perform a cursory visual inspection of all piers on both bridges to assess the condition of both the piers and the ICCP systems.
- For the piers selected to perform an in-depth study, the following tasks were performed:
  - Detailed visual inspections of the selected study areas, including removal of the junction box covers for inspection of electrical wiring, connections, and accessories
  - Electrical testing
    - "On" and "Instant Off" potential measurements with installed reference electrodes within each footing
    - Using a shunt resistor, measure total current output between system negatives and positives with ICCP system on and off.
      - Metalizing is directly connected to the reinforcing steel in certain repair areas and, therefore cannot be disconnected without disabling the metalizing system.
    - AC resistance between system negatives and the titanium mesh leads, with leads removed from rectifier
    - Continuity testing between system negative wires.
    - Perform decay potential measurements with reference electrodes inside the jacket and in the water (minimum of 24 hours after disconnect)
  - Core samples were obtained to perform the following material testing:
    - Surface resistivity of grout
    - Bulk resistivity testing of samples in as-received and saturated conditions
    - Evaluation of bond between original and new concrete placements
    - Microscopic examination of titanium mesh samples using stereoscopic microscope to make observations related to oxidation or consumption
    - Measure thickness and/or weigh samples to determine consumption

Description of Structures and Environment

The Gandy and Howard Frankland (HF) Bridges both span Tampa Bay to connect Tampa with St. Petersburg, with the Gandy Bridge approximately two miles south of the Howard Frankland Bridge. Table 7 provides general descriptions and properties of each bridge.

Table 7. Bridge Descriptions

Bridge	Gandy	Howard Frankland
Structure	SR 600 (US 92)	SR 93 (I-275 NB)
Feature Crossed	Old Tampa Bay	Old Tampa Bay
County	Hillsborough / Pinellas	Hillsborough / Pinellas
Florida Bridge No.	100300	150107
Facility Carried	US Route 92	I-275
Year Constructed	1975	1959
Design Life	50 years (2025)	50 years (2009)
ADT	18,250 (2019)	82500 (2018)
NBI Substructure Rating	6 (2019)	5 (2018)
No. of Spans	296	321
Overall Length	14,778 ft. 6 in.	15,932 ft.
Overall Width	42 ft. 3 in.	62 ft. 0 in.
Roadway Width (curb-to-curb)	40 ft. 0 in.	58 ft. 5 in.
Superstructure	AASHTO Type II, III, & IV Girders	AASHTO Type II, III, & IV Girders
Substructure	(273) Pile bents (5-7 Piles per Bent) & (24) Piers with prestressed concrete piles	(288) Pile bents (8-10 Piles per Bent) & (30) Piers with prestressed concrete piles

Gandy Bridge

The Gandy Bridge was constructed in 1975 and is approximately 14,778 feet long, consisting of 296 spans. Of the 297 bents, 22 are pier footings, 273 are pile bents, 2 are abutments, and 2 are pier crash walls. Pier footing bents consist of two footings per bent, each 8 feet, 6 inches by 12 feet, 6 inches by 5 feet deep, and cast atop eight prestressed concrete piles. Columns are constructed on each footing, each of which is four feet in diameter. Columns are connected by struts measuring 2 feet, 6 inches wide, and 4 feet 6 inches deep, which are constructed directly above the top surface of the footings. The center-to-center spacing of the columns is 25 feet, and clear spacing between the pier footings is 16 feet, 6 inches. Pile bents include five to seven prestressed piles per bent, including some bents with battered piles. Prestressed piles are between 1 foot 6 inches and 2 feet square and are connected to a pile cap measuring 3 feet deep and are generally 41 feet wide.

Referenced design specifications for the Gandy Bridge included the following:

- Florida State Road Department Standard Specifications for Road and Bridge Construction (1966)
- 1969 Edition of AASHTO Standard Specifications for Highway Bridges and Approved Revisions

A review of the design documents and the aforementioned design specifications, also provided geometric and material information, which is summarized below in Table 8.

Table 8. Detailing Information for Gandy Bridge

Substructure Element	Description	Concrete Class	Min. Design Cover (in.)	Elevation (ft. vs. MLW, ref. bottom of element)
Piles	Prestressed piles - end bents: 50 ton; intermediate bents: 60 ton; pier piles: 70 ton	P	3	Cut-off 1 ft. above bent/footing bottom
Pile Bent Caps	CIP pile bents cast atop piles	A	4	Varies: +2 to +10
Pier Footings	CIP footings above 8 piles, two per pier. 9-inch thick footing seal shown as underside form for structural footing	A (Option for 9 in. seal to be A or seal concrete)	4 (no reinforcement in seal concrete)	-1.5 (including 9 in. underside seal)
Pier Struts	CIP struts span atop two footings at pier bents	A	4	+3.5
Columns	CIP columns extending from footings to bent caps at pier bents	A	4	NA

Howard Franklin Bridge

The HF Bridge is the northbound bridge that was constructed in 1959 and is often referred to as the Old HF Bridge. A sister bridge was constructed to carry the southbound lanes and was not assessed in this field investigation. The Old HF bridge is approximately 15,932 feet long, consisting of 318 spans. Of the 319 bents, 28 are pier footings, 286 are pile bents, 2 are abutments, and 2 are pier crash walls. Pier footing bents consist of three footings per bent, each 8 feet, 6 inches by 11 feet by 4 feet deep, and cast atop six 24-inch square prestressed concrete piles. Rectangular columns are constructed on each footing, each of which is 3 feet 4 inches wide with tapered depth based on elevation. Columns are connected by struts measuring 2 feet, 6 inches wide, and 5 feet deep, which are constructed directly above the top surface of the footings. Design documents allow for struts to be precast; however, struts appeared to be cast-in-place. Center-to-center spacing of the columns is 22 feet, 6 inches and the clear spacing between the columns is 19 feet, 2 inches. Typical pile bents consist of eight 24-inch square precast piles per bent, with the exterior piles on each bent being battered 2 inches per foot. Pile caps are 3 feet deep, 3 feet 4 inches wide, and 61 feet wide.

Referenced design specifications for the Old HF Bridge included the following:

- 1953 Edition of AASHO Standard Specifications for Highway Bridges

The review of the design documents, as well as the aforementioned design specifications, provided geometric and material information, which is summarized below in Table 9.

Table 9. Detailing Information for HF Bridge

Substructure Element	Description	Concrete Class	Min. Design Cover (in.)	Elevation (ft. vs. MLW, ref. bottom of element)
Piles	Precast piles – 50 ton	P	2.25	Cut-off 1.5 ft. above bent/footing bottom
Pile Bent Caps	CIP pile bents cast atop piles	A	3 bottom and sides; 2 top	Varies
Pier Footings	CIP footings above 6 piles, three per pier	A	3	+1.0
Pier Struts	CIP struts span atop footings at pier bents; two per bent	A	3	+5.0
Columns	CIP columns extending from footings to bent caps at pier bents	A	3	NA

While detailing and geometry vary slightly between the two bridges, overall construction and material specifications as they apply to the elements evaluated in this study were similar enough to develop relative comparisons of the CP systems installed on the bridges.

As described later in this section, multiple generations of CP pile jackets and impressed current CP jackets have been installed in various construction projects over the life of both bridges. Similar to previous sections, the descriptions of each of these corrosion control systems and installation histories, are summarized in two independent subsections below.

Description of Galvanic Corrosion Control Systems

A total of 406 sacrificial CP pile jackets have been installed between the Gandy and HF bridges, summarized in Table 10. This table omits replacements, repairs, and manufacturer variations. These variables, however, were accounted for when selecting pile jackets for in-depth assessments. Additionally, electrical commissioning data for the 2012 installations were unavailable for review, limiting the ability to assess these jackets. Therefore, these jackets were also omitted from this investigation. The field investigation of galvanic corrosion control systems focused on the long-term performance of structural and non-structural CP pile jackets from the 2001, 2005, and 2009 installations.

Table 10. Summary of Jacket Installation History

Installation Year	Gandy Non-Structural Jackets	Gandy Structural Jackets	HF Non-Structural Jackets	HF Structural Jackets
2001	4	0	137	1
2005	0	0	8	117
2007	0	0	2	0
2009	41	24	17	1
2012	0	0	15	39
Total	45	24	179	158

Only the construction documents for the 2009 (Financial Project ID 420666-1-52-01) and 2012 (Financial Project ID 427455-2-52-01) installations were available for review. However, installation detailing appeared extremely similar between the two generations, and it is assumed that previous generations were also very similar. Two types of CP pile jackets are installed on these two bridges: non-structural and structural jackets. Three trial jackets were installed using systems provided by a different manufacturer. These jackets were not evaluated as part of this field investigation.

Non-Structural CP Jackets

Typical non-structural CP pile jackets consist of two C-shaped, 1/8-inch thick fiberglass stay-in-place forms installed around the piles and connect at a vertical seam on each side. Each jacket contains a diamond pattern zinc mesh anode, which serves as the sacrificial anode for the CP system within the annular space of the jacket. After installing the fiberglass jacket, the 2-inch nominal annular space was filled with a portland cement grout that serves as the CP system electrolyte. Fifty-pound submerged bulk anodes, which are oftentimes installed in conjunction with these systems to provide a supplemental source of current to the submerged portion of the pile, were installed 2 feet below mean low water using a bolted steel channel assembly strapped to each pile. The height of pile jackets varied depending on pile geometry, however, the bottom of the form was detailed to be installed approximately at the elevation of mean low water. Negative connections to the reinforcing steel and prestressing were made using No. 10 AWG copper strand, and installation notes required verification of electrical continuity around the entirety of the pile. Positive connections to the zinc mesh anode within the jacket and the submerged bulk anode are established and fed through a PVC conduit and are connected within a PVC terminal box mounted to the pile above the jacket, where they are connected through a 0.1 ohm shunt. Additionally, access points through the jacket were installed 6 inches above mean high water to allow for monitoring. An elevation view and cross-sectional view of typical non-structural CP pile jackets are provided in Figure 6 and Figure 7, respectively.

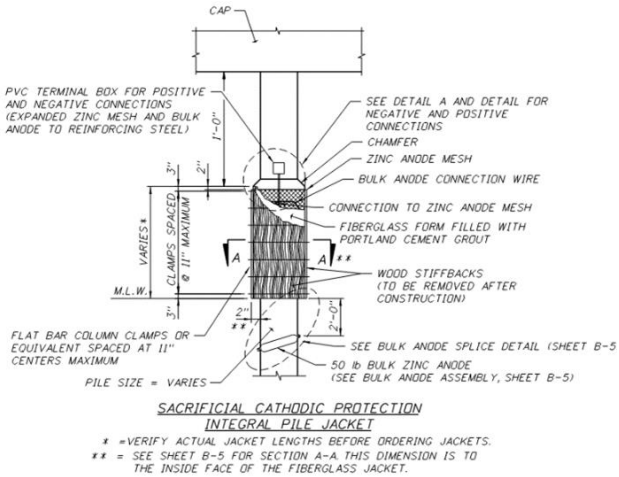

Figure 6. Typical elevation view detail of non-structural CP pile jackets.

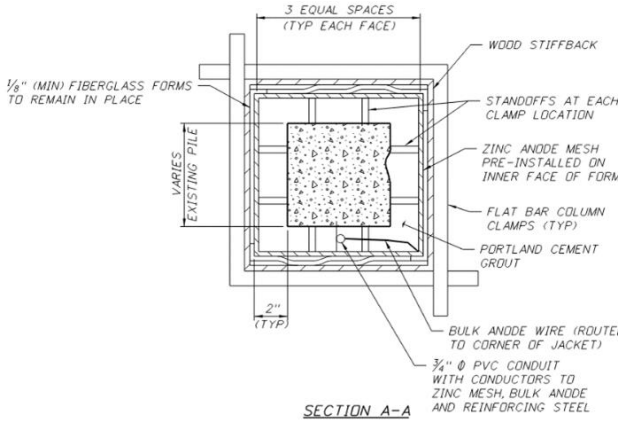

Figure 7. Typical cross section of non-structural CP pile jackets.

Structural CP Jackets

Typical structural CP pile jackets are very similar to non-structural jackets; however, installation detailing and techniques vary slightly. The primary difference is that supplemental reinforcing steel is installed around the perimeter of the existing pile for structural jackets, which is supported by steel bars doweled into the existing pile. To facilitate installation and electrical isolation of the additional steel, the annular space between the fiberglass stay-in-place forms is increased from 2 to 4 inches. As a result of this increased volume of fill material, Class IV concrete is used to fill the annular space instead of portland cement grout. Similar detailing is utilized between the two jacket types, including form and anode materials, detailing of negative and positive electrical connections, and routing of wiring through a terminal box installed above the top of the jacket. An elevation view and cross-sectional view of typical structural CP pile jackets are provided in Figure 8 and Figure 9, respectively.

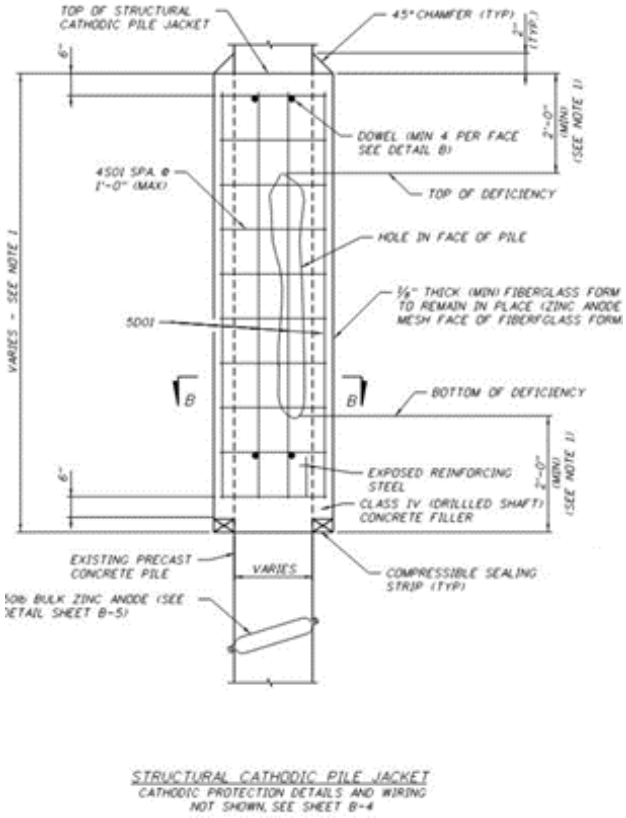

Figure 8. Typical elevation view detail of structural CP pile jackets.

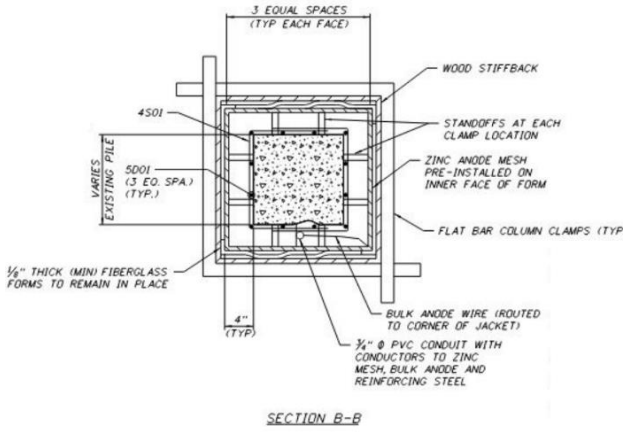

Figure 9. Typical cross section of structural CP pile jackets.

Assessment Findings of Galvanic Corrosion Control Systems

FDOT protocols specify that routine monitoring and inspection of galvanic CP pile jackets be performed approximately three years after installing and commissioning of the CP jackets. For the two bridges included in this investigation, typical monitoring data included output currents measured across the shunt, while for a subset of pile jackets, electrical connections were disconnected to allow for depolarized potentials to be measured and polarization decays to be calculated. This investigation focused on 38 CP

pile jackets with complete routine monitoring data. Prior to the issuance of this research contract, the most recent routine monitoring inspection was completed in 2013. FDOT retained a contractor to obtain more recent monitoring data for these CP pile jackets, including current outputs and depolarization measurements in late 2020, to incorporate into this investigation. A list of the 38 CP pile jackets with detailed monitoring data is summarized below in Table 11, and complete routine monitoring data is provided in APPENDIX A. The routine monitoring data included obtaining electrical data for 39 CP piles. However, Pile 316-8 was omitted from this study because it was the only pile from the subset installed in a small repair contract in 2007.

Table 11. Inventory of Piles with Detailed Routine Monitoring Data

Gandy Bridge		Howard Frankland Bridge					
46-3	82-6*	12-1*	14-4	44-5*	53-3*	65-8	73-5*
85-4	94-3	80-6	99-9	105-9*	116-4	120-1	123-8
104-1	106-7*	129-6	133-5*	138-7	138-8	177-4	182-3
137-4*	144-4	190-6	191-3*	198-1	214-3	214-6*	236-7*
		263-1*	270-2*	289-2	289-5*	304-4	308-5

*2001 Install, 2005 Install, 2009 Install, * indicates a structural jacket*

Data Processing Findings

To assess the galvanic CP pile jackets, routine monitoring data was first evaluated to identify trends based on the ages of installed jackets. Such trends were identified based on the initial installation age of jackets and sorted between non-structural and structural CP jackets for further evaluation. Processed and summarized data for 2001, 2005, and 2009 CP jacket installations are provided below in Table 12, Table 13, and Table 14, respectively. The data includes current outputs and polarization/depolarization measurements from initial commissioning and routine monitoring data from 2013 and 2020 and the changes in these values between commissioning and 2020. Additionally, average decay potentials from 2013 and 2020 are presented along with the change in potential. However, only instant-off potentials values were obtained during commissioning, which does not generally allow a direct comparison with decay potentials.

Scatter is expected in electrical field measurement data for CP systems installed in marine environments. Individual measurements can be affected by multiple factors, including but not limited to water levels at the time of the measurement, temperature, condition of wiring and connection elements, varied performance of the jacket, and allotted decay time.

Table 12. Gandy and HF Galvanic Pile Jacket CP Test Data Summary – 2001 Install

Measurement	Combined	Non-Structural	Structural
Number of Jackets	15	15	
Avg. Total Current Output at Commissioning	66	66	
Avg. Total Current Output in 2013	31	31	
Avg. Total Current Output in 2020	16	16	
Avg. Δ Current Output	-51	-51	
Avg. Polarization at Port at Commissioning	162	162	
Avg. Depolarization at Port in 2013	102	102	
Avg. Depolarization at Port in 2020	64	64	
Avg. Δ Polarization / Depolarization at Port	-98	-98	
Avg. Polarization in Water at Commissioning	199	199	NA
Avg. Depolarization in Water in 2013	74	74	
Avg. Depolarization in Water in 2020	69	69	
Avg. Δ Polarization / Depolarization in Water	-130	-130	
Avg. Decay Potential at Port in 2013	-730	-730	
Avg. Decay Potential at Port in 2020	-627	-627	
Avg. Δ Decay Potential at Port	103	103	
Avg. Decay Potential in Water in 2013	-955	-955	
Avg. Decay Potential in Water in 2020	-934	-934	
Avg. Δ Decay Potential in Water	24	24	

Units: Amperage = mA, Polarization / Depolarization = mV, Potentials = mV vs. CSE

Table 13. Gandy and HF Galvanic Pile Jacket CP Test Data Summary – 2005 Install

Measurement	Combined	Non-Structural	Structural
Number of Jackets	13	1	12
Avg. Total Current Output at Commissioning	60	94	55
Avg. Total Current Output in 2013	39	47	48
Avg. Total Current Output in 2020	21	38	19
Avg. Δ Current Output	-39	-56	-36
Avg. Polarization at Port at Commissioning	133	116	134
Avg. Depolarization at Port in 2013	98	9	106
Avg. Depolarization at Port in 2020	83	19	89
Avg. Δ Polarization / Depolarization at Port	-50	-97	-45
Avg. Polarization in Water at Commissioning	169	222	165
Avg. Depolarization in Water in 2013	109	21	116
Avg. Depolarization in Water in 2020	107	117	106
Avg. Δ Polarization / Depolarization in Water	-62	-95	-59
Avg. Decay Potential at Port in 2013	-614	-631	-612
Avg. Decay Potential at Port in 2020	-496	-586	-489
Avg. Δ Decay Potential at Port	118	45	123
Avg. Decay Potential in Water in 2013	-893	-1009	-884
Avg. Decay Potential in Water in 2020	-832	-926	-824
Avg. Δ Decay Potential in Water	61	83	60

Units: Amperage = mA, Polarization / Depolarization = mV, Potentials = mV vs. CSE

Table 14. Gandy and HF Galvanic Pile Jacket CP Test Data Summary – 2009 Install

Measurement	Combined	Non-Structural	Structural
Number of Jackets	10	7	3
Avg. Total Current Output at Commissioning	127	132	116
Avg. Total Current Output in 2013	54	37	77
Avg. Total Current Output in 2020	37	36	39
Avg. Δ Current Output	-90	-83	-77
Avg. Polarization at Port at Commissioning	108	126	65
Avg. Depolarization at Port in 2013	128	105	181
Avg. Depolarization at Port in 2020	116	109	134
Avg. Δ Polarization / Depolarization at Port	8	-17	69
Avg. Polarization in Water at Commissioning	171	181	147
Avg. Depolarization in Water in 2013	102	92	124
Avg. Depolarization in Water in 2020	92	89	106
Avg. Δ Polarization / Depolarization in Water	-79	-92	-41
Avg. Decay Potential at Port in 2013	-697	-730	-619
Avg. Decay Potential at Port in 2020	-641	-676	-560
Avg. Δ Decay Potential at Port	56	54	59
Avg. Decay Potential in Water in 2013	-943	-947	-932
Avg. Decay Potential in Water in 2020	-911	-903	-931
Avg. Δ Decay Potential in Water	32	44	1

Units: Amperage = mA, Polarization / Depolarization = mV, Potentials = mV vs. CSE

The data shows a downward trend in CP performance as a function of time based on almost all criteria for each installation generation. No significant differences in CP performance are discernable between non-structural and structural variations. To illustrate these downward trends, Table 15 highlights the percent changes in applicable CP measurements between the initial installation of the CP pile jackets and the routine monitoring data in 2020. Apart from polarization/depolarization shifts for the 2009 installation, each change in CP measurement over time indicates lesser protection than that measured at the initial installation. The following sections provide commentary on the trends evaluated for each measurement criteria.

Table 15. Percent Change in Measurement from Initial Installation to 2020

Criteria	2001	2005	2009
Current Output	-76	-67	-71
Polarization / Depolarization at Port	-60	-38	7
Polarization / Depolarization in Water	-65	-37	-46

Current– A review of total current output data for the three generations of jackets indicated a clear downward trend between commissioning and 2020. Although the average total current measured for the 2009 CP pile jacket installations was measured approximately double the 2001 and 2005 installations, average total current outputs have lessened at approximately a linear rate since initial installation, as

shown in Figure 10. While there are no direct criteria for the minimum total current required to provide adequate CP within pile jackets, higher current flows are generally associated with greater levels of protection and larger polarization decays, if similar system resistances are present. As such, lower current can be indicative of lower CP; however, polarization development and/or decay are not directly proportional to the total current.

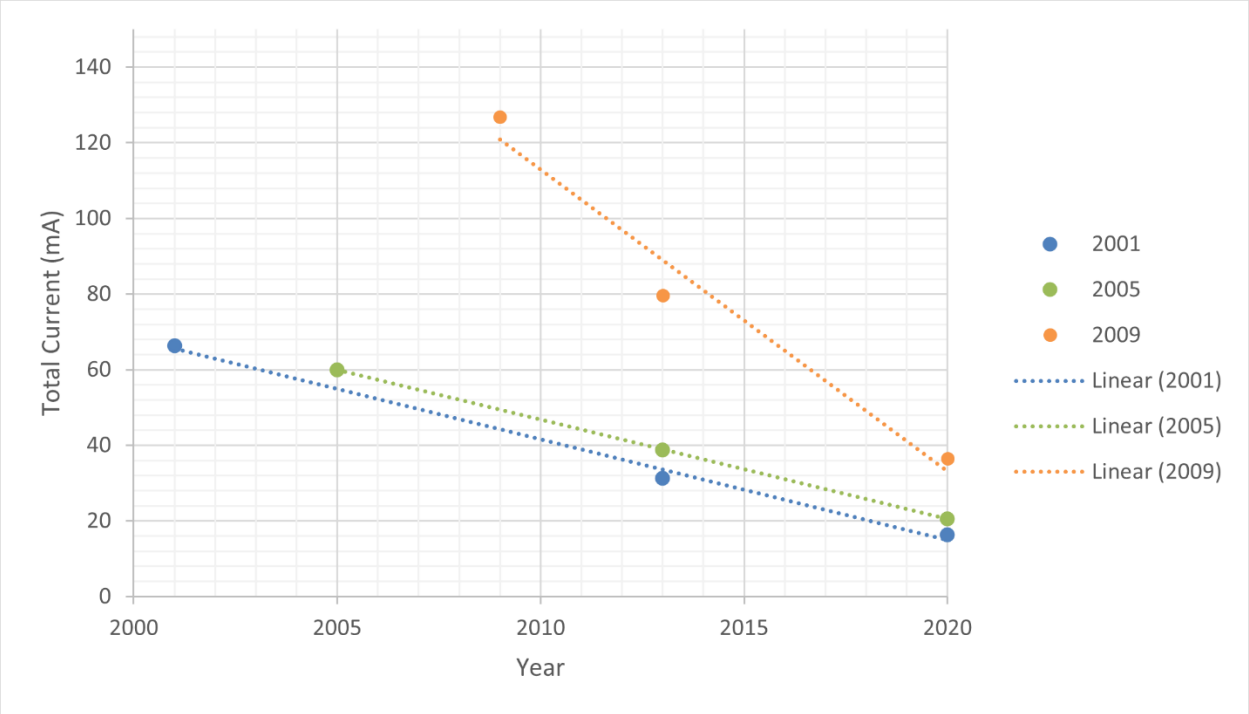

Figure 10. Overview of total current as a function of time.

In addition to the total current output shown above, the routine monitoring data recorded jacket anode current output with the bulk zinc anode connected, bulk zinc anode current output with the jacket anodes connected, the current between the jacket anodes and bulk zinc anode (with the positive test lead connected to the jacket anodes), jacket anode current output with the bulk zinc anode disconnected, and bulk zinc anode current output with the jacket anodes disconnected. Each of these measurements can provide an indication of which anode(s) the structure is receiving CP current flow from and the relative magnitude of that current.

For the majority of piles, current measurements were higher from the bulk anode than the jacket anode mesh, as would be expected due to the lower circuit resistance below the water line. In some cases, extremely low or negative current output measurements were recorded between mesh, bulk, or both anodes and the structure, which may indicate discontinuity of the anode(s) and/or structure from the system. While the diagnosis of the variable current flow routes was not thoroughly evaluated in comparison with its role on CP criteria for the purposes of this research, lesser current output due to increased resistance or discontinuity between either anode(s) and/or the associated structure would likely lead to a lesser amount of CP.

Polarization/Depolarization – A review of polarization/depolarization showed similar trends in decline as a result of the age of the CP pile jacket, which is displayed in Figure 11. Although the data trends were slightly less linear, the decline in depolarization measurements in 2020 ranged from 37 to 65 percent less than polarization measured at initial commissioning, with the exception of the 2020 measurement of the 2009 installation within the port. A likely explanation for this observation is that five of the ten pile jackets evaluated out of the 2009 installation lot decayed for 70 days due to access, over one month longer than the remainder of evaluated pile jackets. A portion of the polarization decay can occur within the first 24 to 48 hours. However, it is rarely enough time to achieve full depolarization of the steel owing primarily to slow migration of oxygen to the steel surface, especially in partially saturated concrete cover. Full depolarization may take months for the structure to finish decaying, particularly above the waterline, as illustrated in this data.

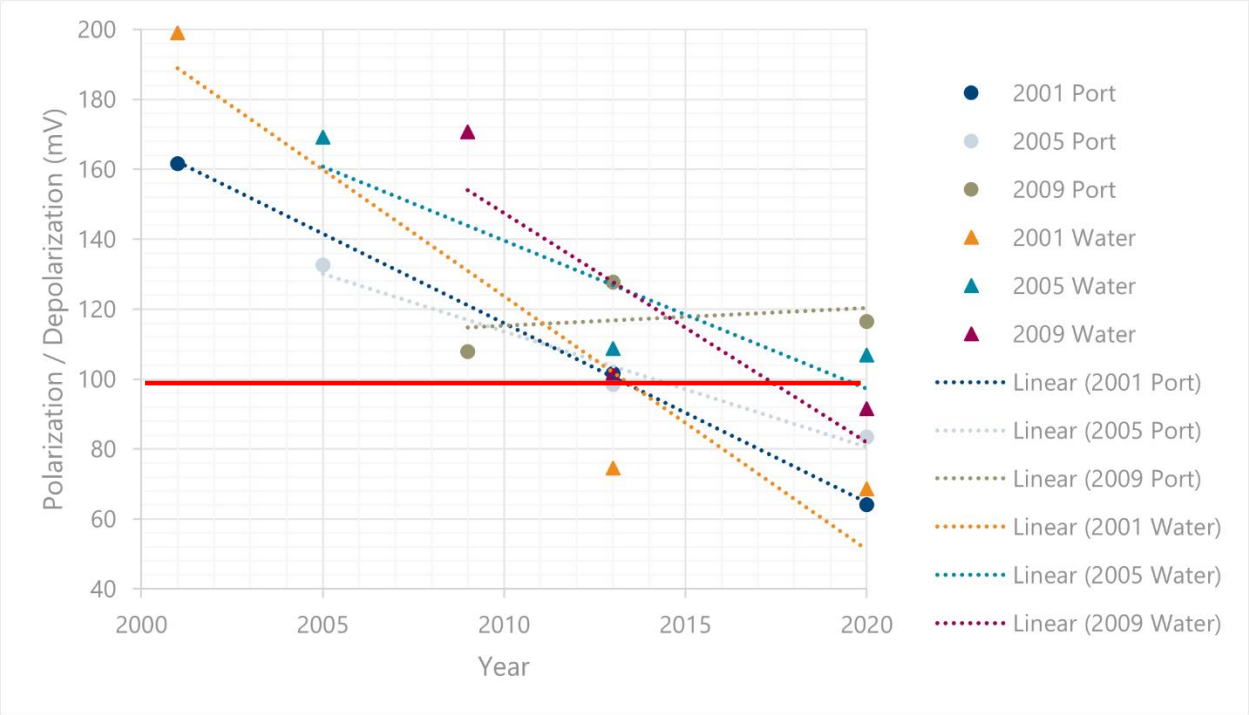

Figure 11. Overview of polarization/depolarization decay as a function of time. The red line indicates the minimum 100 mV polarization/depolarization recommended threshold for adequate CP.

As shown in the discrepancy in the 2009 data, it is likely that depolarization values for the other installations would also increase if allowed more decay time; however, the magnitude of the increase is unknown. Even if assuming a slight increase in depolarization if decay time is increased, the data shows that the average depolarization value for each generation of jackets is declining to be near or less than the 100mV minimum criteria defined by industry standards.

Decay Potential – Similar to current output and polarization/depolarization data, measured decay potentials indicate a decline (more positive) shift in potential, ranging from approximately 2 to 19 percent over the 7-year time period, as shown in Figure 12. Another clear observation regarding this data is the significantly more negative decay potentials measured from within the water than those measured within the port above the waterline. To further illustrate this trend, average decay potentials are plotted side-by-

side with a relative CP pile jacket elevation in Figure 13, with the port measurement shown at 2′-0″ above MHW (0′-6″ above MLW) and the water measurement 3′-0″ below the waterline. In this figure, the elevation of water measurements may vary, and decay potentials are shown as linear; however, these assumptions may not be entirely accurate. Regardless of these potential variations, it is clear that the average decay potentials are likely more positive than the -720 mV vs. CSE threshold within a maximum of 2′-0″ above the waterline, although exact elevations will vary by CP pile jacket and environmental conditions. Additionally, although data was not obtained at higher elevations on the CP pile jackets, it can be assumed that decay potentials will be more positive as elevation increases.

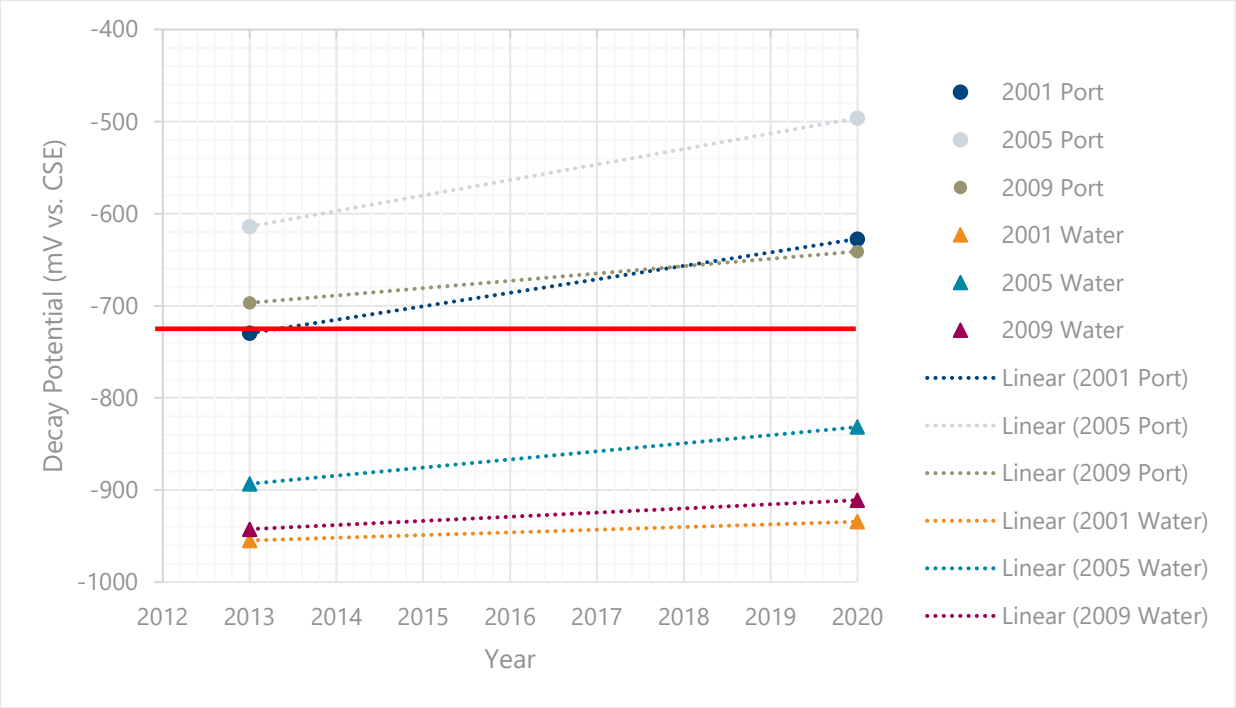

Figure 12. Overview of decay potential as a function of time. The red line indicates the maximum -720 mV vs, CSE decay potential recommended threshold for adequate CP.

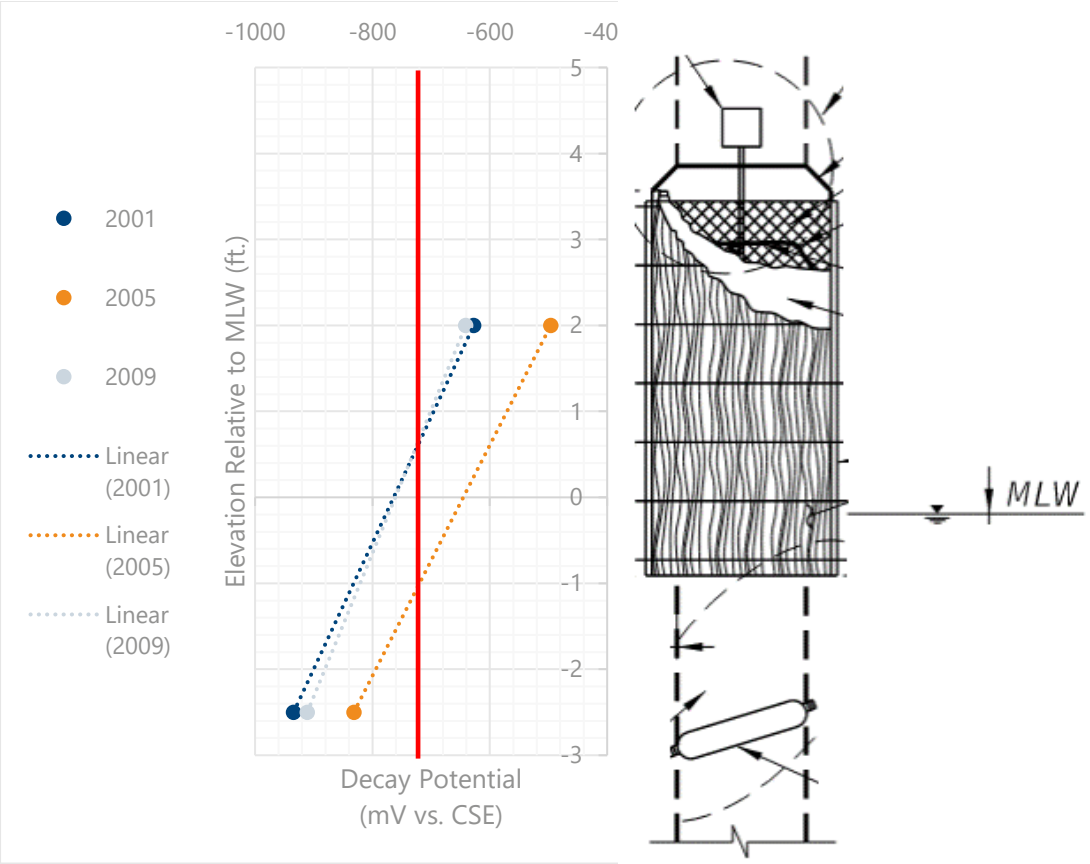

Figure 13. Relative side-by-side comparison of average decay potentials as a function of CP pile jacket elevation. The red line indicates the maximum -720 mV vs. CSE decay potential recommended threshold for adequate CP.

Visual Observation Findings

In addition to evaluating provided CP pile jacket commissioning and monitoring data for trends, this investigation included a limited visual survey of the 38 CP pile jackets and visible portions of the piles. The following distress mechanisms were commonly observed during the visual survey. This investigation did not include observing or documenting the condition of the electrical wiring, junction box, or miscellaneous items, which were assessed and documented during the 2021 routine monitoring survey. APPENDIX B summarizes observed distress between individual piles and associated figures.

Fiberglass Jacket Distress – Approximately 55 percent of the 38 observed fiberglass jackets exhibited some form of distress with variable degrees of severity. The most commonly observed distress was cracking of the fiberglass, which was observed on 12 jackets, ranging from minor corner cracks to vertical cracking extending the entire length of the jacket (Figure 14). In worse cases, entire sections of the jackets had been broken off, exposing the fill grout, as observed in 9 jackets (Figure 15). When entire sections of fiberglass were missing, cracking appeared to initiate at the bottom portion of the jacket and extend upwards. The exact mechanism of the jacket failures was unable to be determined. However, a likely assumption is that cracking initiates first, allowing water and marine growth to penetrate between the jacket and the grout, eventually breaking off.

Figure 14. Full-height cracking of fiberglass jacket (Pile 289-5 shown).

Figure 15. Sections of fiberglass jacket broken off entirely (Pile 105-9 shown)

Pile Distress –Twentyone of the 38 piles observed in this investigation exhibited distress such as cracking or spalling. Cracking typically propagated upward from the top of the jackets and ranged in width from 5 to 50 mil, likely indicative of underlying corrosion of the embedded steel (Figure 16). In some cases, reddish-brown staining was visibly discharging from the crack, further evidence of likely corrosion of the reinforcing steel (Figure 17). In most cases, the cracking was observed two to four inches from the corner(s) of the pile, suggesting that the corner prestressing strands are experiencing ongoing corrosion, as would be expected due to the two-sided exposure. In isolated cases, the cracking resulted in delamination and/or spalling at the corners of the piles.

Figure 16. Typical vertical cracking propagating upward from top of pile at corner (Pile 198-1 shown)

Figure 17. Example of vertical cracking exhibiting minor rust staining (Pile 236-7 shown)

Miscellaneous Observations – Separation between the top portion of the grout material and/or cracking of grout material was commonly observed. The separation was between either the fiberglass jacket and grout interface, the grout and pile interface, or both. The jacket to grout interface separation is of minor consequence, as is transverse cracking within the grout. Separation of the grout-to-concrete pile interface may negatively affect CP performance depending on severity due to the increased resistance disruption of the ionic current path. However, it is likely that the observed separation is limited to the sloped portion of

the top of the grout (top 2 or 4 inches that extend above the jacket for non-structural and structural jackets, respectively). This grout layer is often dry-packed on after the placement of the infill grout to facilitate water drainage away from the pile.

Multiple pile caps had been coated with arc-spray metalizing, and several piles below had received some level of coating due to overspray (Figure 18 and Figure 19). While it did not appear the intent was for the metalizing to protect the top of the piles, they may be receiving some residual protection if reinforcing steel from the piles and pile caps are continuous.

Additionally, there appeared to be previous repairs on multiple piles. The purpose of these repairs is unknown, as they could have been installed to repair corrosion damage or damage to the piles during initial installation.

Figure 18. Cracking of sloped grout material above jacket (Pile 198-1 shown).

Figure 19. Metalizing overspray observed on pile (Pile 14-4 shown)

In-Depth Assessment

To illustrate electrical performance against criteria established by industry standards, Figure 20 and Figure 21 plot depolarization versus decay potentials for the 2021 measurements obtained within the monitoring port and water for the three different generations of CP pile jackets, respectively. As expected, significant scatter is observed in the data, making a correlation difficult between these electrical measurements and differentiating the performance of the jacket generations on an individual CP pile jacket basis. However, one clear trend that is further illustrated is the significantly more negative decay potentials within the water than in the port, while depolarization values remain similar. The submerged portions of the piles would be expected to have more highly negative potentials because the oxygen availability is limited and thus affects the electro-chemical behavior of the bar. Additionally, the presence of the submerged bulk anode and low resistivity of seawater interacting with the grout creates a lower resistance and more favorable path for the ionic current to flow through, compared to the grout above the waterline, particularly at the higher elevations.

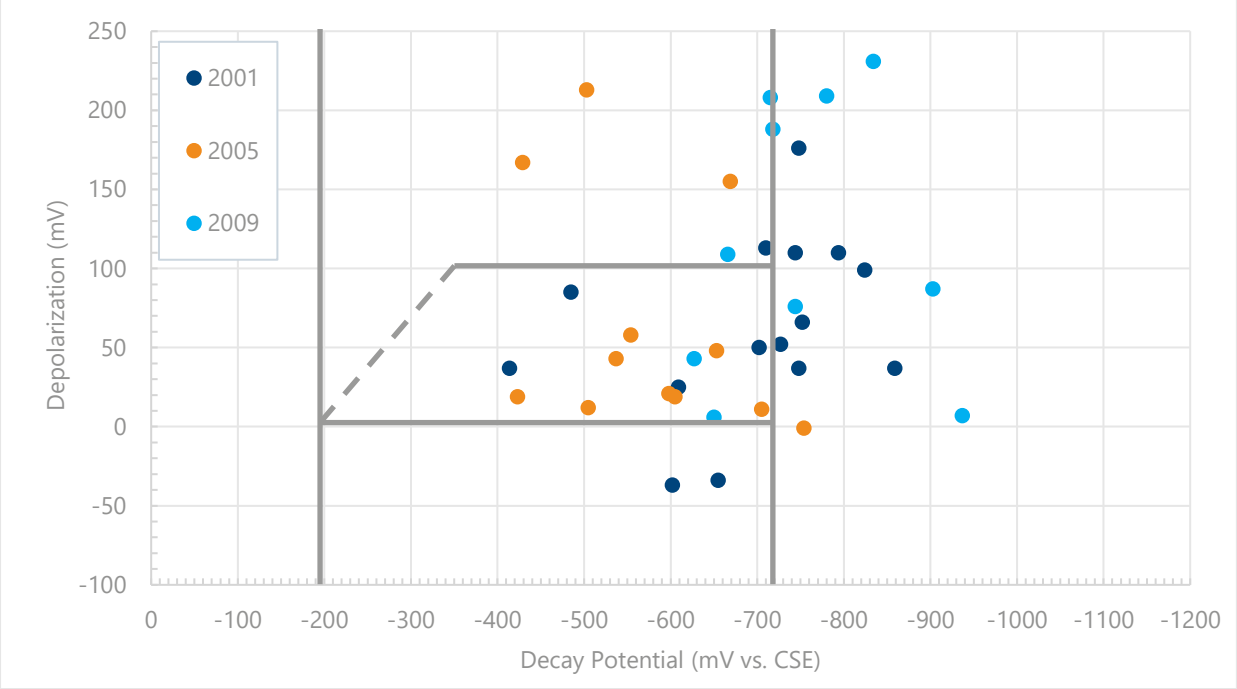

Figure 20. Plot showing depolarization versus decay potentials measured in the monitoring port for the three generations of installations

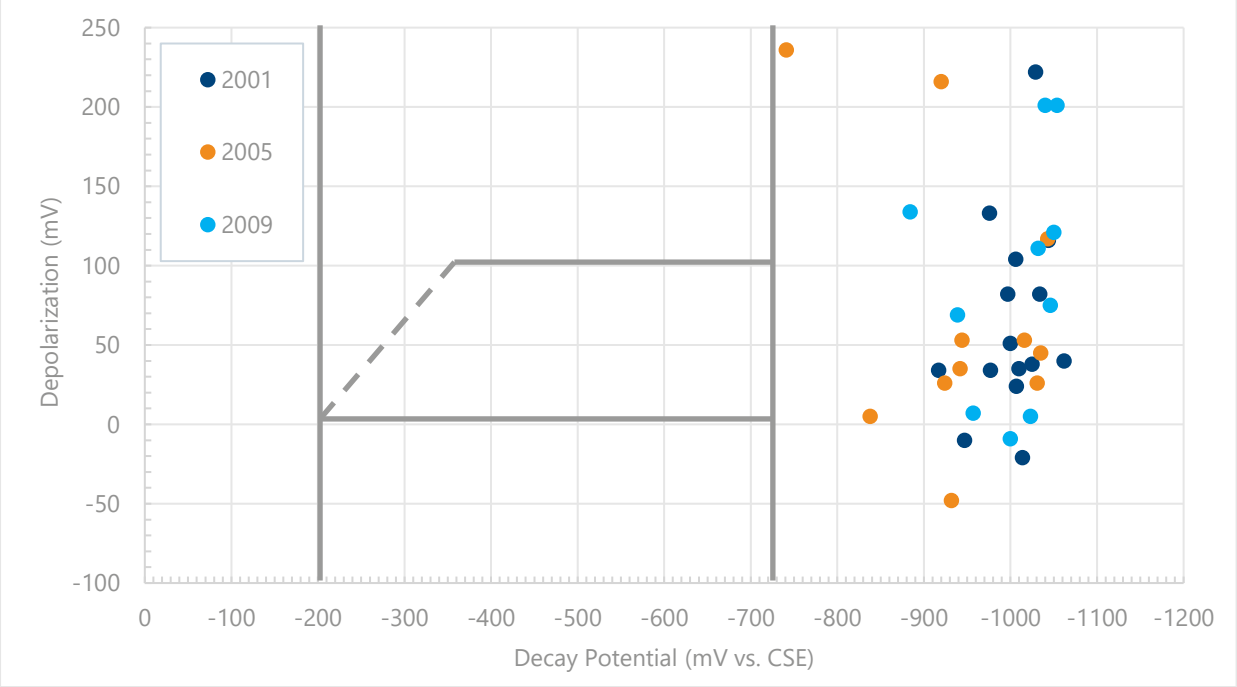

Figure 21. Plot showing depolarization versus decay potentials measured in the water for the three generations of installations

Furthermore, in an attempt to correlate electrical performance with visible distress on the select piles, individual pile data was evaluated in comparison with observed distress on the pile above the top of the

jacket, specifically distress deemed a result of ongoing corrosion of the embedded steel, which is provided in Figure 22. Similar to the data sorted by CP pile jacket installation previously presented, no clear correlation is present between electrical data within the monitoring port and distress observed above the top of the jacket. While previously displayed trends illustrate lesser CP from the CP pile jacket at higher elevations of the pile, the depolarization values and decay potential values measured from within the port do not reflect the actual protection provided at the top or just above the jacket. To illustrate the lack of correlation between CP pile jacket electrical data and visible distress above, 11 of the 21 pile jackets falling within the "100% protected" categories within the jacket exhibited distress above the jacket, while the two pile jackets within the "Unprotected" category did not exhibit distress above the jacket.

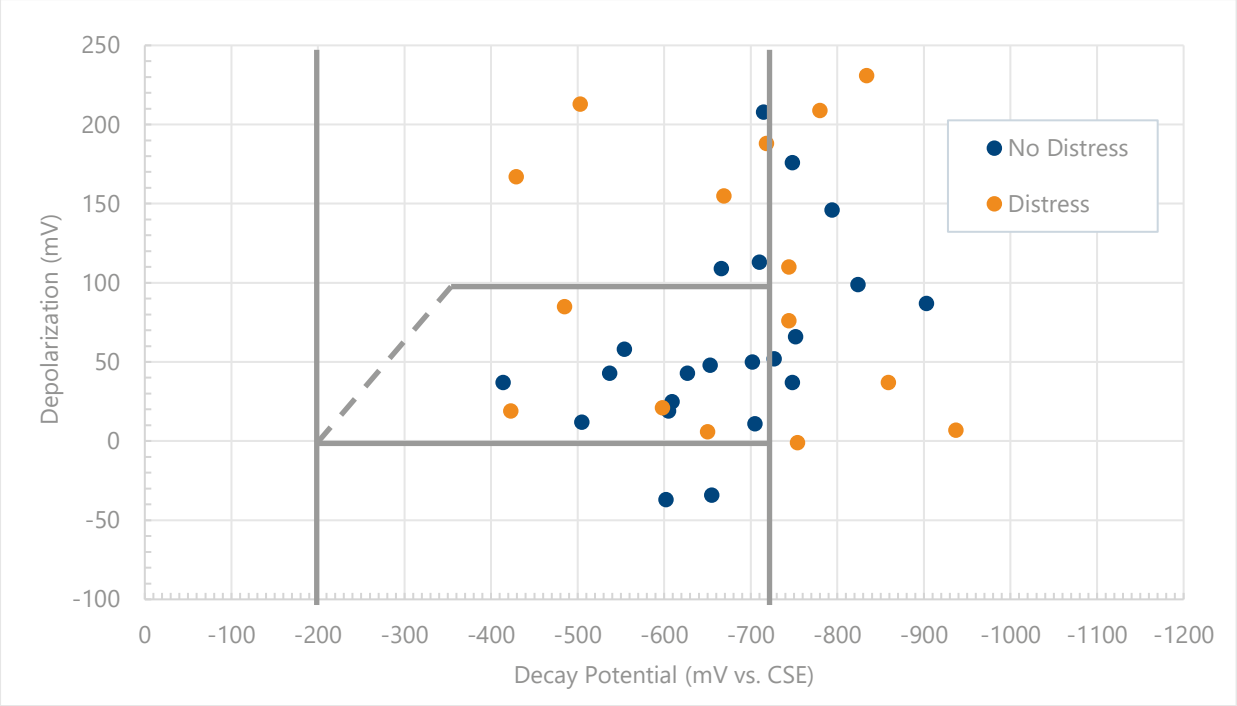

Figure 22. Plot showing depolarization versus decay potentials measured in the monitoring port for piles with and without distress.

To further analyze the possible factor(s) contributing to the diminishing performance of CP pile jackets over time, monitoring data was also used to select individual piles for in-depth assessments in an attempt to identify the factor(s) leading to variation in performance for the different generations of jackets. To perform this in-depth assessment, current data from individual CP pile jackets was compared to average values for each generation to select CP pile jackets with variable performance data, which were selected primarily based on depolarization values. For this investigation, data for an individual pile near the average values for its generation is referred to as performing typical, while those performing better and worse than the average values are referred to as better than typical and worse than typical, respectively. In total, ten CP pile jackets were selected for the in-depth assessment: three from 2001, three from 2005, and four from 2009. Selected CP pile jackets, as well as their associated electrical measurements, are summarized below in Table 16, Table 17, and Table 18.

Table 16. Summarized Data for CP Pile Jackets Selected for In-Depth Assessment – 2001 Installation

Pile Identification	Average	138-7	177-4	182-3
Performance Rating[1]	NA	2	1	3
Total Current Output in 2020	16	5	9	12
Avg. Depolarization at Port in 2020	64	66	176	37
Avg. Depolarization in Water in 2020	69	133	222	40
Avg. Decay Potential at Port in 2020	-627	-686	-572	-822
Avg. Decay Potential in Water in 2020	-934	-911	-754	-989

Units: Amperage = mA, Depolarization = mV, Potentials = mV vs. CSE

[1] *1 = Better than Typical, 2 = Typical, 3 = Worse than Typical*

Table 17. Summarized Data for CP Pile Jackets Selected for In-Depth Assessment – 2005 Installation

Pile Identification	Average	12-1	53-3	270-2
Performance Rating[1]	NA	3	2	1
Total Current Output in 2020	21	3	20	30
Avg. Depolarization at Port in 2020	83	-1	48	167
Avg. Depolarization in Water in 2020	107	35	45	216
Avg. Decay Potential at Port in 2020	-496	-755	-605	-262
Avg. Decay Potential in Water in 2020	-832	-907	-990	-704

Units: Amperage = mA, Depolarization = mV, Potentials = mV vs. CSE

[1] *1 = Better than Typical, 2 = Typical, 3 = Worse than Typical*

Table 18. Summarized Data for CP Pile Jackets Selected for In-Depth Assessment – 2009 Installation

Pile Identification	Average	46-3 [2]	82-6 [2]	106-7 [2]	138-8
Performance Rating[1]	NA	2	3	1	2
Total Current Output in 2020	37	120	46	38	37
Avg. Depolarization at Port in 2020	106	109	6	188	43
Avg. Depolarization in Water in 2020	92	134	5	201	69
Avg. Decay Potential at Port in 2020	-641	-557	-644	-530	-584
Avg. Decay Potential in Water in 2020	-911	-750	-1018	-853	-870

Units: Amperage = mA, Depolarization = mV, Potentials = mV vs. CSE

[1] *1 = Better than Typical, 2 = Typical, 3 = Worse than Typical*

[2] *Indicates piles selected from the Gandy Bridge*

At each of these CP pile jackets, corner sections of the CP pile jackets were removed for material evaluation by an angle grinder at similar elevations on each pile. In the field, surface resistivity measurements were obtained on the exposed surface of infill grout, and samples were transported to the research team's laboratory, where zinc mesh anode samples were examined. This was completed using a stereoscopic microscope at magnifications up to 160X to observe for consumption or any visual properties of the anode.

Microscopical observations and measurements were conducted on the zinc mesh embedded in nine concrete and grout samples. Each sample was saw-cut in a direction perpendicular to the mesh. A saw-cut surface of each sample was lapped with progressively finer grinding media until the edges of the mesh were clearly delineated. The thickness of the intact mesh (or the corroded portion) was measured using a stereomicroscope equipped with a digital camera and a calibrated reticle. Photographs are attached to illustrate the appearance of the cross sections of the samples and the zinc mesh in each sample.

Table 19 provides brief descriptions of the mesh conditions. The mesh was generally well embedded in the concrete or grout but varied in condition from free of visible or frequent corrosion (e.g., Samples 177-4 and 270-2) to widespread corrosion and significant section loss (e.g., Sample 106-7). Many samples exhibited more frequent or more severe corrosion at the exposed corners of the specimens than the edges, probably due to general weathering in the service, such as exposure to moisture and air. Sample 12-1 contained a sub-surface parallel crack that was at the depth of the outboard plane of the zinc mesh (Figure 61). The crack was lined with white secondary deposits. The deposits are likely corrosion products of zinc. Delamination along the crack is expected to occur with further corrosion.

Visually intact zinc mesh was measured approximately 90 to 110 mils thick (Figure 58 and Figure 61) among the nine samples.

Additionally, both surface resistivity and bulk resistivity of the grout samples were measured to understand the material properties as it relates to ionic flow and the overall performance of the CP system. A summary of the findings from the material evaluation is presented in Table 19.

Table 19. Material Evaluation Summary

Pile ID	Year Installed	Performance Rating [1]	Grout Surface Resistivity (kohm-cm)	Grout Bulk Resistivity (kohm-cm)	Zinc Mesh Observations	Figures
137-7	2001	2	1.6	4.0	Localized corrosion and minor section loss near the corner; free of significant corrosion or section loss elsewhere.	Figure 58
177-4	2001	1	1.6	4.2	Only localized corrosion and minor section loss observed. White efflorescence on lapped section.	Figure 59
182-3	2001	3	1.9	5.0	Localized corrosion and minor section loss near the corner; free of significant corrosion or section loss elsewhere.	Figure 60
12-1	2005	3	1.0	5.3	Frequent corrosion and minor section loss; incipient delamination on outboard face of the mesh (0.16 inch deep)	Figure 61
53-3	2005	2	4.2	7.6	Frequent corrosion and minor section loss; a mesh joint observed at the corner.	Figure 62
270-2	2005	1	4.1	7.5	Generally free of visible corrosion or section loss.	Figure 63
46-3[2]	2009	2	NA	NA	NA	NA
82-6[2]	2009	3	2.3	4.0	Significant corrosion and section loss at the corner; less severe corrosion and section loss along edges.	Figure 64
106-7[2]	2009	1	1.6	3.3	Appeared to be the most corroded sample among examined; widespread corrosion and significant section loss.	Figure 65
138-8	2009	2	1.2	3.0	Minor corrosion along edges; more severe at the corner with minor section loss.	Figure 66

[1] *1 = Better than Typical, 2 = Typical, 3 = Worse than Typical*

[2] *Indicates piles selected from the Gandy Bridge*

Description of Impressed Current Corrosion Control Systems

Impressed current CP systems are installed on select footings for the main span piers on both the Gandy and HF bridges, for which there are 24 and 30 piers in total, respectively. Similar to the installation of the ICCP jackets occurred over several years and construction projects. As the only rehabilitation construction drawings provided and reviewed as part of this assessment were 2009 (Financial Project ID 420666-1-52-

01) and 2012 (Financial Project ID 427455-2-52-01) rehabilitations, this investigation focused on the ICCP jacket systems installed from these two rehabilitation projects. Installation dates of ICCP systems are summarized below in Table 20.

Table 20. ICCP System Installation Dates

Year	Gandy Pier Numbers	Howard Frankland Pier Numbers
2009	226, 227, 230 - 232	147, 152, 153, 157 – 159, 166, 168, 171, 176
2013	222 – 225, 228, 229, 235 - 245	None

The review of the ICCP jacket system details showed that similar systems were used for both rehabilitation projects. However, one primary difference was that the 2009 jackets encapsulated the footings, struts, and up to 4-feet 6-inches above the top of the strut (9-feet above the top of the footings), while the 2013 generation only encapsulated the footings. With regards to the ICCP jackets installed on footing elements, detailing appeared very similar with ICCP jackets consisting of titanium mesh anodes and electrically isolated supplemental steel reinforcement encapsulated in a structural concrete jacket on the vertical and top surfaces. On the side surfaces, the titanium mesh was placed against the side of the footings, and supplemental reinforcing steel was installed outside of the mesh. On the top surface, supplemental reinforcing steel was installed adjacent to the top surface of the footing, and the titanium mesh was embedded in an overlay. This overlay was comprised of structural concrete and gunite in the 2009 and 2013 generations, respectively. A cross-section of the typical ICCP jacket is provided in Figure 23.

At each pier, a minimum of three silver-silver chloride reference electrodes are installed within the existing footing, which were specified to be installed at the most anodic location on each element as located by the CP specialist. In the 2009 generation, the ICCP jackets on the footings and struts/columns are electrically isolated to create separate zones and allow for variable current output to be distributed to each area.

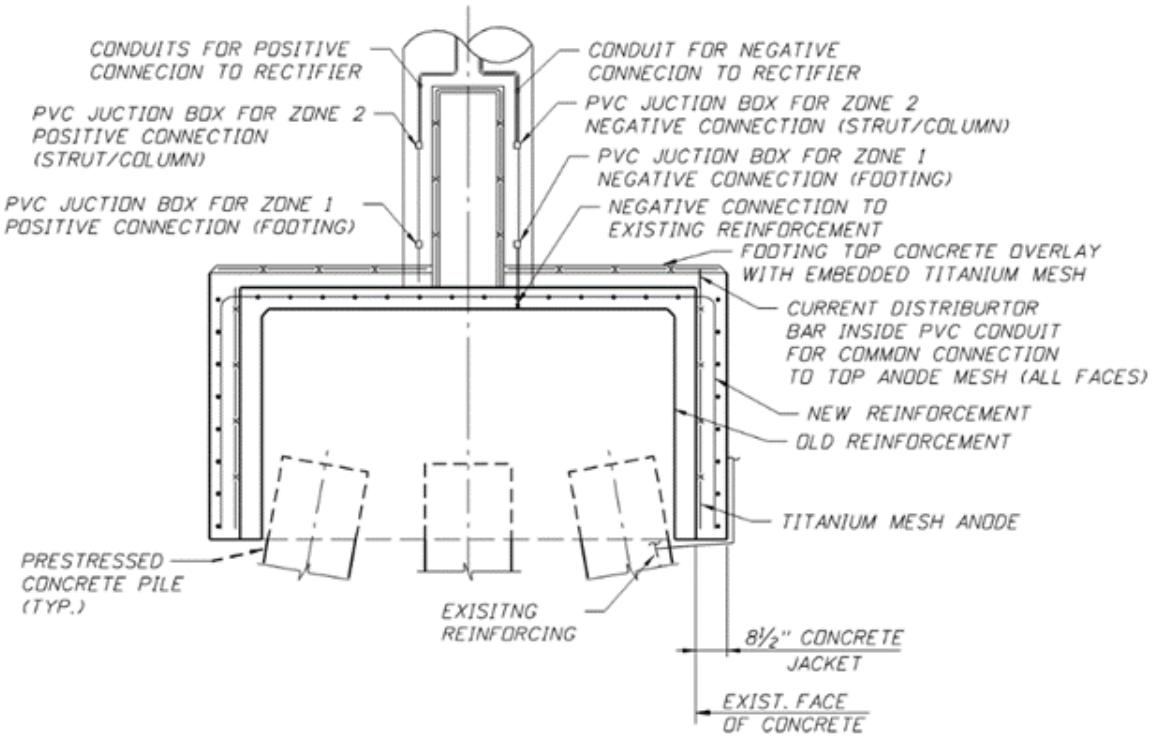

Figure 23. Cross-sectional view of pier footing ICCP system from Drawing Set from Financial Project ID 420666-1-52-01 (2009 Installation).

Current for each ICCP system is provided by rectifiers, which convert alternating current input to direct current output. Rectifiers are installed within electrical junction boxes, along with remote monitoring units (RMUs) that allow monitoring of electrical data. Data obtained by the RMUs was not obtained as part of this assessment, and therefore, it is unclear the capabilities of the remote monitoring systems.

Assessment Findings of Impressed Current Corrosion Control Systems

FDOT personnel indicated that the typical protocol is to perform routine monitoring and inspection of impressed current cathodic protection jackets on an approximately annual basis after installation and commissioning of the systems to confirm performance. For the two bridges included in this investigation, commissioning data for both bridges was provided only for the 2009 installation, and the most recent routine monitoring data for all systems, which was obtained in September 2020 and December 2020 for the HF and Gandy bridges, respectively. Additionally, remote monitoring units (RMUs) are installed to provide FDOT the ability to monitor select electrical parameters remotely; however, this data was not provided for review and was not incorporated into this study. Therefore, assessment of the ICCP systems for these two bridges was performed using three data sets, each briefly described below.

1. Commissioning Data from 2008/2009 (CONCORR Florida, Inc., 2009)
2. Routine Monitoring Data provided by FDOT (2020)
3. Data obtained at select elements during the site visit portion of this study (February 2021)

Two primary restrictions were implemented to sufficiently compare the performance of ICCP systems. Firstly, this assessment focuses on the systems installed on the footings, typically associated as Zone 1,

and omits detailed evaluation of Zone 2 (and 3) systems that are installed on column/strut elements of select piers. Secondly, multiple generations of ICCP systems were installed over several construction projects; however, detailed information, including system detailing and commissioning data, was only provided for the systems installed in 2009. As such, commissioning information was only available for a portion of ICCP systems evaluated as part of this assessment. Additionally, data obtained during commissioning and routine monitoring was obtained using permanent Ag/Ag-Cl reference electrodes, however, all data has been converted to CSE for continuity purposes throughout this report.

Commissioning Data - Commissioning of the 2009 ICCP system installations on both bridges was performed by CONCORR Florida, Inc. Information regarding electrical continuity testing, embedded reference electrode installation, inspections during installation, and pre- and post-energization test data is summarized, as well as additional pertinent information. This report reproduces information from CONCORR Florida, Inc.'s 20009 report applicable to this research, however, refer to the 2009 report for complete information regarding the commissioning of these systems.

CONCORR Florida, Inc.'s 2009 report summarizes the distribution of embedded reference electrodes for each ICCP system installed in 2009 between both bridges, reproduced below in Table 21 and Table 22.

Table 21. Distribution of Embedded Reference Electrodes in Gandy Bridge (Zone 1, 2009 Install Only)

Pier No.	North Footing		Center Footing		South Footing	
	Old Steel	New Steel	Old Steel	New Steel	Old Steel	New Steel
226	X	X	NA	NA	X	
227		X	NA	NA	X	
230	X	X	NA	NA		X
231	X		NA	NA	X	X
232		X	NA	NA	X	

Table 22. Distribution of Embedded Reference Electrodes in Howard Frankland Bridge (Zone 1, 2009 Install Only)

Pier No.	North Footing		Center Footing		South Footing	
	Old Steel	New Steel	Old Steel	New Steel	Old Steel	New Steel
147		X	X			X
152				X	X	
153	X					X
157		X	X			
158	X			X	X	
159	X					X
166		X	X			X
168		X [1]		X	X	
171	X			X	X	
176		X	X			X

[1] *Installed inadvertently*

The following text from CONCORR Florida, Inc.'s 2009 report describes the energization testing process.

> *It was decided to initially energize each zone at 50% of the CP current determined from the ElogI tests. Since old and new reinforcing steel were monitored during ElogI tests on footings, the larger of the two resulting CP currents was used to calculate the initial current setting….*
>
> *… After the CP system was energized and allowed to stabilize a potential decay test was conducted over a period of approximately 40 hours. Based on the results of the potential decay test, adjustments were made to the outputs in several zones and then a final set of test data were obtained. Potential decay test data and the final set of system operating data are included in Table 4 [of the CONCORR Florida, Inc. report]. All test data obtained during the energization process were satisfactory and the power and control system operated as intended.*

As noted above, the determination of necessary cathodic protection was made using ElogI testing. However, the appendices were omitted from the version of the report provided for review, and as such, these test results could not be reviewed. Regardless, CP system energization and potential decay test data was reviewed to establish baseline levels of protection for Zone 1 of the systems installed in 2009, which are summarized below in Table 23, and were confirmed by the CP specialist to have met specified operating criteria.

Table 23. Summary of 2009 ICCP Commissioning Data

Measurement	Gandy Bridge	Howard Frankland Bridge
Number of Reference Electrodes	13	26
Average Initial Required Current	3.0	2.5
Average Static Potential	-464	-416
Average On Potential	-866	-730
Average IO Potential	-798	-657
Average Polarization	334	241
Average Adjusted Required Current	0.9	1.4
Average IO Potential	-854	-712
Average Decay Potential	-793	-599
Average Depolarization	62	113
Average Voltage	1.5	1.6

Units: Amperage = mA, Depolarization = mV, Potentials = mV vs. CSE

Routine Monitoring Data - While ElogI testing was used for the commissioning of the system, this technique is more often used to determine the initial cathodic protection current requirement.This is not commonly used for the evaluation of existing systems. As such, this testing was not performed during FDOT routine monitoring efforts, which were provided and reviewed as part of this assessment. Electrical components for the ICCP systems varied between the HF and Gandy bridges as well as obtained data. For both bridges, recorded data typically included the voltage setting in the on and instant-off configuration and potentials for each reference cell for comparison versus static potentials obtained during commissioning[1]. For the Gandy Bridge, current outputs were also measured. FDOT personnel indicated any adjustments made to the systems, which were reportedly performed to ensure a minimum of 100mV more negative than the static potentials.

Records indicated that ICCP systems are generally not allotted time to depolarize during the routine monitoring efforts, meaning decay potentials are not obtained to determine depolarization. However, it was apparent that the instant-off potentials are being compared to the static potentials obtained during commissioning to determine polarization development. While polarization development is typically used on new installations and less for the evaluation of existing systems, it is reasonable for this method to be used when static potentials are available.

A review of provided data showed that current and voltage output had increased over time, as shown below in Table 24. Over the approximately 11-year time period, FDOT personnel increased the current output on four of the five rectifiers evaluated in this assessment, increasing the average current output for the Gandy Bridge by over 30 percent. Similarly, voltage outputs were increased for both bridges over the same time frame.

[1] For the Gandy Bridge, potentials were measured in the “On” and “IO” configurations. For the HF Bridge, only one potential measurement was documented, and it was unclear as to whether it was in the “On” or “IO” configuration. For the purposes of this assessment, it is assumed that this data was obtained in the “On” configuration.

Table 24. Comparison of Average Rectifier Outputs

Bridge	Gandy Bridge		Howard Frankland Bridge	
Year	2009	2020	2009	2020
Current (A)	0.9	1.21	1.35	NA [1]
Voltage (V)	1.48	1.53	1.58	1.75

[1] *Current output was not recorded for the HF bridge in 2020*

A second observation is that of the 39 reference electrodes installed within the pile footings (26 and 13 within the HF and Gandy bridges, respectively), IO potentials were more positive than static potentials at 13 reference electrodes (9 and 4 within the HF and Gandy bridges, respectively). In many cases, IO potentials were over 100mV more positive than the respective static potentials. Reference electrodes may be affected by external factors such as temperature, lighting, and/or significant changes in concrete concentration or contaminants (Ansuini and Dimond, 1994). However, it is unlikely these ambient factors resulted in significant potential shifts because each is installed at least 10 inches from the exterior surface of the concrete jackets. Therefore, for these reference electrodes, it is assumed that data may be erroneous due to poor electrical connections or other factors.

Of the 26 reference electrodes that are assumed to be functional between the two bridges, "On" and "IO" potential data was also compared for cumulative performance as a function of time. Despite current and voltage outputs being manually increased between 2009 and 2020, Table 25 shows a significant decline in average potential measurements for both bridges. Because decay potentials are not measured as part of typical routine monitoring, the only data comparison to be made is between "On" and "IO" potential measurements as a function of time, and depolarization values could not be calculated or evaluated using provided data.

Table 25. Comparison of Average Potential Measurements

Bridge	Gandy Bridge		Howard Frankland Bridge	
Year	2009	2020	2009	2020
"On" Potentials	-866	-566	-730	-433
"IO" Potentials	-854	-553	-712	NA

Units: Potentials = mV vs. CSE

2021 Assessment Data – As part of the 2021 scope, additional in-depth assessments were performed on nine ICCP jackets, four and five from the HF and Gandy bridges, respectively. These assessments included measurement of on and off voltages, AC circuit resistance, and potential measurements for each of the permanent reference electrodes and select monitoring ports on the vertical faces of the pile caps by using portable reference electrodes. For each set of potential measurements, "On" and "IO" measurements were obtained. Additionally, the structure was allowed a minimum of 24 hours decay time in order to obtain decay potentials and calculate depolarization. A summary of data obtained as part of this assessment is provided in APPENDIX C, while a summary of obtained potential data is provided below in Table 26.

Table 26. Summary of Average Potential Measurements from 2021

Bridge	Gandy Bridge		Howard Frankland Bridge	
Location	Perm. Ref. Electrode	Monitoring Port	Perm. Ref. Electrode	Monitoring Port
No. Measurements	12	8	12	6
"On" Potentials	-586	-828	-501	-564
"IO" Potentials	-559	-792	-459	-527
Decay Potentials	-453	-681	-316	-396
Depolarization	106	111	143	131

Units: Potentials = mV vs. CSE

As shown above, ICCP systems globally appear to be functioning as intended, as average depolarizations exceed 100 mV for both bridges using the permanent reference electrodes and data obtained in the monitoring ports. A closer look into the data shows that the minimum depolarization of 100 mV was achieved on a minimum of one measurement location at each of the nine piers and cumulatively on 26 of 38 measurement locations, as summarized in Table 27. Additionally, of the 12 measurement locations receiving less than 100 mV depolarization, 9 appeared to be providing partial protection to the structure. Three locations showed negative shifts (reverse polarization), measured on Reference Cell 1 on the Gandy Bridge (Piers 226, 231, and 241). For each of these piers, ICCP systems appeared to be functional, as full and/or partial protection were measured at each of the other measurement locations. As such, it is likely that these measurements are erroneous due to electrode error, wiring discontinuities, shorting of the electrode to the structure, and/or other factors.

Table 27. Count of Reference Cells

Bridge	Gandy Bridge		Howard Frankland Bridge		Combined	
Depolarization	Perm. Ref. Electrode	Monitoring Port	Perm. Ref. Electrode	Monitoring Port	Perm. Ref. Electrode	Monitoring Port
< 0 mV	3	0	0	0	3	0
0 – 100 mV	1	4	4	0	5	4
> 100 mV	8	4	8	6	16	10
Total	12	8	12	6	24	14

Further review of obtained data shows that increased current output appears to correspond with higher average depolarization measurements at the respective piers, as shown in Figure 24. However, with such a limited amount of applicable data, it is difficult to thoroughly compare the current output with depolarization measurements and substantiate a given conclusion.

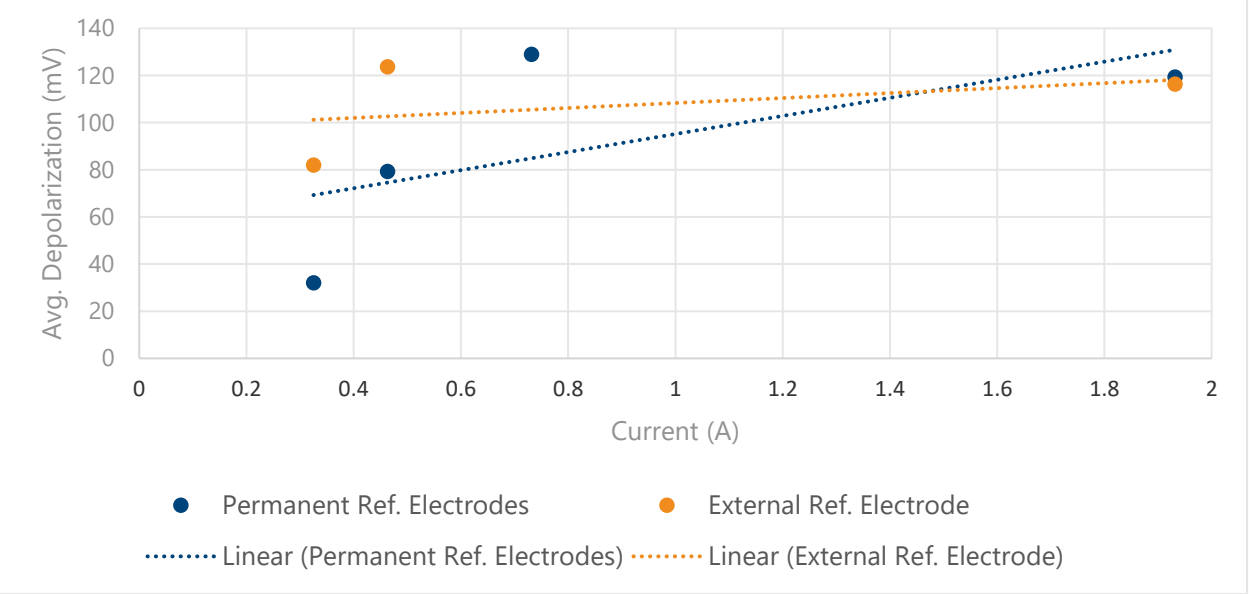

Figure 24. Current versus average depolarization measurements for the Gandy Bridge.

In addition to evaluating the performance of the ICCP jackets versus current and voltage input into the circuits, this study attempts to determine if and to what extent variability in material properties affects performance. To perform this in-depth assessment, core samples were extracted from four ICCP pier jackets selected on a random basis for laboratory evaluation. Piles selected were Piers 226, 231, and 241 on the Gandy Bridge and Pier 158 on the Howard Frankland Bridge. Electrical performance data obtained as part of the 2021 assessment for the select ICCP pier jackets is summarized below in Table 28.

Table 28. Summary of Average Potential Measurements for Select Piers

Pier	**Gandy 226**		**Gandy 231**		**Gandy 241** [1]		**HF 158**	
Location	Perm. Ref. Electrode	Mon. Port	Perm. Ref. Electrode	Mon. Port	Perm. Ref. Electrode	Mon. Port	Perm. Ref. Electrode	Mon. Port
Current [1]	1.932		1.216		0.513		NA	
Voltage [1]	1.513		1.491		1.68		1.821	
No. Measurements	3	3	3	3	2	NA	3	2
"On" Potentials	-671	-807	-597	-808	-651	NA	-610	-609
"IO" Potentials	-636	-770	-579	-765	-614	NA	-589	-590
Decay Potentials	-517	-654	-500	-641	NA	NA	-422	-472
Depolarization	119	116	79	124	NA	NA	167	118

Units: Amperage = mA, Voltage = V, Depolarization = mV, Potentials = mV vs. CSE

[1] Data for Pier 241 on the Gandy Bridge not obtained as part of 2021 assessment, reproduced from data provided by FDOT from 2020 survey

As shown above, the electrical performance data between the four selected ICCP pier jackets did not significantly vary. However, constituents were evaluated to determine if variation in materials correlated with the minor variations in performance. The two primary materials that may factor into the performance of the ICCP systems are the titanium mesh and the concrete replacement material, for which the laboratory evaluation methods and summaries of findings are summarized below.

Titanium Mesh – Embedded titanium mesh within core samples obtained from the Gandy 226, Gandy 231, and HF 158 piers (Figure 67). Mesh samples were examined using both optical stereomicroscope and SEM/EDX. Each of the three laths was similar in composition and composed of pure titanium with only trace amounts of other elements. The thickness of the original titanium sheet used to manufacture the lath was 1 millimeter (40 mils), and no evidence of corrosion or alteration, other than that expected as a result of obtaining and preparing the samples, was observed (Figure 68 and Figure 69). On the exterior surface, Nickel and Phosphorus were detected locally, which are likely a result of surface treatment of the lath. In summary, titanium mesh samples between the three samples appeared similar in composition. Nothing was noted from a material standpoint that would indicate the titanium mesh itself affected the performance of the ICCP systems.

Jacket Concrete Material – Similar to pile jackets as described above, the jacket concrete material used to encase the existing footings serves as a part of the corrosion cell electrolyte and, therefore, may affect the overall performance of the ICCP system based on its material properties and ability to facilitate ionic flow. To evaluate the concrete material, bulk resistivity was measured in the laboratory. Because of the presence of the near-surface titanium mesh, surface resistivity could not be accurately measured. Bulk resistivity data is presented below in Table 29.

Table 29. Bulk Resistivity Data for Jacket Concrete Material

Pier	Gandy 226	Gandy 231	Gandy 241	HF 158
Bulk Resistivity (kohm-cm)	14.0	6.5	34.8	5.8

Based on a review of the limited bulk resistivity data obtained as part of this investigation, few global trends were identified when data was compared to electrochemical performance data for the footing ICCP systems. One isolated observation was noted regarding the relatively high concrete resistivity at Gandy 241, where current output was much less than similar typical footings evaluated in this study. The voltage-controlled rectifier output similar voltage to that observed at other footings, however, the current was much less. The output voltage at Gandy 241 and the average output voltages from the Gandy bridge in 2020 were 1.68V and 1.53V, respectively, while output currents from the same data sets were measured at 0.513A and 1.21A, respectively. Although multiple factors can attribute to this observation, the relatively high bulk resistivity of the jacket concrete is likely attributed to the overall resistance of the circuit. Because depolarization measurements were not obtained at this footing, further conclusions regarding overall performance are difficult to make based on obtained data.

Field Investigation 2 – Melbourne Causeway Bridges

Bridge Nos. 700174 and 700181 are the westbound and eastbound routes of the Melbourne Causeway (US 192) spanning the Indian River in Melbourne, Florida. The bridge substructures are similar construction types. However, 700174 and 700181 are reinforced with black and epoxy-coated reinforcing steel, respectively, and provided an opportunity to evaluate the effectiveness of epoxy-coated reinforcement in similar construction detailing and identical exposure conditions. A thorough corrosion assessment was performed by Concorr Florica, Inc. (Concorr) in 2011, which documented visual observations and construction properties of both bridges at the ages of 33 and 26 years, respectively.

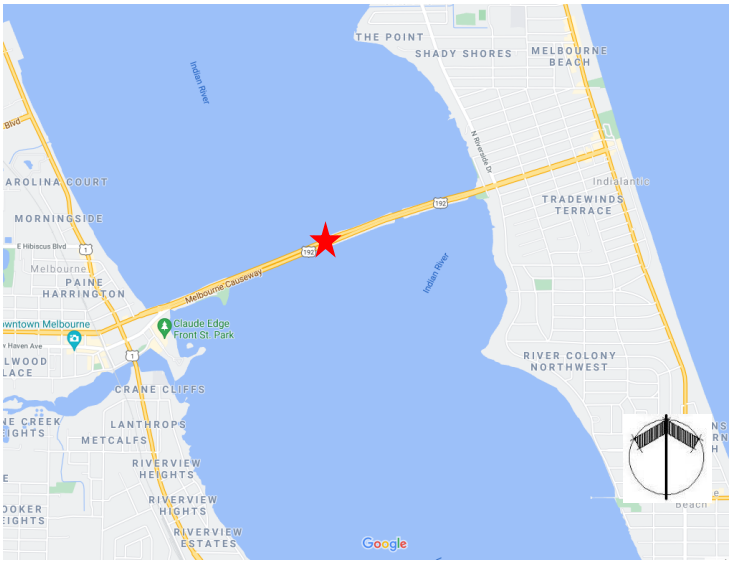

Figure 25. Location of the Melbourne Causeway Bridges across the Indian River, identified by the red star (image from Google Maps©).

Additionally, rehabilitation drawings were issued in 2014 with primary efforts of concrete repair, epoxy injection, and installation of ICCP systems on Bridge No. 700174. This investigation performed a cursory review of ICCP data on Bridge No. 700174.

Assessment Objectives and Methodology

By performing a similar corrosion assessment of Bridge No. 700181 in 2021, a more applicable comparison can be made in terms of the age of the bridge when evaluating the benefit(s) of ECR. Bridge No. 700174 was 33 years of age in 2011, and Bridge No. 700181 was 36 years of age at the time of this investigation in 2021.

This investigation was designed to assess the long-term performance of epoxy-coated reinforcing steel compared to the black bar for similar bridges in identical exposure conditions. Additionally, by obtaining similar information for Bridge No. 700181 in 2021 to Concorr in 2011 for Bridge No. 700174, this investigation aims to determine which of the following three variables (or a combination thereof) contribute to the variation in performance.

- Construction Geometry and Materials (concrete properties, design covers, etc.)
- Exposure Conditions
- Epoxy-coating of the reinforcing steel

Note: Limited data provided in the 2011 Concorr report indicates that concrete specifications and design cover appear similar between the two bridges; however, typical variations may exist in terms of construction and material tolerances.

Concorr performed a corrosion condition assessment with respect to the pile caps and crash walls in 2011, including the following scope of services (paraphrased for conciseness):

1. Visual and sounding surveys on five pile caps, five columns, five struts, and one crash wall on each bridge.
2. Perform the testing and sampling described below on one pile cap, one column, one strut, and one crash wall on each bridge:
   a. Obtain 2" diameter cores for chloride content testing (two cores per element for a total of 8 cores per bridge). Measure reinforcing steel depth at core locations.
   b. Obtain corrosion potential measurements at 6" spacing on each element.
   c. Obtain concrete resistivity measurements at select locations.
3. Obtain a water sample to determine the environmental classification at the bridges.

Table 30 below summarizes obtained data for the subset of elements for which in-depth data was obtained by Concorr in 2011.

Table 30. Components Selected for Comprehensive Testing and Sampling

Bridge No. 700174		Bridge No. 700181	
Pier No.	Component	Pier No.	Component
14	Crash Wall	13	Pile Cap 1
20	Pile Cap 1	13	Column 2
20	Column 1	13	Strut
20	Strut	15	Crash Wall

To provide an applicable comparison between Bridge No. 700174 in 2011 and Bridge No. 700181 in 2021, a similar test plan was developed in order to obtain similar data for side-by-side comparison purposes. As such, the following tasks comprised the field assessment. The intent was to evaluate the same components on Bridge No. 700181 that were assessed in 2011 (Pile Cap 1, Column 2, Strut of Pier No. 13, and the Crash Wall at Pier No. 15).

1. Perform visual and sounding surveys on the four components to document and quantify observed distress.
2. Perform the testing and sampling described below on one pile cap, one column, one strut, and one crash wall on Bridge No. 700181:
   a. Obtain concrete core samples for chloride content testing (two cores per element for a total of 8 cores). Cores were to be located at similar elevations to those obtained in 2011. Measure reinforcing steel depth at core locations.
   b. Obtain corrosion potential measurements at 6" spacing on each element
   c. Obtain concrete resistivity measurements at select locations
   d. Select cores are to be located to sample the ECR
3. The following laboratory tests will be performed on concrete core and reinforcing steel samples:

a. Acid-Soluble Chloride Content Measurements will be obtained per ASTM C1152. The depths of sample slices will be determined to provide a comparison to 2011 data.
b. Examination of epoxy coating on select reinforcing bars

Titanium mesh ICCP systems were installed on the substructure at all piers for Bridge No. 700174 in approximately 2014, making these elements inaccessible up to approximately 12 feet above MLW, making visual or other observation of Bridge No. 700174 impossible. As such, only a cursory review of ICCP data provided by FDOT was performed on Bridge No. 700174.

Description of Structures and Environment

The Melbourne Causeway bridges are twin bridges carrying SR 500 (US 192) to connect Melbourne with Indialantic and are approximately one-half mile long. Table 31 provides general descriptions and properties of each bridge. As-built drawings were not provided or reviewed for this investigation, and therefore, exact detailing and material specifications are unknown; however, a visual comparison of bridges shows that layout and member sizes are nearly identical.

Table 31. Bridge Descriptions

Bridge	**WB Melbourne Causeway (Black bar)**	**EB Melbourne Causeway (Epoxy coated bar)**
Structure	SR 500 (US 192)	
Feature Crossed	Indian River IWW	
County	Brevard	
Florida Bridge No.	700174	700181
Facility Carried	State Road No. 500 (US Route 192)	
Year Constructed	1978	1985
Design Life	Unknown	
ADT	19,250	
NBI Substructure Rating	6 (2018)	
No. of Spans	27	
Overall Length	2,591 ft.	
Overall Width	42 ft. 9 in.	52 ft.
Roadway Width (curb-to-curb)	45 ft. 9 in.	55 ft.
Superstructure	Precast prestressed I-Beams approach spans and steel open girders for main span	
Substructure	Piles with caps supporting columns, typ. two per bent. Either side of main span consists of pier walls supported by piles	

Description of Corrosion Control Systems

Epoxy-Coated Reinforcement (Bridge No. 700181) – As mentioned in the section above, exact detailing and material specifications are unknown for both bridges, including ECR specifications. Three segments of

epoxy coated bars were included within the collected cores, as shown in Figure 26. Brown epoxy coating was used. Laboratory evaluation of the ECR found that the coating thickness averaged between 8 to 12 mils. No corrosion (rated 1) is observed in one of the bars. Minor corrosion (rated 2) is present in the other two bars, with corrosion observed to be active in one. The knife adhesion rating for the epoxy coating ranged from a rating of 3, moderate adhesion (epoxy peels from bars in 1/4" sections), to a rating of 4 (epoxy peels from bars in 3/8" sections. The backside contamination rating for the epoxy coating is less than 5% for the three bars.

Table 32. Results of ECR Evaluation

Bar ID	Bar Size	Epoxy Type (Brown/Green)	Corrosion Rating (1-5)[1]	Active Corrosion?	Average Coating Thickness (mils)	Knife Adhesion Rating (1-5)[2]	Backside Contamination [3]
C2	#14	Brown	1	N	11.8	4	4
C5	#5	Brown	2	Y	8.2	3	3
C8	#8	Brown	2	N	11.9	3	3

(1) Rating 1 indicates no corrosion; Rating 5 indicates corrosion area greater than 60% of total surface area.

(2) Rating 1 indicates excellent adhesion; Rating 5 indicates poor adhesion.

(3) Backside contamination rating is based on the percentage of the backside surface of peeled epoxy coating exhibiting contamination.

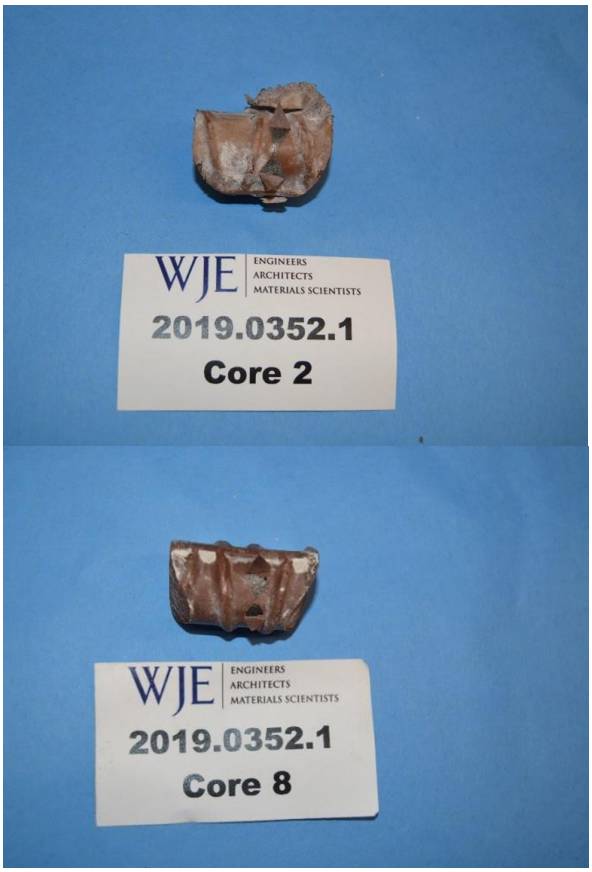

Figure 26. Photographs of evaluated ECR samples from Bridge No. 700181.

Assessment Findings

As discussed in the previous sections, the primary goal of this investigation was to assess long-term performance of epoxy-coated reinforcing steel compared to a black bar for similar bridges in identical exposure conditions. This report section presents data obtained during the 2021 field investigation for Bridge 700181 next to data provided by Concorr in their 2011 report for Bridge No. 700174. By comparing these data sets, a more accurate comparison can be made, as the bridges being investigated were at similar ages at the time of their respective assessments:

- Bridge 700174 (Black Bar)– Constructed circa 1978 (33 years old at time of 2011 assessment)
- Bridge 700181 (Epoxy Coated Bar) – Constructed circa 1985 (36 years old at time of 2021 assessment)

This section is organized by outlining assessment findings and comparing them to the 2011 test results in the following order:

- Construction Geometry
- Concrete Materials
- Exposure Conditions
- Visual Findings
- Corrosion Potentials
- Material Sampling and Testing

Data presented from the Concorr 2011 report is reproduced for comparative purposes only. Complete visual findings, non-destructive evaluation data, and location of samples are presented in APPENDIX D of this report.

Construction Geometry – Although exact geometric information and detailing information regarding the construction of both bridges is unknown, the concrete cover is an important variable to consider when evaluating corrosion performance. As such, Concorr presented concrete cover data for each element as part of their report. Subsequently, this investigation obtained additional cover measurements to verify measurements, which were obtained by measuring bars exposed by concrete coring, drilling to bars for electrical connections, and/or ground penetrating radar (GPR). As construction tolerances are difficult to predict for an entire element when evaluating a localized area, ranges of measured concrete covers are provided for bars measured at the predetermined elements as part of the field investigations. Data from the 2011 and 2021 investigations are provided below in Table 33.

Table 33. Measured Concrete Cover Ranges

Element	2011		2021
	Bridge 700174	Bridge 700181	Bridge 700181
Pile Cap	3.75 - 4.5	3.88 – 4.13	4.25 – 4.75
Column	4.25 - 5.75	3.94	3.25 – 3.75
Strut	4.13 - 4.25	4.25	4.13 – 4.75
Crash Wall	3.88 - 4.25	4.13	4.25 – 4.75

[1] *Measured to outermost bar, units = inch*

Although exact ranges of measured concrete covers vary slightly, these ranges lead to the assumption that design covers for each element were similar between the two bridges. Although it is impossible to know the statistical distribution of concrete covers for each element between the two bridges without a comprehensive concrete cover investigation, the data provided above allows the comparison of distress between the two bridges while omitting concrete cover as a major variable.

Concrete Materials – Similar to concrete cover, concrete properties are important variables to consider when evaluating corrosion performance. To confirm similar composition and properties of concrete between Bridge Nos. 700174 and 100181, limited petrographic studies were performed. Core 1 and Core 10 were extracted from Bridge No. 7001181 and 700174, respectively, and examined to compare the concrete composition and hardened properties (core locations and additional information are provided later in this section). Primary findings from the petrographic examination are provided below, and Table 34 summarizes the general core characteristics. The full petrographic report can be found in APPENDIX E.

1. **Main Cracks:** None observed. Short and shallow hairline cracks were observed in Core 10, likely due to restrained drying shrinkage.
2. **Surface Loss and Surface-Parallel Cracks:** Minor surface loss and short microcracks were observed in Core 10, likely due to drying shrinkage and coring.
3. **ASR:** No evidence of alkali-silica reactions or other significant deleterious chemical reactions such as delayed ettringite formation (DEF) was observed in the cores.
4. **Distress Related to Seawater Exposure:** Minimal in Core 10; None observed in Core 1.
5. **Reinforcement:** Core 1 contained an imprint of No. 8 epoxy-coated steel reinforcing bar. The imprint is free of significant rust or staining, suggesting the bar is likely in good condition. No radiating cracking was observed surrounding the bar. No reinforcement bars or imprints were observed in Core 10.
6. **Carbonation:** Negligible in Core 1 and 0.3 inches in Core 10.
7. **Concrete Condition:** Appeared to be good overall in both cores.

Table 34. General Core Characteristics and Petrographic Findings

	Core 1	Core 10
Length	5.5 inches	2.8 inches
Exterior Surface	Overall flat formed/cast surface exhibited localized discolored areas due to biological growth and carbonate secondary deposits	Flat smooth formed surface exhibited two small spalled areas at edge and a few shallow hairline cracks.
Location	Bridge No. 700181 with epoxy-coated reinforcement; Pier 13 pile cap, S. face, 2" above MGL	Pier 15 on Bridge No. 700174 with black steel bar reinforcement; column above crash wall
Interior Surface	Rough fractured surface extended mainly through coarse aggregate particles. An imprint of likely No. 8 steel reinforcing bar observed on the interior surface (4-3/8 inch cover), with minimal rust	Rough fractured surface extended mainly through coarse aggregate particles. No reinforcement or imprint was observed in the core
Coarse Aggregate	Similar in the two cores, composed of crushed fossiliferous limestone, with a nominal top size 3/4 inch. Vugs and voids associated with the rock diagenesis and formation are frequently observed, but these features did not connect or form a network.	
Fine Aggregate	Similar in the two cores, natural siliceous sand composed of mainly quartz/quartzite with small amounts of feldspar and miscellaneous rocks and minerals.	
Paste	Overall similar in composition (portland cement without SCMs), physical characteristics and estimated water-to-cement ratio (w/c). Medium gray, moderately hard to hard, and moderately low in water absorptivity. Estimated w/c was 0.39 to 0.44.	
Estimated W/C	0.39 to 0.44 in both	
Paste-Aggregate Bond	Interrelated to be tight in both cores	
Secondary Deposits	Ettringite frequently lines air voids in both cores. Likely minor seawater-related alteration in exterior 0.3 inch in Core 10. Small amounts of salts (NaCl) appeared to be present in the region.	
Materials-Related Distress	None observed	Probably minor paste alteration due to seawater exposure in the exterior 0.3 inch
Cracking/Micro cracking	Infrequent microcracking	Minor shallow surface perpendicular cracks likely due to drying shrinkage
Overall Condition	Good	Good

In addition to petrographic evaluation, surface resistivity was measured on the elements selected for in-depth assessment. Surface resistivity measurement values are summarized below in Table 35.

Table 35. Average Measured Surface Resistivity

Element	2011		2021
	Bridge 700174	Bridge 700181	Bridge 700181
Pile Cap	8.7	5.3	9.6
Column	24.8	30.6	29.2
Strut	26.3	38.0	197.6 [2]
Crash Wall	12.0	16.3	52.7 [2]

[1] *Findings above indicates averages of between three and five individual measurements, units = kohm-cm*
[2] *Measured at higher elevations than those in 2011*

As illustrated in Table 34, concrete properties between the two bridges contain similar constituents and exhibit similar properties as it relates to corrosion resistance. Both coarse and fine aggregates are similar between the two core samples, and both contain portland cement paste without fly ash or any other supplementary cementitious material, and water-to-cementitious material ratios were also determined to be similar.

Additionally, surface resistivity measurement data shows similar values between the two bridges, as shown in Table 35. Elevations of measurements (and associated moisture content of concrete), the orientation of measurements relative to reinforcing steel, and other several other factors can contribute to variability in surface resistivity measurements. However, measured values for the pile cap and column appear very comparable between the two investigations, as well as values from the struts and crash walls from 2011. Values obtained from the strut and crash wall in 2021 were taken at a much higher elevation, which generally results in a higher resistivity as a result of decreased moisture content.

For the purposes of this investigation, findings as they relate to concrete materials and physical properties indicate that concrete mixes utilized for the substructures of each bridge are similar and would not play a significant role in differentiating corrosion resistance for either bridge when compared against each other.

Exposure Conditions – Given that the physical locations of the bridges are nearlyidentical, it is assumed that the exposure conditions for the bridges are identical. Additionally, although chemistry and chloride content can change over time, it is assumed that changes over time are slow and did not provide different exposure conditions for Bridge No. 700174 in the approximately seven years prior to the construction of Bridge No. 700184. Table 36 below reproduces the results of the laboratory testing of the water sample collected and tested in 2011 by FDOT-SMO, as presented in the Concorr 2011 report.

Table 36. Reproduced Results of Laboratory Testing of Water Sample

Chloride Content, ppm	Sulfate Content, ppm	Resistivity, ohm-cm	pH
12,046	3,383	20	7.96

Visual Findings – In 2011, Concorr performed cursory visual and sounding surveys of each of the select substructure components on both bridges to identify global trends related to observed distress. Outlined below is the summary of distress findings for Bridge No. 700174, reproduced from their 2011 report:

Pile Caps – Most of the pile caps have moderate to severe cracking with corrosion staining and efflorescence on multiple corners starting at the MGL and extending up vertical faces and onto top faces.

Columns – Approximately 50% of the columns have moderate to large incipient spalls with moderate to severe cracking in areas where the columns intersect with with struts.

Struts – Most of the struts have severe cracking and large incipient spalls with corrosion staining and efflorescence on the bottom face and extending up approximately 16" to 24" onto vertical faces.

Additionally, Concorr performed comprehensive visual and sounding surveys of the specific elements selected for in-depth assessment on both bridges in order to identify and quantify observed distress. A similar survey was completed in 2021 for Bridge No. 700181. For this investigation, distress mechanisms and quantities are compared between the 2011 findings for Bridge No. 700174 and the 2021 findings for Bridge No. 700181. A summary of observed distress for the pier and crash wall at bents 13 and 15, respectively, is provided below:

Pile Caps – Pile caps exhibited cracking on the vertical faces with crack widths ranging from approximately 10 to 40 mil in width. With the exception of one 15 mil crack observed within the face of the north pile cap, cracking was observed to be located within six inches of an outside corner, presumably caused by corrosion of the vertical bars placed in the corners. Lengths of these cracks varied, but most of them extended upward from the mean growth line (MGL) (Figure 27 and Figure 28). Sounding of these areas did not identify any concrete surfaces that were delaminated.

Figure 27. Representative vertical cracking extending upward from the MGL.

Figure 28. Crack width gauge indicating an approximate crack width of 25 mil.

Figure 29. Typical cracking of column at elevation of top of strut.

Columns – Columns exhibited minimal distress except for circumferential cracking adjacent to the top of the strut. This cracking exhibited minor efflorescence and appeared to have had parge coat repairs at some time in the past. With the elevation of this cracking matching the top of the strut, this cracking is assumed to be flexural cracking as the columns sway above the struts that provide lateral constraint. Because this cracking is not believed to be a result of corrosion activity, it is omitted from the quantitative summary of distress provided later in this section.

Struts – The strut on Pier 13 exhibited no visible distress.

Crash Wall – Only approximately 25 percent of the surface area of the crash wall at Bent 15 was visually observed due to schedule and access restrictions from the fender. Of the portion of the crash wall observed, approximately 20 linear feet of cracking was observed. This cracking was measured to be equal to or less than 10 mils and was primarily oriented vertically, however, one short horizontal crack was observed.

In summary, distress described in 2011 regarding Bridge No. 700174 significantly exceeds that observed on Bridge No. 700181 in 2021 for all elements observed. Although cracking was not quantified in 2011 to allow a comparison with that observed in 2021, both quantities and severity of cracking were significantly less on Bridge No. 700181. Furthermore, corrosion staining was not observed on Bridge No. 700181, which provides further indication that corrosion had not advanced to the severity observed in Bridge No. 700174 in 2011. Although cracking was not quantified, the Concorr 2011 report quantified the surface area of each element that was identified as being delaminated, which is reproduced in Table 37. Delaminations were not observed in Bridge No. 700181 in 2011 or 2021; however, they are also presented for consistency in the tabulated data comparisons.

Table 37. Tabulated Delamination Quantities

Element	2011		2021
	Bridge 700174	Bridge 700181	Bridge 700181
Pile Cap	27.1	0	0
Column	27.6	0	0
Strut	26.3	0	0
Crash Wall	109.5	0	0

[1] *Units = square foot (ft^2)*

Corrosion Potentials – While it was unclear how this testing was performed for the 2011 assessments, electrical connections were made to the reinforcement by drilling holes in the outermost bars. To ensure electrical continuity for each HCP test location, a minimum of two connections were established, and the

resistance between the two points was measured and recorded. As expected, much greater circuit resistances were measured than would be expected for uncoated reinforcing steel; however, continuity was able to be established with measurements less than 5 mOhms at each location.

As HCP data is not directly comparable between structures with a black bar and those with ECR, this section does not present comparative data between the two bridges. However, contoured HCP data can be viewed in APPENDIX D for each of the four elements evaluated as part of this assessment. The magnitude of HCP values was significantly more negative at the pile cap and crash wall elements than at the strut or column, as would be expected given the increased moisture content of the concrete. In summary, HCP data obtained for this investigation is inconclusive for locating and quantifying locations of on-going corrosion.

Material Sampling and Testing – Concrete core sampling was performed on the elements selected for in-depth assessment on both bridges in 2011 and Bridge No. 700181 in 2021. Material sampling was performed for two primary reasons. First, core extraction over steel bars allows for visual examination of the bars and in the case of ECR, evaluation of the epoxy coating. Secondly, concrete core extraction allows for chloride content analysis, which allows for the determination of chloride contents at variable depths from exterior surfaces and the calculation of chloride diffusion coefficients.

Table 38 and Table 39 below are reproductions of Table 5 and Table 6 from the Concorr 2011 report, summarizing core samples obtained from Bridges Nos. 700174 and 700181, respectively. Additionally, Table 40 summarizes the locations and details of core samples obtained during the 2021 investigation. Contrary to the 2011 investigation, select cores were obtained to not intersect epoxy-coated reinforcing steel for the purpose of evaluating chloride contents at and beyond the depth of the reinforcing steel.

Table 38. Core Sampling and Condition of Reinforcing Steel on Bridge No. 700174 (Concorr 2011)

Core No.	Component	Core Elevation	Concrete Condition	Steel ***	Steel Condition
9	Pile Cap 20-1	At MGL	Sound **	V	Severe corrosion
10		21" above MGL	Sound	V	Moderate corrosion
11 *		At MGL	Delam.	V	Severe corrosion
12	Column 20-1	6" above Pile Cap	Sound	V & H	Minor corrosion
13		80" above Pile Cap	Sound	H	Minor corrosion
14 *		24" above Pile Cap	Delam.	V	Severe corrosion
15	Strut 20	22" above bottom	Sound	H	Moderate corrosion
16		9" below top	Sound	V	Minor corrosion
17 *		6" above bottom	Delam.	V & H	Severe corrosion
18	Crash Wall 14	12" above MGL	Sound	H	Minor corrosion
19		81.5" above MGL	Sound	H	Minor corrosion

** Indicates additional core samples taken in delaminated areas for corrosion exploration purposes.*
*** No delamination was detected during the sounding survey, however, two obvious delaminations (at different depths) were found inside the core hole.*
**** V = vertical bar and H = horizontal bar.*

Table 39. Core Sampling and Condition of Reinforcing Steel on Bridge No. 700181 (Concorr 2011)

Core No.	Component	Core Elevation	Concrete Condition	Steel *	Steel Condition
1	Pile Cap 13-1	3″ below MGL	Sound	VEC	No corrosion
2		19″ above MGL	Sound	VEC	No corrosion
3	Column 13-2	6″ above Pile Cap	Sound	VEC	No corrosion
4		76″ above Pile Cap	Sound	HEC	No corrosion
5	Strut 13	7″ above bottom	Sound	HEC	No corrosion
6		6″ below top	Sound	VEC	No corrosion
7	Crash Wall 15	14″ above MGL	Sound	HEC	No corrosion
8		78″ above MGL	Sound	VEC	No corrosion

** VEC = vertical epoxy-coated bar and HEC = horizontal epoxy-coated bar.*

Table 40. Core Sampling and Condition of Reinforcing Steel on Bridge No. 700181 (2021)

Core No.	Component	Core Elevation	Concrete Condition	Steel *	Steel Condition
1	Pile Cap 13-1	2″ above MGL	Sound	VEC	No corrosion
2		22″ above MGL	Sound	VEC	No corrosion
3		24″ above MGL	Sound	NA	NA
4	Strut 13	8″ below top	Sound	HEC	No corrosion
5	Column 13-1	6″ above Pile Cap	Sound	HEC	Minor corrosion
6	Pile Cap 13-2	18″ above MGL	Sound	NA	NA
7		23″ above MGL	Sound	VEC	No corrosion
8		20″ above MGL	Sound	VEC	No corrosion
9	Crash Wall 14	18″ above MGL	Sound	HEC	No corrosion
10	Crash Wall 15 (Bridge 700174)	NA	Sound	NA	NA

** VEC = vertical epoxy-coated bar and HEC = horizontal epoxy-coated bar.*

To establish chloride content profiles as a function of the depth of the concrete substrate, concrete core samples were sliced to perform chloride content testing as a function of depth. The 2011 chloride content analysis was performed in accordance with Florida Method 5-516 and assuming a concrete unit weight of 3,800 lb/yd^3. Testing was performed on ½-inch slices, with select cores including slices at ½-inch increments to the approximate depth of the reinforcing steel, while the remaining cores just included one test of a ½-inch slice at the approximate depth of the reinforcing steel. Chloride testing for the 2021 study was performed in general accordance with ASTM C1152 *Standard Test Method for Acid-Soluble Chloride in Mortar and Concrete*. Slice thickness was selected to be ¼-inch, and depth of testing was selected to determine chloride content profiles as a function of depth.

In 2011, Bridge No. 700181 had seven fewer years of exposure than Bridge No. 700174, and as expected, chloride contents were measured to be less in Bridge No. 700181. The primary purpose of chloride content testing in this investigation is to determine if the chloride profiles, and specifically the chloride

content at the depth of the reinforcing steel, are comparable between Bridge No. 700174 in 2011 and Bridge No. 700181 in 2021. In total, chloride profiles were developed and compared between four concrete core samples from each bridge: one from each pile cap, column, strut, and crash wall. Chloride profiles for these samples are provided in Figure 30 through Figure 33.

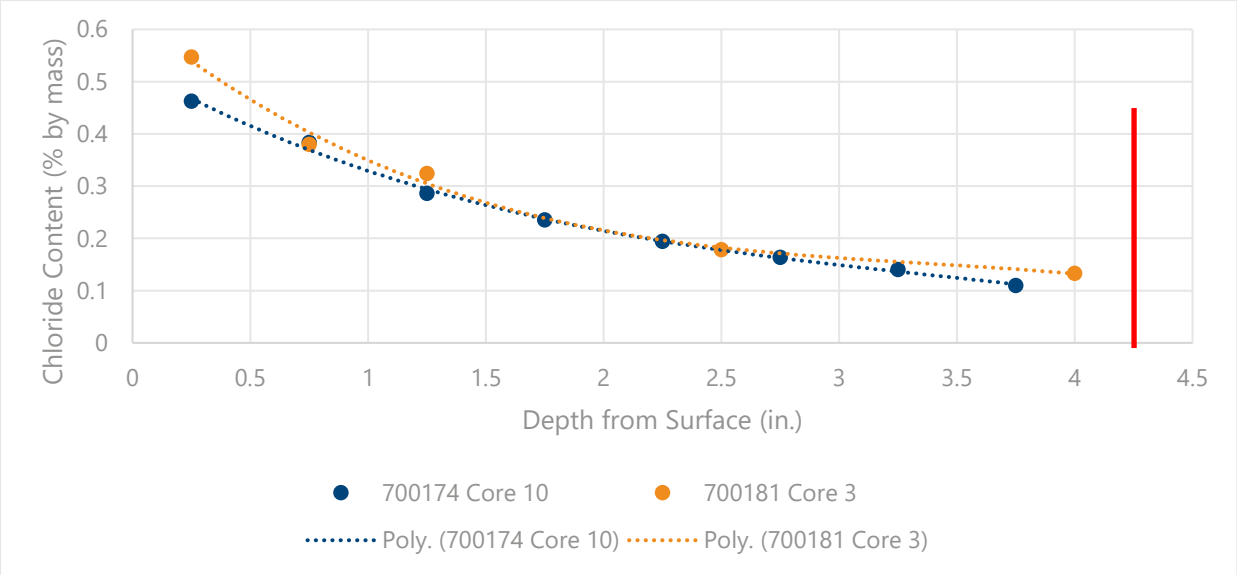

Figure 30. Chloride profiles for pile cap core samples. Cores shown are Core 10 (Bridge No. 700174, 2011) and Core 3 (Bridge No. 700181, 2021). The red line indicates an approximate depth of the reinforcing steel (4.25 in.)

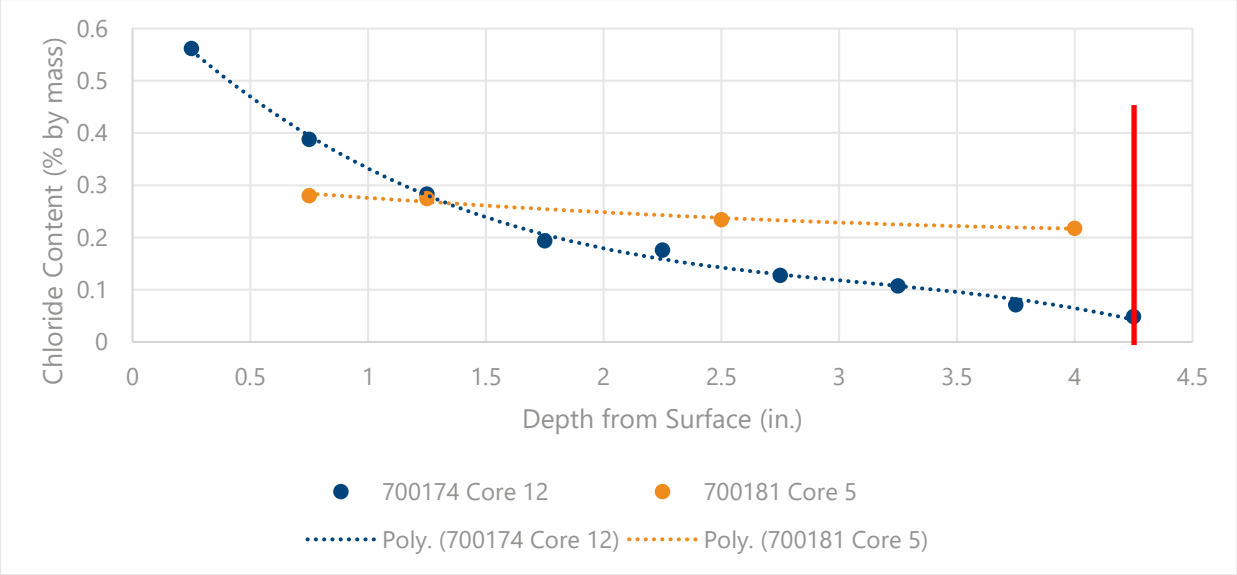

Figure 31. Chloride profiles for column core samples. Cores shown are Core 16 (Bridge No. 700174, 2011) and Core 4 (Bridge No. 700181, 2021). The red line indicates an approximate depth of the reinforcing steel (4.25 in.)

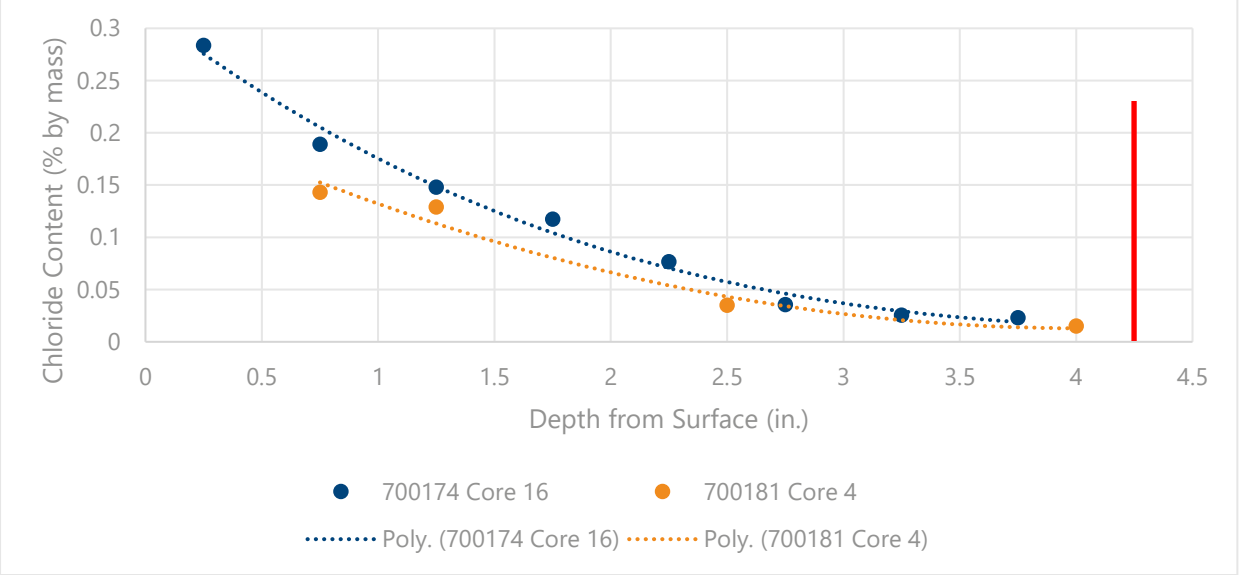

Figure 32. Chloride profiles for strut core samples. Cores shown are Core 16 (Bridge No. 700174, 2011) and Core 4 (Bridge No. 700181, 2021). The red line indicates an approximate depth of the reinforcing steel (4.25 in.)

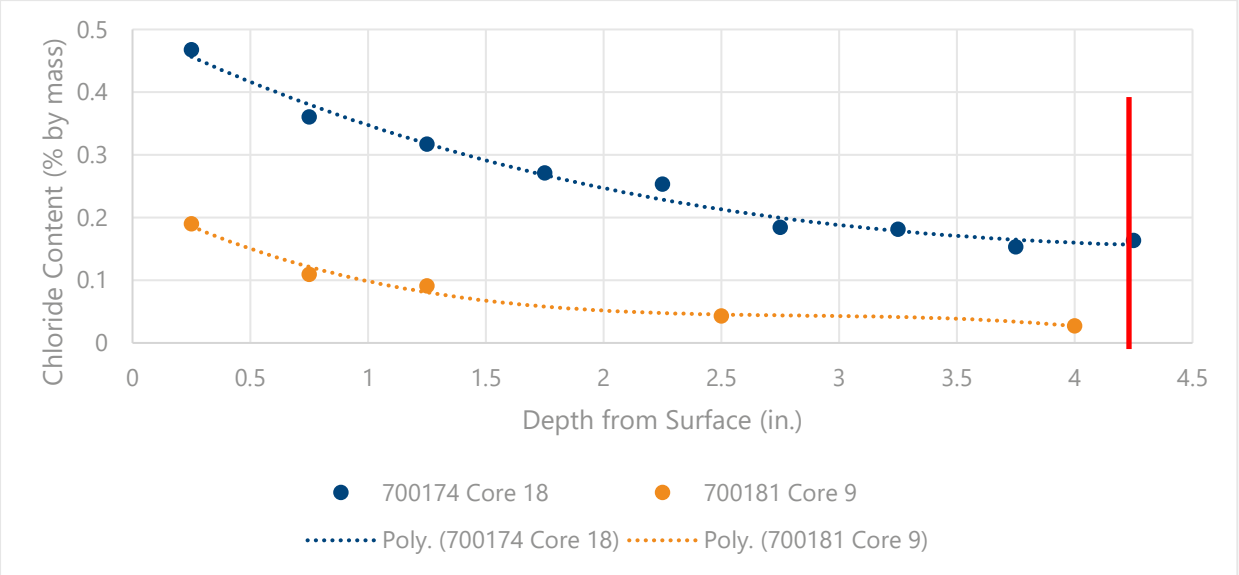

Figure 33. Chloride profiles for crash wall core samples. Cores shown are Core 18 (Bridge No. 700174, 2011) and Core 9 (Bridge No. 700181, 2021). The red line indicates an approximate depth of the reinforcing steel (4.25 in.)

A review of chloride profiles shows an extremely close correlation for the pile cap and column elements, with similarly sloped profiles and measured chloride contents at bar depth between 0.1-0.15 and 0.02-0.04, respectively. For the strut and crash wall samples, significant variability was observed. By performing chloride testing on only one concrete core sample per element, a thorough statistical comparison is unable to be performed between the two bridges, as exact values and profiles would be expected to vary from sample to sample even if obtained at similar elevations. As such, it is difficult to conclude that chloride profiles and measured contents at the bar depths are within a certain percentage; however, it

appears that the order of magnitude chloride contents is comparable between Bridge No. 700174 in 2011 and Bridge No. 700181 in 2021.

When evaluating chloride contents, 0.03 percent by weight of concrete represents a commonly accepted lower-bound chloride content required to initiate corrosion of uncoated reinforcing steel embedded in concrete (Broomfield 2007). However, several other variables, including but not limited to moisture content, oxygen availability, and concrete pH, affect the minimum accumulation of chloride content at the bar level to initiate corrosion activity. Regardless, except for strut elements, chloride contents appeared to significantly exceed this 0.03 percent by weight concrete threshold for the other three elements for both bridges. It was clear that the initiation of corrosion of the uncoated reinforcing steel within Bridge No. 700174 had begun long before 2011, as distress was significantly advanced on each of the four elements within the study area. Contrary, similar chloride contents had accumulated at or near the epoxy-coated reinforcing steel, which was only exhibiting minimal corrosion-related cracking distress in the pile caps. In other elements, only flexural cracking of the columns was observed, however, this was presumably caused by movement of the columns relative to the struts and unrelated to corrosion.

Field Investigation 3 – EB Sunrise Boulevard, WB Sunrise Boulevard, and St. Andrews Avenue Bridges

Bridge Nos. 860467 and 860466 are the eastbound and westbound routes of Sunrise Boulevard spanning over the intercoastal waterway, west of the State Road A1A, and east of SR-5 (Figure 34). The bridge substructures are similar constructions and concrete mixes, yet, a key difference is that 860467 contains a Fly Ash admixture, while Fly Ash was not used as part of the concrete mix at 860466. In addition, Bridge No. 860319 is on the eastbound and westbound route of S. Andrews Ave, spanning over New River & New River Drive, and located 0.2 miles south of Broward Blvd (Figure 35). All three bridges are currently coated with an acrylic coating. All bridges had been reinforced with epoxy-coated reinforcing steel and provided an opportunity to evaluate the effectiveness of the Fly Ash admixtures in similar construction detailing and identical exposure conditions. Marlin Engineering performed a thorough condition assessment in April 2021 and 2020, which documented visual observations and construction properties of Bridge Nos. 860467 and 860466 at ages 34 and 31, respectively. A study assessing the conditions of Bridge No. 860319 was performed on August 22, 2019, by Transystems Corporation Consultants. This assessment documented visual observations and construction properties of Bridge No. 860319 at age 38.

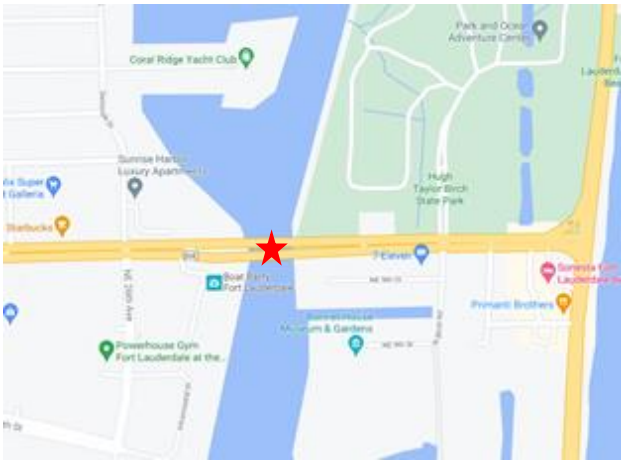

Figure 34. Location of the eastbound and westbound routes of Sunrise Blvd over the intercoastal waterway, identified by the red star (image from Google Maps©).

Figure 35. Location of the eastbound and westbound route of S. Andrews Ave, over New River & New River Drive, identified by the red star (image from Google Maps©).

Assessment Objectives and Methodology

By performing a corrosion assessment of Bridge Nos. 860467, 860466, and 860319, a comparison can be made in terms of the age of the bridge when evaluating the benefit(s) of ECR supplemented by a Fly Ash admixture in the concrete mix. Bridge No. 860467 was 34 years of age, Bridge No. 860466 was 32 years of age, and Bridge No. 860319 was 40 years of age at the time of this investigation in 2021.

This investigation was designed to assess the long-term performance and durability of epoxy-coated reinforcing steel with the use of a Fly Ash admixture in the concrete mix in similar bridges with very similar exposure conditions. In addition, by obtaining similar information for Bridge Nos. 860467 and 860466 to that obtained by Marlin Engineering in 2021 and 2020, and for Bridge No. 860319 to that obtained by

Transystems Corporation Consultants in 2019, this investigation aims to determine which of the following three variables (or a combination thereof) contribute to the variation in performance.

- Construction Geometry and Materials (concrete properties, design covers, etc.)
- Exposure Conditions
- Epoxy-coating of the reinforcing steel

To provide a comparison between the performance of the Fly Ash admixture in the concrete mix at Bridge Nos. 860467, 860466, and 860319, the research team developed a test plan to obtain similar data for side-by-side comparison purposes. As such, the following tasks comprised the field assessment. The intent was to evaluate the depth of chlorides and effects of corrosion at similar locations at Bridge No. 860467, containing Fly Ash, Bridge No. 860319, and Bridge No. 860466, which did not contain Fly Ash.

Two mobilizations were performed for this assessment. The first mobilization included a full assessment as described later in this section and included obtaining nine core samples: Cores SE1, SE2, and SE3 from Bridge No. 806466, Cores SW1, SW2, and SW3 from Bridge No. 806467, and Cores A1, A2, A3 from Bridge No. 860319. A second mobilization was scheduled to obtain four additional core samples for the primary purpose of confirming chloride diffusion profiles. These cores were identified as Cores SE4 and SE5 from Bridge No. 806466 and Cores SW4 and SW5 from Bridge No. 806467. Additional information regarding core samples and material testing is provided later in this section.

Description of Structures and Environment

The Sunrise Boulevard bridges are twin bridges spanning over the intercoastal waterway and are approximately 360 feet long. The South Andrews Avenue bridge spans over New River & New River Drive and is approximately 620 feet long. Table 41 provides general descriptions and properties of each bridge. As-built drawings were not provided or reviewed for this investigation, and therefore, exact detailing and material specifications are unknown. However, a visual comparison of bridges shows that the layout and member sizes of the eastbound and westbound Sunrise Boulevard bridges are similar, if not the same.

Table 41. Bridge Descriptions

Bridge	EB Sunrise Boulevard	WB Sunrise Boulevard	EB and WB S. Andrews Ave
Structure	Sunrise Blvd		S. Andrews Ave
Feature Crossed	Intercoastal Waterway		New River & New River Drive
County	Broward		Broward
Florida Bridge No.	860467	860466	860319
Facility Carried	EB Sunrise Boulevard	WB Sunrise Boulevard	EB and WB S. Andrews Ave.
Year Constructed	1987	1989	1981
Design Life	34	32	40
ADT	11,250	11,250	20,500
NBI Substructure Rating	7 (2018)	7 (2018)	7 (2017)
No. of Spans	5	5	13
Overall Length	361.9	361.9	621.1
Overall Width	53ft 6in	53ft 10in	53ft 3in
Roadway Width (curb-to-curb)	44ft 11in	44ft 11in	49ft 11in
Superstructure	Precast prestressed I-Beams approach spans and steel open girders for the single-leaf main span	Precast prestressed I-Beams approach spans and steel open girders for the single-leaf main span	Precast prestressed I-Beams approach spans and steel open girders for the double-leaf main span
Substructure	Five vertical piles with two batter piles on each end. Either side of the main span consists of pier walls supported by piles	Five vertical piles with two batter piles on each end. Either side of the main span consists of pier walls supported by piles	Column piers on each side, typ. two. Either side of the main span consists of bascule piers walls supported by piles

Description of Corrosion Control Systems

Epoxy-Coated Reinforcement (Bridge No. 860466, 860467, and 860319) – As mentioned in the section above, exact detailing and material specifications are unknown for the three bridges, including ECR specifications. However, laboratory evaluation of the ECR for the 860466 and 860319 bridges indicated that the coating thickness averaged between 6.7 to 12.4 mils. The results of the ECR evaluation are presented in Table 42, and the bar samples are illustrated in Figure 36. No corrosion (rated 1) was observed on three bars (A2-2, SE1-1, and SE1-2); minor corrosion (rated 2) was observed on three bars (A2-1, SE2-1, and SE2-2). The knife adhesion rating for the epoxy coating was 5 (poor adhesion as epoxy peeled from bars in 1/2inch sections) for the majority of the samples and 1 (excellent adhesion) for sample SE1-1. The backside contamination for the epoxy coating was less than 5% for four bars (A2-2, SE1-2, SE2-1, and SE2-2) and 30-40% for one bar (A2-1) as seen in Figure 37.

Table 42. Results of ECR Evaluation

Bar ID	Bar Size	Epoxy Type (Brown/Green)	Corrosion Rating (1-5)[1]	Active Corrosion?	Average Coating Thickness (mils)	Knife Adhesion Rating (1-5)[2]	Backside Contamination[3]
A2-1	#6	Green	2	Y	9.6	5	30 to 40
A2-2	#8	Green	1	N	12.4	5	≤ 5
SE1-1	#5	Green	1	N	9.2	1	N/A
SE1-2	#5	Green	1	N	6.7	5	≤ 5
SE2-1	#5	Green	2	Y	11.8	5	≤ 5
SE2-2	#5	Green	2	Y	7.6	5	≤ 5

(1) Rating 1 indicates no corrosion; Rating 5 indicates corrosion area greater than 60% of total surface area.

(2) Rating 1 indicates excellent adhesion; Rating 5 indicates poor adhesion.

(3) Backside contamination rating equals the percentage of the backside surface of peeled epoxy coating exhibiting contamination. The rating was not available in Bar SE1-1 since the epoxy coating did not peel off.

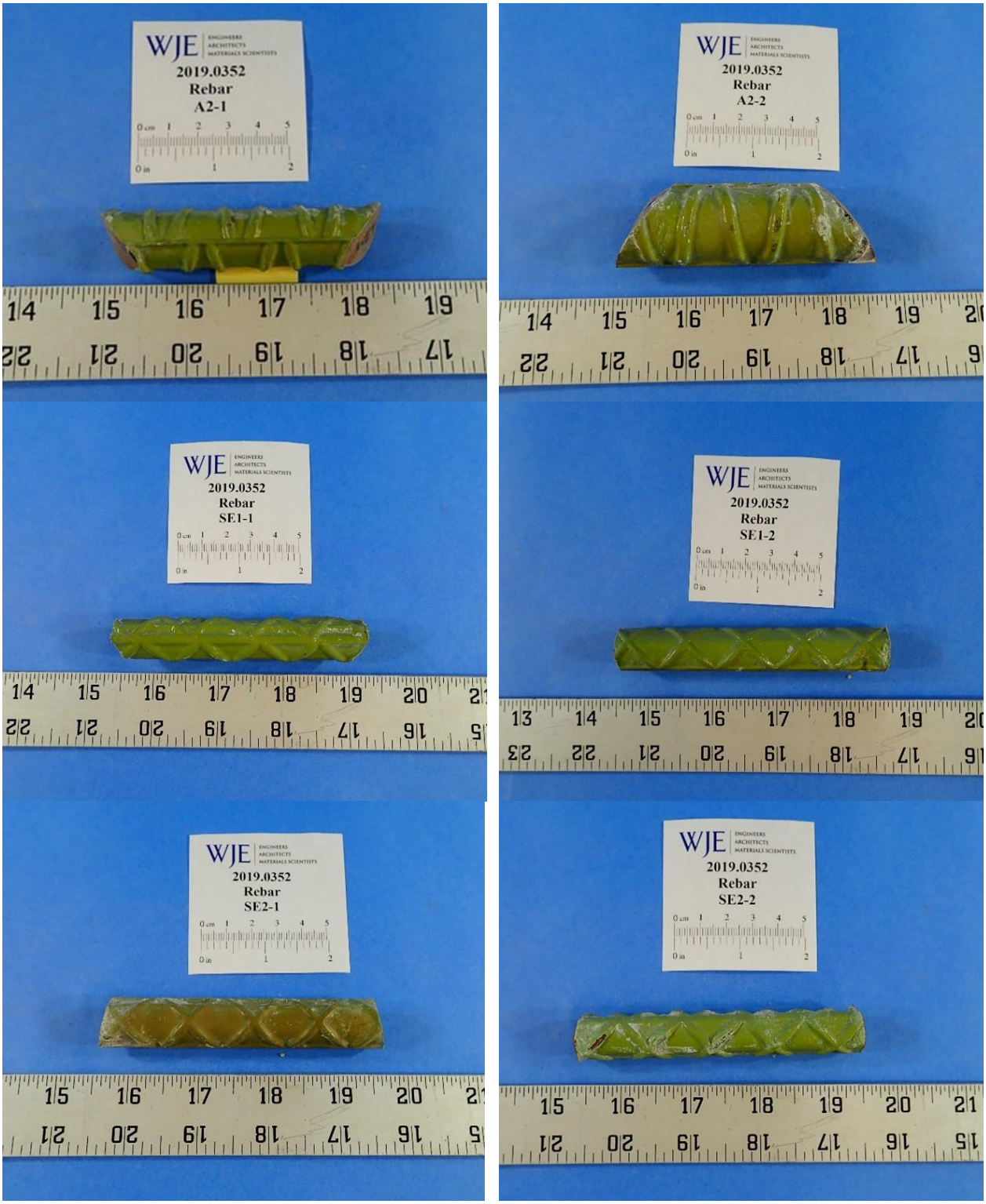

Figure 36. Photographs of evaluated ECR samples.

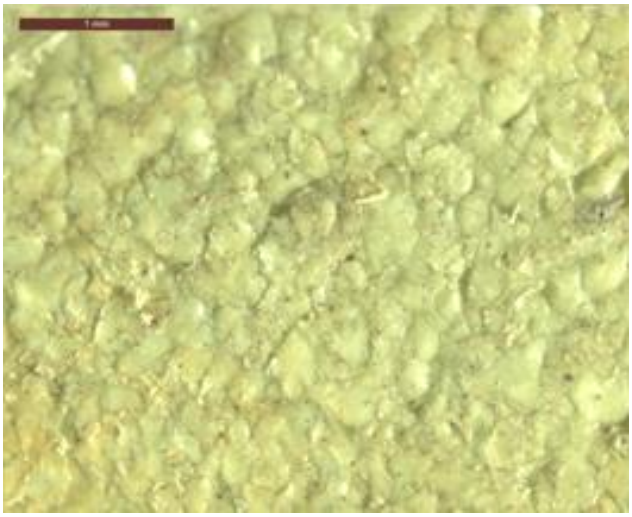

Figure 37. A2-1 30-40% Backside Contamination.

Assessment Findings

The primary goal of this investigation was to assess the long-term performance of epoxy-coated reinforcing (ECR) steel for bridges of similar construction and concrete mixes, supplemented by a Fly Ash admixture in the concrete mix. The report section presents data obtained during the research team's 2021 field investigation for Bridge Nos. 860466, 860467, and 860319, next to observations from Marlin Engineering performed in April 2021 and 2020 of Bridge Nos. 860467 and 860466, and Transystems Corporation Consultants on August 22 of Bridge No. 860319. The bridges being investigated were at similar ages at the time of their respective assessments:

- Bridge 860467 – Constructed circa 1987 (34 years old at time of 2021 assessment)
- Bridge 860466 – Constructed circa 1989 (32 years old at time of 2021 assessment)
- Bridge 860319 – Constructed circa 1981 (40 years old at time of 2021 assessment)

This section is organized by outlining assessment findings and test results in the following order. Select data and photographs are also summarized in APPENDIX F of this report.

- Construction Geometry
- Concrete Materials
- Exposure Conditions
- Visual Findings
- Corrosion Potentials
- Material Sampling and Testing

Construction Geometry - Although the exact design and specifications information regarding the construction of these bridges are not known, the concrete cover is an important variable to consider when evaluating corrosion performance. This investigation obtained cover measurements obtained by measuring bars exposed by concrete coring, drilling to bars for electrical connections, and/or ground-penetrating radar (GPR). As construction tolerances are difficult to predict for an entire element when

evaluating a localized area, ranges of measured concrete covers are provided for bars measured at the predetermined elements as part of the field investigations. Data from the 2021 investigations are provided below in Table 43.

Table 43. Measured Concrete Cover Ranges

Element	2021	
	Bridge 860466 Concrete Cover (in)	Bridge 860467 Concrete Cover (in)
Approach Pier	3.50-5.50	4.04-5.44

[1] *Measured to outermost bar, units = inch*

The average measured covers for Bridges 806466 and 806467 were 4.70in. Although exact ranges of measured concrete covers vary slightly, these ranges lead to the assumption that design covers for each element were similar between the two bridges. Although it is impossible to know the statistical distribution of concrete covers for each element between the two bridges without a comprehensive concrete cover investigation, the data provided above allows the comparison of distress between the two bridges while omitting concrete cover as a major variable.

Concrete Materials – Similar to concrete cover, concrete properties are important variables to consider when evaluating corrosion performance. To confirm similar composition and properties of concrete between Bridge Nos. 806466 and 806467, limited petrographic studies were performed on Cores SE3 and SW2. Primary findings from the petrographic examination are provided below, and Table 44 summarizes the general core characteristics. The full petrographic report can be found in APPENDIX G.

1. **Main Cracks:** None observed in either core. Microcracking is infrequent.
2. **ASR:** No evidence of alkali-silica reactions or other deleterious chemical reactions such as delayed ettringite formation (DEF) was observed in the cores.
3. **Distress Related to Seawater Exposure:** Likely minimal to absent.
4. **Reinforcement:** Core SW2 contained a No. 5 deformed, epoxy-coated steel reinforcing bar. The bar appeared to be in good condition. No radiating cracking was observed surrounding the bar. No reinforcement bars or imprints were observed in Core SE3.
5. **Carbonation:** 0.2 to 0.3 inch in Core SE3 and 0.4 to 0.5 inch in Core SW2.
6. **Concrete Condition:** Appeared to be good overall in both cores.
7. **Coating Layer:** Overall, well bonded to the substrate concrete in both cores.
8. **Major Differences Between Two Cores:** Core SE3 contains fly ash estimated at 15 to 25% of total cementitious materials. No fly ash was observed in Core SW2 based on powder mount examinations. Core SW2 contains an overall higher air content and more small air voids than Core SE3.

Table 44. General Core Characteristics and Petrographic Findings

	Core SE3	Core SW2
Dimensions	Diameter=1.5 inches; Length=7.3 inches	Diameter=3.6 inches; Length=5.0 inches
Exterior Surface	Overall flat formed/finished surface covered with a light-gray coating layer approximately 40 mils thick	Overall flat formed/finished surface covered with a light-gray coating layer that is approximately 20 mils thick
Interior Surface	Rough fractured surface extended mainly through coarse aggregate particles.	Rough fractured surface extended mainly through coarse aggregate particles. A No.5 deformed, epoxy-coated reinforcing steel bar observed on the interior surface (4-1/8 inch cover); the bar is free of rust.
Coarse Aggregate	Similar in the two cores, composed of crushed fossiliferous limestone, with a nominal top size 3/4 inch. Many particles are also arenaceous (i.e., containing quartz sand grains in the limestone).	
Fine Aggregate	Similar in the two cores; appeared to be sand manufactured from rocks similar in lithology to the coarse aggregate; consisting mainly of limestone and smaller amounts of siliceous quartz sand. Different composition from fine aggregate in Core 1 and Core 10 studied previously.	
Paste	• Portland cement and fly ash paste • Fly ash estimated 15 to 25% of total cementitious materials by mass (Figure 38) • Medium to dark gray, moderately hard to hard, and moderately low in water absorptivity.	• Portland cement paste without supplementary cementitious materials based on powder mount examination. • Medium, moderately hard to hard, and moderately low in water absorptivity.
Estimated W/C	0.39 to 0.44	0.40 to 0.45
Paste-Aggregate Bond	Interpreted to be tight in both cores	
Estimated Air Content	3 to 4%, likely air-entrained; contains both coarse and fine air voids.	4 to 6%; air-entrained; mainly small spherical air voids.
Secondary Deposits	Ettringite frequently lines air voids in both cores, consistent with exposure to moisture.	
Materials-Related Distress	None observed in either core	
Cracking/Micro cracking	Infrequent microcracking in both cores	
Overall Condition	Appeared to be good in both cores.	

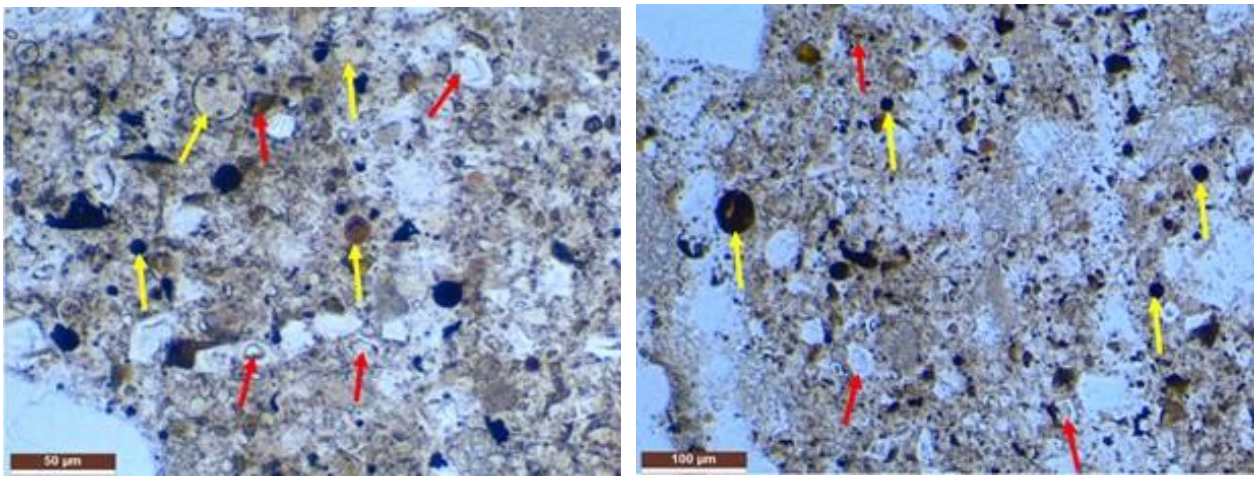

Figure 38. Core SE3. Thin section photographs show the cement paste composition and micro texture. Portland cement (red arrows) appeared to be well hydrated. Fly ash was observed (yellow arrows) and estimated at 15 to 25 percent by mass of total cementitious materials. Plane-polarized light for both.

In addition to petrographic evaluation, surface resistivity was measured on the elements selected for an in-depth assessment. Surface resistivity measurement values are summarized below in Table 45.

Table 45. Average Measured Surface Resistivity Closest to High Water Line

Element	2021		
	Bridge 860466	Bridge 860467	Bridge 860319
Approach Pier	62.1	56.8	
Rest Pier			39.2

[1] *Findings above indicates averages of between three and five individual measurements, units = kohm-cm*

As shown in Table 44, concrete properties between Bridge Nos. 860467 (Core SE3) and 860466 (Core SW2) contain similar coarse and fine aggregate constituents; however, Bridge No. 860466 contains fly ash. In addition, surface resistivity data shows similar values between Bridge Nos. 860466 and 860467, which are both higher than the resistivity measured at Bridge No. 860319. It should be noted that elevations of measurements (and associated moisture content of concrete), the orientation of measurements relative to reinforcing steel, and several other factors can contribute to variability in surface resistivity measurements. Generally, resistivity measurements taken at higher elevations result in a higher resistivity due to decreased moisture content.

The findings relating to concrete materials and physical properties confirm that Bridge Nos. 860466 and 860467 provide an opportunity to compare the effects of Fly-ash as they relate to enhancing the corrosion resistance of the concrete mixture by potentially reducing the depth of the chloride intrusion.

Exposure Conditions – Given that the physical locations of the bridges are near identical, it is assumed that the exposure conditions for the bridges are identical. Additionally, although chemistry and chloride content can change over time, it is assumed that changes over time are slow and did not provide different exposure conditions for Bridge No. 860467 in the approximately two years before the construction of

Bridge No. 860466. The research team did not perform laboratory testing of the water sample at either bridge.

Each of the three bridges was coated with an acrylic coating likely intended to provide both aesthetics and a partial barrier restricting chloride accumulation at the surface of the concrete. The research team did not receive any specifications of the existing coating or information regarding previous or scheduled maintenance efforts for review in this intestigation. To provide a broad understanding of the existing coatings at Bridge No. 860466 and Bridge No. 860319, two samples were submitted for laboratory evaluation, respectively designated SW2 and A2.

The thickness of the coating samples was evaluated using a stereomicroscope, and the generic type of polymeric binder was analyzed using Fourier transform infrared (FTIR) spectroscopy. The results are summarized below:

- The coating system for Bridge No. 860319 (A2) appeared to have two layers, a red top coat and a white base coat. The layers were consistent with a reference spectrum of styrenated acrylic copolymer. A micrograph showing the cross-section and some thickness measurements is presented in Figure 39.
  - On average the thickness of the red topcoat measured 4.2 mils. Measurements ranged from 1.7 to 7.3 mils.
  - The thickness of the white base layer averaged 42.9 mils and ranged from 33.5 to 53.8 mils.
- The coating system for Bridge No. 860466 (SW2) appeared to have only one layer consistent with a reference spectrum of styrenated acrylic copolymer. A micrograph showing the cross-section and some thickness measurements is presented in Figure 40.
  - On average the coating thickness measured 13.3 mils, and the measurements ranged from 5.4 to 20 mils.

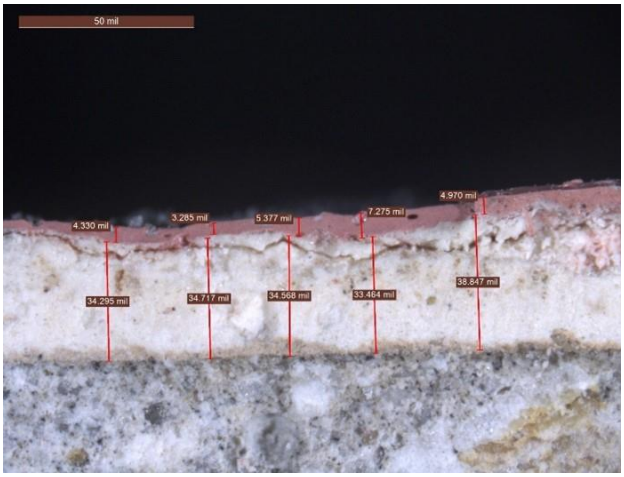

Figure 39. Micrograph of Core A2 cross-section with coating thickness measurements.

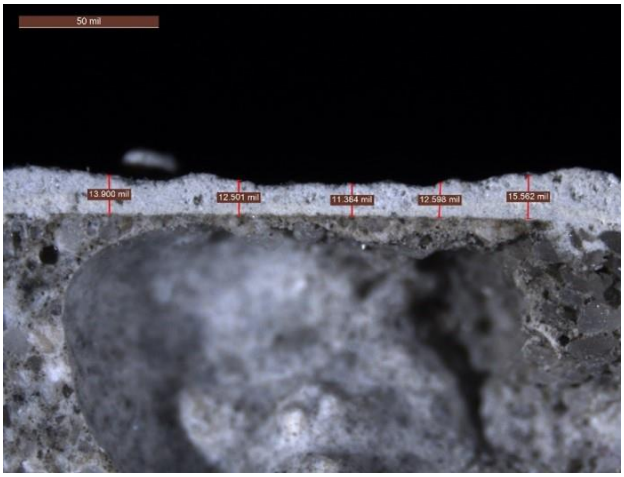

Figure 40. Micrograph of Core SW2 cross-section with coating thickness measurements.

Visual Findings - The research team conducted a visual survey of the select portions of substructure components at Bridge Nos. 860466, 860467, and 860319. No indications of cracking, spalling, or other distress were noted in the areas observed. Due to the overall intact condition of the coating, it was evident that maintenance efforts have been made to maintain the coating system..

Corrosion Potentials - Electrical connections to exposed reinforcing steel within the core holes were made to determine electrical continuity of the reinforcement prior to performing half-cell potential testing. To determine continuity, two connections were established, and the resistance between the two points was measured and recorded. At Bridge Numbers 860467 and 860319, reinforcing steel was determined to be electrically discontinuous acrossthe study area, likely due to ECR electrically isolating intersecting bars due to the non-conductive nature of the epoxy coating. As such, this must be accounted for when interpreting the HCP data.

Material Sampling and Testing – Concrete core sampling was performed on the Bridge Nos. 860466, 860467, and 860319. Material sampling was performed for two prim reasons. First, core extraction over steel bars allows for visual examination of the bars and in the case of ECR, evaluation of the epoxy coating. Secondly, concrete core extraction allows for chloride content analysis, which allows for the determination of chloride contents at variable depths from exterior surfaces and the calculation of chloride diffusion coefficients.

In order to establish chloride content profiles as a function of depth of the concrete substrate, concrete core samples were sliced to perform chloride content testing as a function of depth. Chloride testing for the 2021 study was performed in general accordance with ASTM C1152 *Standard Test Method for Acid-Soluble Chloride in Mortar and Concrete*. Slice thickness was selected to be ¼-inch for cores that were four inches in diameter (SW1, SW4, SW5, SE1, SE2, SE4, SE5, and A2) and 1/2 inch for cores that were two inches in diameter (SW3). Depth of testing was selected to adequately determine chloride content profiles as a function of depth.

Chloride concentration data is presented below in Table 46 and graphically illustrated in Figure 41.

Table 46. Acid-Soluble Chloride Contents

Core ID	Slice IDs	Average Slice Depth (in.)	Acid-Soluble Chloride, % by mass of sample
SW1	A	0.213	0.023
	B	0.439	0.037
	D	1.096	0.031
	F	1.602	0.022
	H	2.088	0.023
	J	3.593	0.025
SW3	A	0.410	0.016
	B	1.027	0.059
	C	1.644	0.055
	E	2.768	0.044
	G	3.859	0.039
SW4	A	0.275	0.009
	B	0.514	0.023
	D	1.081	0.034
	F	1.662	0.031
	H	2.170	0.026
SW5	A	0.176	0.005
	B	0.442	0.014
	D	1.005	0.020
	F	1.540	0.031
	H	2.003	0.018
SE1	A	0.292	0.149
	B	0.506	0.172
	D	1.149	0.107
	F	1.678	0.025
	H	2.207	<0.003
	J	3.540	<0.003
SE2	A	0.198	0.311
	B	0.433	0.545
	D	1.033	0.438
	F	1.583	0.272
	H	2.105	0.114
	J	3.544	0.007
SE4	A	0.235	0.005
	B	0.518	0.018
	D	1.015	0.019
	F	1.704	0.018
	H	2.218	0.018
SE5	A	0.224	0.010

Core ID	Slice IDs	Average Slice Depth (in.)	Acid-Soluble Chloride, % by mass of sample
	B	0.480	0.014
	D	1.073	0.017
	F	1.596	0.013
	H	2.132	0.011
A2	A	0.230	0.019
	B	0.449	0.023
	D	1.114	0.081
	F	1.638	0.090
	H	2.174	0.091
	J	3.594	0.056

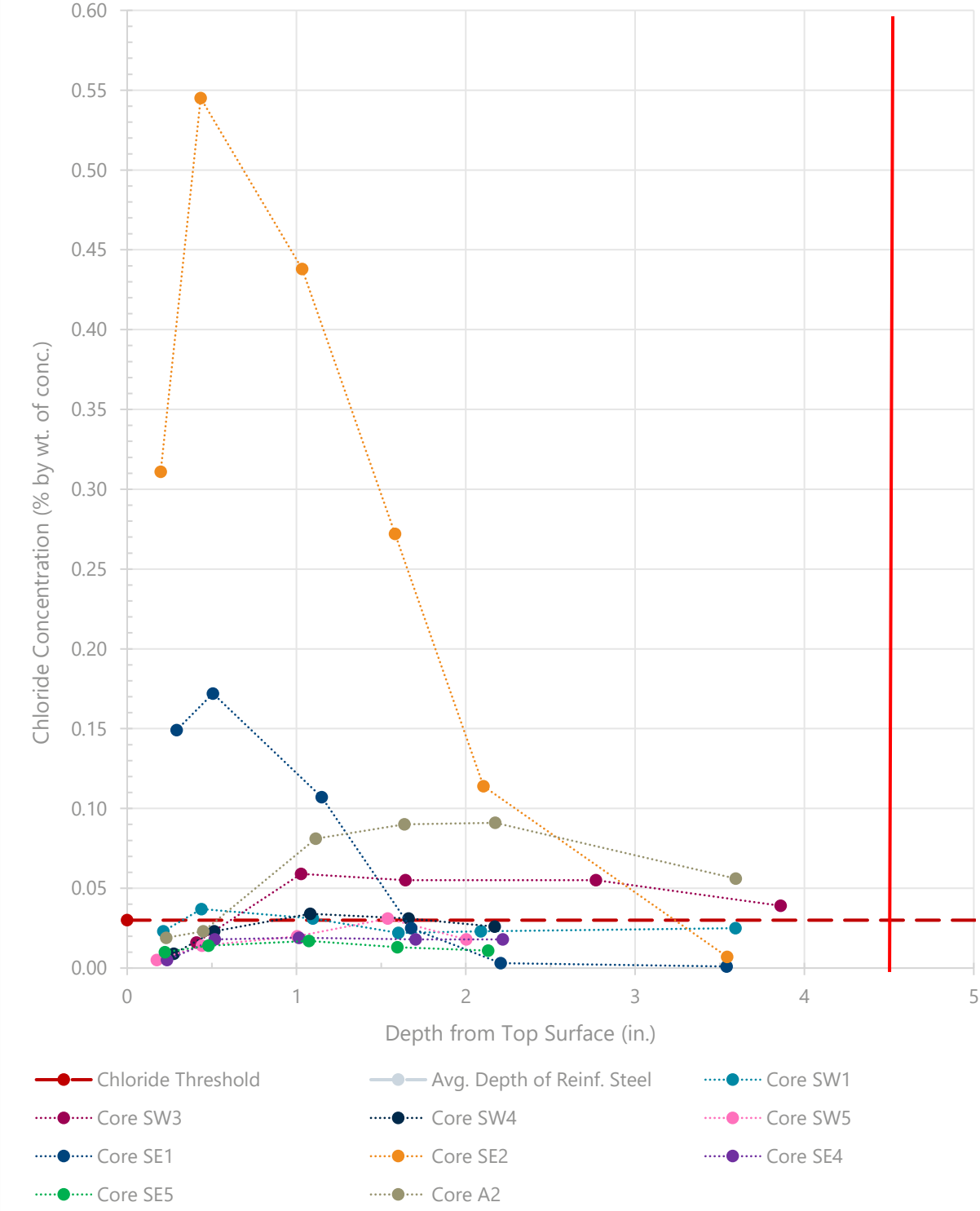

Figure 41. Chloride profiles for the core samples. Cores shown are SE1, SE2, SE4, and SE5 (Bridge No. 860467), SW1, SW3, SW4, and SW5 (Bridge No. 860466), and A2 (Bridge No. 860319). The red line indicates an approximate depth of the reinforcing steel (4.50 in.)

Chloride-related corrosion initiation is governed by the rate at which ions move through the concrete and accumulate at the bar surface. Chloride ion transport in concrete is complex; however, its commonly assumed that diffusion plays the largest role. The apparent diffusion coefficient (D_a) of the concrete was determined by fitting the acid-soluble chloride content at each depth to a model of Fick's law of diffusion. Because of the variability of surface concentrations, the fitting excluded the data point nearest to the exterior surface of the concrete. The average apparent diffusion coefficient, D_a, for Bridge No. 860467 (EB Sunrise) and Bridge No. 860466 (WB Sunrise) was calculated to be approximately $D_a \sim 10^{-9}$ cm^2/s and $D_a \sim 10^{-7}$ cm^2/s, respectively. As outlined above, chloride profiles from the initial core samples seemed non-typical in shape, which was the primary reason for the second mobilization to obtain additional data. However, the chloride profiles from the second round of cores were similar and provided a level of data verification. The diffusion coefficients did not precisely fit the data, but the order of magnitude difference can point to some level of variability in diffusion between the two bridges. Furthermore, diffusion parameters were not strongly correlated to the elevation of the concrete core specimens.

Field Investigation 4 – Bob Graham Sunshine Skyway Bridge – Trial Solar-Powered ICCP System

Bridge No. 150189, referred to herein as the "Skyway Bridge," is the northbound and southbound routes of I-275 spanning over Tampa Bay and connecting St. Petersburg with Bradenton. Limited documentation was provided for review; the most recent FDOT Inspection Report provided was from the September 2018 inspection. ICCP systems are installed on a number of substructure pier footings. However, the detailing is unknown. FDOT has replaced one traditional ICCP rectifier with solar panels to power the ICCP system on a trial basis. The primary long-term intent of this power-source swap was to save on installation costs (refer to the Costs of Installed CP section of this report). However, the long-term performance and limitations of solar-powered ICCP systems are largely unknown.

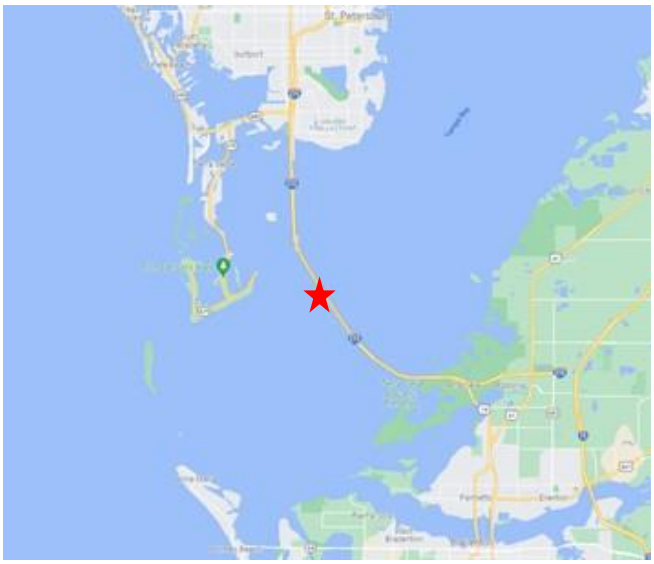

Figure 42. Location of the Skyway over Tampa Bay, identified by the red star (image from Google Maps©).

Assessment Objectives and Methodology

Installation of an alternate power source for an ICCP system on a trial basis allows FDOT to accumulate and evaluate the system prior to widespread implementation. As such, the primary intent of this assessment is to evaluate the overall performance of the solar-powered system with respect to industry-defined performance guidelines and determine system limitations.

- Assess the long-term performance of solar-powered ICCP systems for footing repair/rehabilitation in marine exposures.
  - Evaluate the electrochemical performance of the trial solar-powered ICCP system using remote monitoring unit (RMU) data.
  - Perform a manual hard reset and disconnect system to measure depolarization over a multi-day period for a typical bent and bent, including a solar-powered ICCP system.
  - Consider functionality and installation methods for solar panels.

The time frame for which data was evaluated was over an approximately 3-week period, spanning between October 1 to 20, 2021. The system was disconnected entirely on October 11, 2021, to allow the system to depolarize and was not re-energized until October 14, 2021, allowing approximately 72 hours for depolarization.

Description of Structures and Environment

The Skyway Bridge spans over Tampa Bay and is approximately 22,000 feet long. The bridge consists of five individual units and unit keys: main spans (0), south trestle approach spans (1), south high-level approach spans (2), north high-level approach spans (3), and the north trestle approach spans (4). The bridge unit included in this assessment was the substructure of the main span, which consists of piles

capped with pier footings and columns, both of which are reinforced with ECR. Table 47 provides general descriptions and properties of the main span as listed in the 2018 inspection report. As-built drawings were not provided or reviewed for this investigation, and therefore, exact detailing and material specifications are unknown.

Table 47. Bridge Description

Bridge	Skyway Bridge
Structure	Bob Graham Sunshine Skyway Bridge
Feature Crossed	Tampa Bay
County	Pinellas
Florida Bridge No. / Unit Key	150189 0
Facility Carried	I-275 (SR 93)
Year Constructed	1986
Design Life	Unknown
ADT	62,157
NBI Substructure Rating	7
No. of Spans	11 (Main Unit), 177 (Total)
Overall Length	21,917ft
Overall Width	95ft 3in
Roadway Width (curb-to-curb)	95ft 3in
Superstructure	Precast, post-tensioned, cable-stayed, segmental box girder
Substructure	Column piers on each side, typ. two. Either side of the main span consists of bascule piers walls supported by piles

Description of Impressed Current Corrosion Control Systems

Impressed current CP system jackets are installed on select pier footings and columns on the main span bents. No additional information was provided regarding the age or detailing of the systems. However, FDOT indicated the jackets are titanium mesh ICCP systems, and the detailing is similar to the systems installed on the Gandy and HF bridges previously described in this report.

At Pier 116 of the main span, FDOT has replaced the previous traditional rectifier with six 1.5V-0.5A solar panels installed on the underside of the box girder (Figure 43), three of which are installed in series to provide DC power for the Zone 1 (pier footing) and Zone 2 (piles) systems. Two embedded silver-silver chloride reference electrodes are installed in each zone at the north and the south sides (referred to as North Upper and South Upper in Zone 1 and North Lower and South Lower in Zone 2). Remote monitoring units are utilized at Pier 116 to monitor potentials of the embedded reference electrodes, as well as voltage. Reportedly, current outputs for each zone are in the 0.2 to 1.5A range; however, monitoring data shows 0A

for all data, likely due to to precision limitations of the monitoring equipment. RMUs typically recorded potentials every 2 hours; however, a review of the data showed some inconsistencies regarding reading intervals. In most cases, isolated readings appeared to be missing based on the assumed 2-hour interval; however, potential data from the North Lower (Zone 2) was inconsistent, and on certain days, only one reading was obtained. Therefore, Zone 2 North Lower data is presented below but omitted from thorough analysis.

For comparative purposes, limited electrochemical data was obtained from Pier 115 while on-site, which consisted of a typical ICCP system including an AC-to-DC rectifier. An RMU was not installed on this bent, so long-term data was unavailable.

Figure 43. Overview of solar panels epoxied to the underside of the box girder (photograph provided by FDOT).

Assessment Findings

The primary goal of this field investigation was to assess the overall performance of the trial solar panel-powered ICCP system. In order to perform the assessment, the obtained electrochemical data was split into two separate time frames:

- October 1 through 10 and October 15 through 19, 2021: Typical ICCP system operation
- October 11 through 14, 2021: System disconnected to allow depolarization

Data obtained and stored using the remote monitoring unit was processed to observe general performance data and trends. Plotted RMU data showing output voltages and measured potentials for embedded reference cells during the evaluated time frame are provided in Figure 44 and Figure 45, respectively.

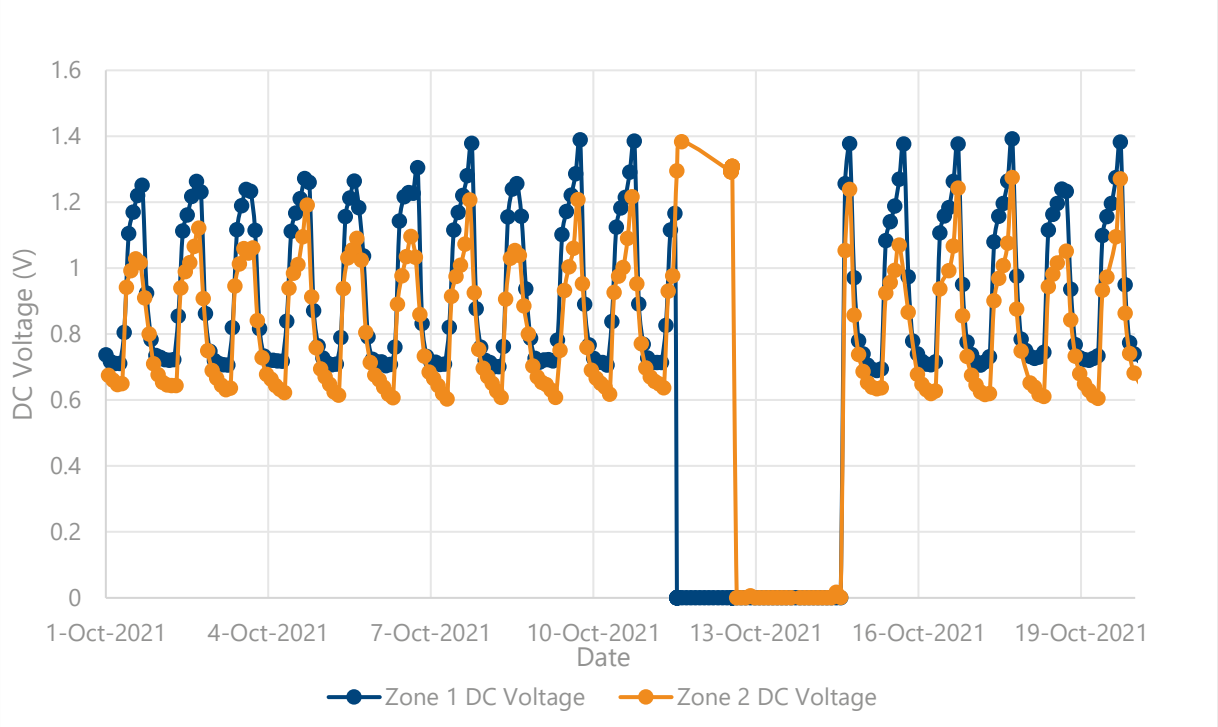

Figure 44. Measured output DC voltage data from RMU.

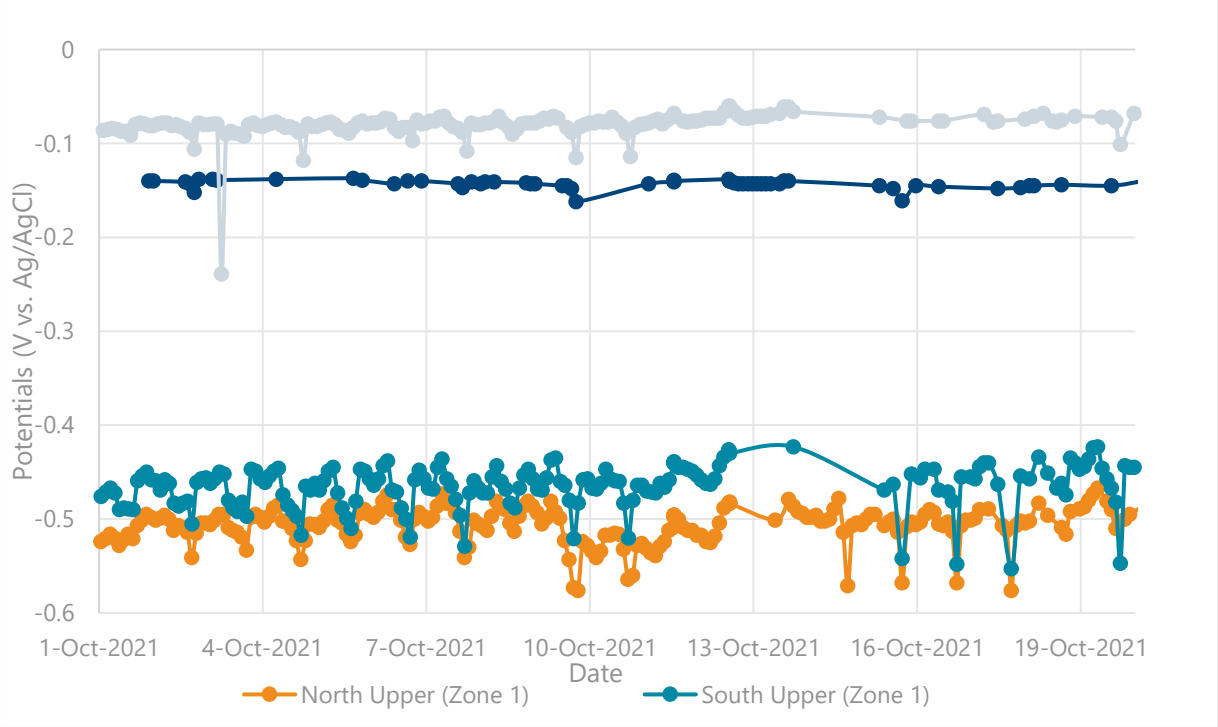

Figure 45. Measured potential data from RMU for Zone 1 and Zone 2.

Review of data showed that output voltages dropped between 0.6 and 0.8 volts overnight, presumably as a result of lack of sunlight exposure to the solar panels reducing current output. Furthermore, recorded potentials typically shifted more positive during similar time frames, particularly for the Zone 1 (Upper) system primarily above the water line. While potentials in reinforced concrete structures in marine environments may shift dependent on environmental factors (tidal conditions, temperature, etc.), the consistent positive shift during the night hours provides significant evidence that the reduced current output of the solar panels does affect potentials of the structure and associated level of cathodic protection.

Further evaluation of the Pier 116, Zone 1 potential data is provided below in Table 48, which provides minimum and maximum "On" potentials during typical operation, the average daily shift in potentials, the decay measurement after manual disconnection of the system, and average depolarization in compared to the daily range of potentials.

Table 48. Summary of Pier 116 RMU Data during Investigation Time Frame

Zone	Avg. Min. "On" Potential	Avg. Max. "On" Potential	Avg. Daily Potential Shift	"Off" Potential	Avg. Depolarization vs. Min. Potential	Avg. Depolarization vs. Max. Potential
1 North	-540	-486	54	-466	74	20
1 South	-515	-441	74	-421	94	20
2 South [1]	-103	-72	31	-60	43	12

Units: Potentials = mV vs. SCE, Depolarization = mV

[1] Readings from the Zone 2 North RMU were obtained at inconsistent frequencies and are omitted from this evaluation

Depolarization measurements vary depending on the exact timing of the obtained "On" potential measurements; however, in no case did the calculated depolarization exceed 100mV. As multiple variables may affect the measured potentials during the "On" measurements, it is difficult to pinpoint exact causations for not achieving the 100mV depolarization compared to even the minimum potential measurements.

In addition to data provided by the RMUs, manual data was obtained while the ICCP systems were turned off and after re-energizing the systems, which is summarized in Table 49. These measurements were to verify readings from the RMU (at Pier 116 only) and obtain real-time measurements not associated with the predetermined time intervals that the RMU obtained measurements. These discrete measurements allow for a direct calculation of polarization after energization as opposed to average, aggregate values presented in the table above.

Table 49. Summary of Manually-Obtained Electrochemical Measurements

Pier	Zone	"Off" Potential	"On" Potential	Calculated Polarization	Output Voltage	Output Current
115	1 North	-409	-762	353	1.27	0.56
	1 South	-440	-923	483		
	2 North	-122	-613	491	1.48	0.33
	2 South	-183	-670	487		
116	1 North	-508	-528	20	1.20	0.29
	1 South	-458	-483	25		
	2 North	-172	-186	14	1.02	0.23
	2 South	-90	-118	28		

Units: Potentials = mV vs. SCE, Depolarization = mV, Voltage = V, Current = A

The manually-obtained data shows a wide discrepancy of calculated polarizations between Piers 115 and 116, with values at both zones of Pier 115 exceeding a 350mV polarization. Measured polarization for both zones of Pier 116 did not exceed 30mV, which slightly exceeded values from RMU data when comparing the maximum daily potentials with the "Off" potentials. In this case, both sets of data are indicative that the as-installed solar-powered system does not provide equal cathodic protection as the typical rectifier-powered ICCP systems. Furthermore, average voltages and current outputs also significantly varied, however, not by the order of magnitude as the polarization measurements. Output voltages and currents at Pier 115 exceeded Pier 116 by an average of approximately 19 and 42 percent, respectively.

4. REVIEW OF FDOT CORROSION PREVENTION AND CONTROL PROGRAMS

The following subsections include the evaluation of various bridge inspection records and publicly available data to evaluate various corrosion protection components and associated bridge inventory, maintenance, and rehabilitation considerations. Three main tasks were performed as part of this review, including:

- A simplified cost assessment of CP systems related to the bridge substructure elements.
- An evaluation of damage progressions and other trends for bridge substructures that use various construction materials and/or practices to reduce corrosion (but without dedicated CP systems)
- An evaluation of damage progressions and other trends for bridges with CP systems installed on the substructures.

More information for each of these tasks is provided in the sections below.

Costs of Installed CP

Historical cost information for commonly used CP systems, publicly available through FDOT records, was evaluated from 2016 to 2020. A five-year period was evaluated to ensure a sufficient number of projects were included and allowed for comparison in cost changes over multiple years. Unit price cost data was plotted as a function of time for select items associated with the following CP systems:

- ICCP Systems with Titanium Mesh (Figure 46)
- Galvanic CP System with Zinc Aluminum Spray (Figure 47)
- Galvanic CP System with Zinc Anode Assemblies (Figure 48)
- Galvanic CP Integral Pile Jackets (Figure 49)

Cost information summarized in this section is limited to that provided by FDOT and did not incorporate additional cost data from other DOTs or outside sources. Pay items are restricted to commonly installed systems/elements utilized in Florida. Based on the provided information, no cost data was available to evaluate the benefit of ECR. FDOT has not specified ECR for many years, and as such, cost information is unavailable for a recent cost analysis when comparing to black bar.

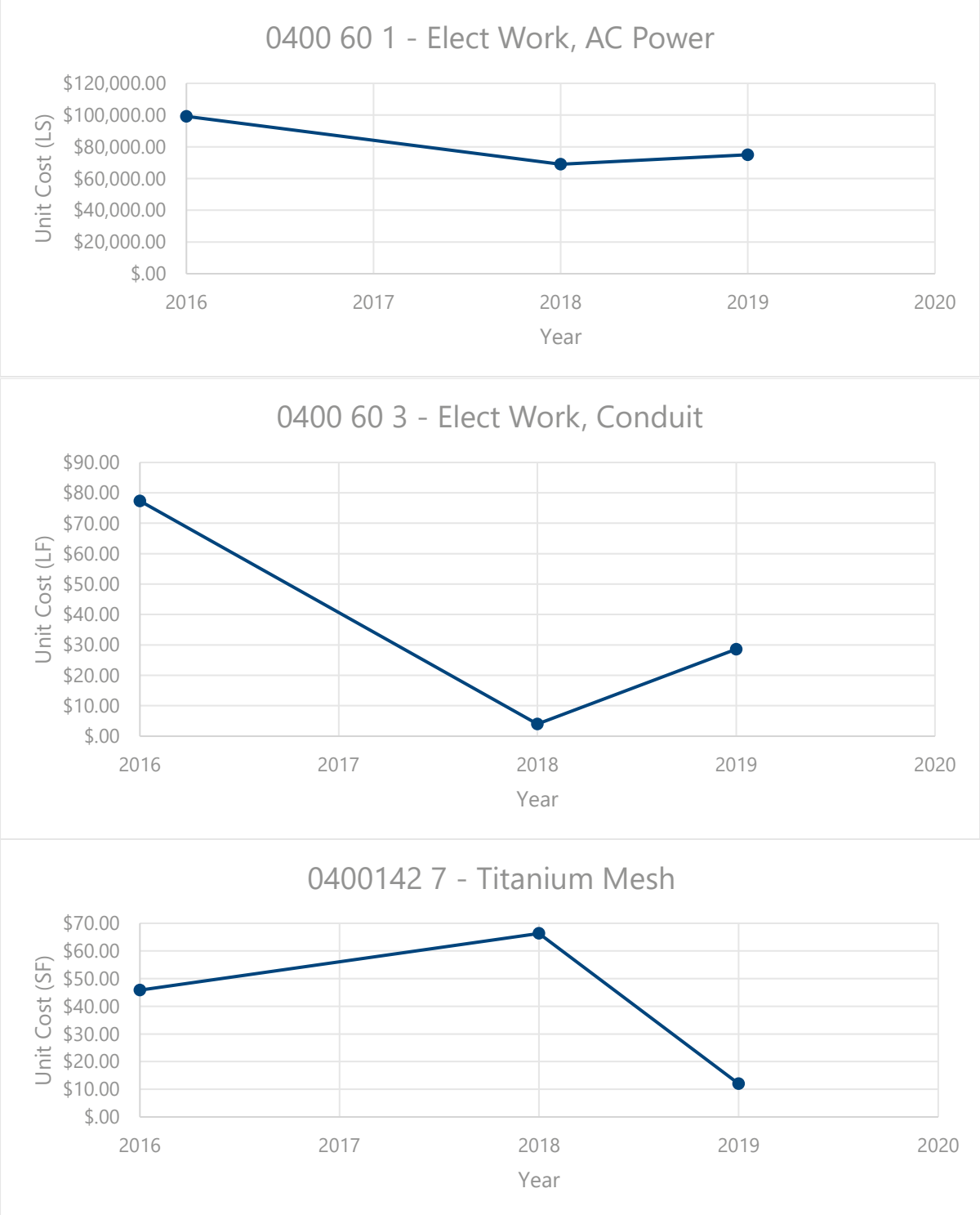

Figure 46. Average statewide costs for CP Systems with Titanium Mesh – Impressed Current Systems. Top, middle, and bottom plots show Electrical Work (Item 0400 60 1), Conduit (Item 0400 60 3), and Titanium Mesh (Item 0400142 7), respectively.

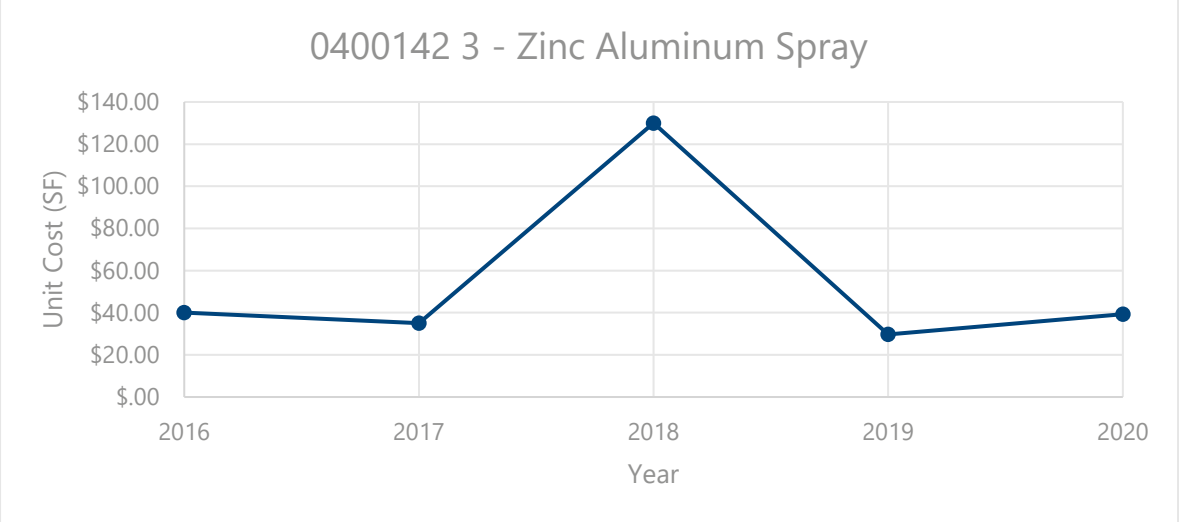

Figure 47. Average statewide costs for CP Systems with Zinc Aluminum Spray – Galvanic Arc-Spray Metalizing Systems. Zinc Aluminum Spray (Item 0400142 3) shown.

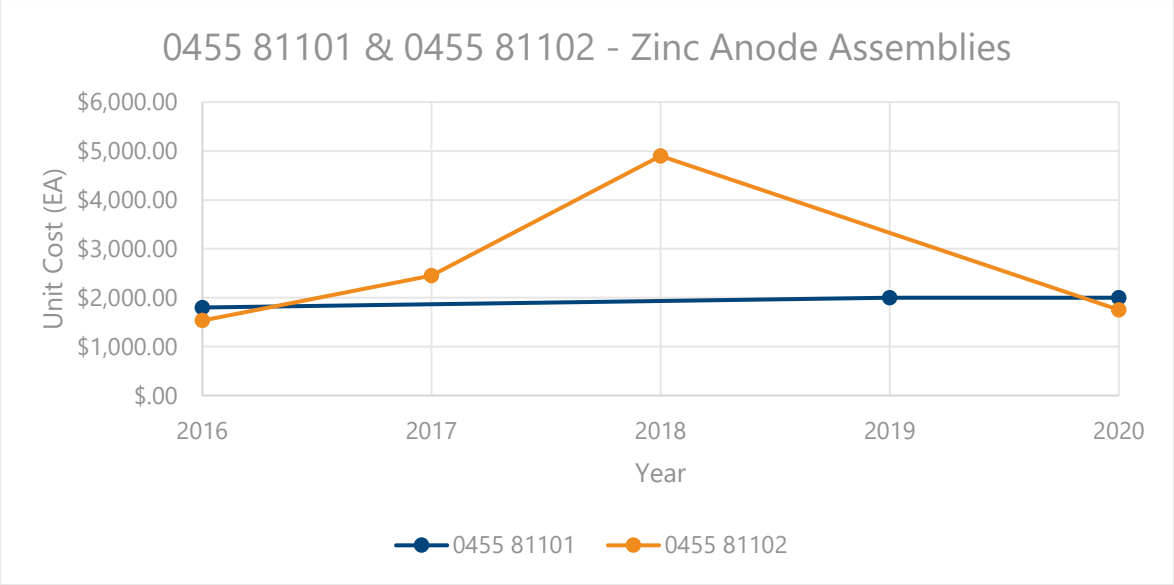

Figure 48. Average statewide costs for CP Systems with Zinc Anode Assemblies – Galvanic Systems. Pile Zinc Anode Assemblies (Item 0455 81101) and Pier Zinc Anode Assemblies (Item 0455 81102) shown.

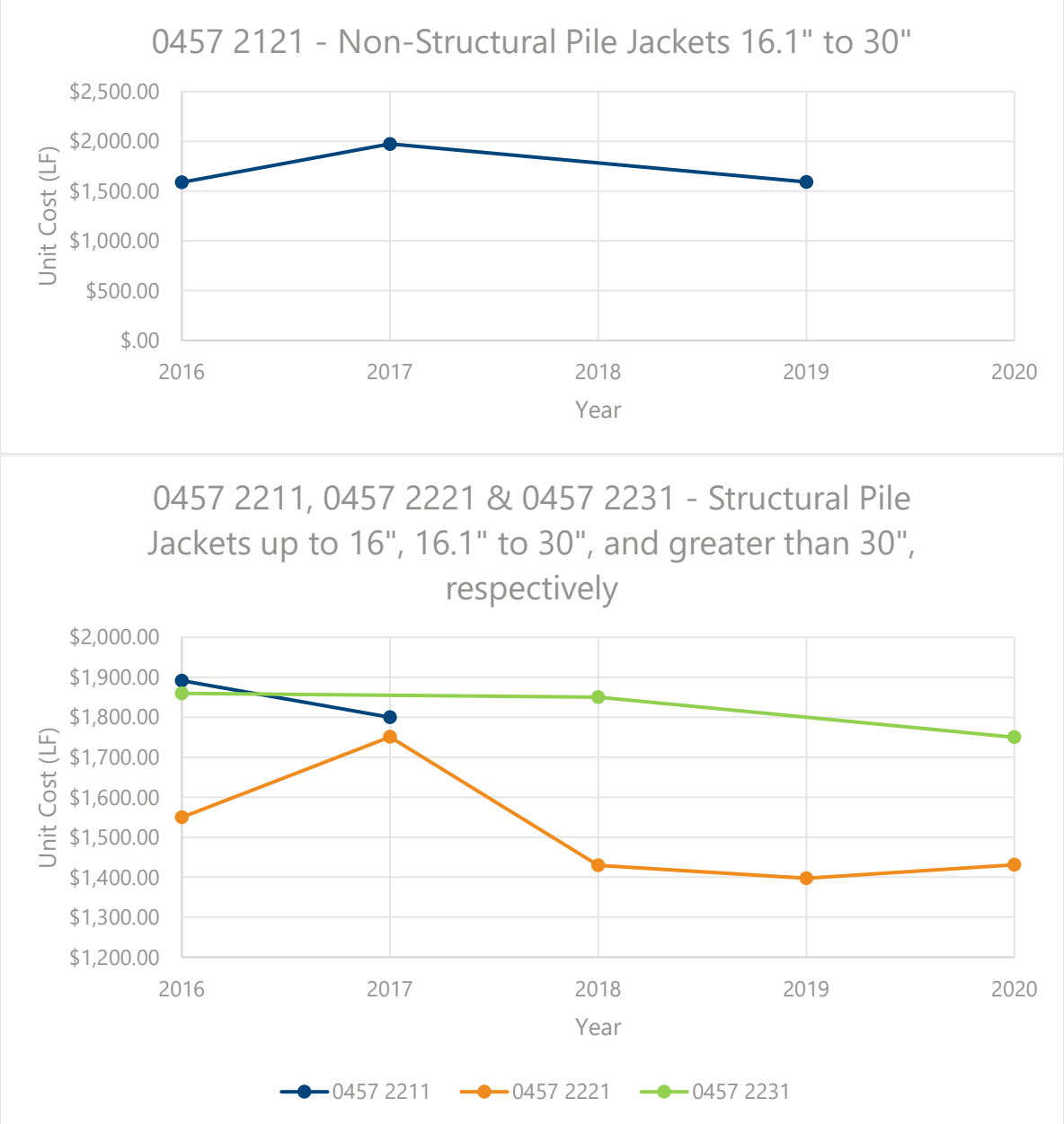

Figure 49. Average statewide costs for CP Integral Pile Jackets – Galvanic Systems. Top and bottom plots show Non-Structural Pile Jackets 16.1" to 30" (Item 0457 2121) and Structural Pile Jackets up to 16" (0457 2211), 16.1" to 30" (0457 2221), and greater than 30" (Item 0457 2231) shown, respectively.

Furthermore, Table 50 and Table 51 provide annual tabulated and average cost data for applicable pay items between 2016 and 2020, respectively.

Table 50. Tabulated Costs for Select Pay Items Statewide (2016 – 2020)

Item	Year	No. of Counts	Weighted Average	Total Quantity	Unit Meas.	Description
0400 60 1	2016	3	$99,179.84 $396,719.35	4.00	LS	Cathodic protection-elect work, AC power
	2018	1	$69,000.00	1.00	LS	Cathodic protection-elect work, AC power
	2019	1	$75,000.00	1.00	LS	Cathodic protection-elect work, AC power
0400 60 3	2016	4	$77.35 $834,149.02	10,784.00	LF	Cathodic protection-elect work, conduit
	2018	1	$4.01 $91,841.03	22,903.00	LF	Cathodic protection-elect work, conduit
	2019	1	$28.57 $79,996.00	2,800.00	LF	Cathodic protection-elect work, conduit
0400142 7	2016	3	$45.83 $2,357,287.05	51,438.00	SF	Cathodic protection system, titanium mesh
	2018	1	$66.32 $182,711.60	2,755.00	SF	Cathodic protection system, titanium mesh
	2019	1	$12.00	7,888.00	SF	Cathodic protection system, titanium mesh
0400142 3	2016	5	$40.06 $4,573,745.00	114,178.00	SF	Cathodic protection system, zinc aluminum spray
	2017	1	$35.00	2,628.00	SF	Cathodic protection system, zinc aluminum spray
	2018	1	$130.00 $1,244,360.00	9,572.00	SF	Cathodic protection system, zinc aluminum spray
	2019	3	$29.70 $650,879.50	21,917.00	SF	Cathodic protection system, zinc aluminum spray
	2020	3	$39.25 $762,085.00	19,417.00	SF	Cathodic protection system, zinc aluminum spray
0455 81101	2016	1	$1,800.00	5.00	EA	Cathodic protection, F&I, pile, zinc anode assembly
	2019	1	$2,000.00	12.00	EA	Cathodic protection, F&I, pile, zinc anode assembly
	2020	1	$2,000.00	1.00	EA	Cathodic protection, F&I, pile, zinc anode assembly
0455 81102	2016	3	$1,533.43 $272,950.00	178.00	EA	Cathodic protection, F&I, pile, zinc anode assembly
	2017	1	$2,450.00	18.00	EA	Cathodic protection, F&I, pile, zinc anode assembly
	2018	1	$4,900.00	62.00	EA	Cathodic protection, F&I, pile, zinc anode assembly

Item	Year	No. of Counts	Weighted Average	Total Quantity	Unit Meas.	Description
	2020	1	$1,750.00	128.00	EA	Cathodic protection, F&I, pile, zinc anode assembly
0457 2121	2016	3	$1,589.07 $417,925.00	263.00	LF	Non-structural cathodic protection integral pile jackets (16.1"-30")
	2017	1	$1,975.00	66.00	LF	Non-structural cathodic protection integral pile jackets (16.1"-30")
	2019	3	$1,591.55 $565,000.00	355.00	LF	Non-structural cathodic protection integral pile jackets (16.1"-30")
0457 2211	2016	2	$1,891.57 $673,400.00	356.00	LF	Structural cathodic protection integral pile jackets (up to 16")
	2017	1	$1,800.00	59.00	LF	Structural cathodic protection integral pile jackets (up to 16")
0457 2221	2016	7	$1,549.55 $1,327,960.30	857.00	LF	Structural cathodic protection integral pile jackets (16.1"-30")
	2017	3	$1,750.81 $661,805.00	378.00	LF	Structural cathodic protection integral pile jackets (16.1"-30")
	2018	5	$1,429.56 $3,864,112.00	2,703.00	LF	Structural cathodic protection integral pile jackets (16.1"-30")
	2019	6	$1,397.50 $1,846,100.00	1,321.00	LF	Structural cathodic protection integral pile jackets (16.1"-30")
	2020	5	$1,430.83 $2,810,144.00	1,964.00	LF	Structural cathodic protection integral pile jackets (16.1"-30")
0457 2231	2016	2	$1,859.80 $1,119,600.00	602.00	LF	Structural cathodic protection integral pile jackets (greater than 30")
	2018	1	$1,850.00	189.00	LF	Structural cathodic protection integral pile jackets (greater than 30")
	2020	1	$1,750.00	630.00	LF	Structural cathodic protection integral pile jackets (greater than 30")

Table 51. Average Costs for Select Pay Items Statewide (2016 – 2020)

Item	No. of Counts	Weighted Average	Total Quantity	Unit Meas	Description
0400 60 1	5	$90,119.89	6.00	LS	Cathodic protection-elect work, AC power
0400 60 3	6	$27.57	36,487.00	LF	Cathodic protection-elect work, conduit
0400142 7	5	$42.44	62,081.00	SF	Cathodic protection system, titanium mesh
0400142 3	13	$43.67	167,712.00	SF	Cathodic protection system, zinc aluminum spray
0455 81101	3	$1,944.44	18.00	EA	Cathodic protection, F&I, pile, zinc anode assembly
0455 81102	6	$2,188.73	386.00	EA	Cathodic protection, F&I, pile, zinc anode assembly
0457 2121	7	$1,627.60	684.00	LF	Non-structural cathodic protection integral pile jackets (16.1"-30")
0457 2211	3	$1,878.55	415.00	LF	Structural cathodic protection integral pile jackets (up to 16")
0457 2221	26	$1,455.09	7,223.00	LF	Structural cathodic protection integral pile jackets (16.1"-30")
0457 2231	4	$1,809.82	1,421.00	LF	Structural cathodic protection integral pile jackets (greater than 30")

Although mobilization costs are omitted from this cost analysis, rough estimates of ICCP footing jackets, metalizing spray, and galvanic CP pile jackets can be estimated.

ICCP footing jackets – A large portion of the cost of the ICCP footing installations is electrical work to provide AC power input to the rectifiers, which is bid on a lump-sum basis. Additionally, a conduit is required to route the electrical wiring through to provide the power, which is bid as a linear foot bid item, which will change cost based on the geometric properties of the bridge. Titanium mesh is bid as a square-foot bid item, which will change cost dependent on the size of the footings. Additional costs, such as reinforcing steel (for jackets with supplemental reinforcing steel) and concrete, are small compared to the above items and omitted from the tabulation; however, they will need to be included in total cost estimates for system installation. As costs for the jacket itself is likely not to change unless material costs change, FDOT could investigate alternate sources of power to the systems to lessen the amount of electrical work required to power the systems (e.g., solar power). In summary, the average cost over the past five years for the electrical work, conduit, and titanium mesh are approximately $90,100/LS, $28/LF, and $42/SF.

Metalizing Spray – Arc-spray zinc aluminum appears to be the most used metalizing spray across the state and is generally bid as a square-foot bid item. The average cost over the past five years was tabulated to be just under $44/SF.

CP Pile Jackets – Costs of pile jackets slightly varied as a function of size and quantity to be installed per mobilization, as unit costs for given sizes appeared to be less when more linear feet were to be installed (as expected). As such, it may be beneficial for the state to perform cost analyses for larger bridges that may require multiple rehabilitation efforts over their life span. Assigning installation of CP pile jackets more conservatively will increase the total cost of a given rehabilitation project; however, it may reduce the unit cost of installation of the jackets and minimize the number of rehabilitation projects over the life span (and associated mobilization costs). In summary, the average cost over the past five years was

tabulated to be approximately $1,630/LF for non-structural CP pile jackets (16.1 – 30 in.) and $1,880/LF, $1,460/LF, and $1,810/LF for structural CP pile jackets (16 in. and less, 16.1 to 30 in., and greater than 30 in., respectively. Additionally, the installation of submerged zinc anodes to supplement the CP pile jackets is not included in the base cost of CP pile jackets and would add an additional unit cost between $1,960 and $2,190/EA.

Damage Analysis of Structures without CP

In an effort to evaluate the performance of various implemented corrosion prevention techniques and construction practices, elemental data from select bridges is presented below as a function of age and construction practices. As information regarding construction practices and materials is not readily available for bridges throughout the state, data was used from 20 bridges for which age and construction material/practice is known. Furthermore, because of the limitations of available data, only the four following categories were differentiated for data comparison:

- Fly ash (FA), ECR (3 bridges)
- FA, black bar reinforcement (5 bridges)
- No FA, ECR (9 bridges)
- No FA, black bar reinforcement (3 bridges)

Table 52 below presents the bridges selected for this analysis, including their year of construction and construction materials/practice.

Table 52. Bridge List for Elemental Data Comparison

Bridge Name	Bridge Number	Year Constructed	FA?	ECR?
Brooks	570034	1964	No	No
Dames Point	720518	1989	No	No
New Smyrna	790152	1990	No	No
Sunshine Skyway	150189	1986	Yes	No
Safety Harbor	150202	1990	Yes	No
Courtney Campbell Cswy	150138	1992	Yes	No
Bay Side	154259	1993	Yes	No
McArthur Cswy	870772	1995	Yes	No
Niles Channel	900117	1980	No	Yes
Indian Key	900095	1981	No	Yes
NB Vaca Cut	900126	1981	No	Yes
S Andrews Ave[1]	860319	1981	No	Yes
Snake Creek	900077	1981	No	Yes
Channel 5	900098	1982	No	Yes
Long Key	900094	1982	No	Yes
Ernest Kouwen Hoven[1]	700181	1985	No	Yes
WB Sunrise Boulevard[1]	860466	1989	No	Yes
Lillian	480140	1981	Yes	Yes
EB Sunrise Boulevard[1]	860467	1987	Yes	Yes
Howard Frankland	150210	1991	Yes	Yes

[1] *Indicates bridge for which the most recent BIR was provided*

In order to quantify the amount of failed corrosion repairs and the effect of the failed repairs on the service life of select bridges, data was mined from publicly available National Bridge Institute (NBI) element data published by the FHWA. Figure 50, Figure 51, Figure 52, and Figure 53 below provide a statistical comparison of elemental distress as a function of bridge age and construction practice for columns (Element Number [EN] = 205), pile caps/footings (EN = 220), piles (EN = 226), and pier caps (EN = 234), respectively.

Although very limited data was provided and included in this analysis, general trends observed in these plots include the following:

- Columns and pier caps with FA and ECR showed less distress than that without FA and ECR.
- Pile caps/footings and piles with FA and ECR showed higher distress than that without FA and ECR.
- Columns, pile caps/footings, and pier caps with FA and without ECR showed less distress than that without FA and with ECR.
- Piles with FA and without ECR showed higher distress than that without FA and with ECR.
- Columns and pier caps with FA showed less distress than that without FA.
- Piles with FA showed higher distress than that without FA.

- Pile caps/footings with FA showed similar distress to that without FA.
- Columns with ECR showed less distress than that without ECR.
- Pile caps/footings, piles, and pier caps with ECR showed higher distress than that without ECR.

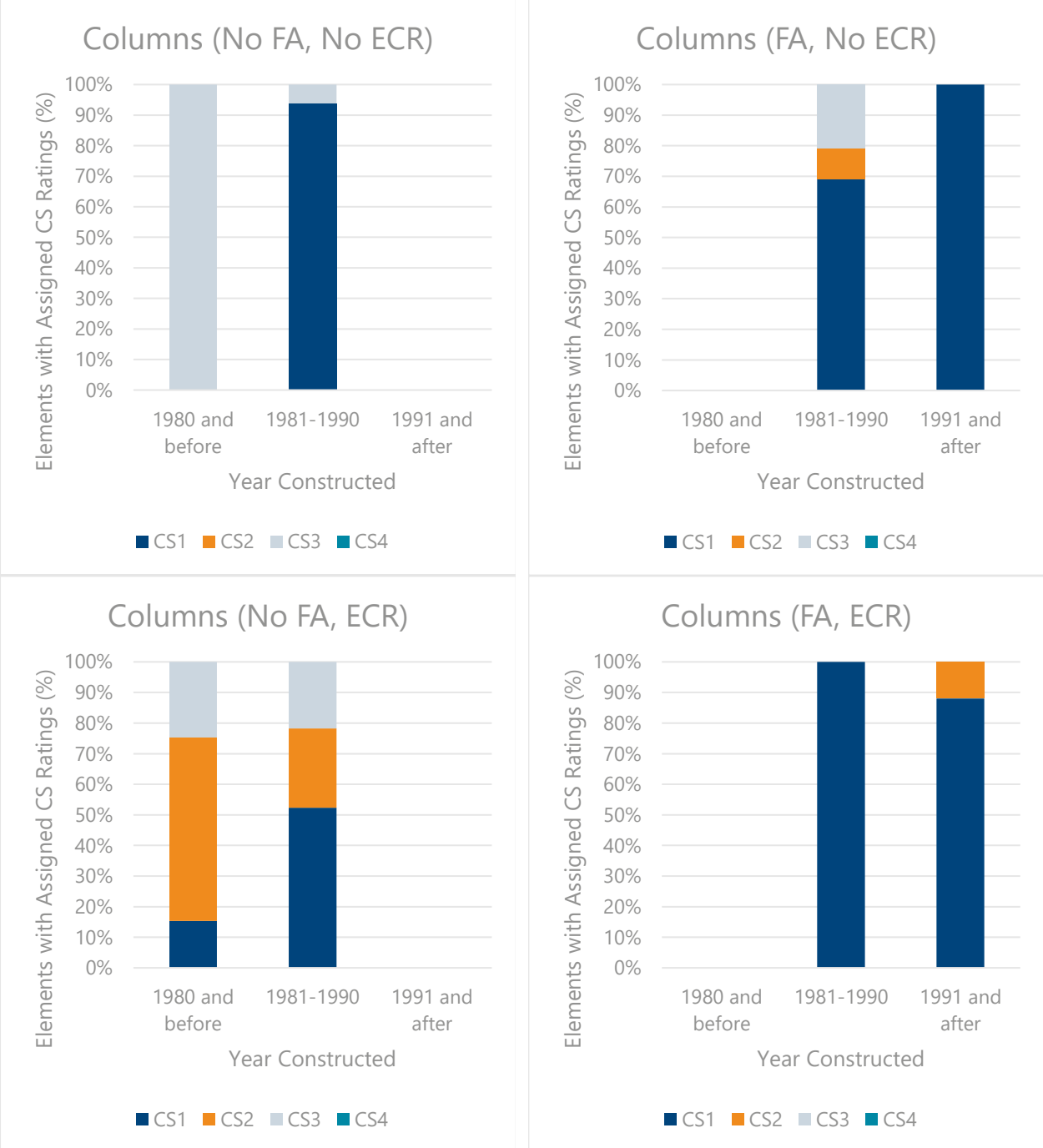

Figure 50. Statistical comparison of elemental distress as a function of bridge age and construction materials for column elements (EN = 205).

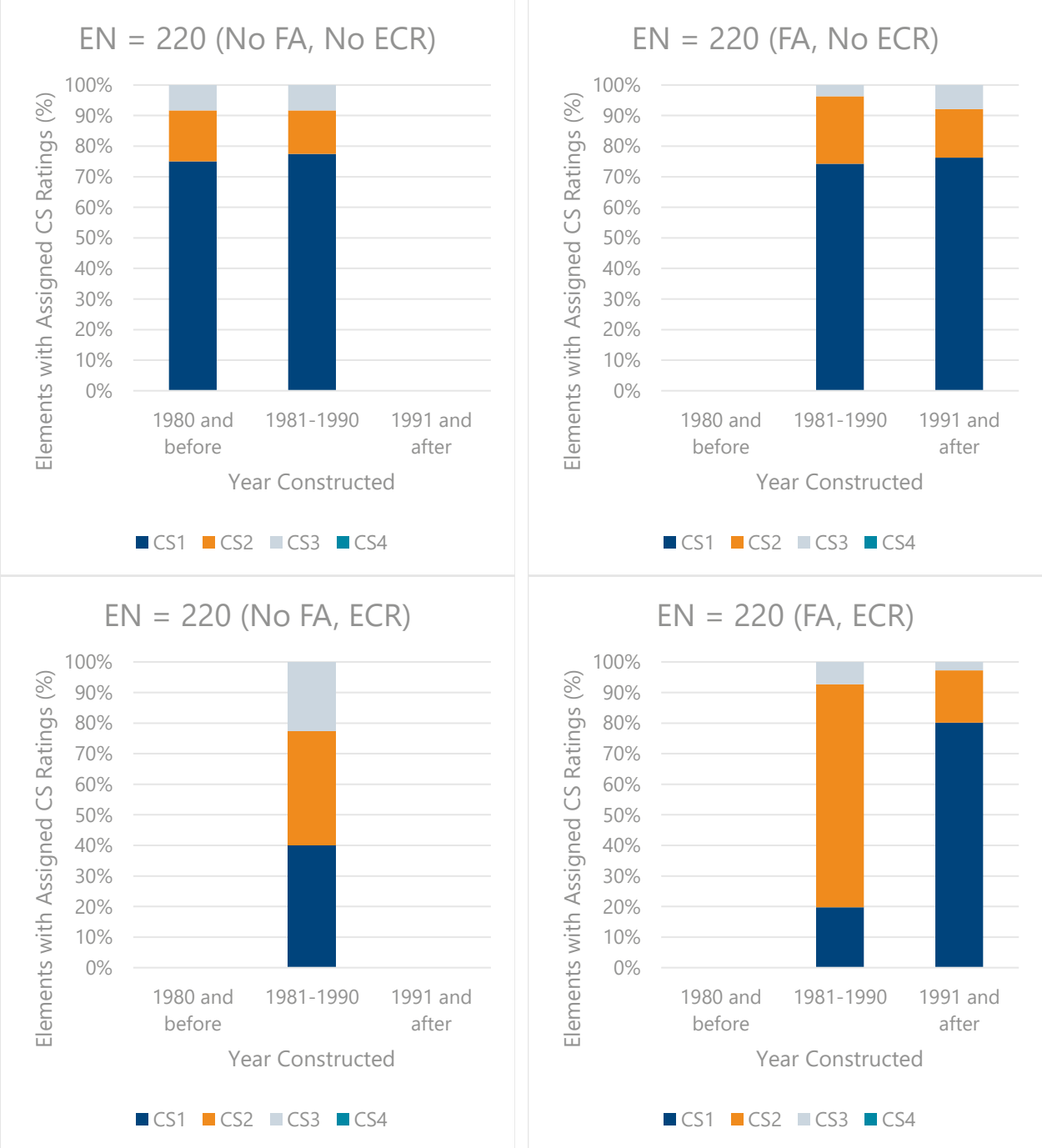

Figure 51. Statistical comparison of elemental distress as a function of bridge age and construction materials for pile cap/footing elements (EN = 220).

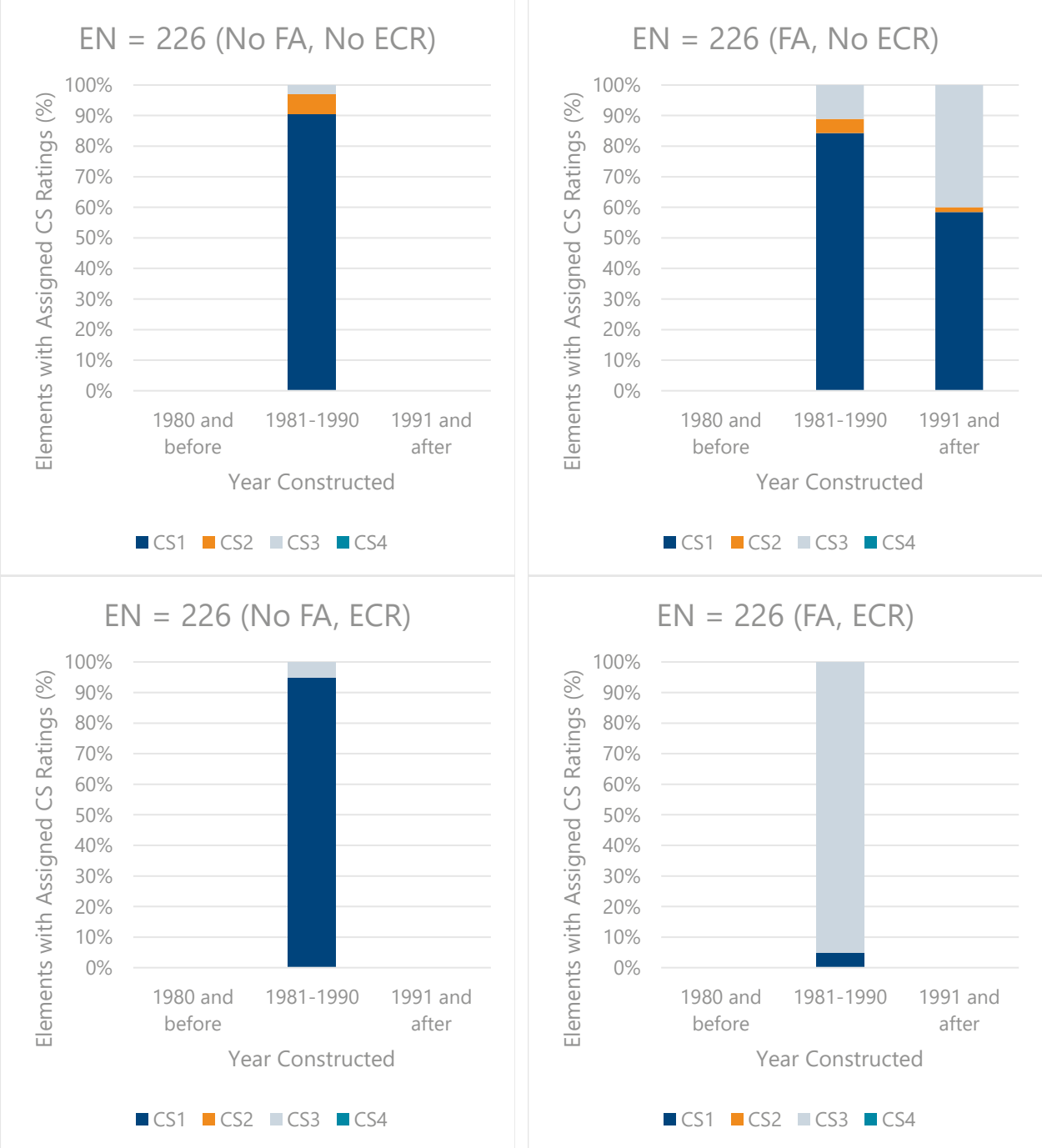

Figure 52. Statistical comparison of elemental distress as a function of bridge age and construction materials for pile elements (EN = 226).

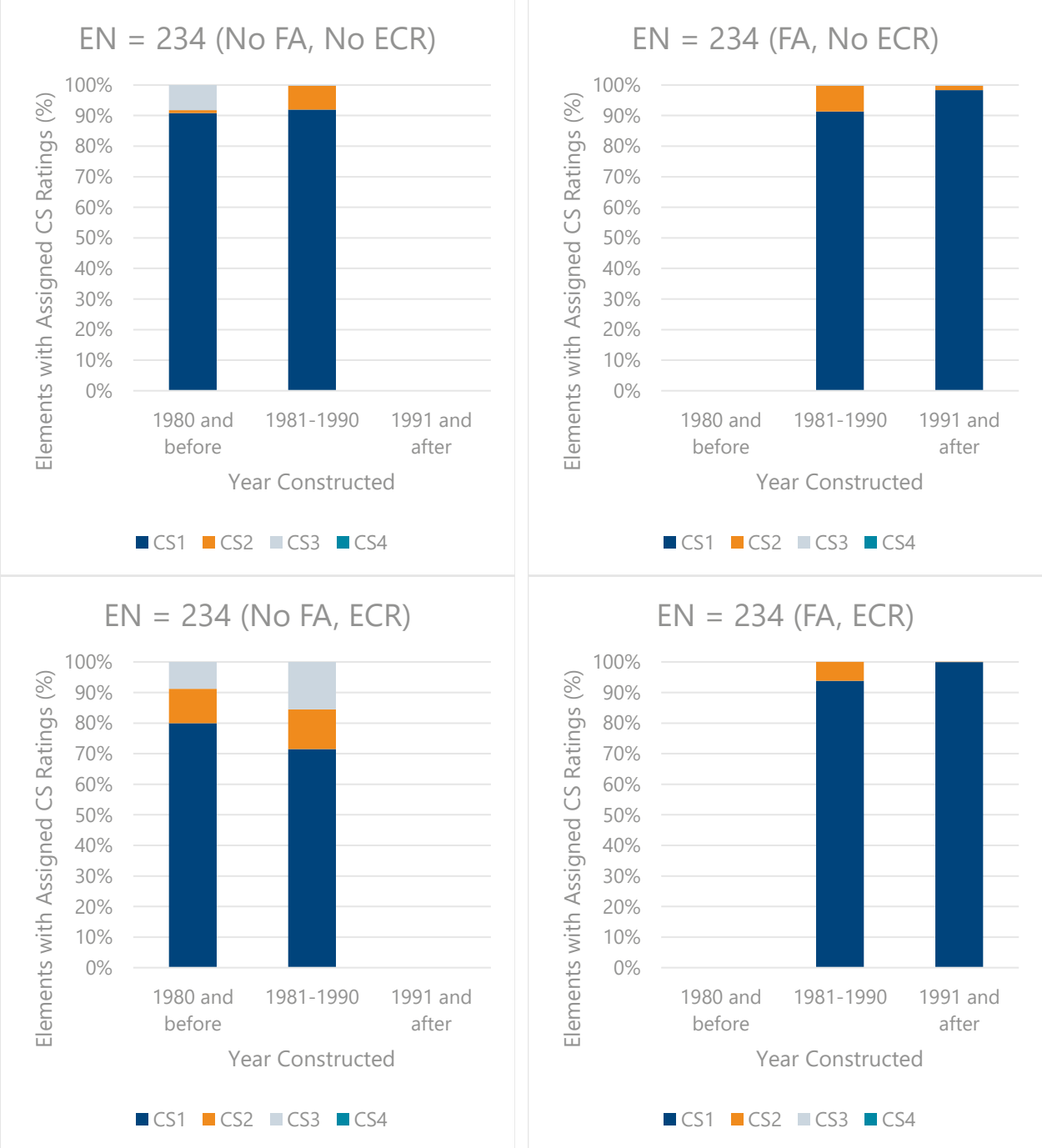

Figure 53. Statistical comparison of elemental distress as a function of bridge age and construction materials for pier cap elements (EN = 234).

Damage Analysis of Structures with CP

Data from BIRs for Gandy and Howard Frankland Bridges

In order to evaluate the overall performance of implemented CP systems, elemental data was evaluated for the Gandy and Howard Frankland bridges. This analysis provides cumulative elemental data for two bridges with various types of CP systems. Because the BIRs available to the research team only included data dating back to 2015, only elements evaluated between 2015 and 2020 were considered for this analysis.

This analysis did not differentiate between various types of systems and intends to provide a cumulative data summary showing the trends in elemental data as a function of time, as shown in Figure 54, Figure 55, and Figure 56.

Distress trends below show that pile cap/footing elements are showing an apparent linear downward trend over the past 5 years in terms of distress (Figure 54). However, only approximately 30 percent of the element exhibited any distress, and approximately two-thirds of that would be considered as minor CS2 damage. Similarly, pile jacket data showed a similar trend over the same time span (Figure 56), with less than 8 percent of pile jackets exhibiting any distress in 2015 to over 10 percent exhibiting significant distress, primarily rated as a CS3. The data for pile elements, however, shows a drastic decline in condition between 2017 and 2018/2019 (Figure 55), with less than 20 percent of piles exhibiting any distress in 2017 to over 80 percent of piles exhibiting significant distress deemed CS3, primarily due to delamination/spall/patched areas. The reason(s) for this large discrepancy over less than a 24-month time frame is difficult to determine using bridge inspection records alone. While some amount of decline in condition is expected, it is likely not at the rate determined between the two inspection records. It should be noted that different consultants performed the two inspections, and while the NBI program intends to train inspectors to use similar criteria for assigning condition states and ratings, it is impossible to eliminate all subjectivity from these inspections, and this subjectivity likely played some role in variable conditions.

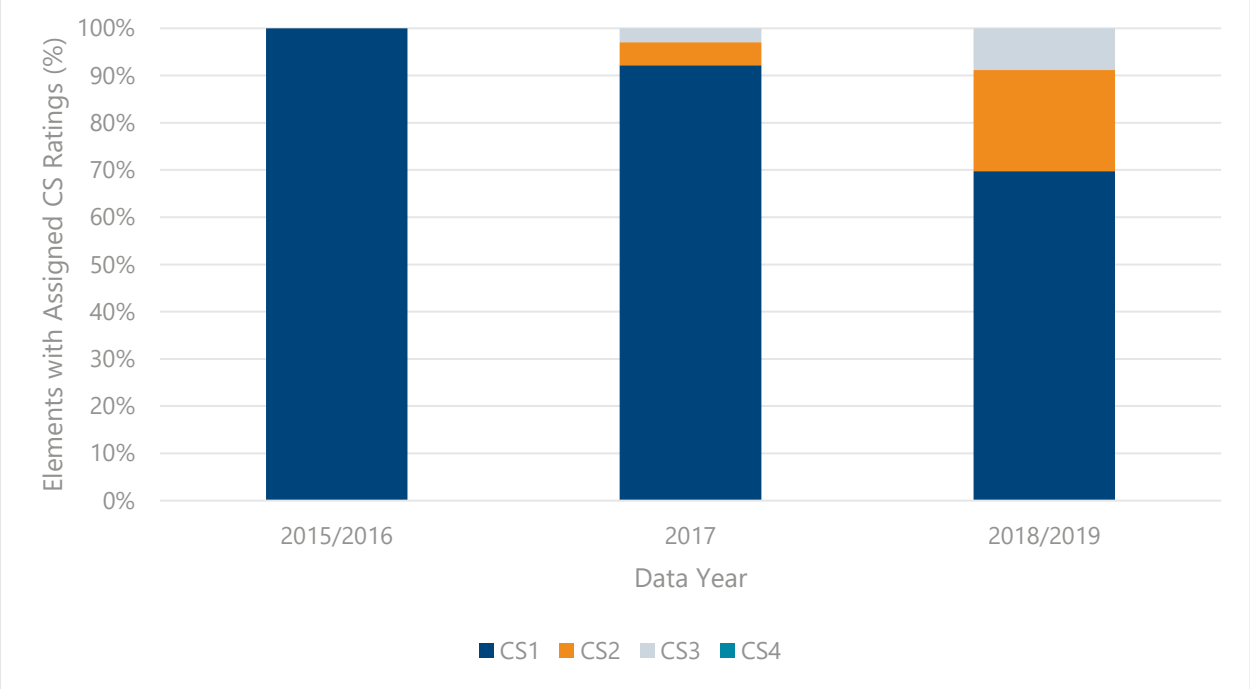

Figure 54. Statistical comparison of elemental distress as a function of cumulative data for pile cap/footing (EN = 220).

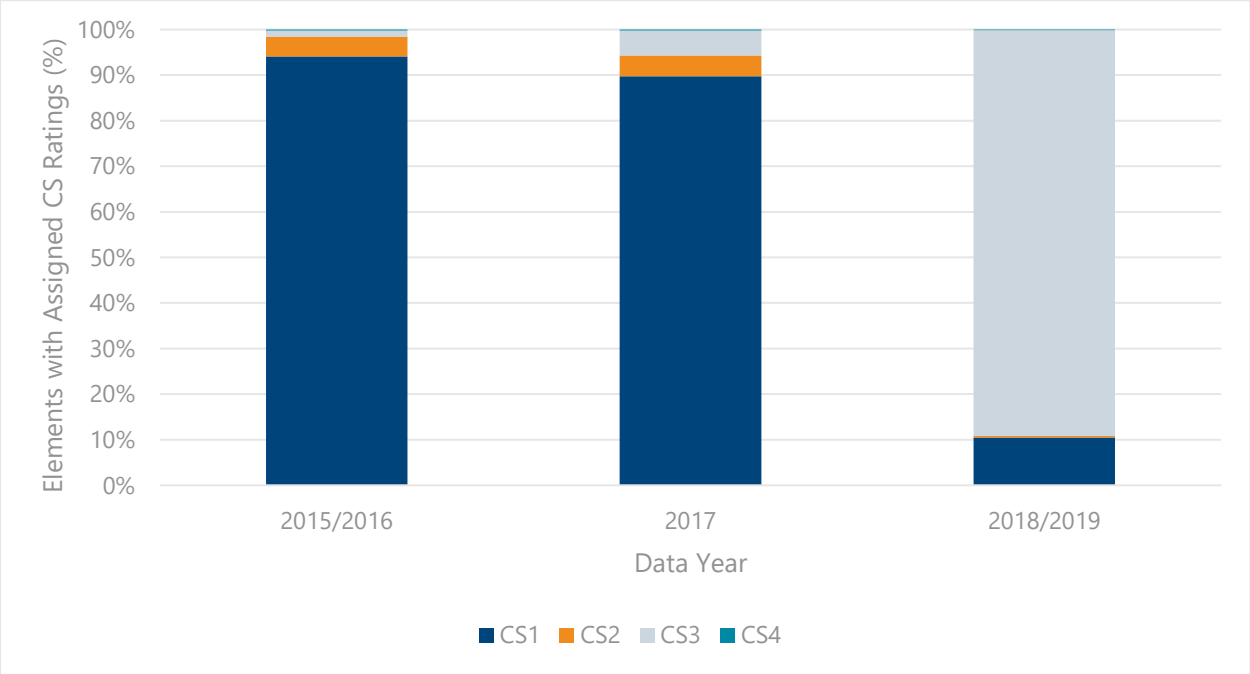

Figure 55. Statistical comparison of elemental distress as a function of cumulative data for prestressed and reinforced concrete pile (EN = 226/227).

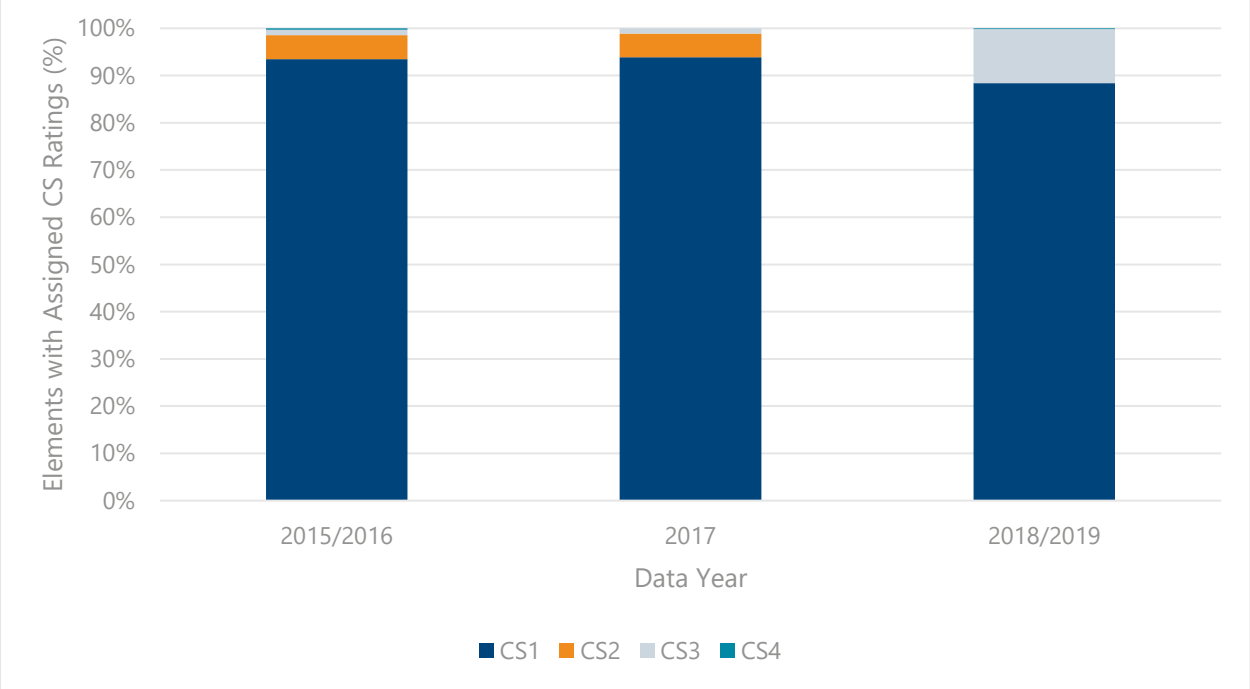

Figure 56. Statistical comparison of elemental distress as a function of cumulative data for pile jackets (EN = 8298).

Publicly Available Data

In order to evaluate the performance of various CP systems, cumulative elemental data was evaluated for additional select bridges with CP, including data both prior to and after installation of such systems. Because elemental data for the state of Florida is only publicly available back to 2016, only bridges that had had CP systems installed between 2016 and 2020 were considered for this analysis. For this analysis, representative data from this time range was only able to be compiled for galvanic CP pile jackets. Insufficient data was publicly available for ICCP and/or metalizing systems to draw reasonable comparisons and, as such, are omitted from this section.

Table 53 below presents the bridges selected for this analysis for galvanic CP pile jackets, including their year of construction, the year the CP system was installed, and a brief description of the systems. This analysis did not differentiate between system detailing and intends to provide a cumulative data summary showing improved trends in elemental data based on the installation of a select system, as shown in Figure 57. For the four bridges with data available for comparison, the installation of galvanic pile jackets reduced the percentage of piles distributing distress by approximately 10 percent and eliminated all CS4 condition state ratings. However, it can be seen that almost 40 percent of piles on the subject bridges still exhibit some amount of distress, mostly that qualifying as a CS3 condition state rating.

Table 53. Bridge List for Galvanic CP Pile Jackets

Bridge Name	Bridge Number	Year Constructed	Year CP Installed	Description
Boca Chica Channel SB	900003	1973	2016	Sacrificial: galvanic Zn pile jackets (463 LF N-Str, 93 LF Str) on 43 piles.
Tea Table Channel	900089	1980	2017	Sacrificial: Galvanic Zn pile jackets (135 LF Non, 42 LF Str) on 17 piles.
Boca Chica Channel NB	900074	1982	2016	Sacrificial: galvanic Zn pile jackets (463 LF N-Str, 93 LF Str) on 43 piles.
SR-20 over Aucilla River	540029	1995	2019	Sacrificial / Zinc mesh pile jackets.

This table omits descriptions of any additional types of CP that may be installed

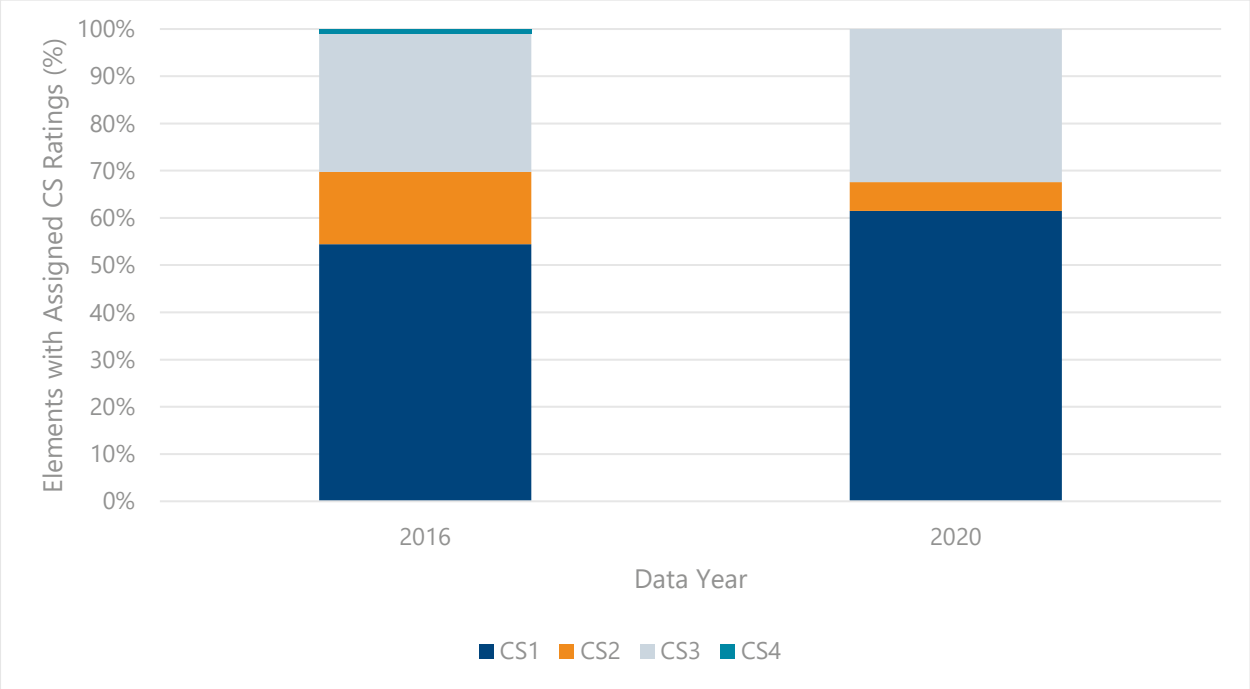

Figure 57. Statistical comparison of elemental distress as a function of cumulative data and installation system for piles (EN = 226/227).

5. COMPREHENSIVE ASSESSMENT OF CORROSION PREVENTION AND CONTROL PROGRAM

To provide a comprehensive assessment into the corrosion prevention and control systems currently installed across the network of over 6,500 bridges in Florida's highway infrastructure system, FDOT and the research team chose to evaluate both durability-based design requirements of new bridges and rehabilitation efforts for existing bridges. This evaluation included a review of both performance and estimated costs of commonly used materials/systems to identify the most robust, effective, and cost-efficient methods for extending service lives of bridges in the future. The research team planned field investigations to focus the scope of the assessments to evaluate one or more corrosion prevention and control system while minimizing external variables. While external variables in field investigations cannot always be eliminated, the data and knowledge obtained during this study provides a solid basis for future decision making regarding corrosion prevention and control systems for FDOT's bridges. In summary, over the eight individual bridges assessed over four mobilizations, the following corrosion prevention and control systems were the primary focus of this research study:

- Cathodic Protection
  - Galvanic Pile Jackets
  - Impressed Current Systems
- Construction Practice
  - Epoxy-Coated Reinforcement
  - Fly Ash Inclusion in Mix Designs

The following subsections provide a summary of findings of the primary systems researched as part of this study.

Cathodic Protection – Galvanic Pile Jackets

To evaluate galvanic pile jackets, historical data was compared to field data obtained in 2020 to not only assess current performance of the systems, but also to evaluate performance trends for multiple generations of jacket installations (2001, 2005, and 2009) over time. The bridges evaluated as part of this field investigation were the Gandy (Bridge No. 100300) and Howard Frankland (Bridge No. 150107) spanning Tampa Bay. Review of electrical data from 2020 provided by FDOT (presented in APPENDIX A) showed a wide scatter, particularly for measurements obtained within the monitoring ports. When compared to protection criteria as defined by industry standards (NACE SP0216-2016 and SP0408-2019), approximately half of the 38 pile jackets evaluated were categorized as fully protected based on potential decay and/or depolarized potential criteria within the monitoring port within the jacket. Only two pile jackets, both from the 2001 installation, were not providing any cathodic protection to the associated piles, and the remainder were providing some amount of partial protection. For electrical measurements obtained within the water using a submerged reference electrode, all 38 pile jackets were fully protected based on potential decay and/or depolarized potential criteria within the water. This is likely due to multiple factors, primarily the presence of a submerged bulk anode at each pile and locally lower resistivity of the grout due to higher moisture and chloride content. As the tidal and splash zones are typically the zones within reinforced or prestressed concrete piles that are of greatest risk for corrosion,

the additional protection within these exposure zones is critical to the overall durability of the piles. The discrepancy in performance data between that obtained within the water and that from within the monitoring port showed the amount of cathodic protection diminishes within the jacket as elevation relative to the water line increases; however, zinc samples obtained within the atmospheric zones indicated that the zinc had activated on each sample obtained for material testing regardless of electrical testing data and age. While the amount of cathodic protection supplied by the system diminishes with increased elevation, it is likely that the amount of cathodic protection required to protect the steel is also less as elevation increases. There was not a clear link between the electrical data of pile jackets and the extent of corrosion-related distress for individual piles (i.e. corrosion-induced cracking was observed above the jacket in cases where electrical data from within the port indicated full protection). This may be because many corrosion-related factors that could not be isolated from this study, including extent of corrosion and pre-existing elevation of cracking relative to the elevation of the top of the standard jacket installations. In such cases where a jacket does not encapsulate ongoing corrosion, cracking, or other distress observed above the top of existing jackets, metalizing or other form of corrosion control may be effective to be installed as a supplement above pile jackets at the higher atmospheric exposure zones.

Evaluating the three generations of pile jackets using data obtained from commissioning through 2020 allowed comparison of performance versus age. As expected, average output current and polarization for each of the three generations typically diminished from commissioning to 2020. The research team believes this is an outlier. Regardless, data from commissioning, 2013, and 2020 shows an approximately linear decline for both current output and polarization, with current outputs reducing from between 67 to 76 percent and polarization reducing by 37 to 65 percent (with the exception of the 2009 polarization measurements within the monitoring port). The higher reduction in current output than polarization is acceptable from a performance standpoint given that after installation and initial polarization of the protected steel, the required current output to maintain polarization will drop. Despite global trends showing declined performance over time, four of fifteen pile jackets from the 2001 installation evaluated in this study were still meeting 100 percent protection criteria, indicative that pile jackets may last 20 or more years.

Lastly, the research team obtained material samples for laboratory evaluation to determine effect of material properties on overall performance. In summary, obvious trends between grout resistivity data or visual properties of the zinc mesh were not identified. For example, Piles 270-2 (2005) and 106-7 (2009) both met 100 percent protection criteria per NACE SP0216-2016 and SP0408-2019l; however, the zinc mesh sample from Pile 270-2 was generally free of corrosion and the zinc mesh sample from Pile 106-7 exhibited widespread corrosion and significant section loss. Furthermore, grout surface resistivities were 4.1 and 1.6 kohm-cm and grout bulk resistivities were 7.5 and 3.3 kohm-cm, respectively.

A major component of the electrical cathodic protection circuit that was not evaluated as part of this study was the electrical connections, including the connection to the reinforcing steel, electrical continuity between embedded steel, and connections within the junction boxes. Each of these connections were required to have been verified during the installation and commissioning process, however, it is unclear the role that age and deterioration may have on these connections and the overall circuit. To ensure ongoing performance of these systems, periodic repairs may be required at accessible connections within

the junction box. Furthermore, future research could be performed on decommissioned piles to evaluate performance of internal connections.

In summary, data presented in this research indicates that galvanic pile jackets appear to be an effective corrosion control measure for protection of pile elements within bridge substructures and the data indicates that these systems have the potential to provide cathodic protection to pile elements for over 20 years. The primary conclusions of this research as it relates to galvanic pile jackets are summarized below:

- Submerged bulk anodes significantly increase the cathodic protection within the tidal and splash exposure zones, where corrosion activity is typically the most aggressive.
- Objective comparison of electrical performance of the galvanic pile jackets is difficult; however, the cathodic protection provided by the various generations of jackets has diminished over the up to 20 years they have been service. The majority of jackets continue to provide variable amounts of cathodic protection to the piles.
- A wide variation in the performance of individual jackets was observed due to factors, such as temperature, tidal elevation, and extent of corrosion at time of installation, and this makes it difficult to determine a single age at which FDOT should consider replacement. Decisions related to jacket life, rehabilitation and/or replacement needs will likely be most effective if made on an individual jacket basis.
- The research team did not identify any obvious material failures that may limit the function of the individual components of the pile jackets, which are up to approximately 20 years old. All systems evaluated appear to be capable of functioning effectively.

Potential future research as it relates to galvanic pile jackets is also summarized below:

- Destructive testing of in-service (or recently removed) piles and associated jackets to evaluate variability in continuity of connections and their effect on performance of cathodic protection.

Cathodic Protection – Impressed Current Systems

ICCP systems evaluated as part of this investigation included jackets installed on footing elements of the bridge substructures for the Gandy and Howard Frankland Bridges. Evaluation of these systems included both analysis of historic electrical data provided by FDOT (summarized in APPENDIX C), as well as obtaining field data for this investigation including depolarization measurements, which are not typically measured or recorded in reviewed electrical data. Of the four piers evaluated during the 2021 field investigations, average depolarization measurements met 100 percent protection criteria per NACE SP0216-2016 and SP0408-2019 using data from both the embedded reference cells and those obtained manually from within the monitoring ports located on the sides of footings. Further evaluation of data from individual footings showed that 100 mV depolarization was achieved at 16 of 24 locations using the permanent reference electrodes and 10 of 14 locations where measurements were taken within the monitoring ports. As expected, higher current outputs from the rectifiers typically corresponded with higher average depolarization measurements for the given zone.

The research team obtained material samples to determine how material properties affect the overall performance of the ICCP systems. Three titanium anode mesh samples were obtained for laboratory analysis, which indicated the samples appeared similar in composition and were generally undeteriorated

and could be expected to provide adequate performance for ICCP. Core samples were obtained to evaluate bulk resistivity data of the jacket grout. No obvious trends were identified between electrical data and bulk resistivity of the grout, which was generally less than 35 kohm-cm, and the electrochemical performance for the footing ICCP systems.

On a trial basis, FDOT has retrofitted existing ICCP jacket systems to be powered by solar panels. The research team evaluated one system at the Sunshine Skyway Bridge and compare its performance to an adjacent traditional system powered by a rectifier. In comparing the two systems over the time period evaluated in this field investigation, polarizations for the traditional system far exceeded the 100mV polarization requirement, while daily average polarization for the solar powered systems did not exceed 28 mV, far less than required for adequate protection. Additionally, based on the RMU data, the "on" potentials fluctuated up to 74 mV over each day for the solar powered system, as a result of variable amounts of sunlight available to power the system. For the purposes of this investigation, depolarization of the solar-powered systems was measured against the average "On" potentials (IR drop was unable to be obtained). The inconsistent current output from the solar powered rectifiers may prevent the system from reaching 100mV depolarization because of limited maximum current outputs or limited durations of sunlight exposure-produced current. This is further illustrated by measured average output currents were roughly 40 percent less for the solar powered system versus the traditional, varying slightly by zone.

In summary, traditional ICCP systems installed with AC power and rectifier units appeared to be performing well as a corrosion control measure for footing and/or other substructure elements within the splash/tidal zones. While the use of solar powered ICCP systems is promising based on this initial trial, greater capacity may be necessary to improve performance to be comparable with traditional rectifier powered ICCP systems. The primary conclusions of this research as it relates to ICCP systems are summarized below:

- There is a direct correlation between current output and structure polarization. With these systems being adjustable, implementation of more stringent program to adjust current output to maintain 100 percent protection should be established.
- After the structure is initially polarized, current demand to remain polarized drops; however, over time, the current required to maintain polarization may increase, meaning optimizing the systems to achieve minimum performance criteria while not over-protecting the structure requires monitoring and periodic adjustments.
- The research team did not identify any obvious material failures that may limit the function of the individual components of the ICCP jackets, which were up to approximately 12 years old.

Potential future research as it relates to ICCP jacket systems is also summarized below:

- Installation of solar systems with higher and more consistent current outputs. This may require additional and/or larger solar panels as well as a rechargeable battery or similar method to provide consistent current.
- Review of costs showed that Items 0400 60 1 Elect Work, AC Power and 0400 60 3 Elect Work, Conduit are large portions of installation costs for ICCP systems. Research into feasibility and methods to provide power not only to the ICCP system but also the associated RMU and eliminate the need for routing of AC power to the junction boxes would be beneficial to the state as a cost savings measure.

Construction Practice – Epoxy-Coated Reinforcing Steel

Application of epoxy coating on reinforcing steel provides a barrier with the intent of preventing depassivation of the steel as a result of chloride buildup at the surface of the bars. Epoxy coating of reinforcing steel also limits the surface of the bars available to supports cathodic reactions and promotes electrical discontinuity between bars, slowing the progression of corrosion. Although no longer specified by the State of Florida due to severe corrosion observed in as little as 5 years in bridges built in the 1980s, fusion-bonded epoxy-coated rebar (ECR) has been in continued use (particularly for bridge decks) in northern states in the country. The early-onset corrosion of bridges in Florida was attributed to the presence of coating defects and holidays that after some time in service (in part relating to moisture and chloride presence as well as mechanisms involving cathodic disbondment) allowed for localized corrosion to occur and subsequently progress to extended damage to the rebar and thus concrete delamination and spalling. These early installations of ECR typically included field-applied coatings, which are much more prone to defects and holidays and thinner than coatings shop-applied today. This investigation found better performance of epoxy coated bars than has been previously reported on other bridges in Florida; this may be because of better quality control during coating application and construction of the bridge.

This investigation assessed the long-term performance of ECR in twin bridges in Melbourne, Florida, in identical exposure conditions and at similar ages. Bridge Nos. 700174 and 700181 are the westbound and eastbound routes of the Melbourne Causeway (US 192) spanning the Indian River in Melbourne, Florida. The bridges are very similar in terms of construction detailing with the exception that Bridge No. 700181 was designed with epoxy-coated reinforcement and 700174 with black steel bar reinforcement. Because ICCP systems have been installed on Bridge No. 700174, the research team utilized a condition assessment report from 2011 to compare Bridge No. 700174 (Bridge age of 33 years) to data obtained from Bridge No. 700181 during the 2021 field investigation (Bridge age of 36 years). While cracking had initiated on the select elements included in the study area that was evaluated on Bridge No. 700181, no delaminations were noted. Contrary to this, moderate to severe cracking, delaminations, and/or spalling was observed on over half of pile cap, column, and strut elements evaluated in 2011. Due to the quantity of advanced distress, initiation of corrosion of the uncoated reinforcing steel within Bridge No. 700174 had likely begun far prior to the 2011 assessment. Core samples were obtained to evaluate chloride diffusion rates and concentrations at the bar levels for both bridges, which were obtained at similar elevations. At two elements (column and crash wall) chloride concentrations at the assumed bar depth was slightly higher in Bridge No. 700174 than Bridge No. 700181, but they were similar in the pile cap and strut samples. Despite similar chloride contents at or near the epoxy-coated reinforcing steel and similar concrete properties, Bridge No. 700181 exhibited only minimal cracking distress at an age three years older than when the delaminations were found on Bridge No. 700174.

The primary conclusions of this research as it relates to ECR are summarized below:

- At 36 years of age, Bridge 700181 did not exhibit corrosion-related distress that would warrant structural repairs and/or installation of corrosion mitigation systems. On the contrary, significant distress was observed on Bridge 700174 at 33 years of age, warranting installation of ICCP systems on the footings. As such, installation of ECR on Bridge 700181 has apparently provided at least three

years and likely more of additional service life to the structure versus the similar bridge constructed with black bar.

Potential future research as it relates to ECR is also summarized below:

- To further evaluate and quantify the benefit of ECR, revisit Bridge 700181 to perform a similar assessment and compare data to that obtained in this study and in 2011.

Construction Practice – Fly Ash Inclusion in Mix Designs

Chloride-related corrosion initiation is governed by the rate at which chloride ions move through the concrete and accumulate at the bar surface. Chloride ion transport in concrete is complex; however, it is commonly assumed that diffusion plays the largest role, especially is marine exposure where the concrete stays wet. Concretes with supplementary cementitious materials, such fly ash, typically have better diffusion and electrical properties than concrete without. This investigation observed the long-term performance of fly ash concrete by comparing the performance of two twin bridges in Fort Lauderdale in identical exposure conditions and at similar ages (i.e built within eight years of each other). Bridge Nos. 860467 and 860466 are the eastbound and westbound routes of Sunrise Boulevard spanning over the intercoastal waterway and were constructed in 1987 and 1989, respectively. Bridge No. 860467 contains a fly ash admixture, while fly ash was not used as part of the concrete mix at Bridge No. 860466. Both bridges are currently coated.

Evaluating diffusion rates based on chloride data plotted as a function of depth, a slower rate of chloride penetration was observed at Bridge No. 860467, which contained fly ash. However, the surface concentrations were as much as thirty times higher for Bridge No. 860467 than for Bridge No. 860466 despite the twin bridges nearly identical environmental conditions, so it is unclear if the concrete exposure was truly similar. It is likely that surface coatings may have affected the data collected, and dates of coating application and/or maintenance records were not available to help understand that effect. For that reason, the research team could not draw any firm conclusions using data obtained during this field investigation. While it is well documented throughout the literature that fly ash provides a benefit towards corrosion control of reinforced concrete, this effect could be quantified based on the obtained data.

Potential future research as it relates to pozzolanic materials is summarized below:

- As supply of fly ash is becoming scarcer, research into alternate pozzolanic materials to reduce pore size and increase electrical resistivity of the concrete would be beneficial.

FIGURES

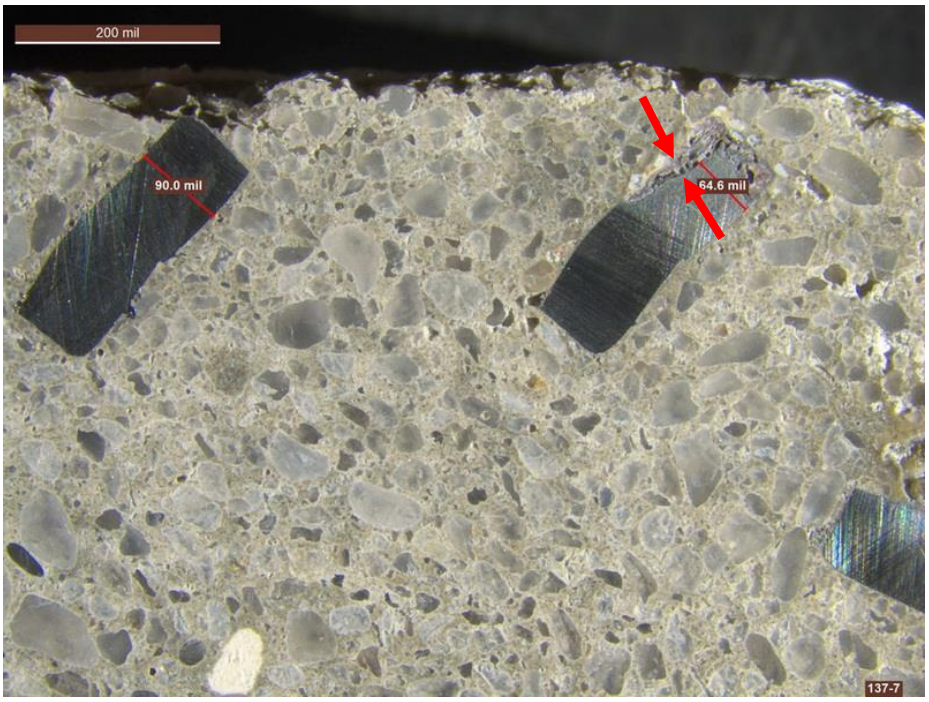

Figure 58. Sample 137-7. Close-up view of zinc mesh shows its condition and thickness measurements. The mesh showed localized corrosion and minor section loss near the corner. Mesh was free of significant corrosion or section loss elsewhere. Arrows indicate corroded portion.

Figure 59. Sample 177-4. Close-up view of zinc mesh shows its condition and thickness measurements. Very localized corrosion and minor section loss were observed. Red arrows indicate locally corroded zinc. White efflorescence was also observed on the lapped section (yellow circle).

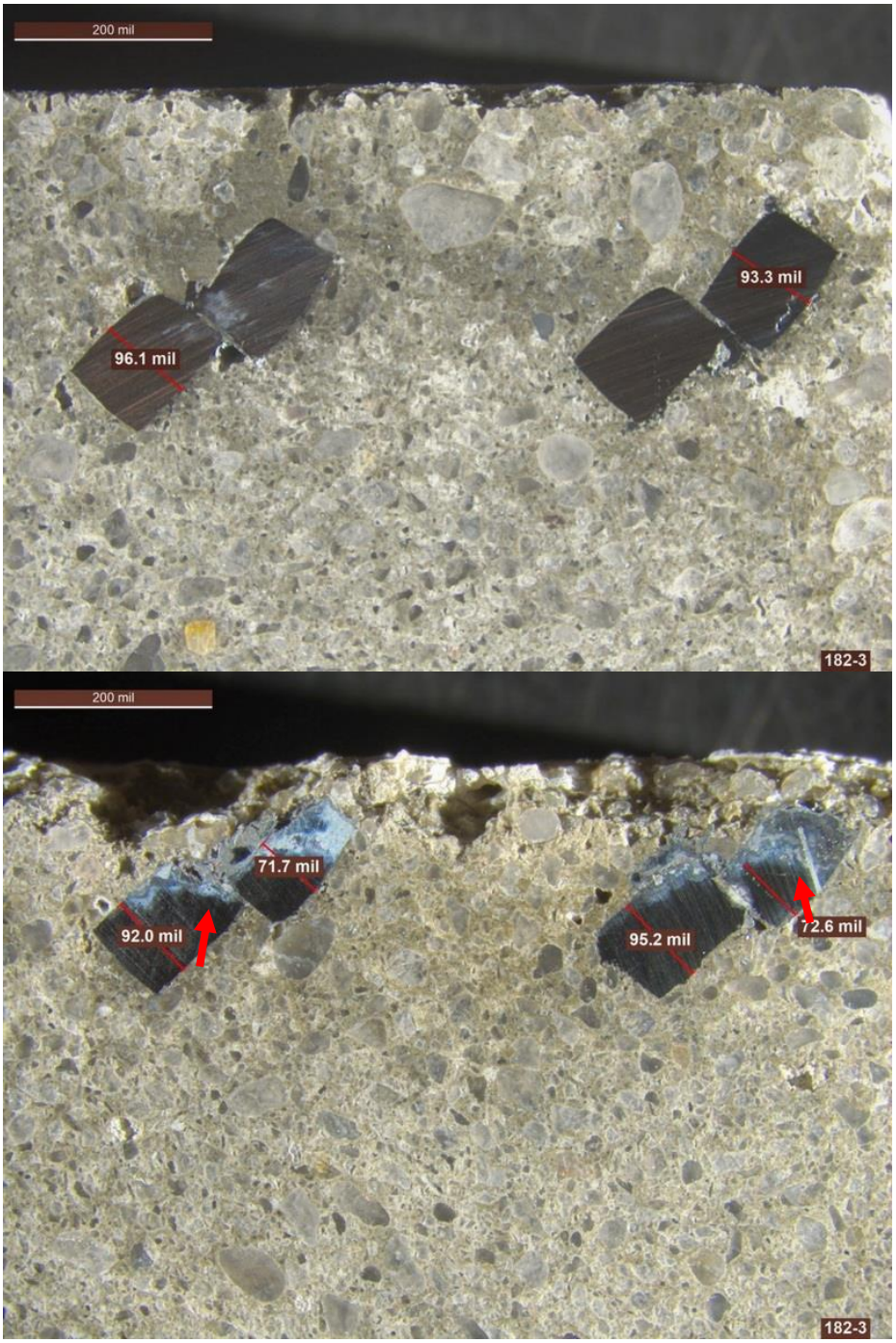

Figure 60. Sample 182-3. Close-up views of zinc mesh show its condition and thickness measurements. Localized corrosion and section loss were observed. Red arrows indicate corroded or partially corroded zinc.

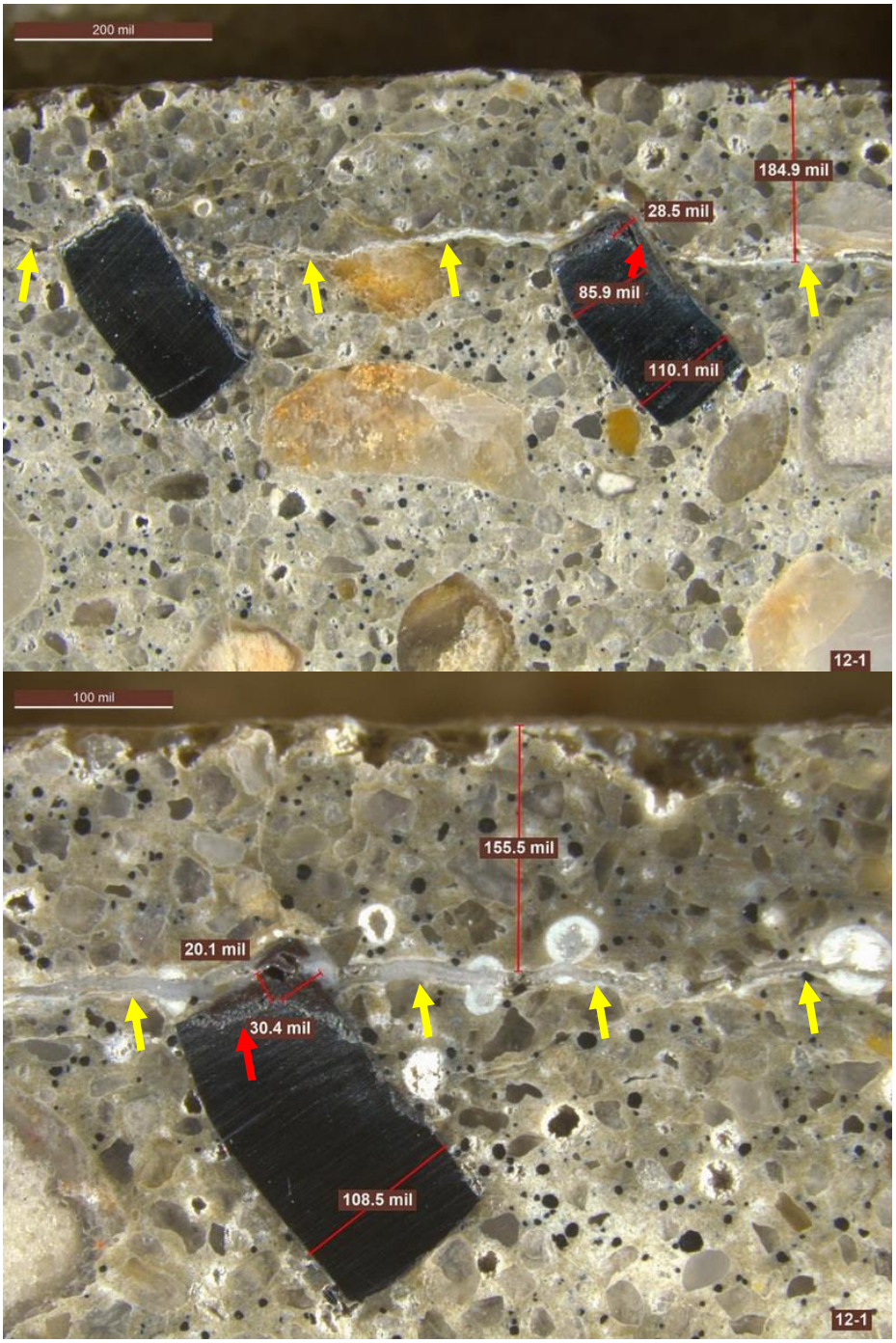

Figure 61. Sample 21-1. Close-up views of zinc mesh show its condition and thickness measurements. Frequent corrosion and minor section loss were observed. Red arrows indicate corroded zinc. Yellow arrows indicate a delamination crack lined with secondary deposits, liekly due to corrosion of the zinc mesh.

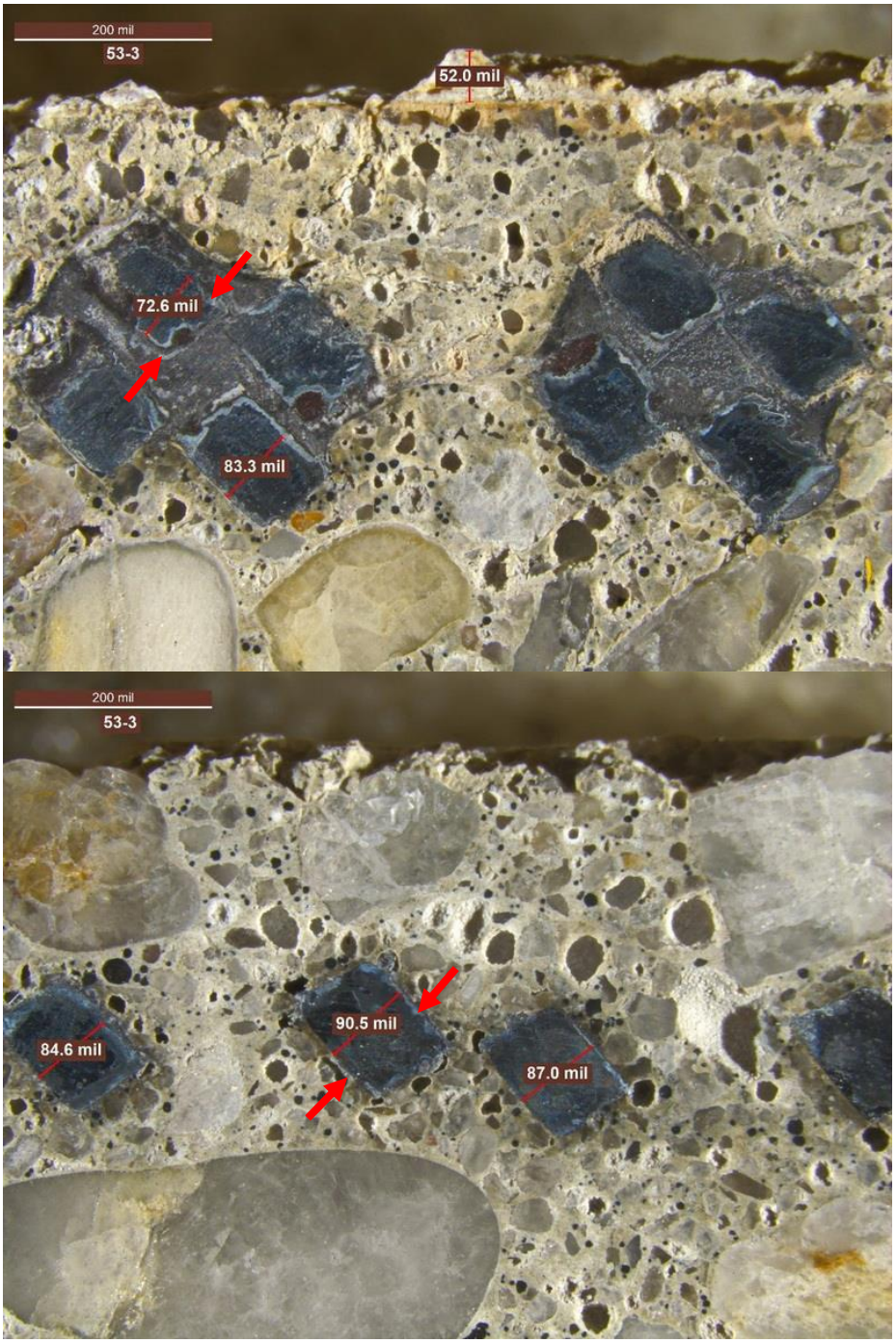

Figure 62. Sample 53-3. Close-up views of zinc mesh show its condition and thickness measurements. A mesh joint appeared to be present at a corner of the concrete sample (top photo). Corrosion and minor section loss were observed.

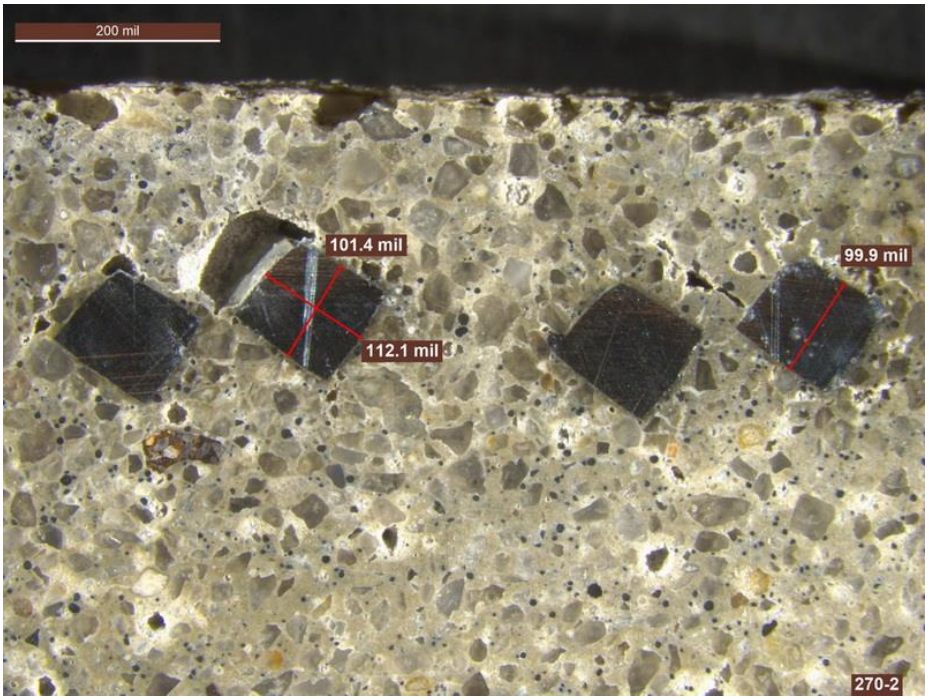

Figure 63. Sample 270-2. Close-up view of zinc mesh shows its condition and thickness measurements. Generally free of significant corrosion or section loss.

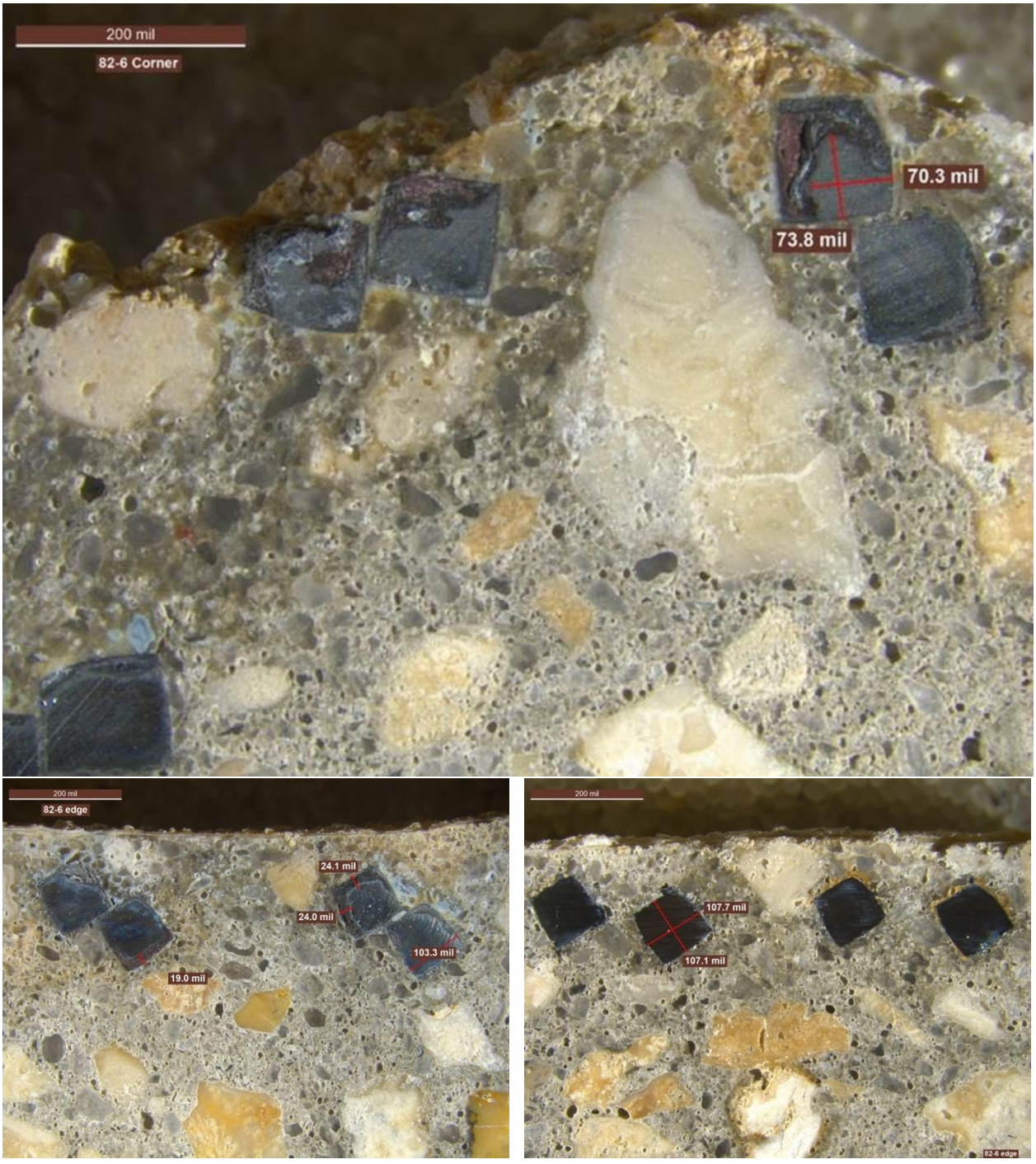

Figure 64. Sample 82-6. Close-up views of zinc mesh show its condition and thickness measurements. Corrosion and minor section loss were observed at the corner (top photo); less corrosion and section loss along the two edges (bottom photos).

Figure 65. Sample 106-7. Close-up view of zinc mesh shows its condition and thickness measurements. Widespread corrosion and significant section loss were observed. Red arrows indicate white deposits suspected to be zinc corrosion product.

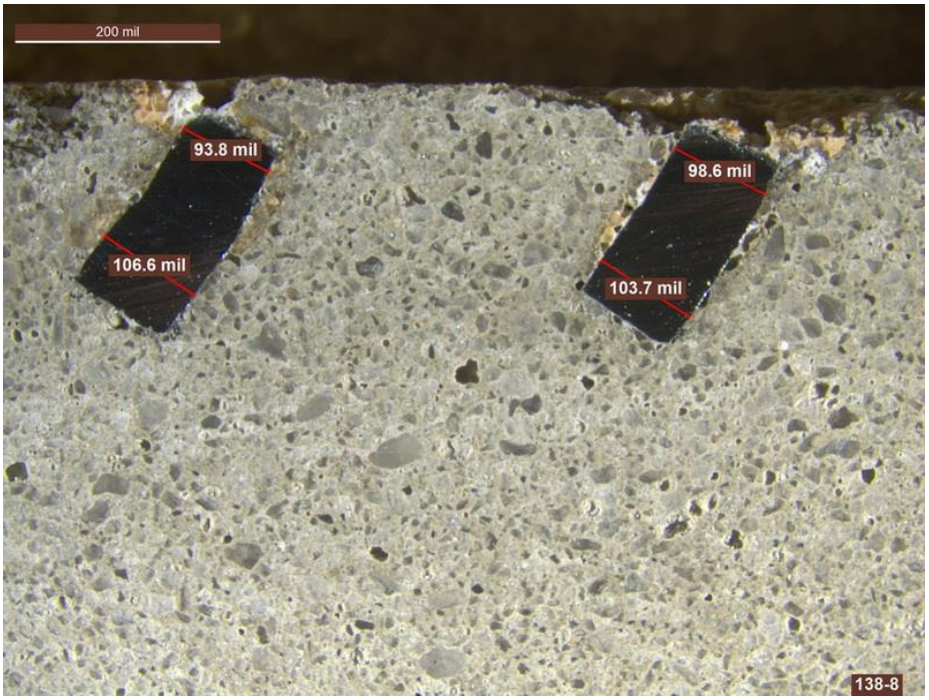

Figure 66. Sample 138-8. Close-up view of zinc mesh shows its condition and thickness measurements. Corrosion and minor section loss were observed.

Figure 67. Representative titanium mesh sample (Gandy 226)

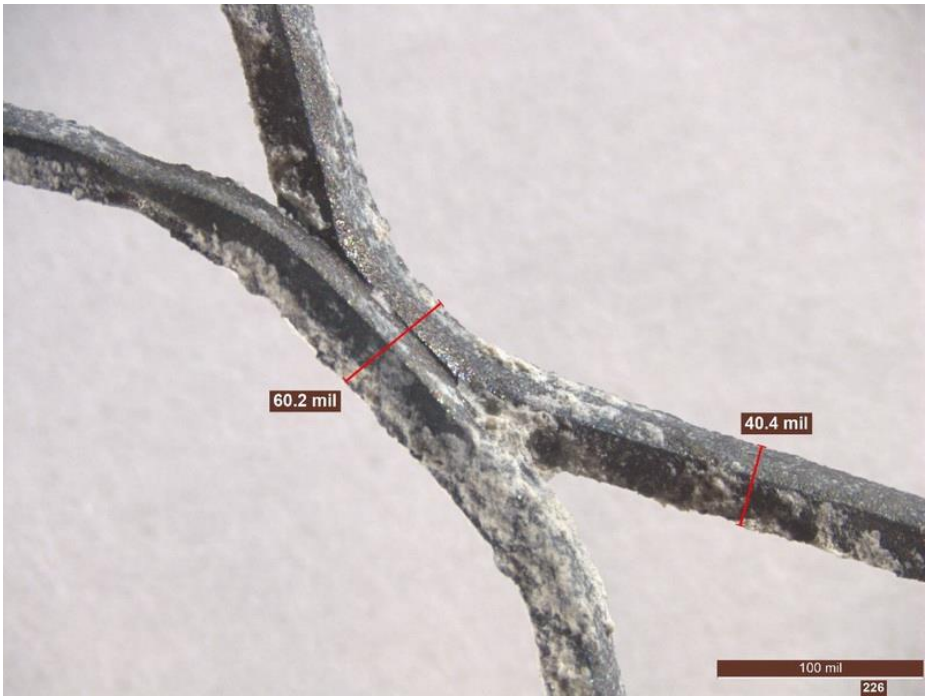

Figure 68. Microscopic view of titanium mesh, including thickness measurements (Gandy 226)

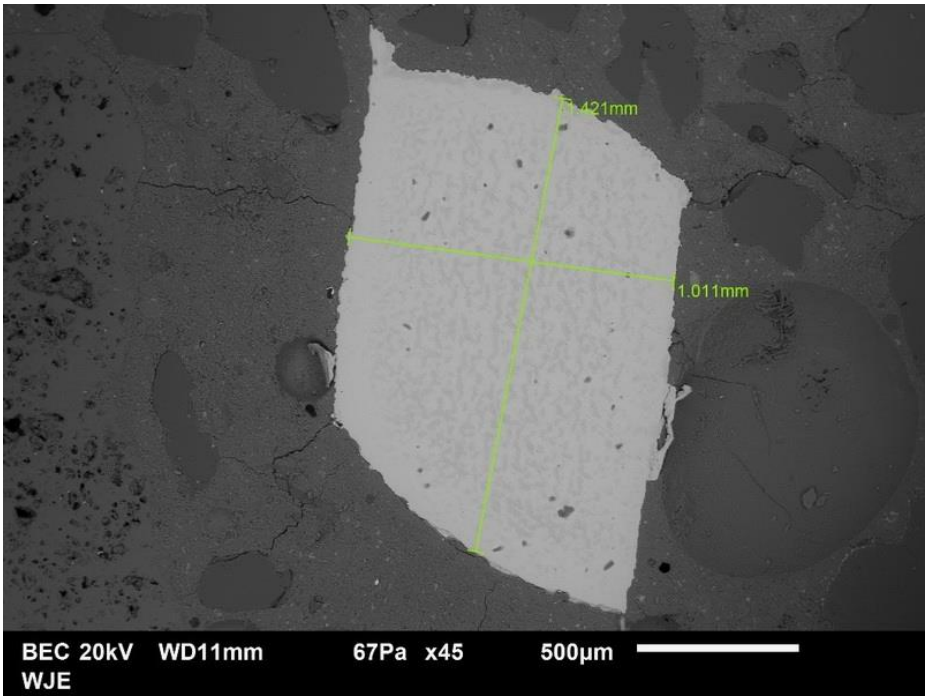

Figure 69. Microscopic view of titanium mesh cross section, including thickness measurements (HF 158)


Figure 70. Missing portion of pile jacket (Pile 12-1)

Figure 71. Vertical cracking with rust staining extending upward from top of pile (Pile 12-1)

Figure 72. Split pile jacket near waterline (Pile 14-4)

Figure 73. Split pile jacket and multiple vertical cracks on pile (Pile 44-5)

Figure 74. Cracking measured up to approximately 50 mil wide (Pile 44-5)

Figure 75. Vertical splitting of jacket (Pile 53-3)

Figure 76. Overview photograph of pile and jacket with no noted distress (Pile 65-8)

Figure 77. Jacket splitting and missing around lower perimeter of pile (Pile 73-5)

Figure 78. Overview photograph of apparent jacket extension on top (Pile 80-6)

Figure 79. Overview photograph of pile and jacket with no noted distress (Pile 99-9)

Figure 80. Significant distress of jacket (Pile 105-9)

Figure 81. Overview photograph of pile and jacket with no noted distress (Pile 116-4)

Figure 82. Significant distress of jacket (Pile 120-1)

Figure 83. Exposed grout exhibiting staining and cracking (Pile 120-1)

Figure 84. Minor spall on the SW corner top that was metalized over (Pile 123-8)

Figure 85. Jacket extension on top, no distress noted (Pile 129-6)

Figure 86. Significant distress of jacket (Pile 133-5)

Figure 87. Repair on NW corner of the pile (Pile 138-7)

Figure 88. Vertical splitting of jacket (Pile 138-8)

Figure 89. Horizontal splitting of jacket (Pile 177-4)

Figure 90. Vertical cracking of jacket (Pile 182-3)

Figure 91. Cracking measured up to approximately 20 mil wide and spalling of pile (Pile 190-6)

Figure 92. Vertical cracking of jacket (Pile 191-3)

Figure 93. Repair and cracking measured up to approximately 30 mil wide (Pile 198-1)

Figure 94. Overview photograph of pile and jacket with no noted distress (Pile 214-3)

Figure 95. Repairs with corroded anchors on pile (Pile 214-6)

Figure 96. Vertical cracking of the pile (Pile 236-7)

Figure 97. Two vertical cracks of the pile measured up to approximately 5 mil wide (Pile 263-1)

Figure 98. Cracking measured up to approximately 50 mil wide with corrosion staining (Pile 270-2)

Figure 99. Overview photograph of pile and jacket with no noted distress (Pile 289-2)

Figure 100. Vertical full length splitting of the jacket (Pile 289-5)

Figure 101. Cracking in repair of pile (Pile 304-4)

Figure 102. Cracking in repair on top of pile (Pile 308-5)

Figure 103. Repair on pile corner (Pile 316-8)

Figure 104. Missing bottom of jacket (Pile 46-3)

Figure 105. Cracking measured up to approximately 25 mil wide (Pile 82-6)

Figure 106. Jacket opening at the bottom (Pile 85-4)

Figure 107. Spalling of pile (Pile 85-4)

Figure 108. Jacket broken at the bottom Pile 94-3)

Figure 109. Cracking of pile (Pile 94-3)

Figure 110. Cracking on repair of pile (Pile 104-1)

Figure 111. Corner cracking of pile (Pile 106-7)

Figure 112. Parge coat cracking, no pile cracking noted (Pile 137-4)

Figure 113. Cracking on pile (Pile 144-4)

REFERENCES

AASHTO LRFD Bridge Design Specifications, 9th Edition, American Association of State Highway and Transportation Officials, Washington DC, 2020.

ACI 222R-19 "Guide to Protection of Metals in Concrete Against Corrosion," American Concrete Institute Committee 222. Farmington Hills, MI.

ACI 222.3R-11 "Design and Construction Practices to Mitigate Corrosion of Reinforcement in Concrete Structures," American Concrete Institute Committee 222. Farmington Hills, MI.

ACI 318-19 "Building Code Requirements for Structural Concrete," American Concrete Institute Committee 222. Farmington Hills, MI.

Angst, Ueli, Bernhard Elsener, Claus K. Larsen, Oystein Vennesland. "Critical chloride content in reinforced concrete - A review." *Cement and Concrete Research 39* (2009) 1122-1138.

Ansuini, F. and Dimond, J. "Factors Affecting the Accuracy of Reference Electrodes." *Materials Performance*, Vol. 33, No. 11 (1994): 14-17. Houston, TX: NACE International.

ASTM A775-16 "Standard Specification for Epoxy-Coated Steel Reinforcing Bars," *Annual Book of ASTM Standards*, Part 02.04, ASTM, West Conshohocken, PA.

ASTM A1055-16 "Standard Specification for Zinc and Epoxy Dual-Coated Steel Reinforcing Bars," *Annual Book of ASTM Standards*, Part 01.04, ASTM, West Conshohocken, PA.

ASTM A1094-18 "Standard Specification for Continuous Hot-Dip Galvanized Steel Bars for Concrete Reinforcement," *Annual Book of ASTM Standards*, Part 02.04, ASTM, West Conshohocken, PA.

ASTM B6-18 "Standard Specification for Zinc," *Annual Book of ASTM Standards*, Part 02.04, ASTM, West Conshohocken, PA.

ASTM B833-20 "Standard Specification for Zinc and Zinc Alloy Wire for Thermal Spraying (Metallizing) for the Corrosion Protection of Steel," *Annual Book of ASTM Standards*, Part 02.04, ASTM, West Conshohocken, PA.

ASTM C1152-20 "Standard Test Method for Acid-Soluble Chloride in Mortar and Concrete," *Annual Book of ASTM Standards*, Part 04.02, ASTM, West Conshohocken, PA.

ASTM C856-20 "Standard Practice for Petrographic Examination of Hardened Concrete," *Annual Book of ASTM Standards*, Part 04.02, ASTM, West Conshohocken, PA.

ASTM C876-15, "Standard Test Method for Corrosion Potentials of Uncoated Reinforcing Steel in Concrete," *Annual Book of ASTM Standards*, Part 03.02, ASTM, West Conshohocken, PA.

ASTM D3963-15 "Standard Specification for Fabrication and Jobsite Handling of Epoxy-Coated Steel Reinforcing Bars, "*Annual Book of ASTM Standards*, Part 01.04, ASTM, West Conshohocken, PA.

ASTM B6-18 "Standard Specification for Zinc, "*Annual Book of ASTM Standards*, Part 02.04, ASTM, West Conshohocken, PA.

ASTM B833-20 "Standard Specification for Zinc and Zinc Alloy Wire for Thermal Spraying (Metallizing) for the Corrosion Protection of Steel, "*Annual Book of ASTM Standards*, Part 02.04, ASTM, West Conshohocken, PA.

Bennett, J., & Schue, T. J. (1993). SHRP-C-260, Evaluation of NORCURE Process for Electrochemical Chloride Removal from Steel-Reinforced Concrete Bridge Components. Washington, DC: Strategic Highway Research Program.

Bennett, J., Fong, K. F., & Schue, T. J. (1993). SHRP-S-669, Electrochemical Chloride Removal and Protection of Concrete Bridge Components: Field Trials. Washington, DC: Strategic Highway Research Program.

Broomfield, J. (1997) Corrosion of Steel in Concrete Understanding, Investigation and Repair. E & FN SPOK, London, 16-21.

Broomfield, J. P. (2007). Corrosion of Steel in Concrete. New York: Taylor and Francis.

Broomfield, J. P. "Electrochemical Realkalization of Steel Reinforced Concrete-A State of Art Report, Technical Notes N 9." Corrosion Prevention Association (CPA) (2004).

Bridge Rehabilitation Contract Plans from Parsons Brinckerhoff Quade & Douglas, Inc. (Financial Project ID 420666-1-52-01), dated May 3, 2007

Bridge Rehabilitation Contract Plans from TY Lin International (Financial Project ID 427455-2-52-01), dated December 2012

C. Andrade, M. Castellote, J. Sarria, C. Alonso, Mater. Struct., 32 (1999) 427–36

Clemena, G. G., & Jackson, D. R. (2000). VTRC 00-R18, Trial Application of Electrochemical Chloride Extraction on Concrete Bridge Deck Components in Virginia. Charlottesville, VA: Virginia Transportation Research Council.

Corrosion Condition Evaluation of Substructure Components on the US-192 Bridges Over the Intracoastal Waterway (Bridge Nos. 700174 and 100181) in FDOT District 5 Report by Concorr Florida, Inc., dated August 2, 2011

Corrosion Condition Evaluation of the Eastbound Gandy Bridge on US 92 (SR 600) Over Old Tampa Bay Bridge No. 100300 Report by CONCORR Florida, Inc., dated November 2, 2005

Corrosion Investigation Report of Concrete Footer at Pier No. 233 Report by Corrosion Research Laboratory, dated April 23, 1990.

COST 509, European Commission, Corrosion and Protection of Metals in Contact with Concrete, Final Report, 1996.

Druga, Melina. "Florida's budget includes nearly $10B for transportation infrastructure development" *Transportation Today News* (Washington DC), November 20, 2019.

Eastbound Gandy Bridge Condition Evaluation and Cost Analysis (Financial Project ID 4125931-1-32-03) by CONCORR Florida, Inc. on July 16, 2007

Guo, Bingbing, Guofu Qiao, Ditao Niu, and Jinping Ou. "Electrochemical Corrosion Control for Reinforced Concrete Structures-A Review." Int. J. Electrochem. Sci 15 (2020): 5723-5740.

FHWA-RD-01-096 - Long-Term Effectiveness of Cathodic Protection Systems on Highway Structures. Federal Highway Administration, McLean, VA, 2001.

Halstead, Woodrow J. *Report 127 - Use of Fly Ash in Concrete*. National Cooperative Highway Research Program Project 20-5, Washington DC, October 1986.

Included as appendices with above report: Corrosion Damage Projections for the Eastbound Gandy Bridge (Bridge No. 100300) Addendum to the November 2, 2005 Final Report Report by PB Americas, Inc., dated March 29, 2007

Inspection/CIDR Report (FDOT Bridge Management System) by Volkert, Inc., dated January 31, 2019

Installation and Energization of an Impressed Current Cathodic Protection System Report (Financial Project ID 420666-1-52-01) by CONCORR Florida, Inc., dated June 12, 2009

Installation and Energization of an Impressed Current Cathodic Protection System (Financial Project ID 420666-1-52-01) by CONCORR Florida, Inc. on June 23, 2009

Installation of Cathodic Protection Systems on 81 Piles Report (Financial Project ID 420666-1-52-01) by CONCORR Florida, Inc., dated June 12, 2009

Inventory, Routine Monitoring, and Maintenance of Sacrificial CP Systems Installed on Piles on the Old Howard Frankland Bridge (Bridge No. 150107) and the Gandy Bridge (Bridge No. 100300) by CONCORR Florida, Inc., on September 21, 2013.

J. Mietz, Electrochemical Rehabilitation Methods for Reinforced Concrete Structures. A state-of-the-art report, Publication no. 24, European Federation of Corrosion, The Institute of Materials, London, U.K. (1998).

Koch, Gerhardus H., Michiel P.H. Brongers, Neil G. Thompson, Y. Paul Vermani, and JH Payer. *Corrosion Costs and Preventative Strategies in the United States*. NACE International, Houston, Texas, 2005.

Lankard, D. R., Slater, J. E., Hedden, W. A., & Niesz, D. E. (1975). FHWA-RD-76-60, Neutralization of Chloride in Concrete. Columbus, OH: Battelle Columbus Laboratories.

Lau et al. *Florida Department of Transportation Bridge Work Plan for 2015*. 2018.

Lee, Seung-Kyoung, and Paul Krauss. *FHWA-HRT-04-090 - Long Term Performance of Epoxy-Coated Reinforcing Steel in Heavy Salt-Contaminated Concrete.* Federal Highway Administration, McLean, VA, 2004.

Morrison, G. L., Virmani, Y. P., Stratton, F. W., & Gilliland, W. J. (1976). FHWA/KS/RD-74/1, Chloride Removal and Monomer Impregnation of Bridge Deck Concrete by Electro-osmosis. Topeka, KS: Kansas Department of Transportation.

NACE SP0216-2016 "Sacrificial Cathodic Protection of Reinforcing Steel in Atmospherically Exposed Concrete Structures," NACE International, Houston, TX.

NACE SP0408-2019 "Cathodic Protection of Reinforcing Steel in Buried or Submerged Concrete Structures," NACE International, Houston, TX.

NACE TR21463-2020 "Criteria for Evaluation of Cathodic Protection Methods for Steel in Existing Concrete Structures — A State-of-the-Art Report," NACE International, Houston, TX.

PB Bamforth, "Enhanced Reinforced Concrete Durability: Guidance on selecting Measures for Minimizing the Risk of corrosion of Reinforcement in Concrete," Concrete Society Technical Report No. 61, (2004)

Permeh, S., C. Reid, M. Echeverria-Boan, K. Lau, B. Tansel, M. Duncan, and I. Lasa, "Microbiological Influenced Corrosion (MIC) in Florida Marine Environment: A Case Study." CORROSION 2017, paper no. 9536. Houston, TX: NACE International, 2017.

Pfeifer, Donald W., J. Robert Landgren, and Alexander Zoob. *FHWA/RD-86/193 - Protective Systems for New Prestressed and Substructure Concrete*. Federal Highway Administration, Washington D.C., April 1987.

Pfeifer, D.W. and M. J. Scali. *Report 244 - Concrete Sealers for Protection of Bridge Structures*. National Cooperative Highway Research Program Project 12-19A, Washington DC, December 1981.

Proceq SA. (2017). Resipod Family: Operating Instructions. Switzerland: Author.

R.A. Gummow, "A Viewpoint on the CP Criteria Applied to Reinforced Concrete Structures," presented at CORROSION 29 2018, TG 545 Meeting, Phoenix, AZ, April 15, 2018

Sagüés, Alberto A., Jae Bong Lee, Xiaoyuan Chang, Howard Pickering, Eric Nystrom, William Carpenter, S.C. Kranc, Tonya Simmons, Bruce Boucher, Sherry Hierholzer. *Corrosion of Epoxy Coated Rebar in Florida Bridges*. Final Report to Florida D.O.T. WPI 0510603. May 1994.

Sagüés, Alberto A., S.C. Kranc, Franciesco Presuel-Moreno, David Rey, Andres Torres-Acosta, Lan Yao. *Report No. BA502 - Corrosion Forecasting for 75-Year Durability Design of Reinforced Concrete*. Final Report to Florida D.O.T. WPI 0510805. December 2001.

"Section 413 Sealing Cracks and Concrete Structure Surfaces," in *FDOT Standard Specifications for Road and Bridge Construction*. Florida Department of Transportation, Rev. July 2020.

"Section 457 Integral Pile and Column Jackets," Florida Department of Transportation, Jan 7, 2016.

Sharp, S. R., Clemena, G. G., Virmani, Y. P., Stone, G. E., & Kelly, R. G. (2002). FHWA-RD-02-107, Electrochemical Chloride Extraction: Influence of Concrete Surface on Treatment. McLean, Virginia: Federal Highway Administration.

Tinnea, Jack, Lianfang Li, William H. Hartt, & Alberto Sagues. "Corrosion in Bridges in Highways." *ASM Handbook Vol 13C, Corrosion: Environments and Industries* (2006): 558-597.

APPENDIX A. GANDY AND HOWARD FRANKLAND BRIDGES - PILE JACKET ELECTRICAL TESTING DATA

Old Howard Frankland Bridge, 2001 Installation

Table E1. Cathodic protection system test data for select piles at Bridge No. 150107 (Groups 1 to 5).

Pile No.	Year	Current Output, mA						Potential Measurements, mV CSE												
									Reinforcing Steel									LJ Anodes		BZ Anode	
		Total	LJ Curr. w/ BZ	BZ Curr. w/ LJ	LJ Alone	BZ Alone	BZ/LJ	Location	Static	On	IO	Days Decay	Decay Pot.	Polar./ Dep.	Days Decay	Decay Pot.	Depol.	On	IO	On	IO
14-4	2001	35			64	212		Port	-333		-417			84							
								Water	-559		-788			229							
	2013	8	1	8	1	9	4	Port		-828	-824				28	-813	11	-834	-835	-836	-845
								Water		-929	-926					-905	21	-924	-926	-929	-935
	2020	1	1	5	1	5	2	Port		-607	-602				17	-639	-37	-607	-609	-602	-614
								Water		-1011	-1010					-975	35	-1010	-1014	-1011	-1027
	Δ	-34																			
65-8	2001	43			107	202		Port	-272		-459			187							
								Water	-608		-824			216							
	2013	14	4	11	5	12	4	Port		-899	-889				28	-804	85	-898	-900	-901	-914
								Water		-1038	-1036					-967	69	-1039	-1044	-1028	-1041
	2020	9	1	9	0	10	6	Port		-735	-727				16	-675	52	-740	-746	-751	-751
								Water		-1026	-1025					-987	38	-1024	-1024	-1025	-1024
	Δ	-34																			
80-6 [1]	2001	62			103	200		Port	-361		-620			259							
								Water	-619		-818			199							
	2013	13	4	10	5	11	7	Port		-909	-903				28	-824	79	-900	-902	-911	-925
								Water		-1032	-1030					-994	36	-1032	-1034	-1033	-1045
	2020	6	1	5	1	5	4	Port		-710	-710				17	-597	113	-722	-725	-729	-742
								Water		-1008	-1007					-983	24	-1007	-1008	-994	-1004
	Δ	-56																			
99-9 [3]	2001	46			159	211		Port	-250		-365			115							
								Water	-595		-823			228							
	2013	7	6	2	6	2	-1	Port		-879	-871				28	-812	59	-886	-887	-888	-890
								Water		-1007	-1005					-971	34	-1009	-1014	-1008	-1011
	2020	2	4	-2	4	-3	-3	Port		-825	-824				17	-725	99	-840	-840	-834	-831
								Water		-949	-947					-957	-10	-965	-975	-915	-919
	Δ	-44																			
116-4	2001	65			62	177		Port	-375		-494			119							
								Water	-700		-889			189							
	2013	26	4	25	4	27	12	Port		-810	-800				28	-721	79	-808	-810	-811	-828
								Water		-1036	-1031					-982	49	-1036	-1038	-1031	-1049
	2020	17	6	9	7	11	4	Port		-713	-702				16	-652	50	-715	-721	-716	-731
								Water		-997	-997					-915	82	-993	-1001	-995	-1011
	Δ	-48																			
123-8	2001	91			81	253		Port	-317		-462			145							
								Water	-600		-792			192							
	2013	55	5	52	5	53	3	Port		-864	-842				28	-701	141	-859	-865	-867	-896
								Water		-1077	-1072					-1008	64	-1078	-1091	-1076	-1100
	2020	44	5	39	5	41	5	Port		-689	-655				16	-689	-34	-687	-692	-675	-728
								Water		-1035	-1034					-930	104	-1030	-1046	-1034	-1080
	Δ	-47																			
	2001	50			48	177		Port	-330		-563			233							
								Water	-497		-796			299							
	2013	20	1	21	1	21	9	Port		-910	-898				28	-855	43	-914	-915	-916	-942

Routine electrical data obtained and provided by 3e+, Inc. through separate contract with FDOT.

Old Howard Frankland Bridge, 2001 Installation

129-6								Water		-1030	-1027					-985	42	-1030	-1032	-1032	-1052
	2020	19						Port		-762	-748				16	-711	37	-770	-762		
								Water		-1008	-1006					-890	116	-1006	-1026		
	Δ	-31																			
138-7	2001	137			90	260		Port	-412		-574			162							
								Water	-616		-884			268							
	2013	38	3	40	4	42	8	Port		-862	-844				27	-788	56	-879	-881	-884	-910
								Water		-1075	-1069					-997	72	-1076	-1079	-1078	-1097
	2020	5	4	22	4	24	5	Port		-776	-752				16	-686	66	-789	-792	-780	-815
								Water		-1050	-1044					-911	133	-1043	-1066	-1050	-1079
	Δ	-132																			
177-4 [1]	2001	84			93	230		Port													
								Water	-562		-719			157							
	2013	62	-48	97	52	83	101	Port		-972	-930				27	-645	285	-906	-907	-990	-1004
								Water		-1098	-1064					-749	315	-1064	-1066	-1097	-1103
	2020	9	-3	10	6	8	7	Port		-857	-748				16	-572	176	-859	-863	-879	-895
								Water		-1078	-976					-754	222	-1047	-1060	-1080	-1092
	Δ	-75																			
182-3	2001	61			40	155		Port													
								Water	-629		-764			135							
	2013	6	2	7	1	8	4	Port		-879	-871				46	-836	35	-883	-890	-886	-892
								Water		-1030	-1028					-990	38	-1028	-1030	-1034	-1045
	2020	12	3	12	3	12	4	Port		-863	-859				16	-822	37	-861	-872	-868	-898
								Water		-1030	-1029					-989	40	-1028	-1036	-1030	-1049
	Δ	-49																			
190-6	2001	83			63	248		Port													
								Water	-528		-694			166							
	2013	18	12	14	12	15	5	Port		-698	-670				45	-621	49	-712	-716	-688	-711
								Water		-972	-968					-935	33	-973	-996	-974	-990
	2020	31	7	27	7	27	2	Port		-506	-485				17	-400	85	-512	-516	-497	-526
								Water		-1065	-1062					-1011	51	-1061	-1078	-1068	-1093
	Δ	-52																			
214-3	2001	61			240	267		Port													
								Water	-433		-650			217							
	2013	86	28	86	27	89	-2	Port		-802	-782				46	-671	111	-812	-814	-816	-842
								Water		-1080	-1076					-1016	60	-1082	-1096	-1083	-1104
	2020	25	4	26	5	26	5	Port		-609	-609				16	-584	25	-614	-625	-635	-654
								Water		-996	-1000					-1021	-21	-983	-1010	-998	-1005
	Δ	-36																			
289-2	2001	87			171	339		Port													
								Water	-486		-692			206							
	2013	54	25	38	27	42	10	Port		-695	-680				28	-525	155	-698	-709	-699	-720
								Water		-1082	-1075					-991	84	-1081	-1105	-1085	-1101
	2020	19	6	10	11	15	-1	Port		-460	-414				16	-377	37	-454	-472	-460	-480
								Water		-1064	-1014					-980	34	-1046	-1071	-1000	-1039
	Δ	-68																			
	2001	84			239	265		Port													
								Water	-559		-714			155							
	2013	68	71	7	72	9	-21	Port		-822	-809				46	-614	195	-818	-820	-817	-820

Routine electrical data obtained and provided by 3e+, Inc. through separate contract with FDOT.

Old Howard Frankland Bridge, 2001 Installation

308-5								Water		-986	-983					-887	96	-988	-1007	-987	-989
	2020	6	12	1	13	1	-5	Port		-761	-744				16	-634	110	-753	-748	-707	-721
								Water		-931	-917					-883	34	-930	-917	-931	-932
	Δ	-78																			

Old Howard Frankland Bridge, 2005 Installation

Table E1. Cathodic protection system test data for select piles at Bridge No. 150107 (Groups 1 to 5).

Pile No.	Year	Current Output, mA						Potential Measurements, mV CSE													
									Reinforcing Steel								LJ Anodes		BZ Anode	
		Total	LJ Curr. w/ BZ	BZ Curr. w/ LJ	LJ Alone	BZ Alone	BZ/LJ	Location	Static	On	IO	Days Decay	Decay Pot.	Polar./ Dep.	Days Decay	Decay Pot.	Depol.	On	IO	On	IO
12-1 [1]	2005	73			68	121		Port	-624		-772			148							
								Water	-790		-939			149							
	2013	7	2	4	5	6	3	Port		-906	-897				28	-821	76	-855	-861	-903	-909
								Water		-996	-995					-915	80	-993	-996	-991	-999
	2020	3	2	1	3	0	0	Port		-760	-754				17	-755	-1	-759	-767	-759	-764
								Water		-946	-942					-907	35	-944	-951	-944	-947
	Δ	-70																			
44-5 [2]	2005	22			25	31		Port	-530		-681			151							
								Water	-767		-913			146							
	2013	2	-3	5	2	3	5	Port		-770	-749				44	-325	424	-774	-773	-776	-787
								Water		-1076	-1053					-548	505	-1074	-1069	-1078	-1083
	2020	10	-1	-1	10	14	4	Port		-675	-669				16	-514	155	-733	-733	-756	-762
								Water		-1016	-990					-709	281	-1029	-1035	-1060	-1063
	Δ	-12																			
53-3	2005	39			76	169		Port	-518		-639			121							
								Water	-804		-971			167							
	2013	31	6	29	6	31	4	Port		-638	-626				44	-603	23	-642	-647	-643	-671
								Water		-1061	-1054					-973	81	-1061	-1071	-1063	-1084
	2020	20	9	12	16	20	2	Port		-662	-653				16	-605	48	-706	-706	-685	-686
								Water		-1039	-1035					-990	45	-1071	-1090	-688	-688
	Δ	-19																			
73-5 [1]	2005	48			140	161		Port	-630		-749			119							
								Water	-766		-911			145							
	2013	12	-2	15	3	14	10	Port		-742	-727				28	-638	89	-735	-738	-748	-766
								Water		-1032	-1019					-981	38	-1010	-1018	-1036	-1046
	2020	3	2	13	4	14	4	Port		-510	-505				17	-493	12	-511	-513	-549	-549
								Water		-1016	-1016					-963	53	-1006	-1009	-1054	-1054
	Δ	-45																			
105-9	2005	31			92	123		Port	-563		-702			139							
								Water	-739		-870			131							
	2013	7	0	8	5	8	7	Port		-883	-880				28	-775	105	-885	-890	-885	-891
								Water		-1012	-1005					-929	76	-1016	-1019	-1019	-1026
	2020	13	-8	12	1	12	9	Port		-566	-554				17	-496	58	-554	-557	-554	-576
								Water		-961	-924					-898	26	-822	-780	-1011	-1019
	Δ	-18																			
	2005	94			98	236		Port	-380		-496			116							
								Water	-671		-893			222							

Routine electrical data obtained and provided by 3e+, Inc. through separate contract with FDOT.

Old Howard Frankland Bridge, 2005 Installation

120-1	2013	47	-1	54	4	55	25	Port		-657	-640				28	-631	9	-664	-666	-678	-707
								Water		-1035	-1030					-1009	21	-1031	-1034	-1033	-1063
	2020	38	37	-2	35	2	-9	Port		-623	-605				16	-586	19	-620	-627	-599	-602
								Water		-1048	-1043					-926	117	-1049	-1070	-1043	-1046
	Δ	-56																			
133-5	2005	60			149	187		Port	-470		-581			111							
								Water	-761		-913			152							
	2013	47	7	43	17	42	20	Port		-633	-626				28	-522	104	-641	-643	-643	-644
								Water		-948	-942					-862	80	-950	-953	-955	-955
	2020	13	18	30	22	29	9	Port		-600	-598				16	-577	21	-617	-618	-607	-608
								Water		-916	-838					-833	5	-900	-904	-921	-923
	Δ	-47																			
191-3 [4]	2005	69			105	192		Port	-600		-742			142							
								Water	-755		-939			184							
	2013	189	51	171	56	181	36	Port		-704	-678				1	-667	11	-712	-745	-719	-812
								Water		-961	-938					-865	73	-970	-1012	-976	-1055
	2020	12	11	-3	12	0	0	Port		-707	-705				17	-694	11	-717	-717	-745	-746
								Water		-1032	-1031					-1005	26	-1045	-1046	-1038	1058
	Δ	-57																			
214-6	2005	90			107	234		Port	-497		-628			131							
								Water	-702		-858			156							
	2013	110	32	122	32	129	34	Port		-738	-725				28	-682	43	-743	-745	-740	-765
								Water		-1046	-1043					-991	52	-1047	-1052	-1048	-1069
	2020	15	1	0	19	0	0	Port		-542	-537				16	-494	43	-558	-562	-550	-555
								Water		-976	-932					-980	-48	-910	-920	-895	-920
	Δ	-75																			
236-7	2005	43			115	162		Port	-525		-661			136							
								Water	-801		-938			137							
	2013	0	2	-2	0	0	-2	Port		-832	-829				46	-701	128	-759	-775	-743	-748
								Water		-1020	-1018					-917	101	-991	-992	-980	-982
	2020	3	11	11	3	-3	-2	Port		-604	-599				16	-280	319	-631	-628	-575	-574
								Water		-853	-844					-500	344	-862	-862	-810	-808
	Δ	-40																			
263-1	2005	64			118	171		Port	-650		-788			138							
								Water	-730		-877			147							
	2013	99	9	100	14	105	40	Port		-690	-652				27	-596	56	-710	-714	-713	-805
								Water		-894	-875					-746	129	-896	-904	-900	-969
	2020	8	8	-14	12	2	0	Port		-583	-503				16	-290	213	-566	-589	-458	-482
								Water		-797	-741					-505	236	-786	-837	-734	-765
	Δ	-56																			
270-2	2005	64			138	192		Port	-518		-641			123							
								Water	-766		-940			174							
	2013	58	11	31	26	59	25	Port		-651	-642				28	-555	87	-653	-658	-657	-687
								Water		-1028	-1020					-938	82	-1028	-1036	-1029	-1055
	2020	30	-2	11	12	25	4	Port		-467	-429				16	-262	167	-408	-426	-410	-442
								Water		-956	-920					-704	216	-901	-923	-907	-928
	Δ	-34																			
	2005	54			117	229		Port	-580		-729			149							
								Water	-734		-1023			289							

Routine electrical data obtained and provided by 3e+, Inc. through separate contract with FDOT.

Old Howard Frankland Bridge, 2009 Installation

289-5	2013	9	4	6	4	7	2	Port		-593	-589				28	-464	125	-600	-602	-599	-605
								Water		-1035	-1033					-938	95	-1034	-1038	-1034	-1039
	2020	100	105	76	106	91	2	Port		-436	-423				16	-404	19	-475	-491	-448	-466
								Water		-950	-944					-891	53	-941	-954	-918	-932
	Δ	46																			

Old Howard Frankland Bridge, 2009 Installation

Table E1. Cathodic protection system test data for select piles at Bridge No. 150107 (Groups 1 to 5).

Pile No.	Year	Current Output, mA						Potential Measurements, mV CSE														
									Reinforcing Steel										LJ Anodes		BZ Anode	
		Total	LJ Curr. w/ BZ	BZ Curr. w/ LJ	LJ Alone	BZ Alone	BZ/LJ	Location	Static	On	IO	Days Decay	Decay Pot.	Polar./ Dep.	Days Decay	Decay Pot.	Depol.	On	IO	On	IO
138-8	2009	177			49	467		Port	-495		-650			155							
								Water	-761		-1013			252							
	2013	44	11	38	10	40	6	Port		-852	-829				27	-715	114	-854	-857	-852	-885
								Water		-1062	-1055					-995	60	-1060	-1071	-1061	-1093
	2020	37	35	-3	34	1	0	Port		-646	-627				16	-584	43	-652	-657	-617	-619
								Water		-944	-939					-870	69	-940	-973	-939	-939
	Δ	-140																			
198-1	2009	127			80	606		Port	-704		-804			100							
								Water	-737		-901			164							
	2013	16	12	9	11	9	4	Port		-953	-942				28	-875	67	-955	-960	-953	-1009
								Water		-1038	-1037					-976	61	-1039	-1054	-1038	-1099
	2020	14	10	7	116	7	2	Port		-952	-937				16	-930	7	-944	-949	-936	-960
								Water		-966	-957					-950	7	-990	-969	-943	-964
	Δ	-113			92																
304-4	2009	145			18	108		Port	-508		-693			185							
								Water	-809		-983			174							
	2013	30	4	31	5	32	13	Port		-953	-948				29	-825	123	-958	-959	-955	-978
								Water		-1076	-1072					-994	78	-1077	-1079	-1078	-1094
	2020	25	-15	25	1	30	14	Port		-904	-903				16	-816	87	-895	-897	-897	-933
								Water		-1034	-1000					-1009	-9	-1022	-1013	-969	-1019
	Δ	-120																			

Routine electrical data obtained and provided by 3e+, Inc. through separate contract with FDOT.

Gandy Bridge, 2001 Installation

Table F1. Cathodic protection system test data for select piles at Bridge No. 100300 (Gandy Bridge) (Groups 6 and 7).

Pile No.	Year	Current Output, mA						Potential Measurements, mV CSE										
									Reinforcing Steel						LJ Anodes		BZ Anode	
		Total	LJ Curr. w/ BZ	BZ Curr. w/ LJ	LJ Alone	BZ Alone	BZ/LJ	Location	Static	On	IO	Days Decay	Decay Pot.	Polar./ Dep.	On	IO	On	IO
85-4	2001	23			97	105		Port	-260		-411			151				
								Water	-664		-793			129				
	2013	26	10	12	11	14	5	Port		-864	-857	15	-716	141	-871	-873	-873	-889
								Water		-1052	-1048		-944	104	-1053	-1058	-1053	-1063
	2020	39	29	4	18	8	-5	Port		-796	-794	16	-648	146	-831	-833	-825	-817
								Water		-978	-977		-830	147	-1033	-1037	-995	-996
	Δ	16																

Routine electrical data obtained and provided by 3e+, Inc. through separate contract with FDOT.

Gandy Bridge, 2009 Installation

Table F1. Cathodic protection system test data for select piles at Bridge No. 100300 (Gandy Bridge) (Groups 6 and 7).

Pile No.	Year	Current Output, mA						Potential Measurements, mV CSE										
									Reinforcing Steel						LJ Anodes		BZ Anode	
		Total	LJ Curr. w/ BZ	BZ Curr. w/ LJ	LJ Alone	BZ Alone	BZ/LJ	Location	Static	On	IO	Days Decay	Decay Pot.	Polar./ Dep.	On	IO	On	IO
46-3	2009	183			56	453		Port	-663		-692			88				
								Water	-779		-968			189				
	2013	39	5	37	80	40	11	Port		-769	-755	15	-673	82	-770	-774	-773	-805
								Water		-1065	-1053		-916	137	-1062	-1071	-1066	-1090
	2020	120	102	0	111	0	0	Port		-689	-666	16	-557	109	-689	-703	-666	-599
								Water		-894	-884		-750	134	-894	-919	-884	-804
	Δ	-63																
82-6	2009	63			108	169		Port	-630		-669			39				
								Water	-826		-1019			193				
	2013	48	26	27	26	30	8	Port		-815	-809	15	-583	226	-817	-828	-817	-843
								Water		-1075	-1065		-919	146	-1078	-1090	-1079	-1093
	2020	46	28	22	22	25	7	Port		-663	-650	16	-644	6	-631	-675	-640	-623
								Water		-1030	-1023		-1018	5	-1023	-1049	-1017	-1006
	Δ	-17																
94-3 [1]	2009	69			44	263		Port	-612		-729			117				
								Water	-856		-1044			188				
	2013	9	8	32	9	32	7	Port		-846	-829	15	-581	248	-847	-848	-849	-871
								Water		-1079	-1067		-799	268	-1082	-1082	-1084	-1089
	2020	22	11	16	13	17	1	Port		-871	-834	70	-603	231	-877	-880	-857	-879
								Water		-1053	-1040		-839	201	-1045	-1063	-1052	-1065
	Δ	-47																
104-1	2009	130			34	301		Port	-603		-739			136				
								Water	-832		-981			149				
	2013	89	10	91	22	98	32	Port		-722	-709	15	-696	13	-727	-728	-726	-754
								Water		-968	-954		-949	5	-969	-972	-973	-983
	2020	14	3	20	7	21	9	Port		-807	-780	70	-571	209	-798	-800	-793	-829
								Water		-1051	-1050		-929	121	-1056	-1064	-1072	-1097
	Δ	-116																
106-7	2009	153			92	227		Port	-596		-686			90				
								Water	-875		-1031			156				
	2013	131	71	74	80	81	12	Port		-771	-739	15	-502	237	-792	-793	-792	-799
								Water		-1088	-1051		-896	155	-1086	-1091	-1081	-1093
	2020	38	22	26	24	25	15	Port		-723	-718	70	-530	188	-723	-728	-720	-762
								Water		-1063	-1054		-853	201	-1047	-1053	-1064	-1088
	Δ	-115																
	2009	131			65	227		Port	-689		-755			66				
								Water	-910		-1003			93				

Routine electrical data obtained and provided by 3e+, Inc. through separate contract with FDOT.

Gandy Bridge, 2009 Installation

137-4	2013	52	24	41	25	72	11	Port		-857	-854	15	-773	81	-784	-787	-781	-802
								Water		-1058	-1052		-981	71	-955	-958	-958	-972
	2020	32	20	22	16	24	16	Port		-716	-715	70	-507	208	-722	-734	-718	-760
								Water		-1037	-1032		-921	111	-1034	-1048	-1046	-1076
	Δ	-99																
144-4	2009	90			63	300		Port	-688		-790			102				
								Water	-890		-1038			148				
	2013	33	3	32	10	36	8	Port		-844	-831	8	-745	86	-766	-767	-770	-794
								Water		-1052	-1035		-1000	35	-970	-974	-971	-985
	2020	17	-3	19	1	21	11	Port		-759	-744	70	-668	76	-770	-767	-772	-800
								Water		-1056	-1046		-971	75	-1041	-1042	-1057	-1079
	Δ	-73																

Routine electrical data obtained and provided by 3e+, Inc. through separate contract with FDOT.

APPENDIX B. GANDY AND HOWARD FRANKLAND BRIDGES - VISUAL OBSERVATIONS

Pile ID	CP Pile Jacket Observations	Pile Observations	Miscellaneous Observations	Figures
12-1	Splitting at top of jacket in NW corner and missing portion below	Vertical cracking extending upward from top of jacket on W face, also exhibiting rust staining	Apparent repair material at top of pile	Figure 70 Figure 71
14-4	Jacket splitting at bottom SE corner	None	Limited metalizing overspray on pile	Figure 72
44-5	Jacket broken off at bottom S face and split at top NE corner	Vertical cracking extending above top of jacket, measured up to 50 mil wide	Cracking of grout	Figure 73 Figure 74
53-3	Jacket splitting at NE corner and missing lower section	None	None	Figure 75
65-8	None	None	None	Figure 76
73-5	Jacket splitting and broken off around lower perimeter of pile	None	None	Figure 77
80-6	Apparent jacket extension on top, no distress noted	None	None	Figure 78
99-9	None	None	None	Figure 79
105-9	Jacket in poor condition	None	None	Figure 80
116-4	None	None	None	Figure 81
120-1	Jacket in poor condition	None	None	Figure 82 Figure 83
123-8	None	Minor spall on SW corner top, metalized over	None	Figure 84
129-6	Jacket extension on top, no distress noted	None	None	Figure 85
133-5	Jacket splitting and missing all around	Exposed steel with corrosion on S face	None	Figure 86
138-7	None	Repair on NW corner	None	Figure 87
138-8	Jacket splitting	Repair on NW corner	None	Figure 88
177-4	Jacket splitting right above water line at SE corner	None	None	Figure 89
182-3	Jacket cracking on N face	Spall repair on SE and SW corners	None	Figure 90
190-6	None	Cracking and spalling at NE corner	None	Figure 91

Pile ID	CP Pile Jacket Observations	Pile Observations	Miscellaneous Observations	Figures
191-3	Jacket splitting on N face	Failed repair of the bent cap underside	None	Figure 92
198-1	None	Vertical cracking on S face, repair on NE corner	None	Figure 93
214-3	None	None	None	Figure 94
214-6	None	Previous repairs with corroded anchors	None	Figure 95
236-7	Jacket splitting on NE corner	Cracking on NW, SE, and SW faces	None	Figure 96
263-1	None	Two cracks on N face	None	Figure 97
270-2	Jacket splitting on NE corner	Cracking on N face with corrosion staining, cracking on all faces	None	Figure 98
289-2	None	None	None	Figure 99
289-5	Jacket splitting on N face	Piles repair in all faces, cracking in previous repair	None	Figure 100
304-4	None	Cracking in repair on SE corner and S face	None	Figure 101
308-5	None	Cracking in repair at top of the pile	None	Figure 102
316-8	None	Repair on SE corner	None	Figure 103
46-3	Missing jacket at the bottom	Several cracks on E face, repairs on E and S face with cracking, cracking on W face	None	Figure 104
82-6	Minor impact damage to the jacket on E face	Repair on exposed portion of the pile on E and S faces, cracking on N face	None	Figure 105
85-4	Jacket opening at the bottom of E face	Spalling on N face	None	Figure 106 Figure 107
94-3	Jacket broken on E face	Cracking on E face, cracking in a repair on N face	None	Figure 108 Figure 109
104-1	None	Repair and cracking on the N face and NW corner	None	Figure 110
106-7	Jacket splitting at top on the SW corner	Cracking on NE, SE and SW corner, repair on NW corner with cracking	None	Figure 111
137-4	None	Cracking on parge coat, no pile cracking noted	None	Figure 112
144-4	Jacket broken at the bottom of E face	Cracking on S, W and E face, repair on SW corner	None	Figure 113

APPENDIX C. GANDY AND HOWARD FRANKLAND BRIDGES - SUMMARIZED ICCP DATA

Table 54. Gandy Bridge – Summary of Voltage and Resistance Measurement Data

Pier	226	231	241	244	245	Average
"On" Voltage	1.5	1.5	1.77	1.61	1.21	1.52
"IO" Voltage	1.32	1.37	1.5	1.43	1.15	1.35
AC Resistance	0.37	0.37	0.39	0.30	0.25	0.34

Units: Voltage = V, Resistance = Ohms

Table 55. HF Bridge – Summary of Voltage and Resistance Measurement Data

Pier	158	159	171	176	Average
"On" Voltage	1.86	1.65	1.55	1.57	1.66
"IO" Voltage	1.59	1.46	1.42	1.51	1.50
AC Resistance	0.67	0.27	0.26	0.24	0.36

Units: Voltage = V, Resistance = Ohms

Table 56. Summary of Potential Data from Permanent Reference Electrodes

Pier	**Gandy 226**				**Gandy 231**			
Ref. Electrode	1	2	3	Avg.	1	2	3	Avg.
"On" Potential	-310	-828	-876	-671	-327	-631	-834	-597
"IO" Potential	-284	-802	-823	-636	-310	-607	-820	-579
"Off" Potential	-406	-671	-474	-571	-327	-494	-678	-500
Depolarization	-122	131	349	119	-17	113	142	79
Pier	**Gandy 241**				**Gandy 244**			
Ref. Electrode	1	2	3	Avg.	1	2	3	Avg.
"On" Potential	-327	-822	-	-575	-877	-508	-	-693
"IO" Potential	-331	-754	-	-543	-850	-490	-	-670
"Off" Potential	-434	-587	-	-510	-717	-365	-	-541
Depolarization	-103	167	-	32	133	125	-	129
Pier	**Gandy 245**				**HF 158**			
Ref. Electrode	1	2	3	Avg.	1	2	3	Avg.
"On" Potential	-585	-398	-	-492	-540	-668	-621	-610
"IO" Potential	-577	-381	-	-479	-537	-624	-605	-589
"Off" Potential	-456	-354	-	-405	-323	-482	-460	-422
Depolarization	121	27	-	74	214	142	145	167
Pier	**HF 159**				**HF 171**			
Ref. Electrode	1	2	3	Avg.	1	2	3	Avg.
"On" Potential	-630	-177	-561	-456	-466	-241	-381	-363
"IO" Potential	-593	-139	-555	-429	-466	-241	-368	-358
"Off" Potential	-396	-66	-446	-303	-413	-156	-304	-291
Depolarization	197	73	109	126	53	85	64	67

Pier	**HF 176**			
Ref. Electrode	1	2	3	Avg.
"On" Potential	-894	-592	-838	-775
"IO" Potential	-705	-519	-760	-661
"Off" Potential	-577	-253	-516	-449
Depolarization	128	266	244	212

Units: Potentials = mV vs. CSE, Depolarization = mV

Table 57. Summary of Potential Data from External Reference Electrodes

Pier	**Gandy 226**				**Gandy 231**			
Ref. Electrode	1	2	3	Avg.	1	2	3	Avg.
"On" Potential	-852	-760	-808	-807	-752	-865	-807	-808
"IO" Potential	-814	-720	-777	-770	-725	-806	-764	-765
"Off" Potential	-620	-655	-687	-654	-620	-631	-673	-641
Depolarization	194	65	90	116	105	175	91	124
Pier	**Gandy 241**				**HF 158**			
Ref. Electrode	1	2	3	Avg.	1	2	3	Avg.
"On" Potential	-758	-1025	-	-892	-635	-582	-	-609
"IO" Potential	-755	-974	-	-865	-597	-582	-	-590
"Off" Potential	-719	-846	-	-783	-486	-457	-	-472
Depolarization	36	128	-	82	111	125	-	118
Pier	**HF 159**				**HF 171**			
Ref. Electrode	1	2	3	Avg.	1	2	3	Avg.
"On" Potential	-578	-499	-	-539	-559	-532	-	-546
"IO" Potential	-470	-467	-	-469	-540	-506	-	-523
"Off" Potential	-357	-334	-	-346	-383	-359	-	-371
Depolarization	113	133	-	123	157	147	-	152

Units: Potentials = mV vs. CSE, Depolarization = mV

APPENDIX D. MELBOURNE BRIDGE - VISUAL DISTRESS, NDE DATA, AND SAMPLE LOCATIONS

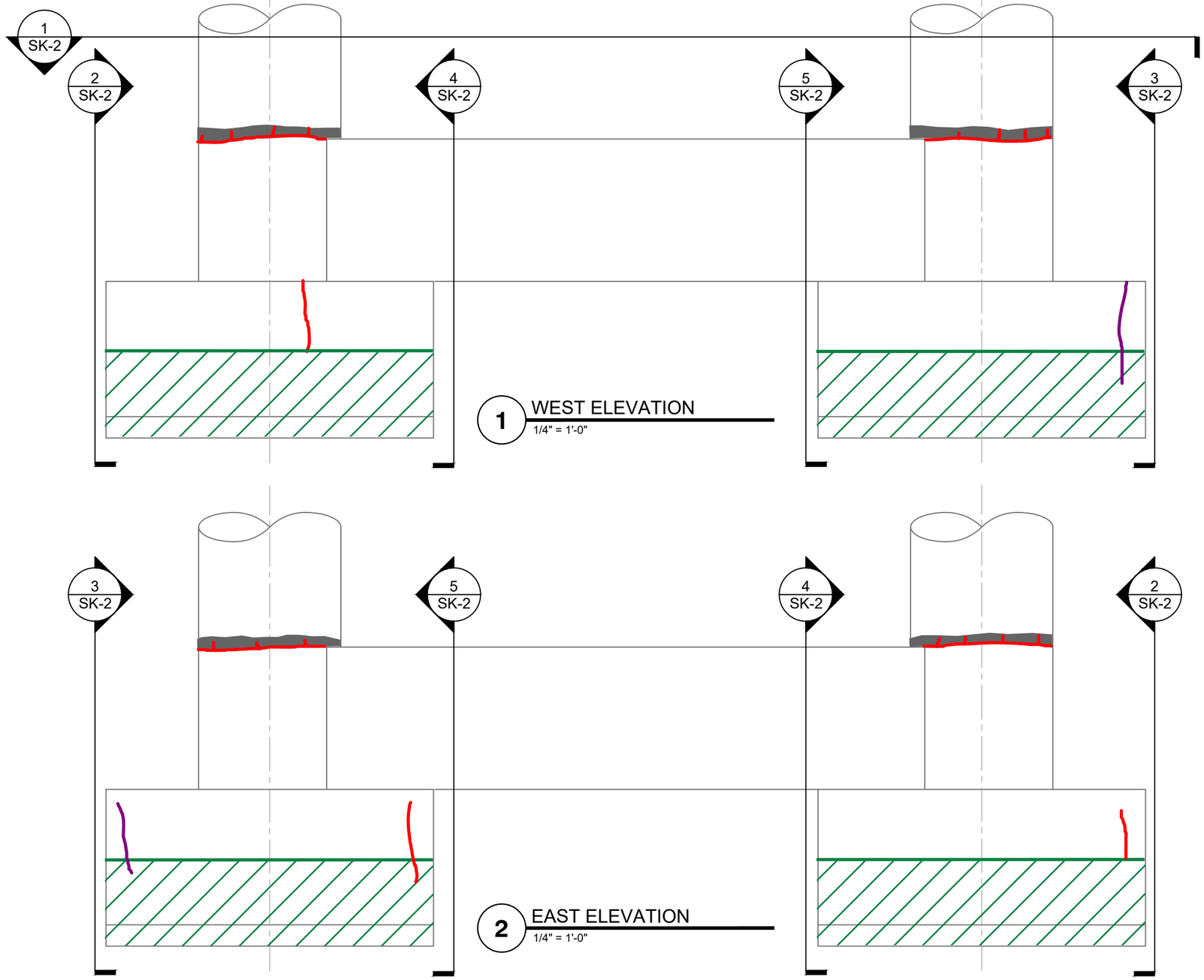

1 WEST ELEVATION
1/4" = 1'-0"

2 EAST ELEVATION
1/4" = 1'-0"

Legend:
- Cracking (<=20 mil)
- Cracking (>20 mil)
- Apparent Previous Repair
- Approximate Mean Growth Line

0 1/2" 1"
THIS SHEET PLOTS FULL SIZE AT 11x17 (INCHES)

Project	MELBOURNE CAUSEWAY (US 192) DISTRESS
Sheet Title	BRIDGE 700181 PIER 13 DISTRESS (1 of 2)
Proj. No.	2019.0352.1
Date	03-05-2021
Drawn	TJH
Checked	CJ
Scale	As Noted
Sheet No.	SK-1

Plotted: 3/5/2021 1:50 PM by Jones, Casey File Name: p:\2019\2019.0xxx\2019.0352.1 - fdot corrosion prevention & inspections (cj)\Drawings\Sketches\SK-DWGS.dwg

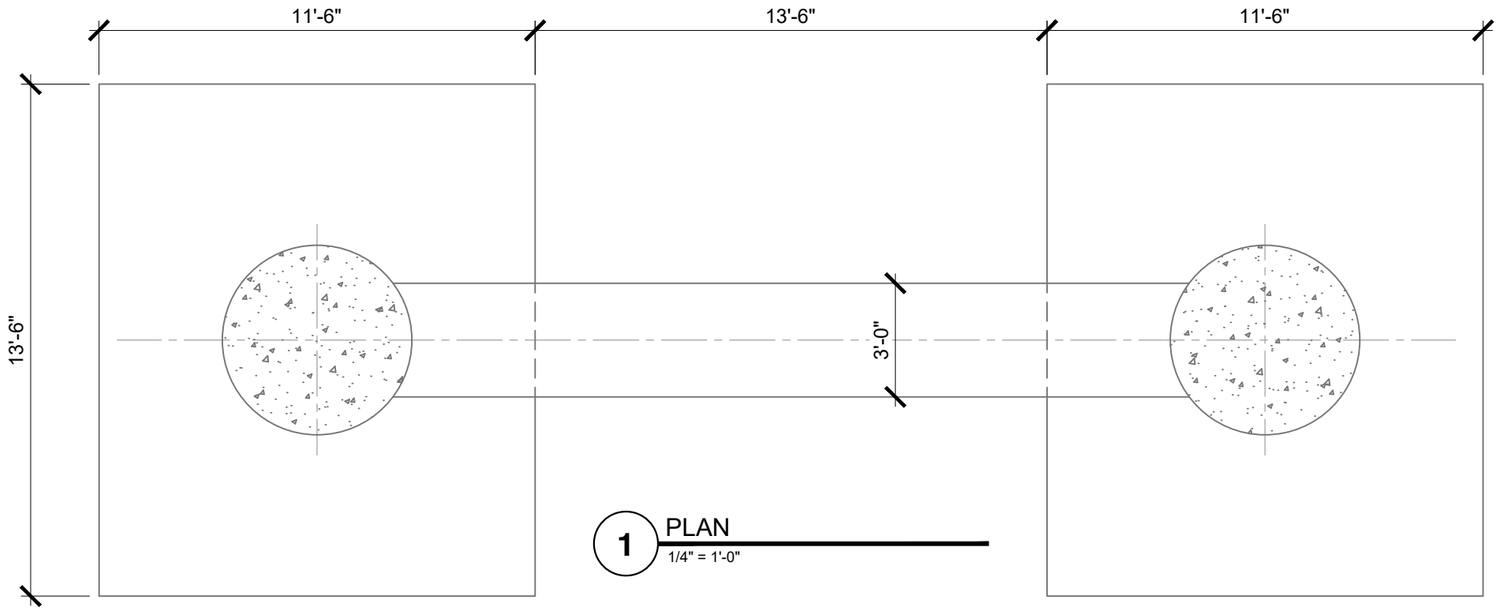

1 PLAN
1/4" = 1'-0"

Legend:
- Cracking (<=20 mil)
- Cracking (>20 mil)
- Apparent Previous Repair
- Approximate Mean Growth Line

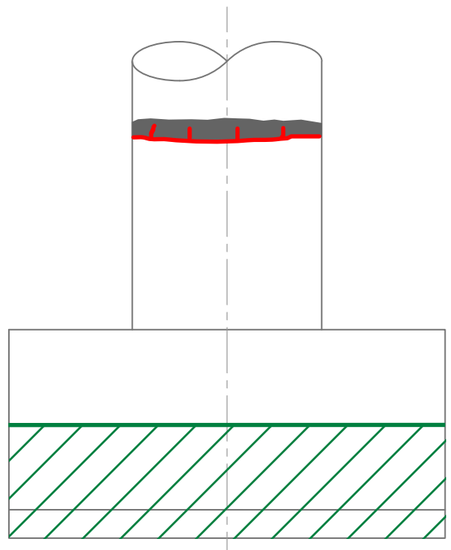

2 NORTH EXTERIOR ELEVATION
1/4" = 1'-0"

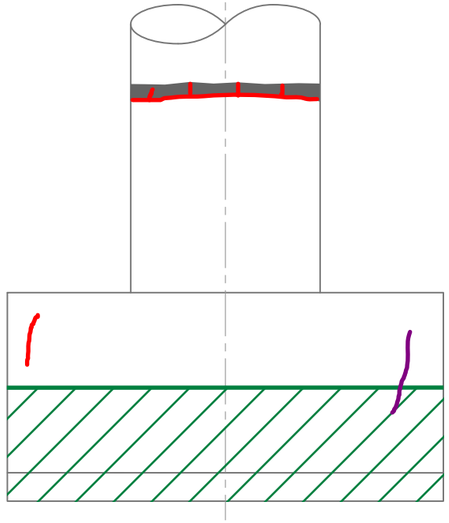

3 SOUTH EXTERIOR ELEVATION
1/4" = 1'-0"

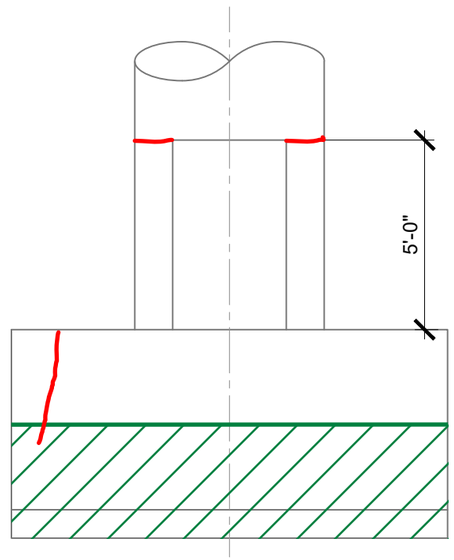

4 NORTH INTERIOR ELEVATION
1/4" = 1'-0"

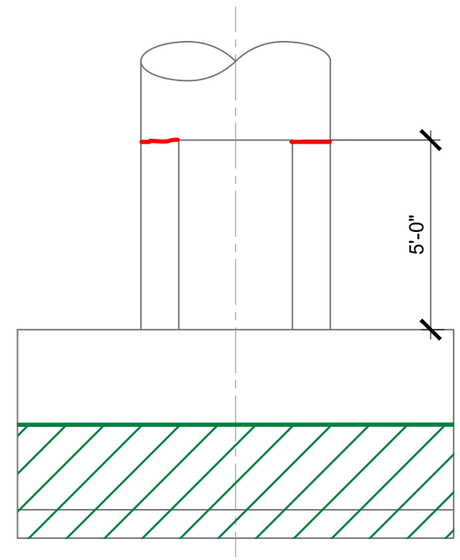

5 SOUTH INTERIOR ELEVATION
1/4" = 1'-0"

0 1/2" 1"
THIS SHEET PLOTS FULL SIZE AT 11x17 (INCHES)

Project	MELBOURNE CAUSEWAY (US 192) DISTRESS
Sheet Title	BRIDGE 700181 PIER 13 DISTRESS (2 of 2)
Proj. No.	2019.0352.1
Date	03-05-2021
Drawn	TJH
Checked	CJ
Scale	As Noted
Sheet No.	SK-2

Plotted: 3/5/2021 1:50 PM by Jones, Casey File Name: p:\2019\2019.0xxx\2019.0352.1 - fdot corrosion prevention & inspections (cj)\Drawings\Sketches\SK-DWGS.dwg

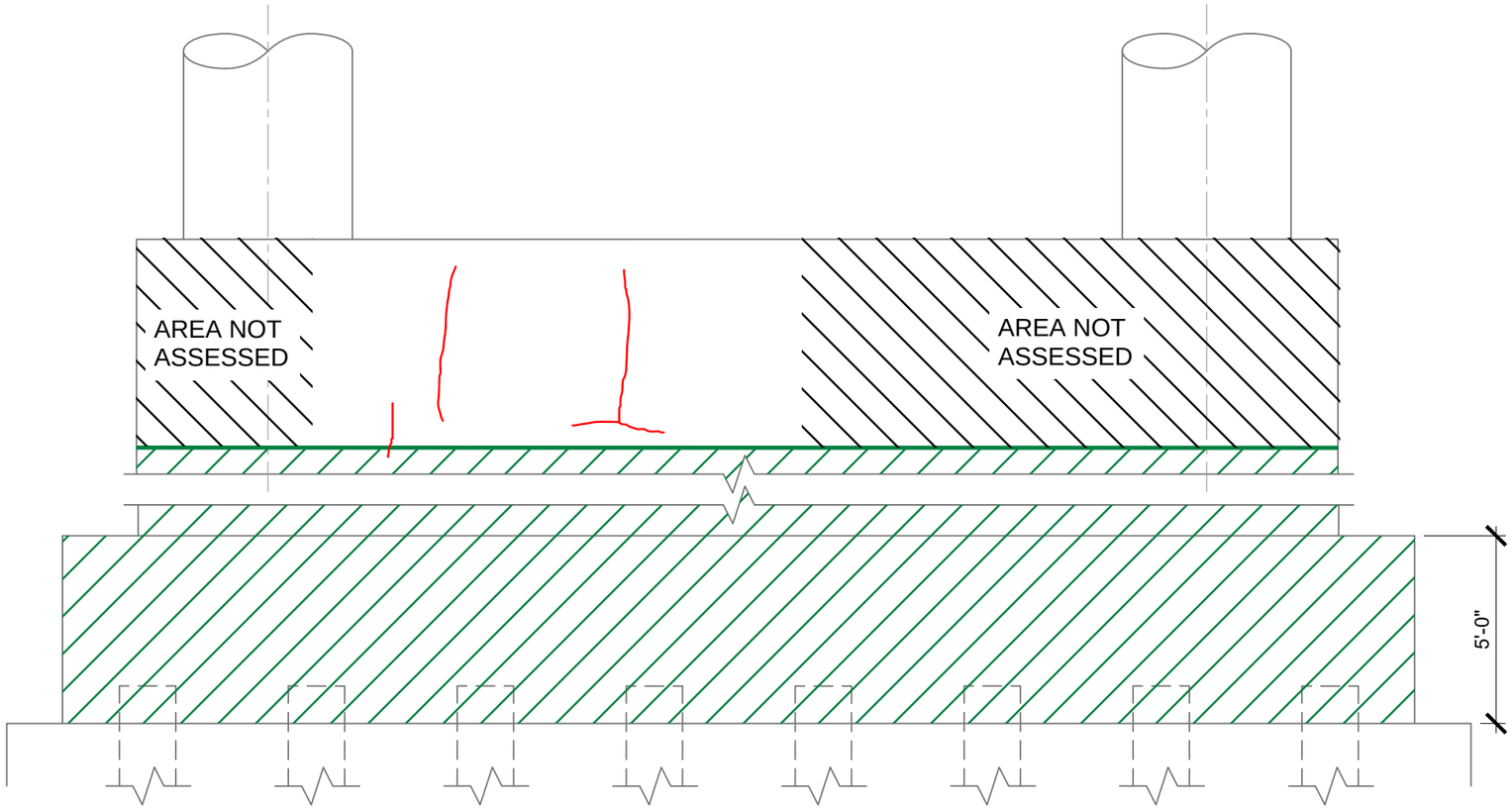

1 EAST ELEVATION
1/4" = 1'-0"

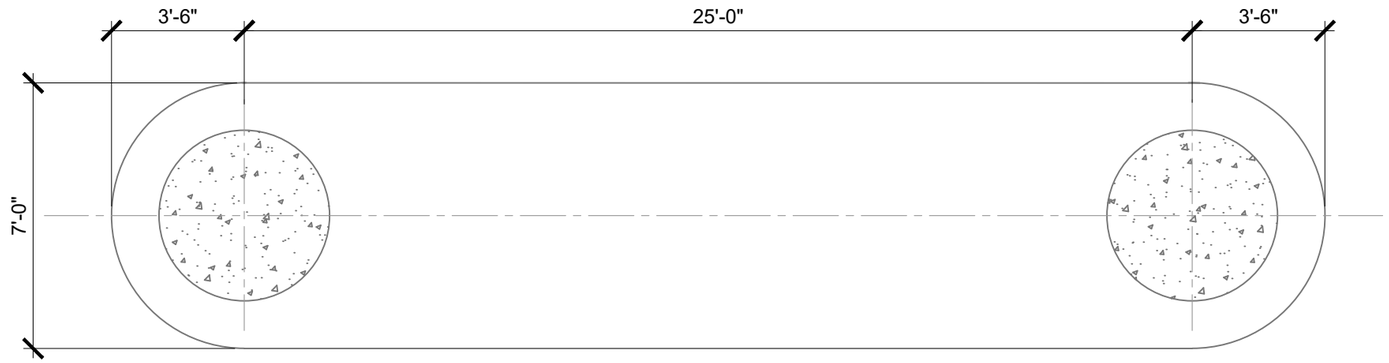

2 PLAN
1/4" = 1'-0"

Legend:
- Cracking (<=20 mil)
- Cracking (>20 mil)
- Apparent Previous Repair
- Approximate Mean Growth Line

N
NORTH

0 1/2" 1"
THIS SHEET PLOTS FULL SIZE AT 11x17 (INCHES)

Project	MELBOURNE CAUSEWAY (US 192) DISTRESS
Sheet Title	BRIDGE 700181 PIER 15 CRASH WALL DISTRESS
Proj. No.	2019.0352.1
Date	03-05-2021
Drawn	TJH
Checked	CJ
Scale	As Noted
Sheet No.	SK-3

Plotted: 3/5/2021 1:50 PM by Jones, Casey File Name: p:\2019\2019.0xxx\2019.0352.1 - fdot corrosion prevention & inspections (cj)\Drawings\Sketches\SK-DWGS.dwg

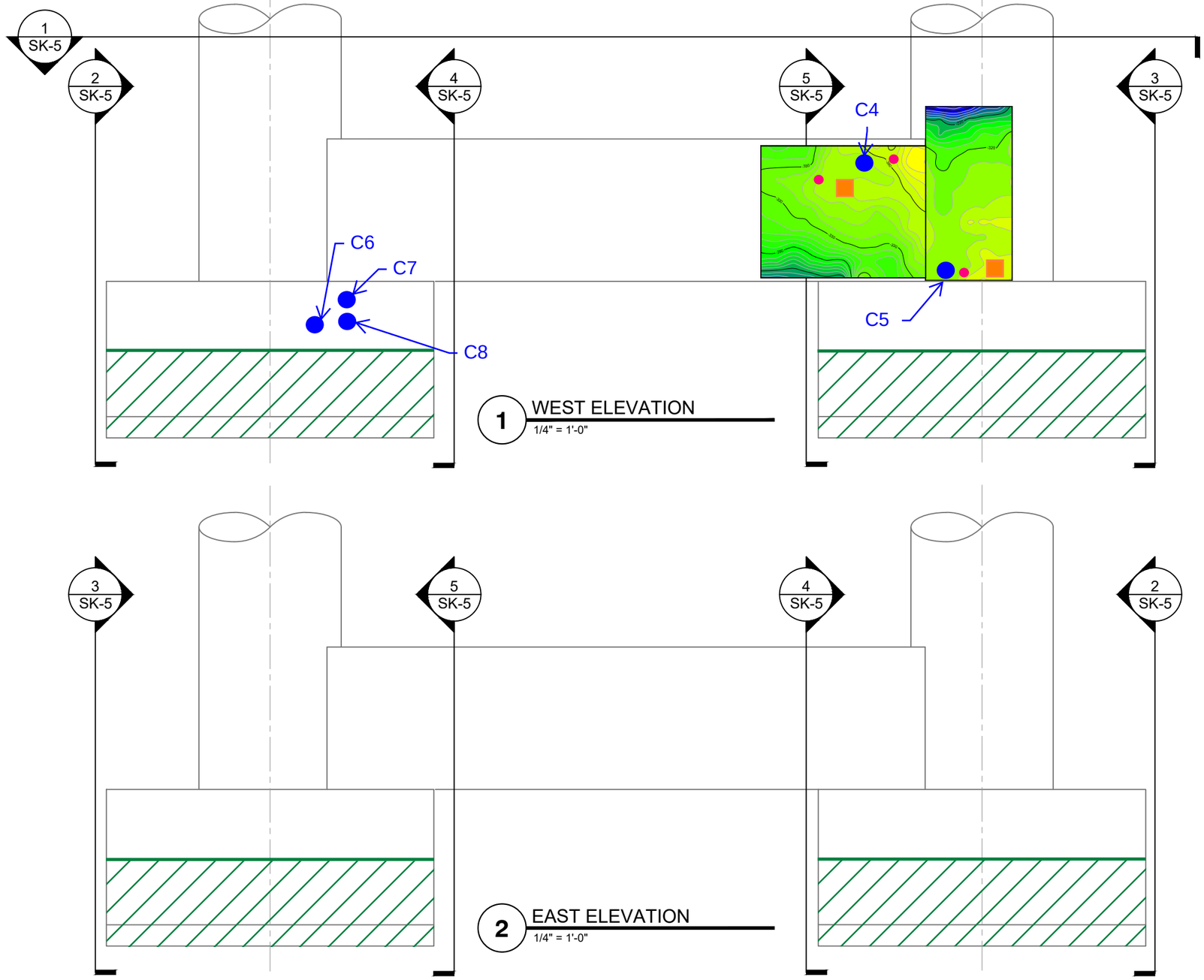

1 WEST ELEVATION
1/4" = 1'-0"

2 EAST ELEVATION
1/4" = 1'-0"

Legend:

- CX — Core Location and ID
- Drill Hole Location
- Surface Resistivity Location
- HCP Testing Location
- Approximate Mean Growth Line

HCP Legend:

-60
-80
-100
-120
-140
-160
-180
-200
-220
-240
-260
-280
-300
-320
-340
-360
-380
-400
-420

0 1/2" 1"
THIS SHEET PLOTS FULL SIZE AT 11x17 (INCHES)

Project	MELBOURNE CAUSEWAY (US 192) DISTRESS
Sheet Title	BRIDGE 700181 PIER 13 SAMPLE LOCATIONS & NDE DATA (1 of 2)
Proj. No.	2019.0352.1
Date	03-05-2021
Drawn	TJH
Checked	CJ
Scale	As Noted
Sheet No.	SK-4

Plotted: 3/5/2021 1:50 PM by Jones, Casey File Name: p:\2019\2019.0xxx\2019.0352.1 - fdot corrosion prevention & inspections (cj)\Drawings\Sketches\SK-DWGS.dwg

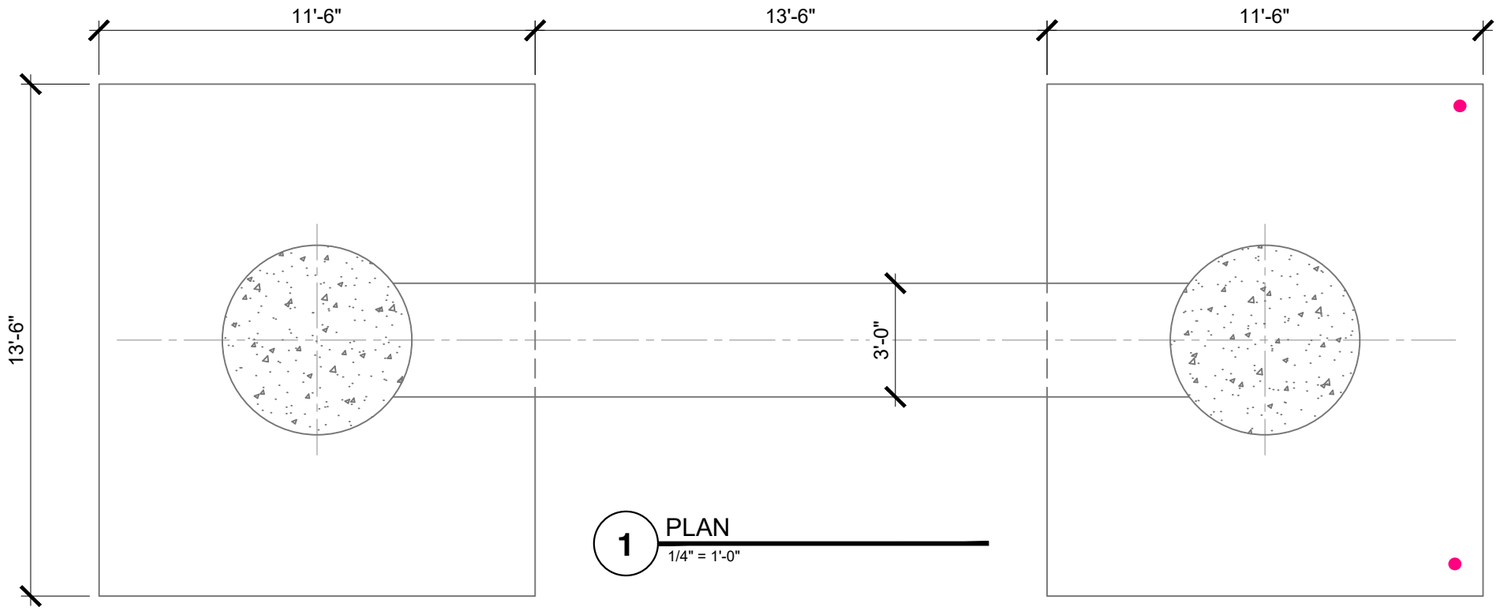

1 PLAN
1/4" = 1'-0"

Legend:
- CX — Core Location and ID
- Drill Hole Location
- Surface Resistivity Location
- HCP Testing Location
- Approximate Mean Growth Line

HCP Legend:

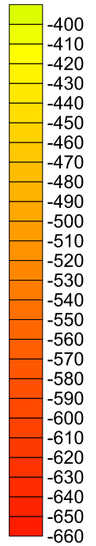

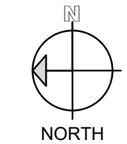

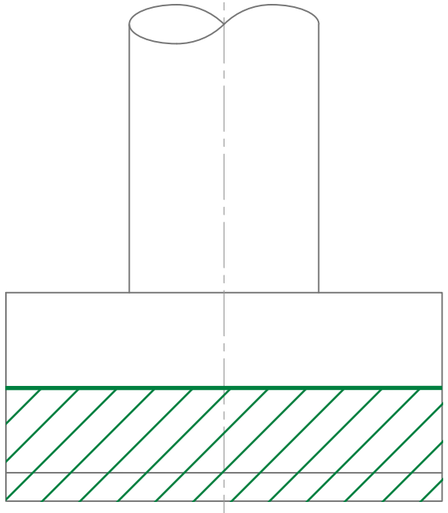

2 NORTH EXTERIOR ELEVATION
1/4" = 1'-0"

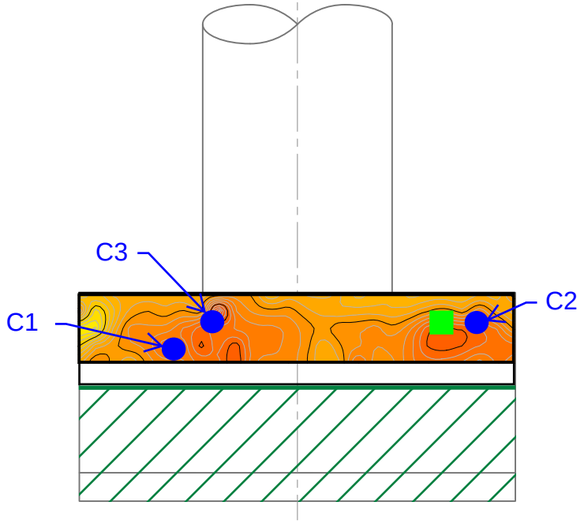

3 SOUTH EXTERIOR ELEVATION
1/4" = 1'-0"

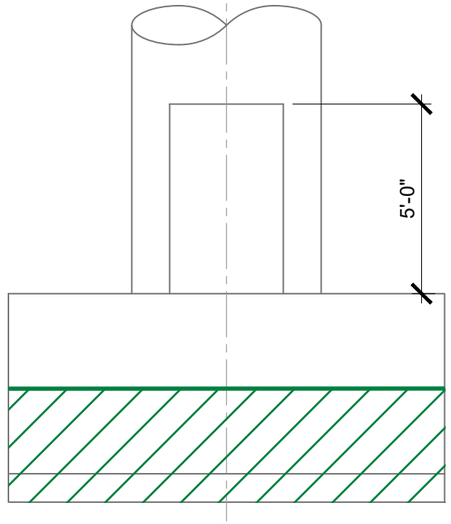

4 NORTH INTERIOR ELEVATION
1/4" = 1'-0"

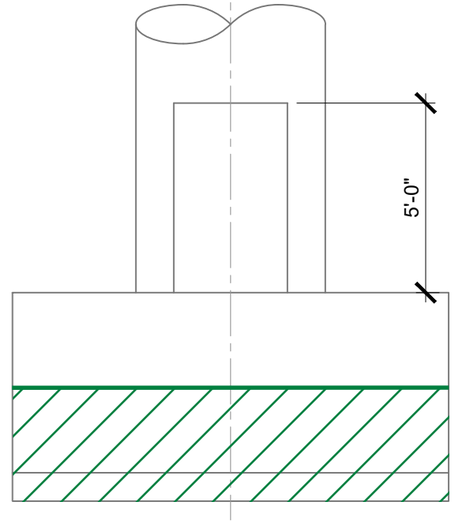

5 SOUTH INTERIOR ELEVATION
1/4" = 1'-0"

0 1/2" 1"
THIS SHEET PLOTS FULL SIZE AT 11x17 (INCHES)

Project	MELBOURNE CAUSEWAY (US 192) DISTRESS
Sheet Title	BRIDGE 700181 PIER 13 SAMPLE LOCATIONS & NDE DATA (2 of 2)
Proj. No.	2019.0352.1
Date	03-05-2021
Drawn	TJH
Checked	CJ
Scale	As Noted
Sheet No.	SK-5

Plotted: 3/5/2021 1:50 PM by Jones, Casey File Name: p:\2019\2019.0xxx\2019.0352.1 - fdot corrosion prevention & inspections (cj)\Drawings\Sketches\SK-DWGS.dwg

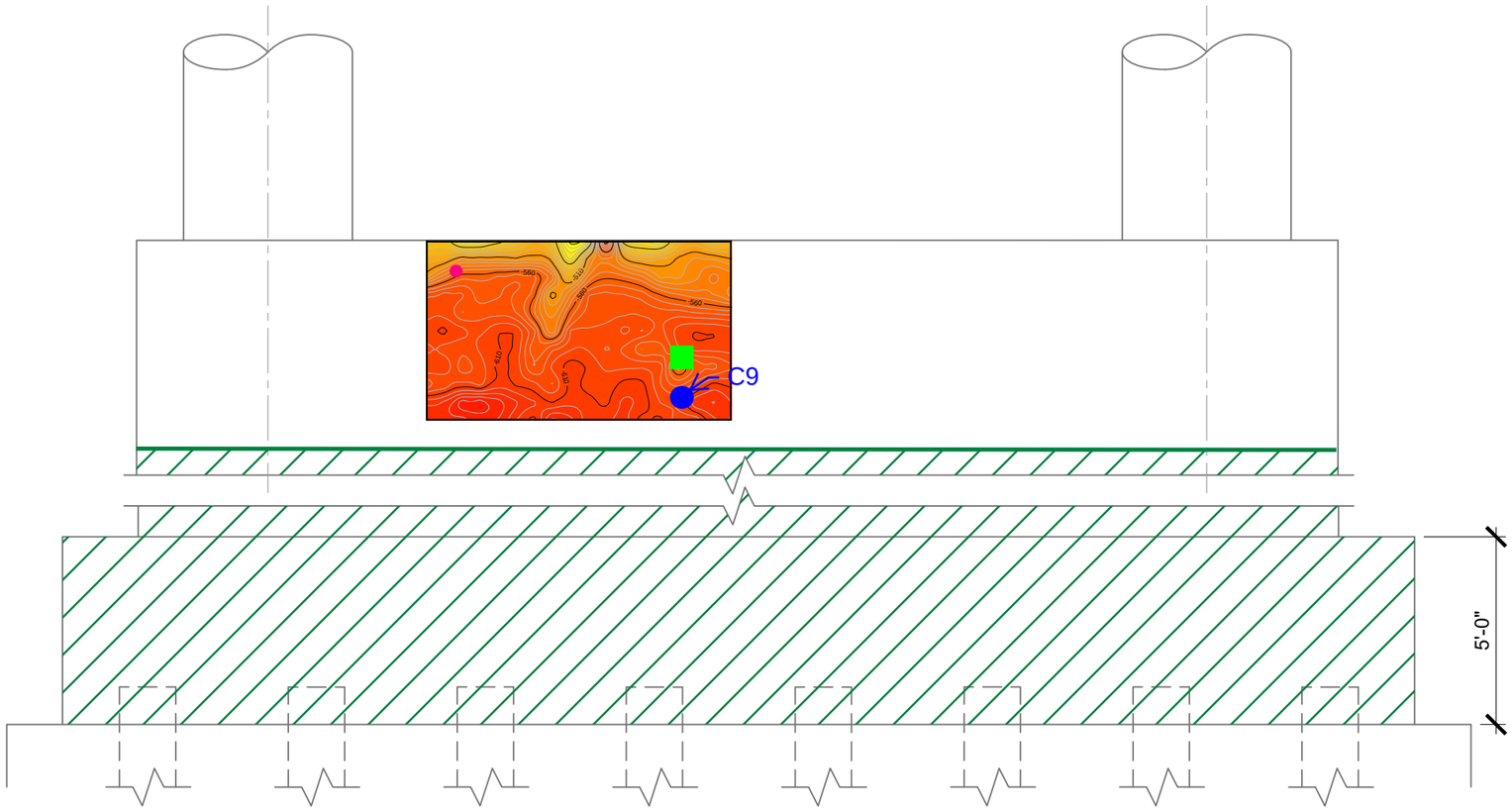

1 EAST ELEVATION
1/4" = 1'-0"

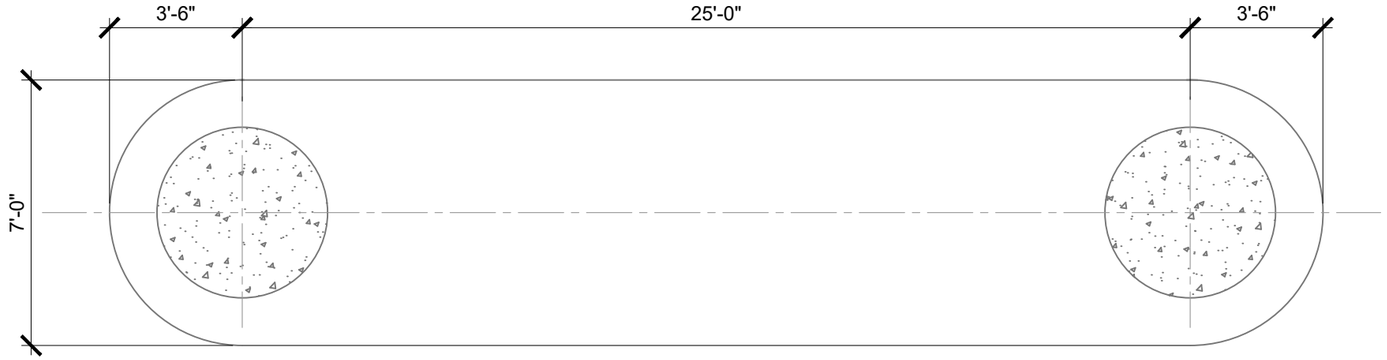

2 PLAN
1/4" = 1'-0"

Legend:
- CX — Core Location and ID
- Drill Hole Location
- Surface Resistivity Location
- HCP Testing Location
- Approximate Mean Growth Line

HCP Legend:

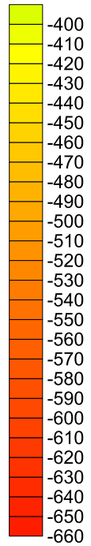

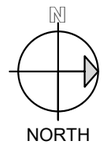

0 1/2" 1"
THIS SHEET PLOTS FULL SIZE AT 11x17 (INCHES)

Project	MELBOURNE CAUSEWAY (US 192) DISTRESS
Sheet Title	BRIDGE 700181 PIER 15 CRASH WALL SAMPLE LOCATIONS & NDE DATA
Proj. No.	2019.0352.1
Date	03-05-2021
Drawn	TJH
Checked	CJ
Scale	As Noted
Sheet No.	SK-6

Plotted: 3/5/2021 1:50 PM by Jones, Casey File Name: p:\2019\2019.0xxx\2019.0352.1 - fdot corrosion prevention & inspections (cj)\Drawings\Sketches\SK-DWGS.dwg

APPENDIX E. MELBOURNE BRIDGE - PETROGRAPHIC EXAMINATION REPORT

Petrographic examinations were conducted on two nominally 4-inch diameter core samples, identified Core 1 and Core 10. Core lengths, locations, and major findings are provided in Table 58. The cores were reportedly extracted from two bridges with different reinforcement (epoxy coated vs. black). Petrographic examinations were conducted in general accordance with ASTM C856, *Standard Practice for Petrographic Examination of Hardened Concrete*. Examinations were conducted on as-received cores (Figure 114 through Figure 117), lapped sections (Figure 118 through Figure 122), and laboratory-induced freshly fractured surfaces. A thin section was prepared from the exterior region of each core to determine the cementitious materials composition and refine water-to-cement ratio (w/c) estimations (Figure 123 and Figure 124). The purposes of the petrographic studies were to assess the general concrete characteristics, quality and condition, as well as evaluate if there are materials-related deleterious chemical reactions that could reduce the service life of the concrete. Brief visual examinations were also conducted on eight cores from the same project.

Major petrographic observations are provided in Table 58 and summarized as follows. Attached figures illustrate the findings.

- Concrete represented by the two cores contained similar constituents in similar proportion and generally exhibited similar physical characteristics.
- The concrete in each core is composed of crushed limestone coarse aggregate (3/4-inch nominal top size) and natural siliceous sand fine aggregate dispersed in non-air-entrained portland cement paste, with an estimated water-to-cement ratio 0.39 to 0.44. No slag or fly ash supplementary cementitious materials was observed.
- The concrete in each core is generally well consolidated. Distribution of constituents is uniform.
- No major cracks were observed. Core 10 contains minor short surface-perpendicular cracks that are typically less than 1 inch deep. The cracks appeared to be related to drying shrinkage.
- Minor surface spalling and surface-parallel cracks/microcracks were observed in Core 10. These features appeared to have been caused by coring. No secondary deposits were observed in the cracks, indicating the cracks are new or recent.
- No evidence of materials-related distress was observed. Both coarse aggregate (fossiliferous limestone) and fine aggregate (natural siliceous sand) appeared to have performed adequately. Ettringite was observed in air voids but no distress such as microcracking was observed associated with ettringite.
- Depth of carbonation was approximately 0.04 inch in Core 1 and approximately 0.3 inch in Core 10. The overall small depth of carbonation is likely relative to the concrete age and is consistent with a hard and dense cement paste in both cores.
- Estimated air content in both cores was 1 to 3 percent. Small spherical air voids were observed, likely due to use of chemical admixtures. No large entrapped voids were observed.
- Concrete represented by both cores appeared to be in good condition overall.

Summary

1. **Main Cracks:** None observed. Short and shallow hairline cracks were observed in Core 10, likely due to restrained drying shrinkage.
2. **Surface Loss and Surface-Parallel Cracks:** Minor surface loss and short microcracks were observed in Core 10, likely due to drying shrinkage and coring.
3. **ASR:** No evidence of alkali-silica reactions or other significant deleterious chemical reactions such as delayed ettringite formation (DEF) was observed in the cores.
4. **Distress Related to Seawater Exposure:** Minimal in Core 10; None observed in Core 1.
5. **Reinforcement:** Core 1 contained an imprint of No. 8 epoxy-coated steel reinforcing bar. The imprint is free of significant rust or staining, suggesting the bar is likely in good condition. No radiating cracking was observed surrounding the bar. No reinforcement bars or imprints were observed in Core 10.
6. **Carbonation:** Negligible in Core 1 and 0.3 inch in Core 10.
7. **Concrete Condition:** Appeared to be good overall in both cores.

Table 58. General Core Characteristics and Petrographic Findings

	Core 1	Core 10
Length	5.5 inches	2.8 inches
Exterior Surface	Overall flat formed/cast surface exhibited localized discolored areas due to biological growth and carbonate secondary deposits	Flat smooth formed surface exhibited two small spalled areas at edge and a few shallow hairline cracks.
Location	Bridge N. 700181 with epoxy-coated reinforcement Pile cap, S. face, 2" above MGL	Pier 15 on Bridge No. 700174 with black steel bar reinforcement
Interior Surface	Rough fractured surface extended mainly through coarse aggregate particles. An imprint of likely No. 8 steel reinforcing bar observed on the interior surface (4-3/8 inch cover), with minimal rust	Rough fractured surface extended mainly through coarse aggregate particles. No reinforcement or imprint was observed in the core
Coarse Aggregate	Similar in the two cores, composed of crushed fossiliferous limestone, with a nominal top size 3/4 inch. Vugs and voids associated with the rock diagenesis and formation are frequently observed, but these features did not connect or form a network.	
Fine Aggregate	Similar in the two cores, natural siliceous sand composed of mainly quartz/quartzite with small amounts of feldspar and miscellaneous rocks and minerals.	
Paste	Overall similar in composition (portland cement without SCMs), physical characteristics and estimated water-to-cement ratio (w/c). Medium gray, moderately hard to hard, and moderately low in water absorptivity. Estimated w/c was 0.39 to 0.44.	
Estimated W/C	0.39 to 0.44 in both	
Paste-Aggregate Bond	Interrelated to be tight in both cores	
Secondary Deposits	Ettringite frequently lines air voids in both cores. Likely minor seawater-related alteration in exterior 0.3 inch in Core 10. Small amounts of salts (NaCl) appeared to be present in the region.	
Materials-Related Distress	None observed	Probably minor paste alteration due to seawater exposure in the exterior 0.3 inch
Cracking/Micro cracking	Infrequent microcracking	Minor shallow surface perpendicular cracks likely due to drying shrinkage
Overall Condition	Good	Good

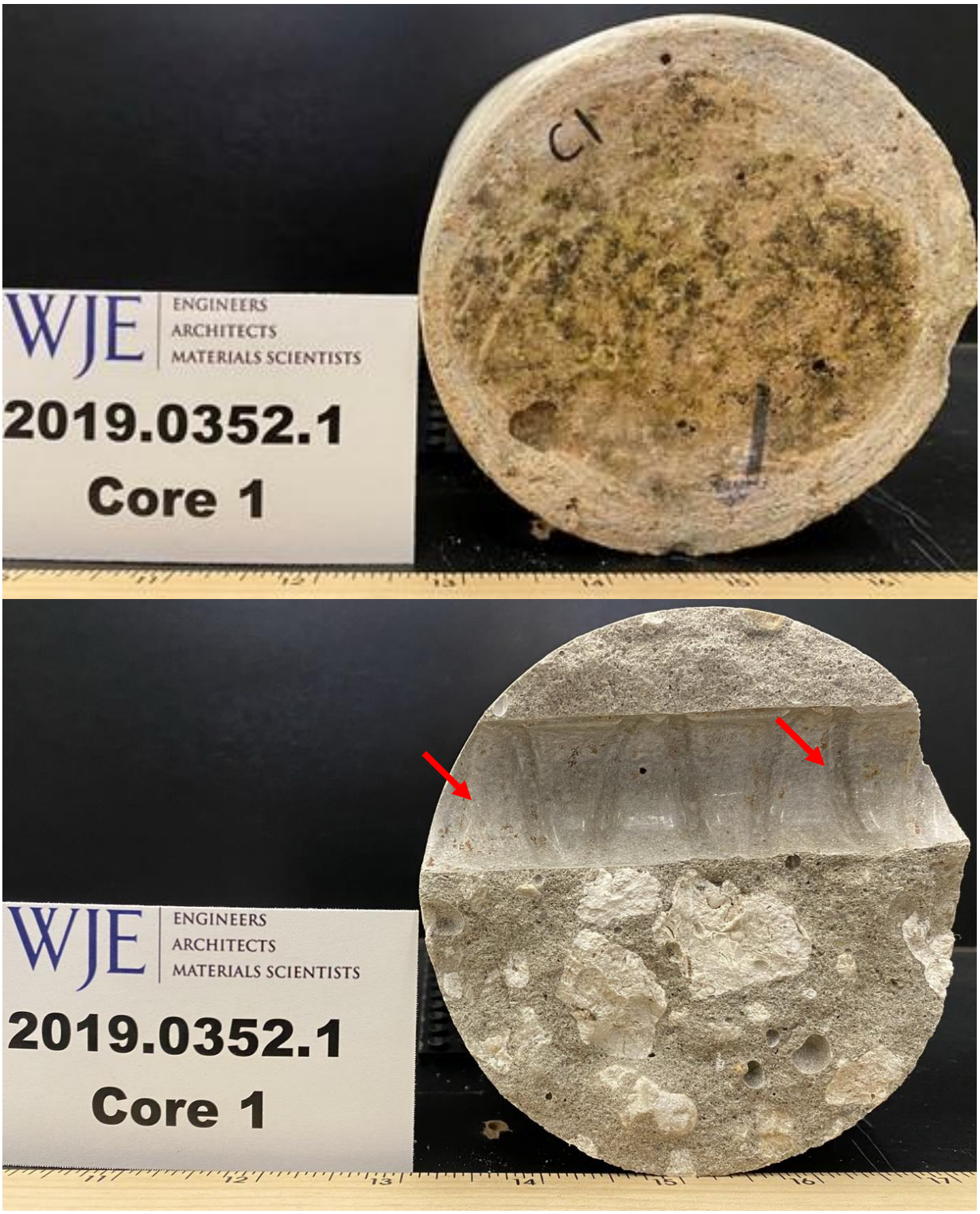

Figure 114. Core 1. Exterior (exposed) surface (top photo) and interior surface (bottom photo). Arrows indicate imprint of coated deformed steel reinforcing bar, with essentially no to minimal stains or corrosion rust. The fractured surface extended mainly through coarse aggregate particles, consistent with a tight paste-aggregate bond. As-received.

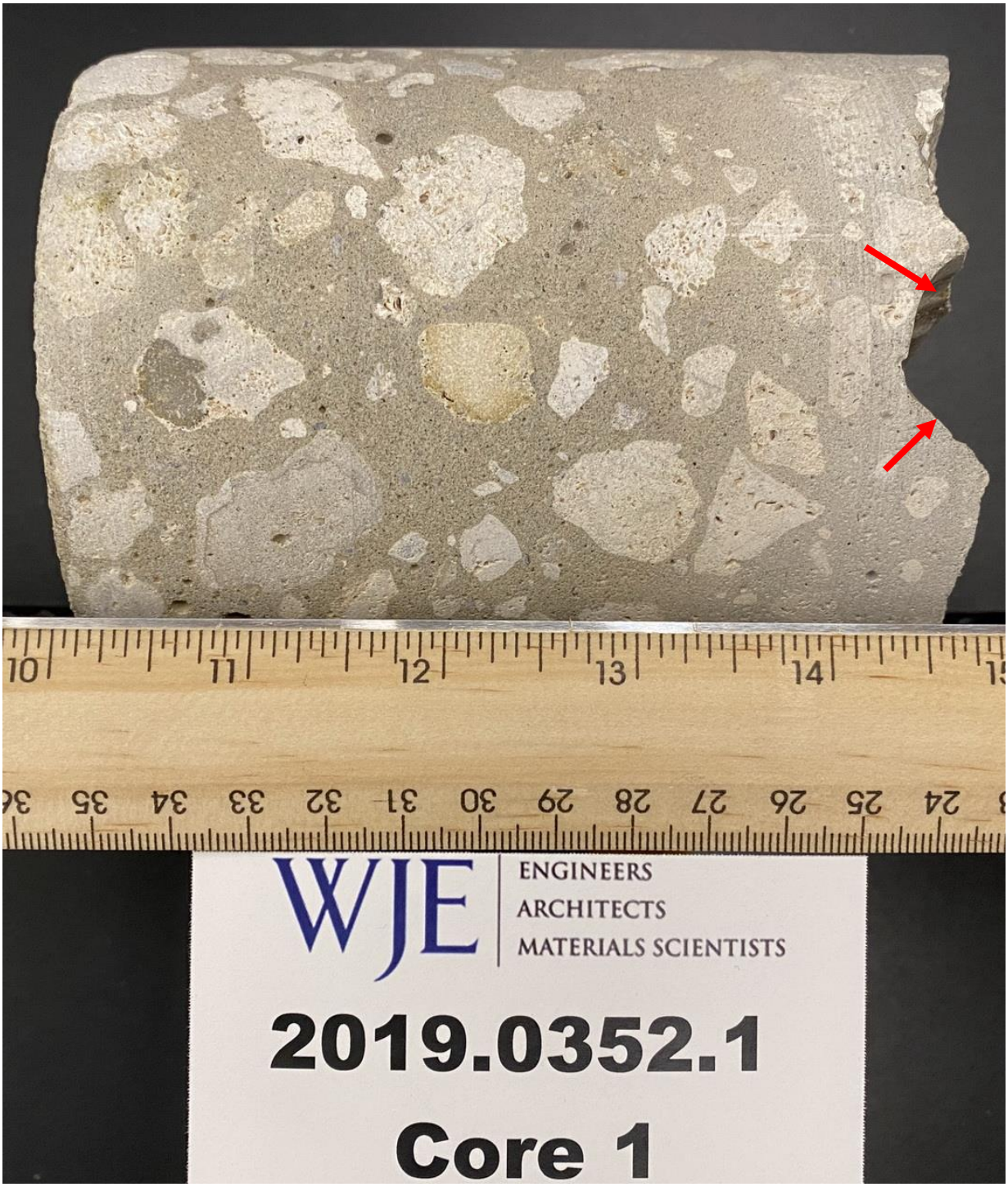

Figure 115. Core 1. Side view. Exterior end of the core is on the left. Arrows indicate the imprint of the rebar.

Figure 116. Core 1. Exterior (exposed) surface (top photo) and interior surface (bottom). Arrows indicate surface spalling or loss that was probably due to coring. The fractured surface extended mainly through coarse aggregate particles, consistent with a tight paste-aggregate bond. Orange arrows indicate hairline cracks. As-received.

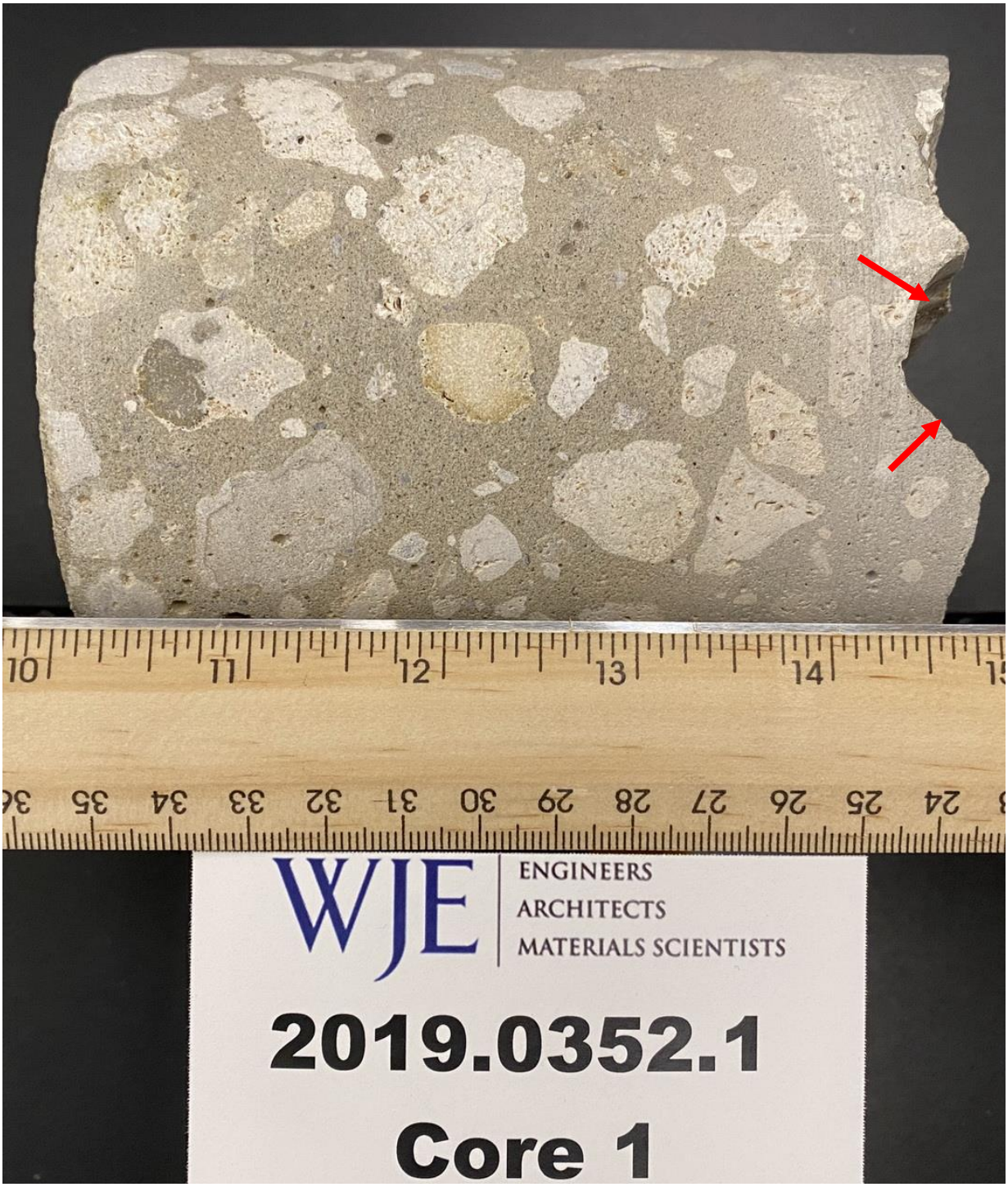

Figure 117. Core 1. Side view. Exterior end of the core is on the left. Arrows indicate the imprint of the rebar.

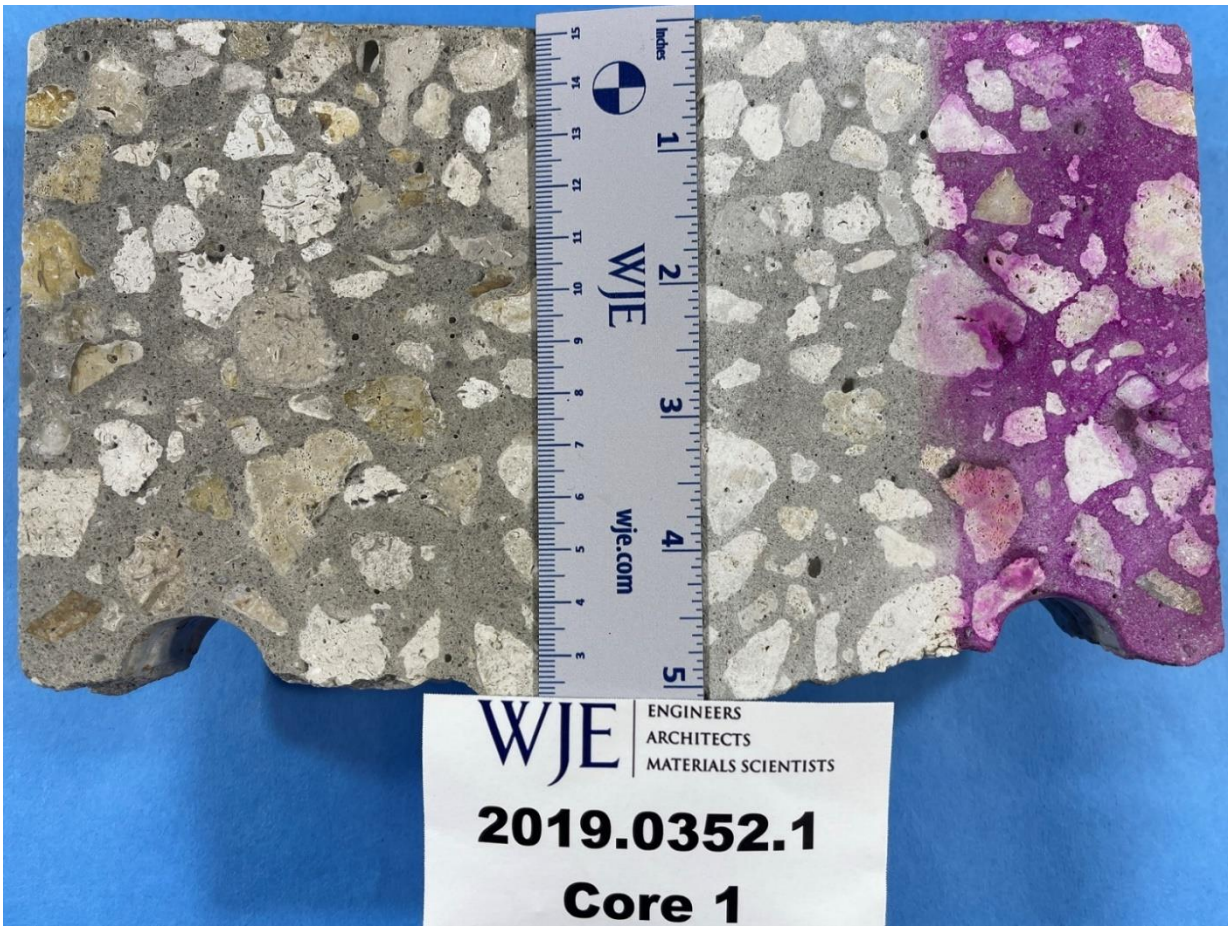

Figure 118. Core 1. Lapped cross section and matching saw-cut section stained with phenolphthalein solution to determine the depth of carbonation, which was less than 0.1 inch. Distribution of paste and aggregate appeared to be uniform and the concrete was well consolidated.

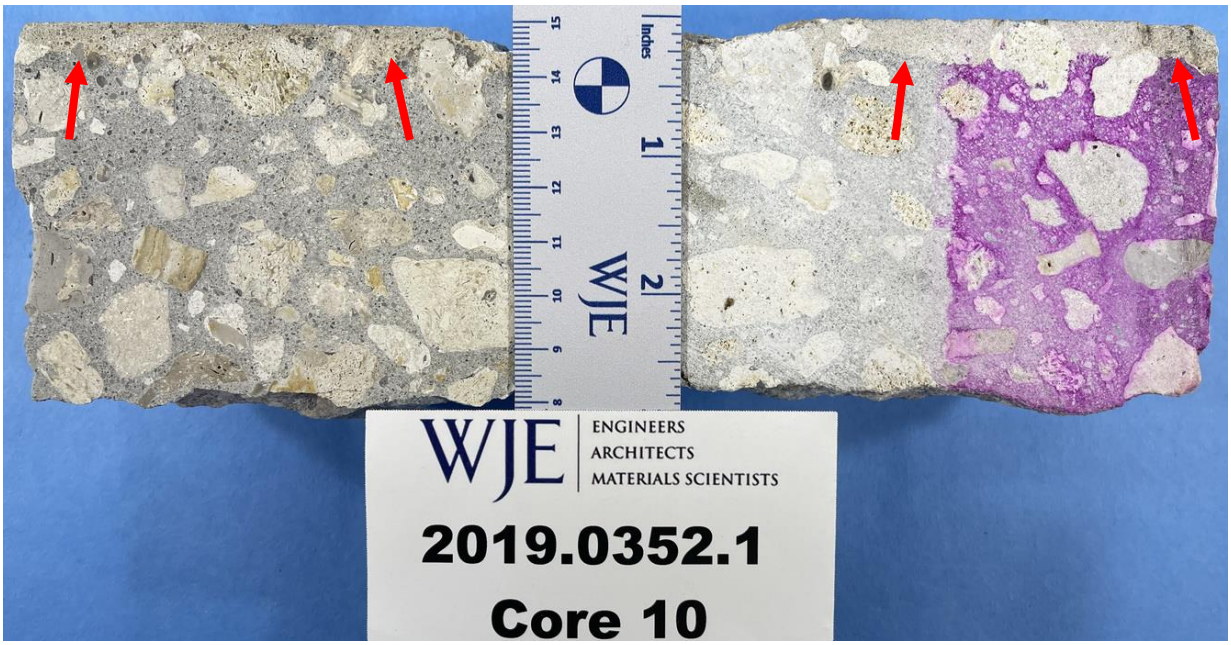

Figure 119. Core 10. Lapped cross section and matching saw-cut section stained with phenolphthalein solution to determine the depth of carbonation, which was approximately 0.3 inch as indicated by red arrows. Distribution of paste and aggregate appeared to be uniform and the concrete was well consolidated.

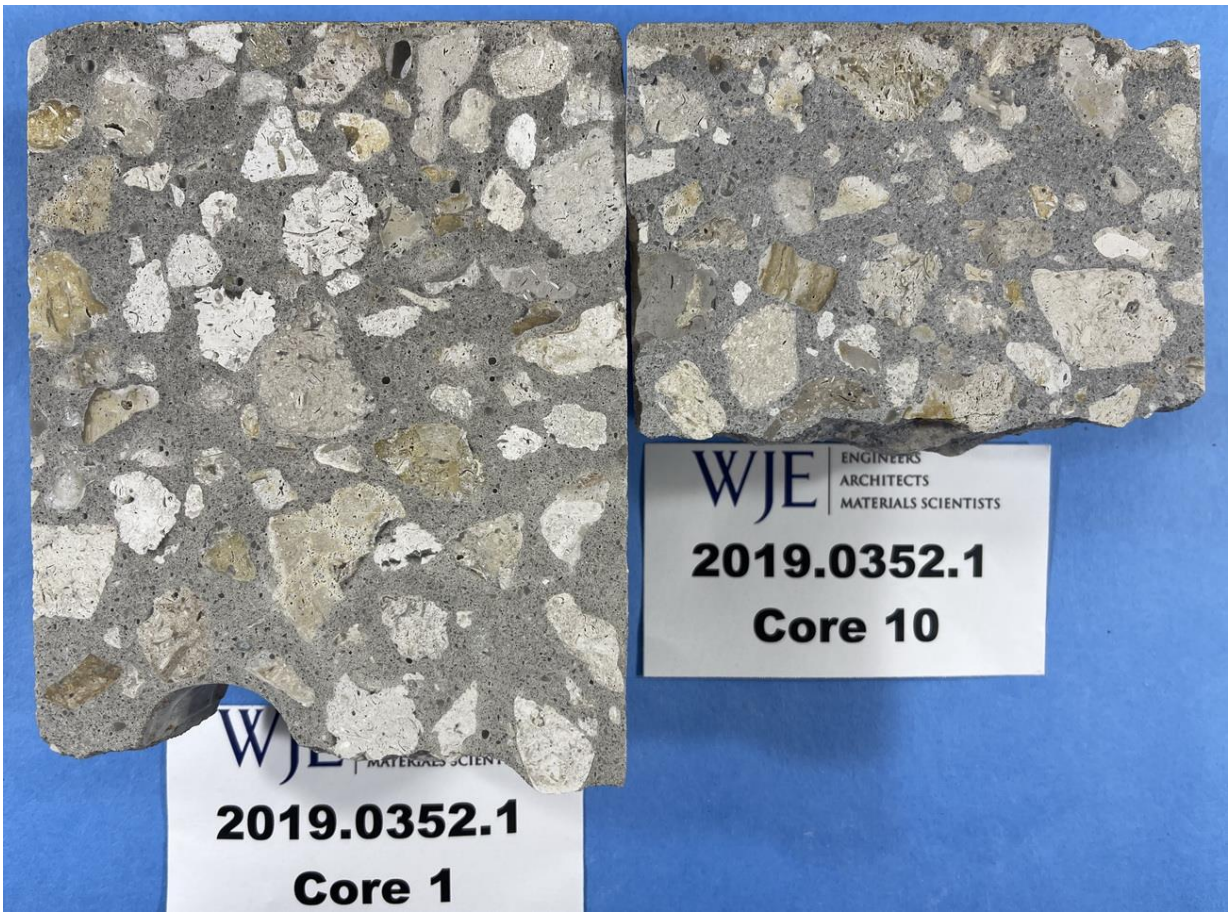

Figure 120. Core 1 and Core 10. Lapped cross sections show the overall similarity between the two cores.

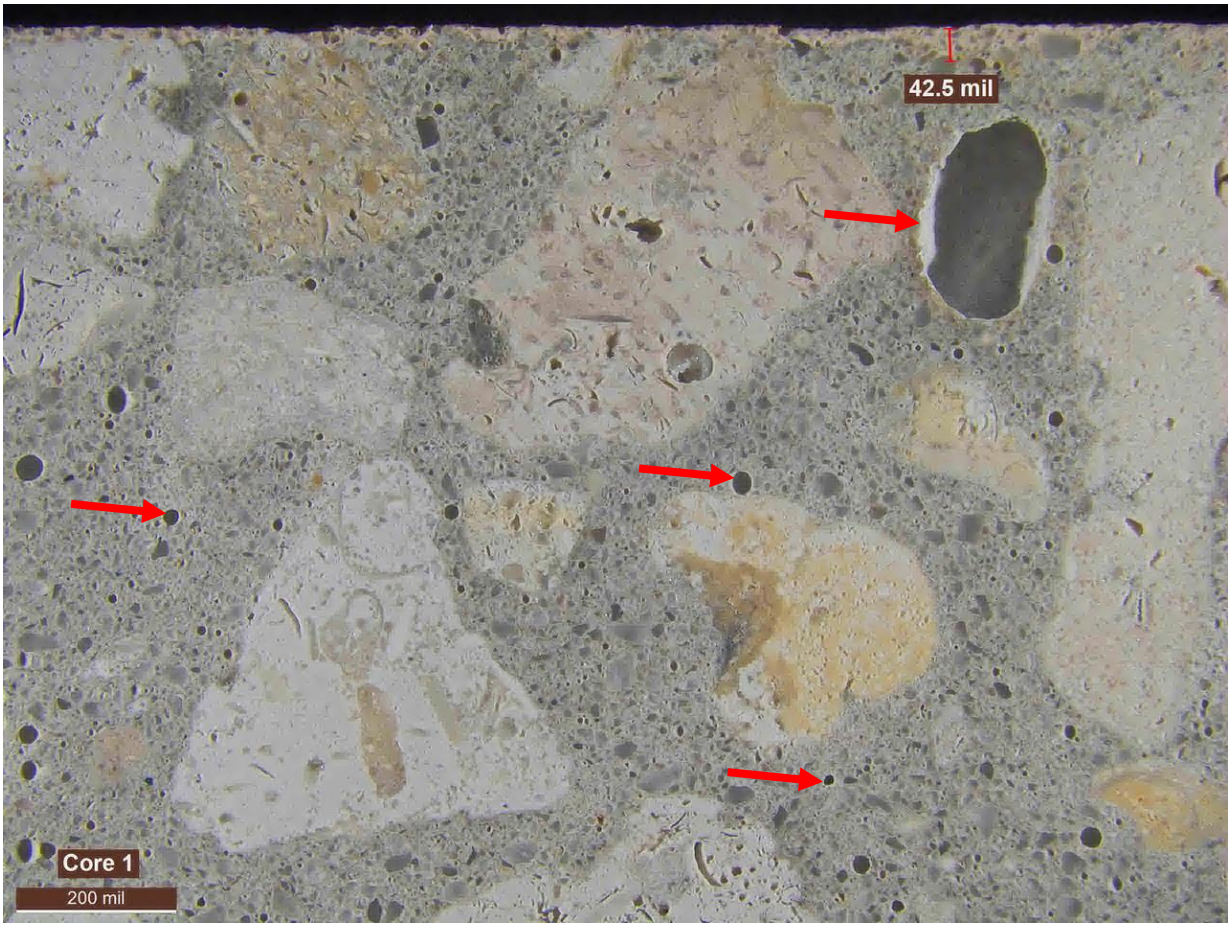

Figure 121. Core 1. Closeup view of the exterior region shows the appearance of aggregate, paste, air voids, and a discolored, carbonated top layer measuring 42.5 mils (0.043 inch). Arrows indicate air voids of varying size.

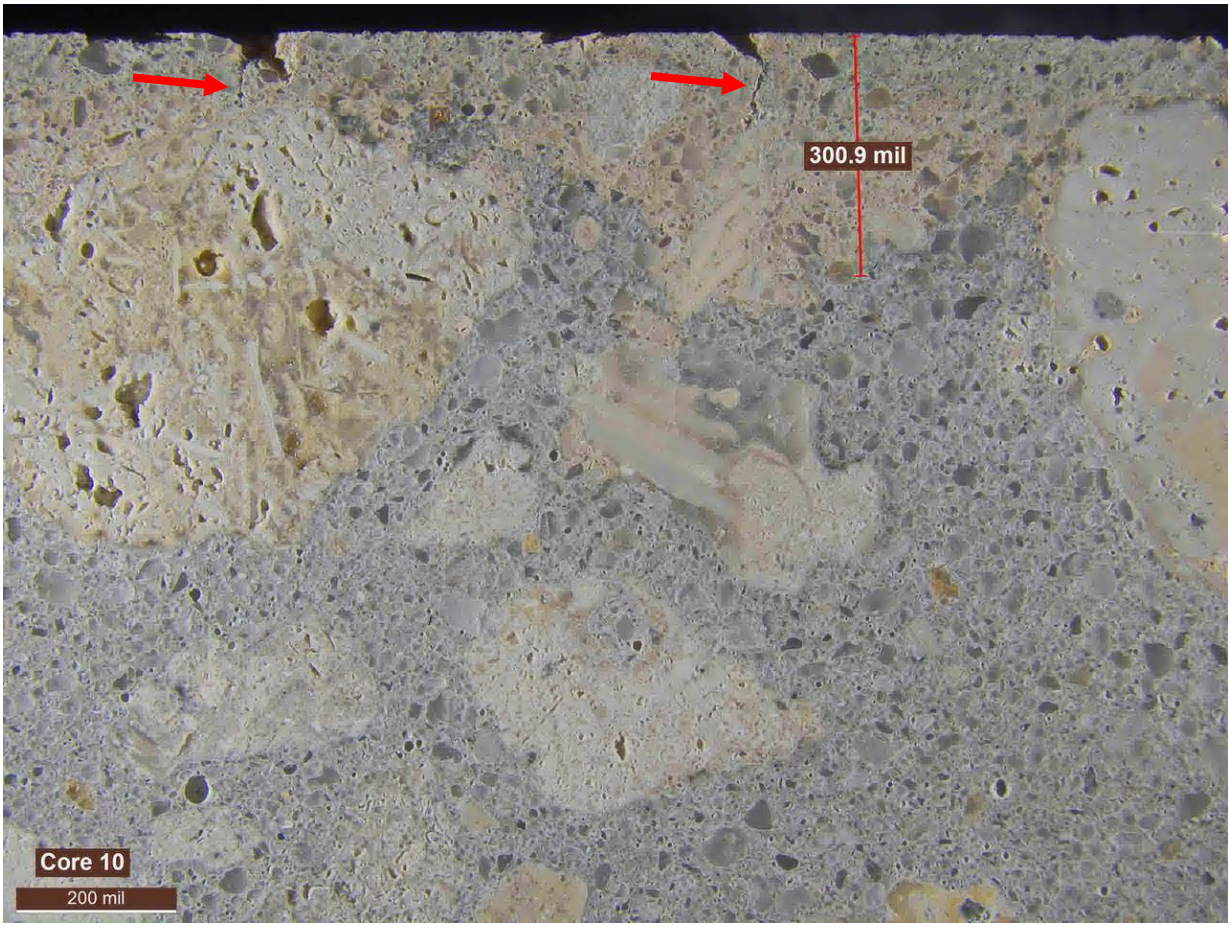

Figure 122. Core 10. Closeup view of the exterior region shows the appearance of aggregate, paste, air voids, and a discolored, carbonated top layer measuring approximately 300 mils (0.3 inch). Arrows indicate short vertical cracks/microcracks.

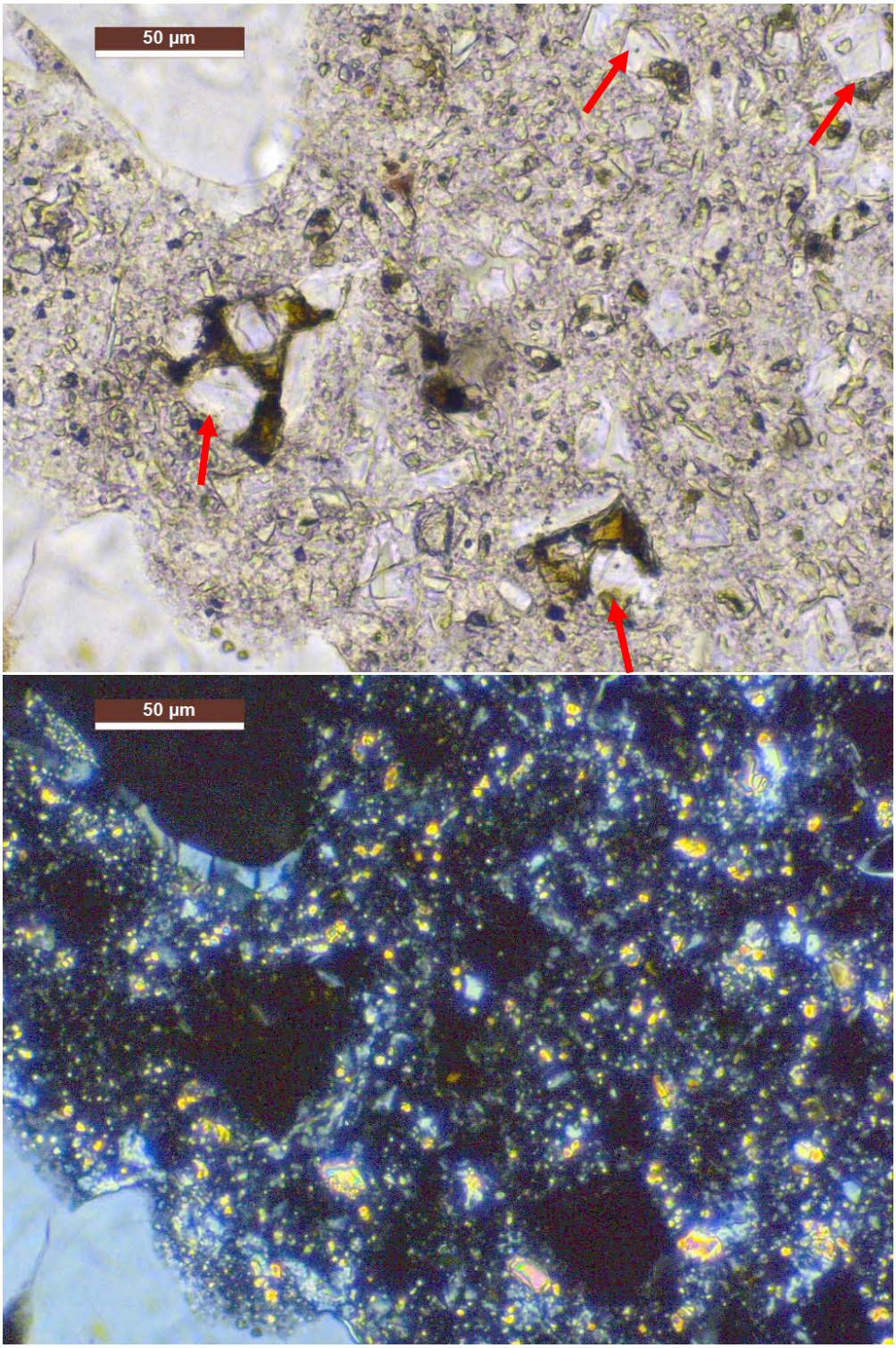

Figure 123. Core 1. Thin section photographs show the cement paste composition and micro texture. Portland cement (arrows) appeared to be well hydrated. No supplementary cementitious materials were observed. Top photo: plane-polarized light. Bottom photo: cross-polarized light.

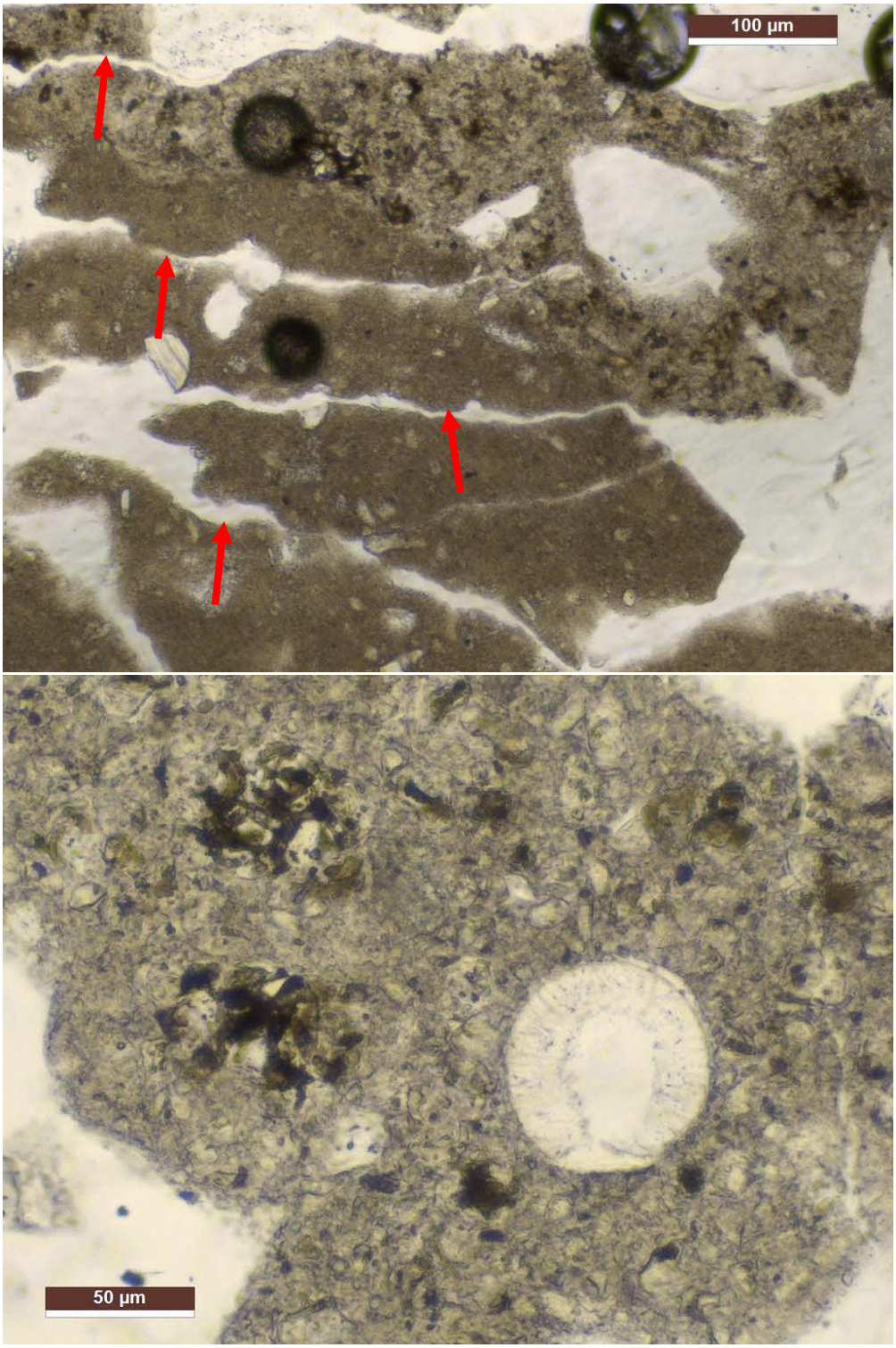

Figure 124. Core 1. Thin section photographs show the cement paste composition and micro texture. Portland cement (arrows) appeared to be well hydrated. No supplementary cementitious materials were observed. Top photo: plane-polarized light. Bottom photo: cross-polarized light.

APPENDIX F. EB SUNRISE BLVD, WB SUNRISE BLVD, AND S. ANDREWS AVE BRIDGES - VISUAL DISTRESS, NDE DATA, AND SAMPLE LOCATIONS

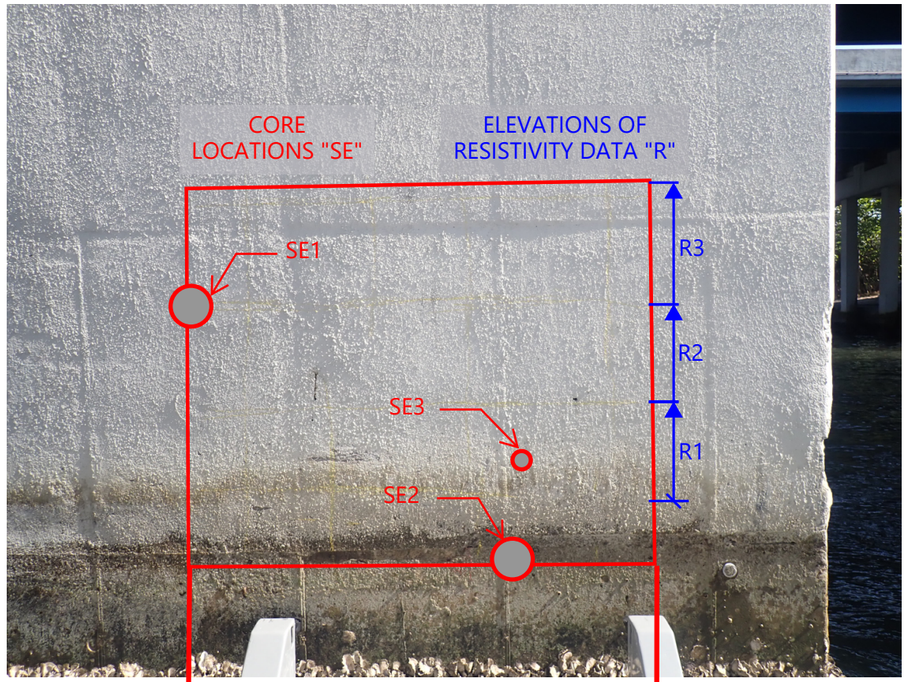

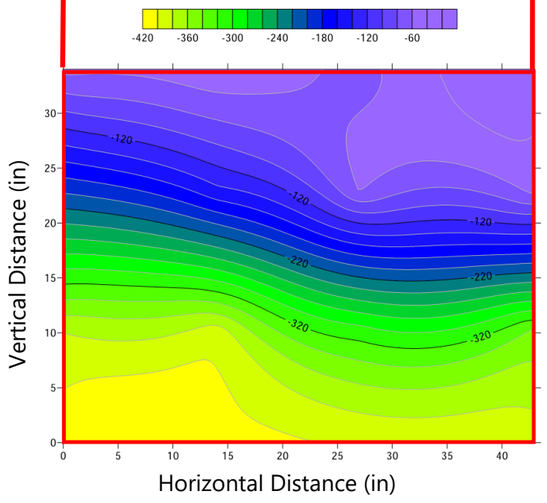

General Information	
Location	FDOT 860467
Date of Assessment	Wednesday, May 5, 2021
Approx. Temperature	83
Cover Data	
No. Bars Measured	6
Avg. Measured Cover (in.)	4.7
Std. Dev. Measured Cover (in.)	0.64
HCP Data Summary (mV vs. CSE)	
Average	0
5th %-ile	0.0
95th %-ile	0.00
Resistivity Data Summary (kΩ)	
Elevation R3	86.0
Elevation R2	214.0
Elevation R1	62.1

0 1/2" 1"
THIS SHEET PLOTS FULL SIZE AT 11x17 (INCHES)

Project	EAST-BOUND SUNRISE BOULEVARD
Sheet Title	SAMPLE LOCATIONS AND NDE DATA
Proj. No.	2019.0352.1
Date	07-08-2021
Drawn	CO
Checked	CJ/MF
Scale	NTS
Sheet No.	**SK-1**

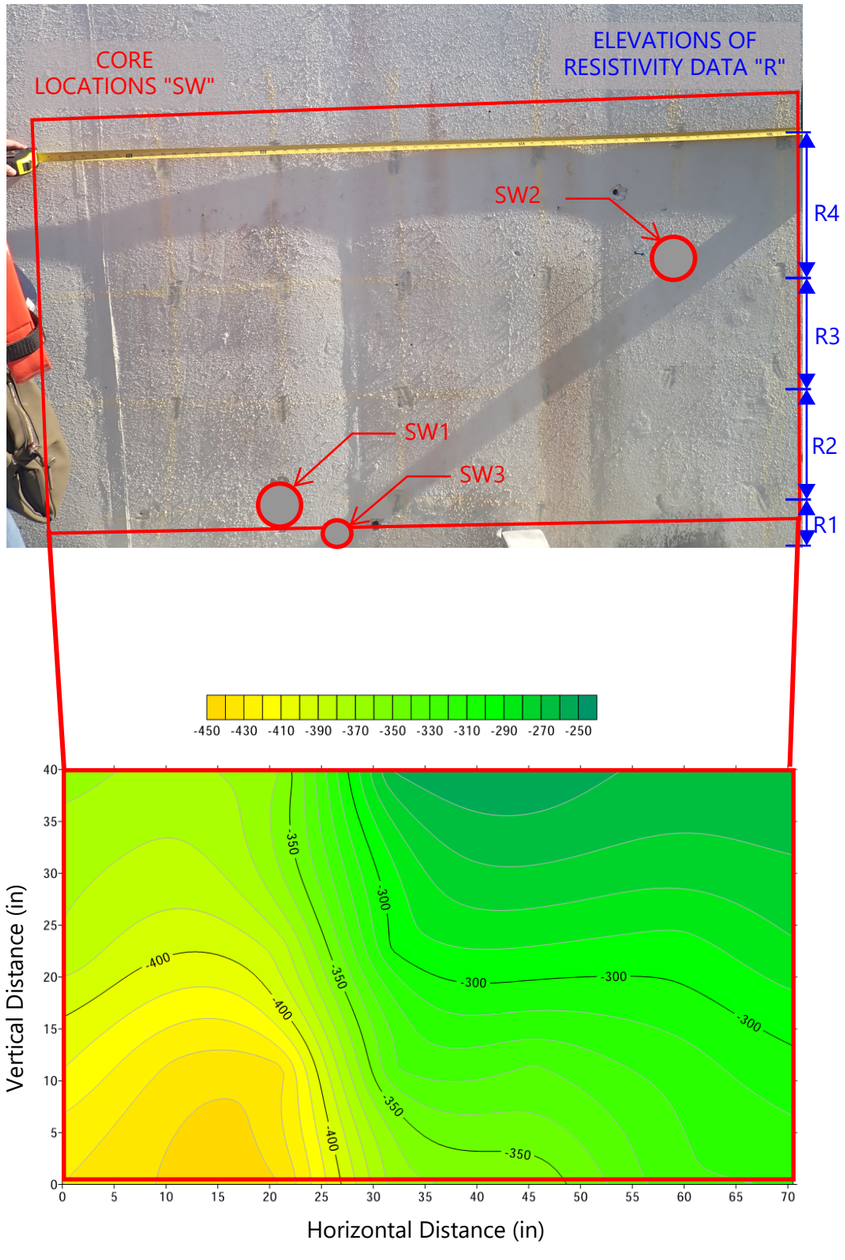

General Information	
Location	FDOT 860466
Date of Assessment	Wednesday, May 5, 2021
Approx. Temperature	83
Cover Data	
No. Bars Measured	3
Avg. Measured Cover (in.)	4.7
Std. Dev. Measured Cover (in.)	0.39
HCP Data Summary (mV vs. CSE)	
Average	0
5th %-ile	0.0
95th %-ile	0.00
Resistivity Data Summary (kΩ-cm)	
Elevation R4	313.6
Elevation R3	159.0
Elevation R2	117.5
Elevation R1	56.8

0 1/2" 1"
THIS SHEET PLOTS FULL SIZE AT 11x17 (INCHES)

Project	WEST-BOUND SUNRISE BOULEVARD
Sheet Title	SAMPLE LOCATIONS AND NDE DATA
Proj. No.	2019.0352.1
Date	07-08-2021
Drawn	CO
Checked	CJ/MF
Scale	NTS
Sheet No.	SK-2

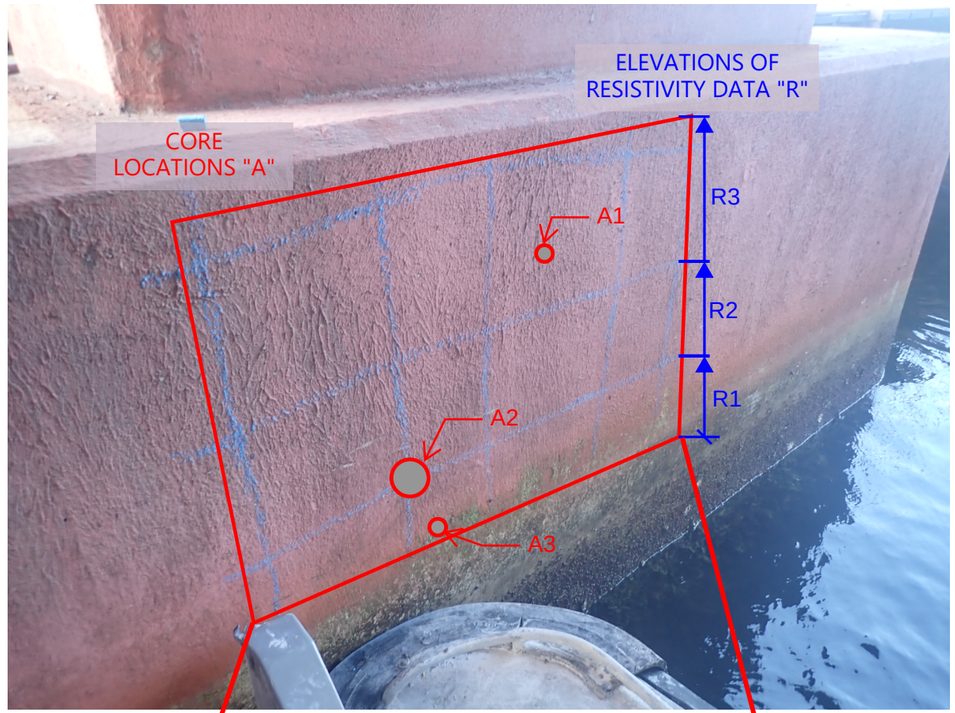

General Information	
Location	FDOT 860319
Date of Assessment	Thursday, May 6, 2021
Approx. Temperature	83
HCP Data Summary (mV vs. CSE)	
Average	0
5th %-ile	0.0
95th %-ile	0.00
Resistivity Data Summary (kΩ)	
Elevation R3	390.8
Elevation R2	140.0
Elevation R1	39.2

0 1/2" 1"
THIS SHEET PLOTS FULL SIZE
AT 11x17 (INCHES)

Project	ST. ANDREWS AVENUE
Sheet Title	SAMPLE LOCATIONS AND NDE DATA
Proj. No.	2019.0352.1
Date	07-08-2021
Drawn	CO
Checked	CJ/MF
Scale	NTS
Sheet No.	SK-3

APPENDIX G. EB SUNRISE BLVD AND WB SUNRISE BLVD BRIDGES - PETROGRAPHIC EXAMINATION REPORT

Petrographic examinations were conducted on two concrete core samples, identified Core SE-3 and Core SW-2. Core dimensions, locations, and major findings are provided in Table 59. Full petrographic examination was conducted on Core SE-3 and limited examination was conducted on Core SW-2, both in general accordance with ASTM C856, *Standard Practice for Petrographic Examination of Hardened Concrete*. Examinations were conducted on as-received cores (Figure 125 through Figure 128), lapped sections (Figure 129 through Figure 132), and laboratory-induced freshly fractured surfaces. A thin section was prepared from Core SE-3 to determine the cementitious materials composition and refine water-cementitious material ratio (w/cm) estimations (Figure 133). Powder-mount examination was conducted on Core SW-2 to assess presence of fly ash. The purposes of the petrographic studies were to assess the general concrete characteristics, quality and condition, as well as evaluate if there are materials-related deleterious chemical reactions that could reduce the service life of the concrete. Petrographic studies were conducted on Core 1 and Core 10 from the same project earlier (see memo dated February 25, 2021).

Major petrographic observations from Core SE-3 and SW-2 are provided in Table 59 and summarized as follows. Attached figures illustrate the findings.

- Concrete represented by the two cores contained similar aggregates but different cementitious materials.
- The aggregates in each core consist of crushed limestone coarse aggregate (3/4-inch nominal top size) and likely manufactured sand fine aggregate.
- Fly ash was observed in Core SE-3 but not in Core SW-2. Fly ash was estimated at 15 to 25 percent of total cementitious materials in Core SE-3.
- Estimated w/cm is 0.39 to 0.44 in Core SE-3 and 0.40 to 0.45 in Core SW-2. Paste in Core SE-3 is darker and marginally harder than Core SW-2 (Figure 118), likely due to presence of fly ash and a lower w/cm.
- Concrete in Core SE-3 is air entrained. Abundant small spherical air voids were observed in the core (Figure 132). Estimated air content was 4 to 6 percent. Concrete in Core SW-2 appeared to be air entrained. Small spherical air voids were observed in the core but much less frequently than in Core SE-3. The air content was estimated at 3 to 4 in Core SW-2.
- The concrete in each core is generally well consolidated. Distribution of constituents is uniform.
- No major cracks were observed. Microcracking is rare in both cores.
- No evidence of materials-related distress was observed. Both coarse aggregate (fossiliferous limestone) and fine aggregate appeared to have performed adequately. Secondary deposits of ettringite was observed in air voids in both cores, consistent with exposure to moisture.
- Depth of carbonation was approximately 0.2 to 0.3 inch in Core SE-3 and 0.4 to 0.5 inch in Core SW-2 (Figure 130, Table 59).
- Each core contains a thin layer of light-gray coating that appeared to be well bonded to the concrete (Figure 131 and Figure 132).
- Concrete represented by both cores appeared to be in good condition overall.

Summary

1. **Main Cracks:** None observed in either core. Microcracking is infrequent.

2. **ASR:** No evidence of alkali-silica reactions or other deleterious chemical reactions such as delayed ettringite formation (DEF) was observed in the cores.
3. **Distress Related to Seawater Exposure:** Likely minimal to absent.
4. **Reinforcement:** Core SW-2 contained a No. 5 deformed, epoxy-coated steel reinforcing bar. The bar appeared to be in good condition. No radiating cracking was observed surrounding the bar. No reinforcement bars or imprints were observed in Core SE-3.
5. **Carbonation:** 0.2 to 0.3 inch in Core SE-3 and 0.4 to 0.5 inch in Core SW-2.
6. **Concrete Condition:** Appeared to be good overall in both cores.
7. **Coating Layer:** Overall well bonded to the substrate concrete in both cores.
8. **Major Differences Between Two Cores:** Core SE-3 contains fly ash estimated at 15 to 25% among total cementitious materials. No fly ash was observed in Core SW-2 based on powder mount examinations. Core SW-2 contains an overall higher air content and more small air voids than Core SE-3.

Table 59. General Core Characteristics and Petrographic Findings

	Core SE-3	Core SW-2
Dimensions	Diameter=1.5 inches; Length=7.3 inches	Diameter=3.6 inches; Length=5.0 inches
Location	Pier	Pier
Exterior Surface	Overall flat formed/finished surface covered with a light-gray coating layer approximately 40 mils thick	Overall flat formed/finished surface covered with a light-gray coating layer that is approximately 20 mils thick
Interior Surface	Rough fractured surface extended mainly through coarse aggregate particles.	Rough fractured surface extended mainly through coarse aggregate particles. A No.5 deformed, epoxy-coated reinforcing steel bar observed on the interior surface (4-1/8 inch cover); the bar is free of rust.
Coarse Aggregate	Similar in the two cores, composed of crushed fossiliferous limestone, with a nominal top size 3/4 inch. Many particles are also arenaceous (i.e. containing quartz sand grains in the limestone).	
Fine Aggregate	Similar in the two cores; appeared to be sand manufactured from rocks similar in lithology to the coarse aggregate; consisting mainly of limestone and smaller amounts of siliceous quartz sand.	
Paste	• Portland cement and fly ash paste • Fly ash estimated 15 to 25% among total cementitious materials by mass • Medium to dark gray, moderately hard to hard, and moderately low in water absorptivity.	• Portland cement paste without supplementary cementitious materials based on powder mount examination. • Medium, moderately hard to hard, and moderately low in water absorptivity.
Estimated W/C	0.39 to 0.44	0.40 to 0.45
Paste-Aggregate Bond	Interpreted to be tight in both cores	
Estimated Air Content	3 to 4%, likely air-entrained; contains both coarse and fine air voids.	4 to 6%; air-entrained; mainly small spherical air voids.
Secondary Deposits	Ettringite frequently lines air voids in both cores, consistent with exposure to moisture.	
Materials-Related Distress	None observed in either core	
Cracking/Micro cracking	Infrequent microcracking in both cores	
Overall Condition	Appeared to be good in both cores.	

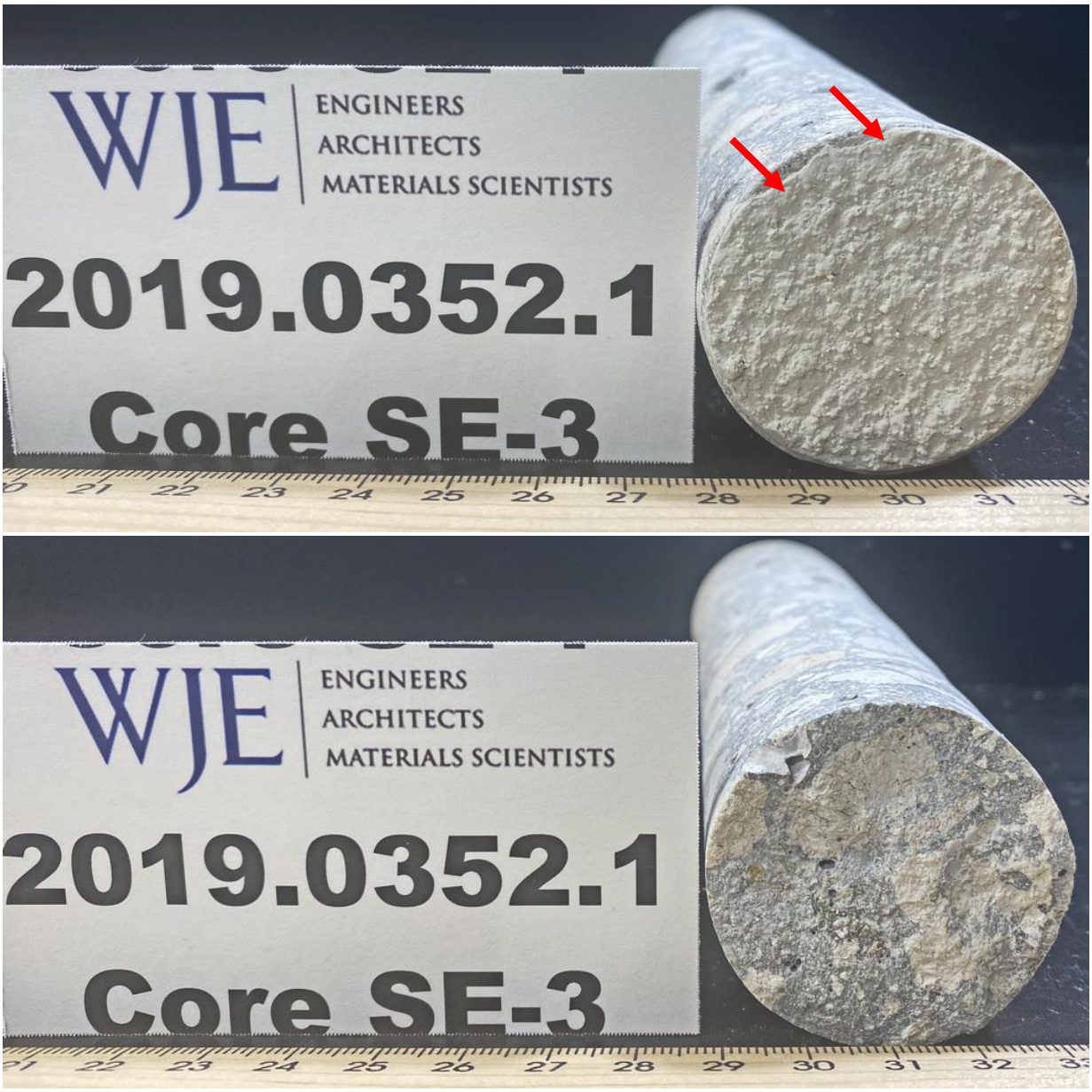

Figure 125. Core SE-3. Exterior (exposed) surface (top photo) and interior surface (bottom photo). Arrows indicate a thin layer of light-gray coating. The interior fractured surface extended mainly through coarse aggregate particles, consistent with a tight paste-aggregate bond. As-received for examination.

Figure 126. Core SE-3. Side view. Exterior end of the core is on the left.

Figure 127. Core SW-2. Exterior (exposed) surface (top photo) and interior surface (bottom). The interior fractured surface extended mainly through coarse aggregate particles, consistent with a tight paste-aggregate bond. Orange arrows indicate a partially exposed No. 5 reinforcing steel bar.

Figure 128. Core SW-2. Side view. Exterior end of the core is on the left. Arrows indicate the reinforcing steel bar.

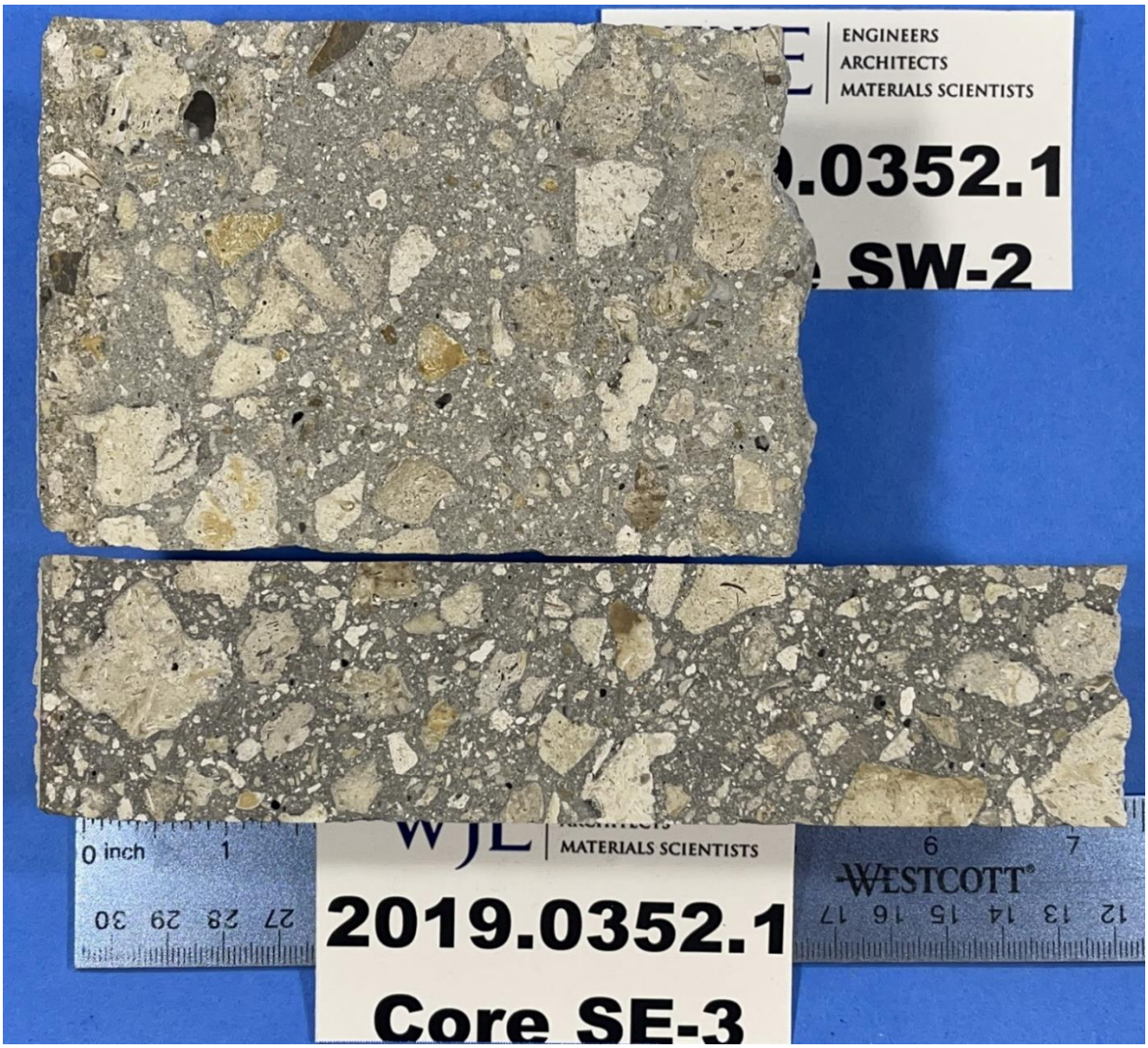

Figure 129. Lapped cross sections of the two cores show the overall appearance and condition of the concrete in each core. Distribution of paste and aggregate appears to be uniform and the concrete in each core is overall well consolidated. The exterior ends are on the left.

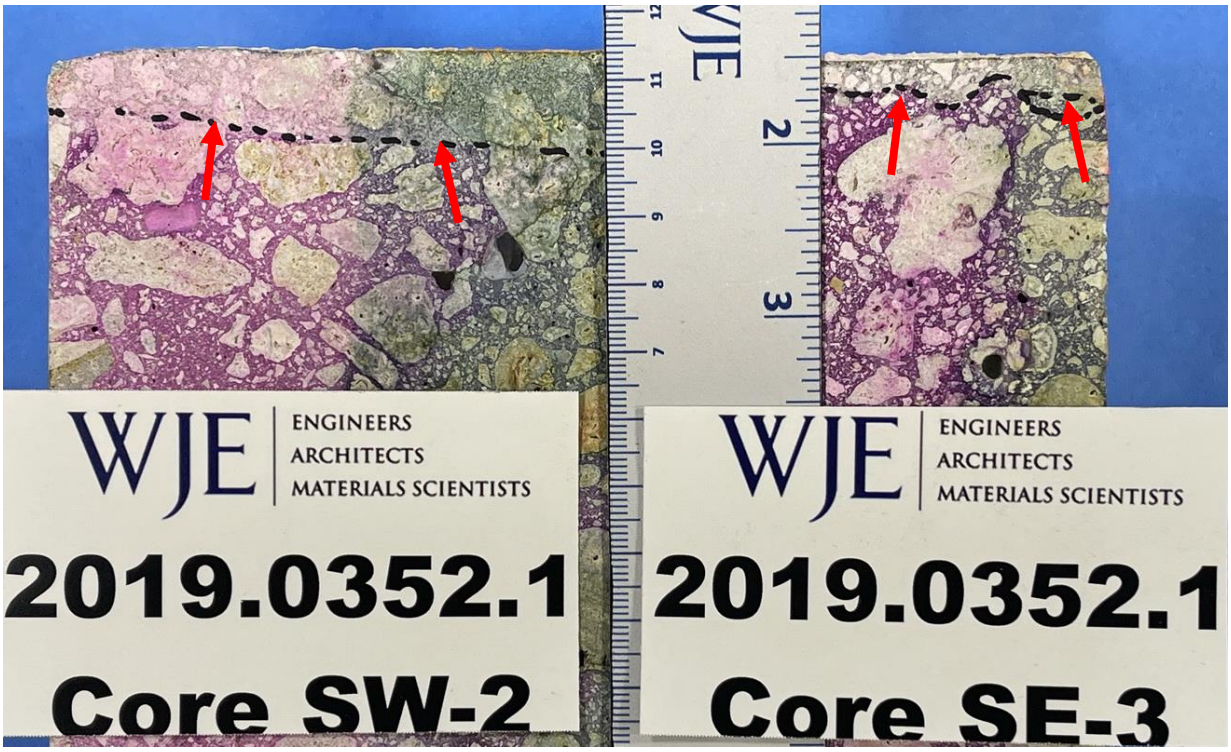

Figure 130. Saw-cut cross sections stained with phenolphthalein solution (left portion in each core) and a rainbow solution to determine the depth of carbonation. Carbonation was 0.4 to 0.5 inch in Core SW-2 and 0.2 to 0.3 inch in Core SE-3, as indicated by the color variation (red arrows).

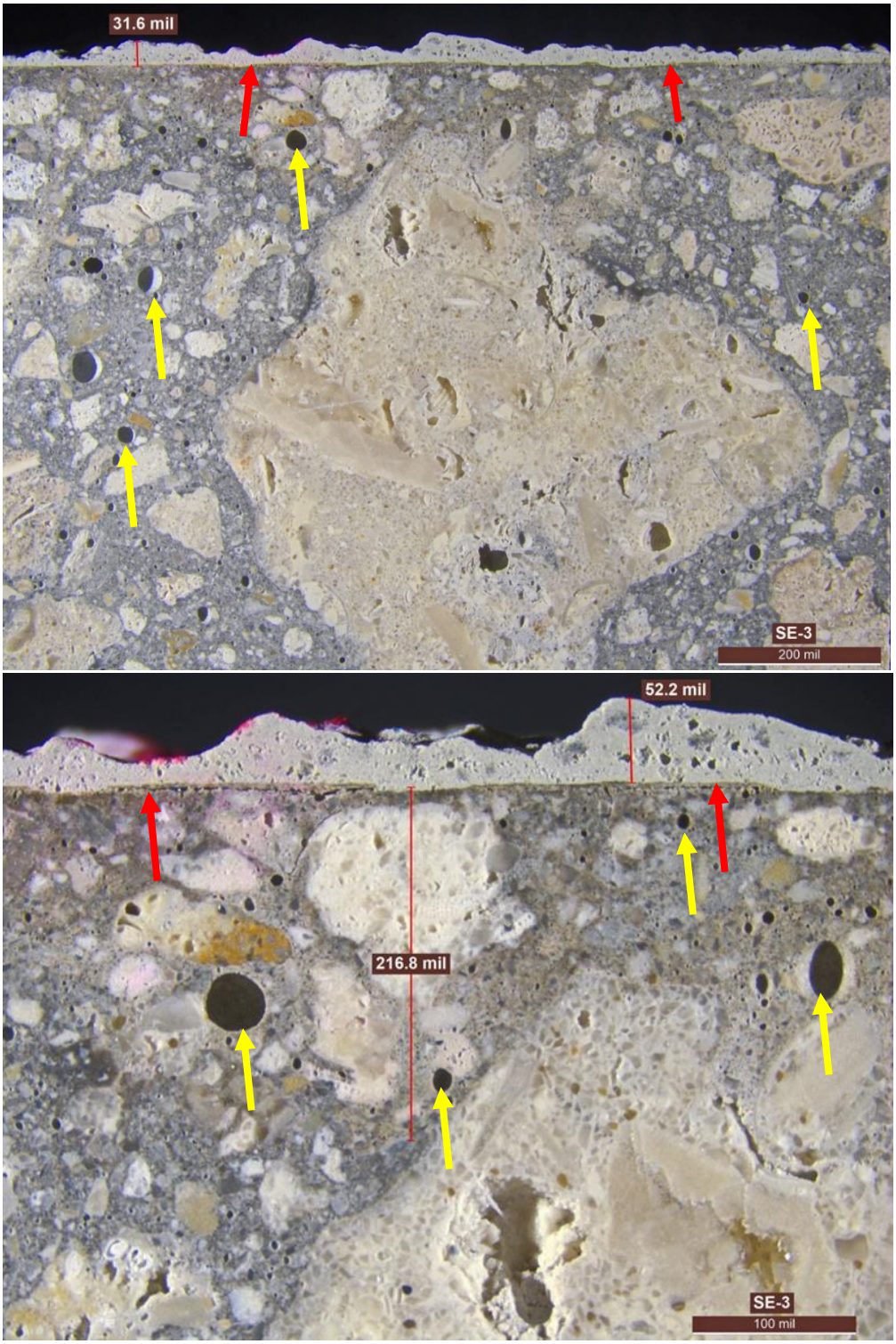

Figure 131. Core SE-3. Closeup views of the exterior region show the appearance of aggregate, paste, air voids, a marginally discolored, carbonated top layer measuring 216.8 mils (0.22 inch), and a light-gray coating layer (red arrows). Yellow arrows indicate air voids.

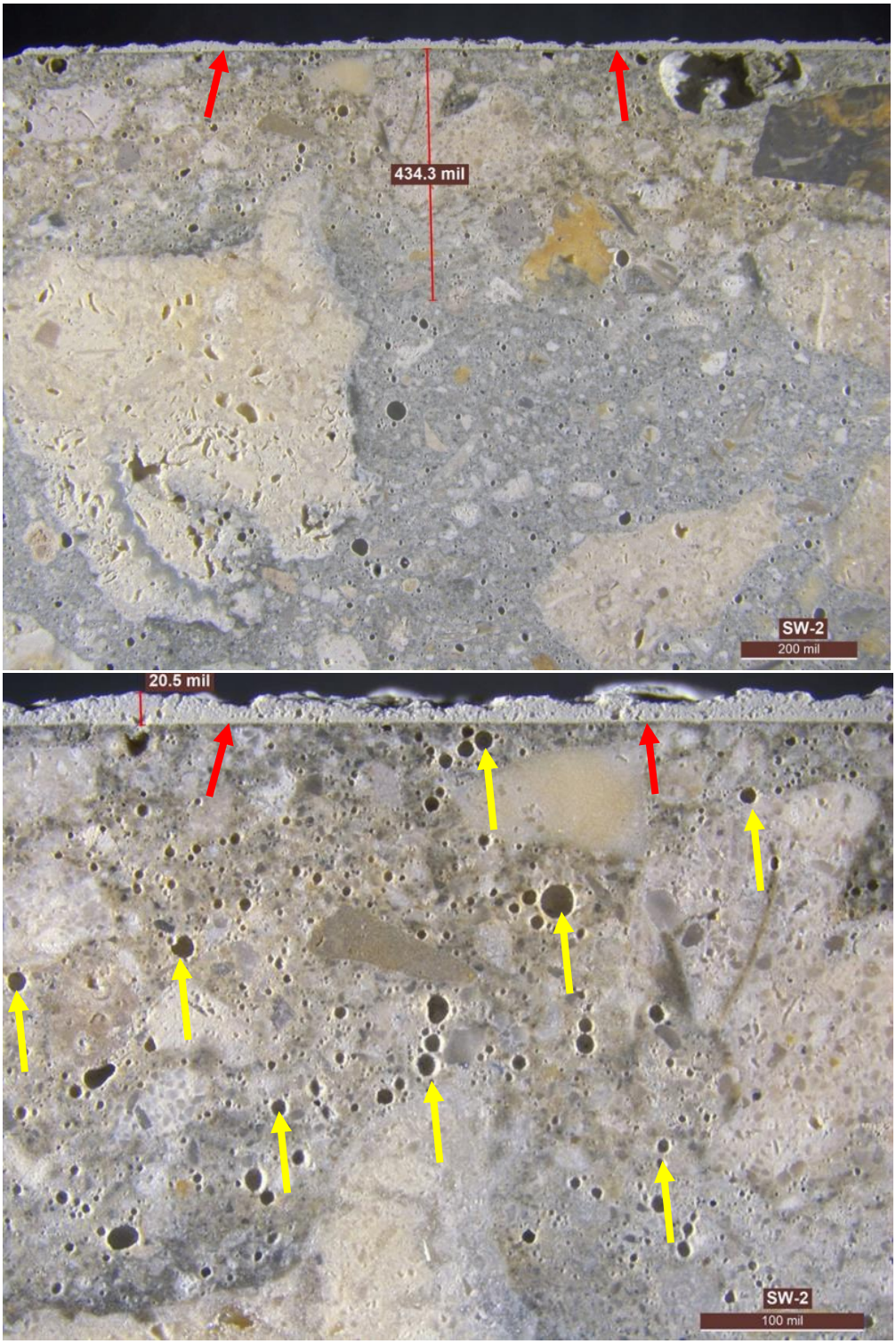

Figure 132. Core SW-2. Closeup views of the exterior region show the appearance of aggregate, paste, air voids, a marginally discolored, carbonated top layer measuring 432.3 mils (0.43 inch), and a light-gray coating layer (red arrows). Abundant small spherical air voids were observed (yellow arrows), consistent with air-entrainment.

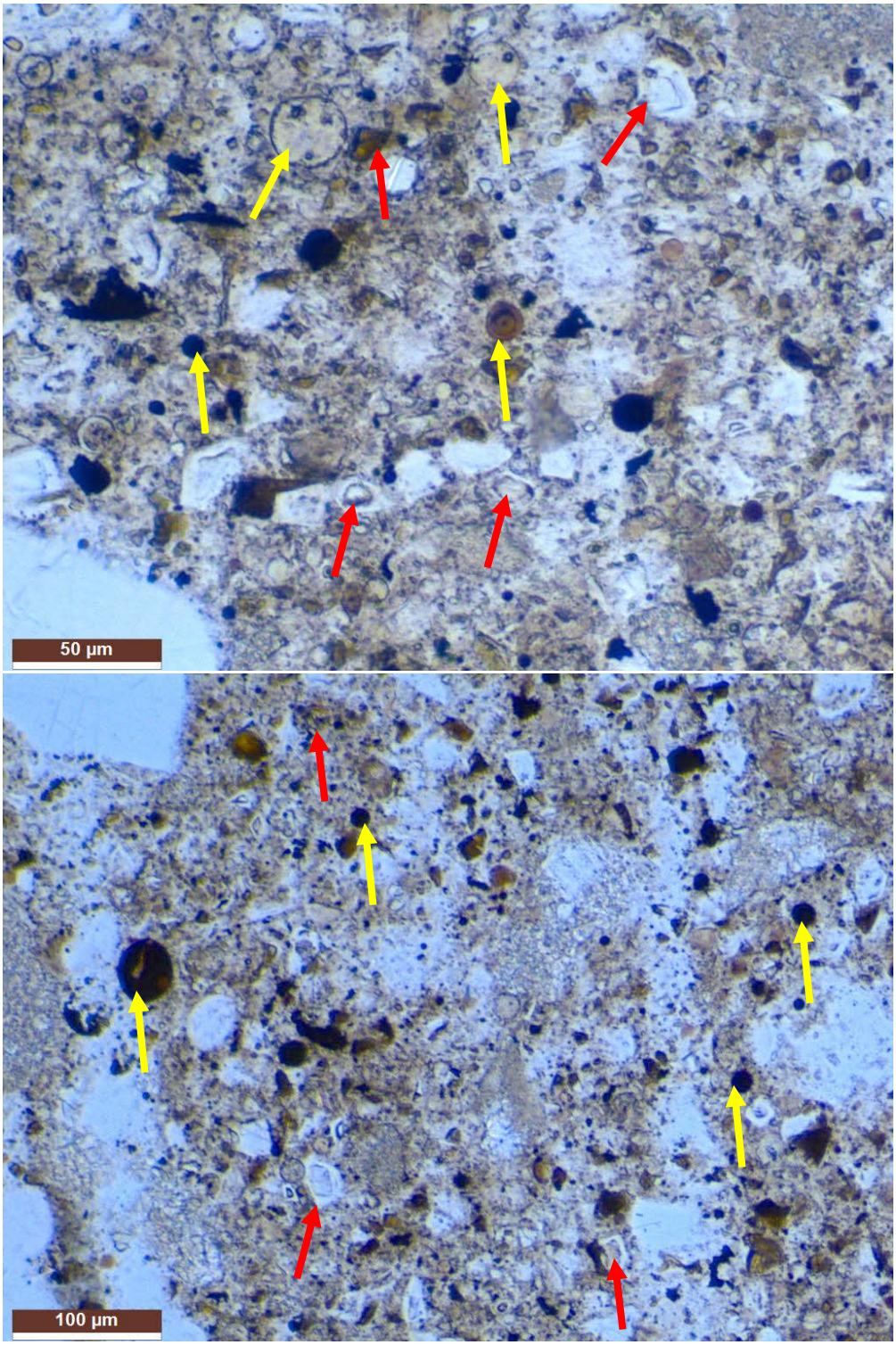

Figure 133. Core SE-3. Thin section photographs show the cement paste composition and micro texture. Portland cement (red arrows) appeared to be well hydrated. Fly ash was observed (yellow arrows) and estimated at 15 to 25 percent by mass of total cementitious materials. Plane-polarized light for both.